CONVENTIONAL AND CARBONATED WATER FLOODING IN HEAVY OIL SYSTEMS: MICROMODEL AND COREFLOODING STUDIES

A Thesis

Submitted to the Faculty of Graduate Studies and Research

In Partial Fulfilment of the degree of

Doctor of Philosophy in

Petroleum Systems Engineering

University of Regina

By

Tayebeh Jamshidi

Regina, Saskatchewan

July, 2018

UNIVERSITY OF REGINA

FACULTY OF GRADUATE STUDIES AND RESEARCH

SUPERVISORY AND EXAMINING COMMITTEE

Tayebeh Jamshidi, candidate for the degree of Doctor of Philosophy in Petroleum Systems Engineering**,** has presented a thesis titled, ***Conventional and Carbonated Water Flooding in Heavy Oil Systems: Micromodel and Coreflooding Studies,*** in an oral examination held on July 26, 2018. The following committee members have found the thesis acceptable in form and content, and that the candidate demonstrated satisfactory knowledge of the subject material.

External Examiner:	*Dr. Hossein Hejazi, University of Calgary
Co-Supervisor:	Dr. Paitoon Tontiwachwuthikul, Industrial Systems Engineering
Co-Supervisor:	Dr. Fanhua Zeng, Petroleum Systems Engineering
Committee Member:	Dr. Nader Mobed, Department of Physics
Committee Member:	Dr. Raphael Idem, Industrial Systems Engineering
Committee Member:	Dr. Yongan Gu, Peetroleum Systems Engineering
Chair of Defense:	Dr. Kathleen McNutt, Faculty of Graduate Studies & Research

*via ZOOM

Abstract

Despite the severe viscosity contrast and low displacement efficiency in heavy oil reservoirs, conventional waterflooding is still considered as one of the feasible recovery processes for such reservoirs. On the other hand, conventional waterflooding has been well studied and has been suggested for light oil reservoirs. However, viability of carbonated waterflooding for heavy oil reservoir and impact of operational parameters, reservoir characteristics, and fluid properties on the performance of this technique are yet to be fully understood. In this study, the performances of conventional and carbonated waterflooding in heavy oil reservoirs were analyzed through various micromodel and coreflooding experiments. Prior to the main tests, a series of experiments were performed to investigate the effect of various parameters such as temperature, pressure, and oil API gravity on the fluid interactions in the binary systems of brine-CO_2 and oil-CO_2.

The solubility of carbon dioxide in 20,000 ppm brine solution was measured at various experimental conditions and compared with previous studies. Furthermore, the solubility of CO_2 in oil and the swelling factor for two heavy oils (Type-I, ^oAPI=20.44 and Type-II, ^oAPI=15.49) were experimentally measured at various conditions. In this regard, CO_2 solubility was measured to be 10.13 and 5.72 (gr CO_2/100 gr oil) in Type-I crude oil when temperature increased from T=21^{o}C to 45^{o}C at the constant pressure of P_{exp}=3.44 MPa. When pressure increased from P_{exp}=1.38 MPa to 3.44 MPa at the constant temperature of T=21^{o}C, solubility of CO_2 in Type-II crude oil was increased from 2.37 to 7.84 (gr CO_2/100 gr oil). A reduction in oil API gravity had adverse effect on the CO_2 solubility. For example, at the temperature of T=21^{o}C and Pressure of P_{exp}=3.44 MPa, CO_2 solubility decreased from about 10.13 (g CO_2/100 gr in oil) Type-I to 7.84 (gr CO_2/100 gr

oil) in oil Type-II. Measured values of swelling factor showed that Type-I and Type-II crude oils could swell to the maximum of 1.079 and 1.052 times of their initial volume at the temperature of T=21^{o}C and Pressure of P_{exp}=3.44 MPa.

Effect of key parameters such as injection rate, temperature, oil API gravity and extreme heterogeneity on the performance of both conventional and carbonated waterflooding in heavy oil systems were extensively studied through series of experiments.

Results of conventional waterflooding conducted with 1.6 PVs of injected water in the single permeability porous media showed ultimate recovery factors of 48%, 62% and 53.7% for water injection rates of q_{inj}=0.025, 0.05, and 0.075 (cm^3/min), respectively. Increasing the temperature from T_{exp}=21^{o}C to 30^{o}C and 45^{o}C improved the ultimate recovery factor of conventional waterflooding in single permeability porous media from 61% to 69.3% and 73%, respectively. These values were achieved at nearly 1.6 PVs of injected water. Analysis of the experimental results at q_{inj}=0.05 (cm^3/min) and T_{exp}=21^{o}C revealed an improvement of 2.44% in ultimate recovery factor when oil API gravity increased from ^{o}API=15.49 to 20.44. Results of this study showed that carbonated waterflooding (CWF) could improve the ultimate recovery factor by 24% compared to WF.

Conventional and carbonated waterflooding tests conducted in a sand-packed model revealed that injection at higher carbonation pressure of 3.1 MPa results in 16.5% additional recovery factor in type-I heavy oil compared to heavier oil of type-II. Among API gravity, carbonation pressure, temperature and injection rate, it was found that the key success for CWF is oil API gravity and carbonation pressure.

Acknowledgements

I would like to express my sincere gratitude to my supervisors Drs. Fanhua (Bill) Zeng and Paitoon Tontiwachwathikul for their continuous support, patience and guidance, during my study and throughout the progress of this work at the University of Regina. I wish to thank Dr. Nader Mobed, Dr. Peter Gu and Dr. Raphael Idem, and Dr. Hejazi (from University of Calgary) for their advice, constructive comments, questions, and their kindness for serving as a member of my examination committee. I am grateful to the dean of FGSR, Dr. Kathleen McNutt, for chairing my defense and her support.

I am thankful to the Petroleum Technology Research Centre (PTRC), Sustainable Technologies for Energy Production System (STEPS) program, Natural Science and Engineering Research Council (NSERC), Heavy Oil Research Network of Excellence (HORNET), Faculty of Graduate Studies and Research (FGSR), and Faculty of Engineering and Applied Science for funding supports and opportunities.

Many thanks to Drs. Abedini, Mosavat, Mohammadpour, Mr. Hongyang Wang, Mr. Nathan David, and Mr. Mohsen Riazi. I would like to express my appreciation to Drs. Karimi, Riazi, Malayeri, and Escrochi and Ms. Sanaz Shojaei (lab manager) and all graduate students at the Enhanced Oil Recovery Centre of Shiraz University for providing space and some equipment to conduct most of my experiments.

Last but not least, I would like to thank my family members, Farshid (my husband), Yasaman (my daughter), Amir and Ryan (my two sons) who supported me to overcome the difficult and busy times during ten years of my undergraduate and graduate studies at the University of Regina.

Dedication

To:

My three reasons of life (Yasaman, Amir, and Ryan),

My husband, Farshid, for his love from childhood until now, trust, patience, and continuous support and encouragement,

My parents Vali and Hamideh for their love, motivation, support, and continues encouragement,

My sister in -law, Safoora for her love and support for over two decades,

To:

All of those who encouraged or tried to discourage, supported or disappointed.

To:

Ali, my 5 years old nephew, who left us behind with so much love and unforgettable memories.

TABLE OF CONTENTS

LIST OF TABLES

LIST OF FIGURES

NOMENCLATURE

Symbols

CL	Carbonation level (%)
D	Grain diameter in porous medium (m)
dP	Differential pressure across the sand-pack (kPa)
k_{abs}	Absolute permeability (mD)
k_{eff}	Effective permeability (mD)
k_h	Horizontal permeability (mD)
k_{ro}	Relative permeability to oil
k_{rw}	Relative permeability to water
L	Length of micro-model's glass (cm^3)
l_p	Length of micro-model's engraved pattern (cm^3)
M	Mobility (D/Pa.s)
$m_{CO2,f}$	Final mass of CO_2 (gr)
$m_{CO2,i}$	Initial mass of CO_2 (gr)
m_{dis}	Mass of CO_2 dissolved in the oil (gr)
m_{oil}	Mass of the oil sample (gr)
MW_{CO2}	Molecular weight of CO_2 (44.01 gr/mol)
MW_o	Oil molecular weight (gr/mole)
N_{CA}	Complete capillary number
P	Pressure (MPa)
P_{atm}	Atmospheric pressure (101.1 kPa)
P_b	Base pressure (14.7 psia)

P_c	Critical pressure (MPa)
P_f	Final pressure (MPa)
P_i	Initial pressure (MPa)
P_{max}	Maximum operating pressure (MPa)
P_R	Reservoir pressure (MPa)
P_s	Saturation pressure (psia)
P_{sat}	Saturation pressure (MPa)
q_{inj}	Injection flow rate (cm^3/min)
R	Universal gas constant (8.314 J/mol.K)
SF	Swelling factor
S_{or}	Residual oil saturation (%)
S_{wi}	Initial water saturation (%)
T	Temperature (°C)
t	Injection time (s)
t_{BT}	Breakthrough time in micro-model study (s)
T_c	Critical temperature (°C)
$T_{c,CO2}$	CO_2 critical temperature (31 °C)
T_{exp}	Experimental temperature (°C)
T_R	Reservoir temperature (°C)
$V_{CO2,f}$	Final CO_2 volume (cm^3)
$V_{CO2,i}$	Initial CO_2 volume (cm^3)
$V_{CO2\text{-}Oil}$	Volume of CO_2–oil mixture (cm^3)
V_{oil}	Oil volume (cm^3)
W	Width of micro-model's glass (cm^3)

w_p	Width of micro-model's engraved pattern (cm^3)
x_{CO2}	Molar fraction of CO_2 in water
Z	Gas compressibility factor

Greeks

ϕ	Porosity (%)
ΔP	Pressure difference (kPa)
μ_d	Liquid dye viscosity (mPa.s)
θ	Contact angel (°)
μ	Viscosity (mPa.s)
μ_b	Water viscosity (mPa.s)
μ_o	Oil viscosity (mPa.s)
ρ_b	Brine density (kg/m^3)
ρ_{CO2}	CO_2 density (kg/m^3)
ρ_o	Oil density (kg/m^3)
χ_b	CO_2 solubility (mole CO_2/kg brine)
$\chi_{b,max}$	Maximum CO_2 solubility (mole CO_2/kg water)
χ_o	CO_2 solubility in oil (gr CO_2/ 100 gr oil)
$\chi_{o,max}$	Maximum CO_2 solubility in oil (gr CO_2/ 100 gr oil)
χ_w	CO_2 solubility (mole CO_2/kg water)

Abbreviations

API	American petroleum institute
ASP	Alkaline Surfactant Polymer
BL	Buckley-Leverett
BPR	Back pressure regulator

BT	Breakthrough time
CW	Carbonated water
CWF	Carbonated Waterflooding
CWI	Carbonated Water Injection
EOR	Enhanced oil recovery
GC	Gas Chromatography
GHG	Greenhouse gas
GWR	Gas to water ratio
HCPV	Hydrocarbon pore volume
IFT	Interfacial tension
IOR	Improved oil recovery
MMP	Minimum miscibility pressure (MPa)
MW	Molecular weight
N.C.	Not critical
N.A	Not available
OOIP	Original oil in place
ppm	Parts per million
PV	Pore volume
RF	Recovery factor
SG	Specific gravity
STB	Stock tank barrel
TDS	Total dissolved solids
UNITAR	United Nations Institute for Training and Research
WAG	Water alternating gas
WF	Water flooding

Unit conversion:

1 mD ≈ 0.000987 μm^2

101.325 kPa=14.65 Psi

1 mPa.s=1 cP

CHAPTER ONE: Introduction

1.1. Past, current, and future of production from hydrocarbon resources

Although literature showed that human interests in discovering and using hydrocarbon resources started four thousand years ago (Chisholm, 1911), and oil well was drilled at around 347 AD or earlier (Vogel, 1993), it is believed that modernization of petroleum industry started in 19th century with extraction of paraffin from coal by Young & Meldrum and Edward William Binney. Development of a processes to extract kerosene from coal, bitumen and oil shale by a Canadian geologist Abraham Pineo Gesner was encouraged the industry to discover more hydrocarbon resources such as oil reservoirs in order to resolve the issue of ever growing the demand for kerosene gaslights.

Since 1848 that the first modern oil well has been drilled (http://www.sjvgeology.org/history/), global demand for energy and in particular crude oil has been increasing. Production of crude oil in the U.S. was increased from 2000 barrels in 1859 to about 126.5 million barrels cumulative in 1906. The demand for the energy was drastically increased after the invention of steam and gasoline engines in the time interval 1850-1900 and commencement of aviation industry in the early 20th century. To provide enough supply to the ever-growing demand for the crude oil, the daily production rate of crude oil in the world has been increased from about 55.7 to nearly 80 million barrels with Canada's share of 1.8 and 3.8 million barrels for 1973 and 2016, respectively. Such increase in production together with limited hydrocarbon resources discovery as well as the global warming resulted from gas emission forced researchers to not only explore the

feasible environmentally friendly enhanced oil recovery techniques but also more seriously consider the renewable energy sources. At the same time, search for new sources of hydrocarbons continues to balance the supply/demand market for the crude oil. **Figure 1.1** shows the cumulative oil production and net reserves added for both OPEC and non-OPEC members for the interval of 2007-2016. The word net reserves refer to the amount of crude oil that can be produced with the current technologies. As it can be seen countless efforts of OPEC and non-OPEC members resulted in balancing the cumulative production of crude oil and net-additions of new crude oil resources.

Until the date, shares of non-OPEC and OPEC members to the conventional oil reserves are about 18.5% versus 81.5% while cumulative production of these two groups are standing at 56.6% and 43.4%, respectively (**Figure 1.2**). This could be translated to the rapid decline of production from the limited crude oil resources of non-OPEC members such as Canada and USA.

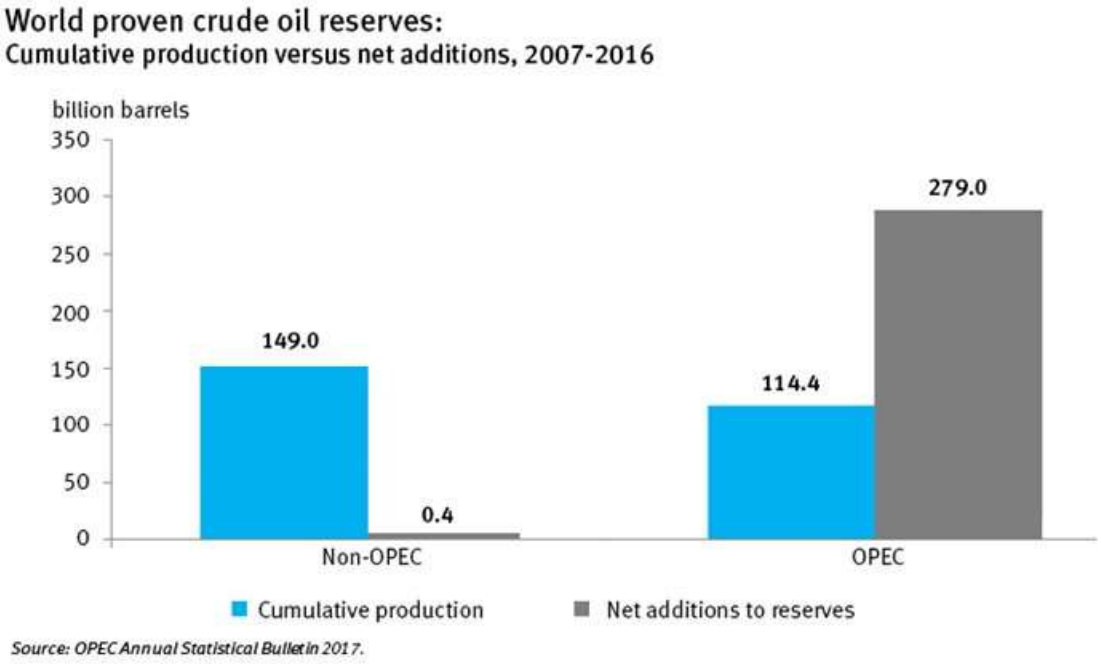

Figure 1.1: World cumulative oil production vs. net additions to oil reserves(OPEC Annual Statistical Bulletin, 2017).

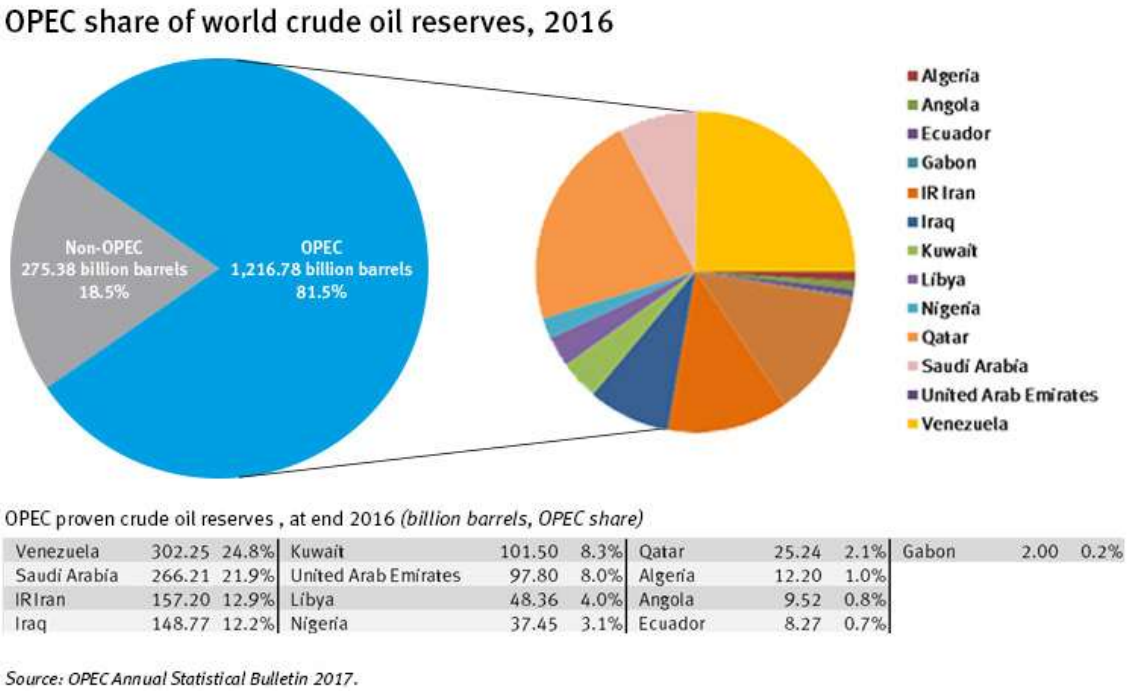

OPEC proven crude oil reserves , at end 2016 *(billion barrels, OPEC share)*

Venezuela	302.25	24.8%	Kuwait	101.50	8.3%	Qatar	25.24	2.1%	Gabon	2.00	0.2%
Saudi Arabia	266.21	21.9%	United Arab Emirates	97.80	8.0%	Algeria	12.20	1.0%			
IR Iran	157.20	12.9%	Libya	48.36	4.0%	Angola	9.52	0.8%			
Iraq	148.77	12.2%	Nigeria	37.45	3.1%	Ecuador	8.27	0.7%			

Source: OPEC Annual Statistical Bulletin 2017.

Figure 1.2: OPEC and non-OPEC shares of crude oil reserves as of 2016 (OPEC Annual Statistical Bulletin, 2017).

In contrast to the conventional light oil resources, North America and in particular Canada and Venezuela have vast resources of heavy, extra heavy, oil sands, bitumen, shale oil and gas, coal, and other unconventional hydrocarbon resources. **Figure 1.3** shows the percentage of world's heavy oil resources in comparison to the conventional light oils (Alboudwarej et al., 2006). As it can be seen, the amount of original oil inplace (OOIP) of heavy, extra heavy and bitumen resources are more than two folds of the conventional light oil. Unfortunately, the higher viscosity of the oil at the reservoir condition and lower initial energy of heavy oil reservoirs resulted in much lower recovery factor from such reservoirs with available technologies in comparison to the light oil reservoirs. Therefore, feasibility of continues production from some of the heavy oil reservoirs is strongly depending on the oil price to an extend that below a certain oil price, many heavy oil production operations might be shut down due to high operational expenditures (OPEX) and insufficient revenue to overcome the costs. Overall, because of the extra low mobility of the heavy oil, higher cost of production, environmental policies and regulations, and lack of highly efficient technologies, more than 70% of the heavy oil and over 90% of extra heavy oil and bitumen in Canada are still remaining underground (Sandrea & Sandrea, 2007).

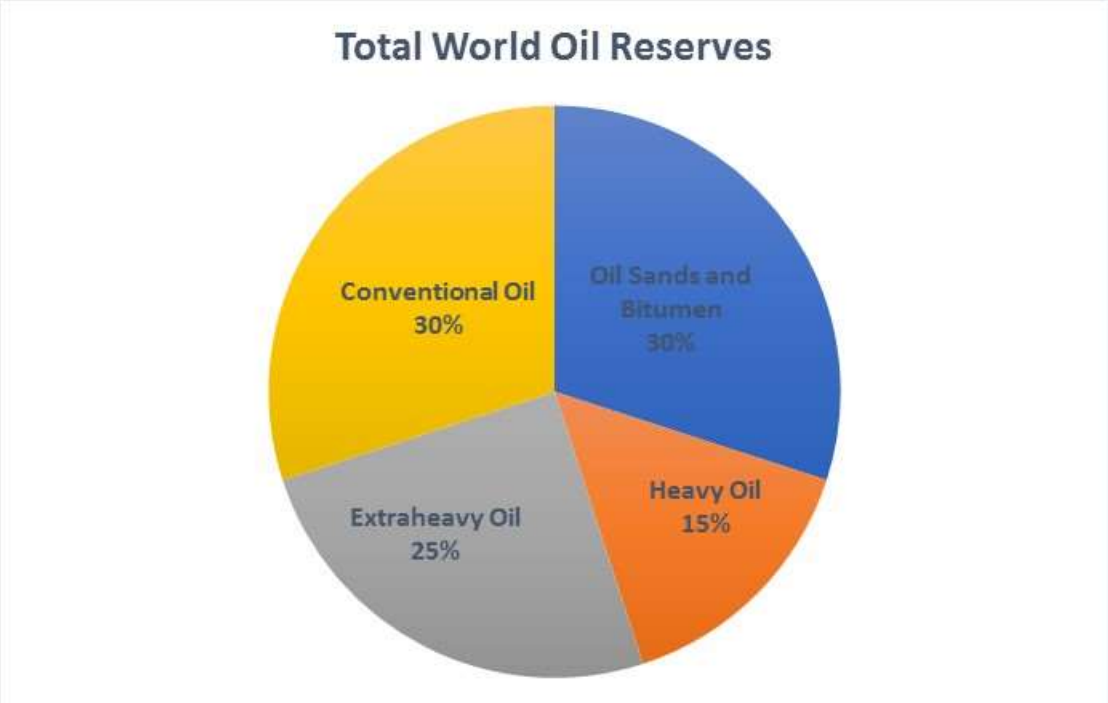

Figure 1.3: Percentage of heavy oil, extra heavy oil, and bitumen resources of the world compared to conventional oil (reconstructed from: Alboudwarej et al., 2006)

1.2. Classifications of crude oils

Crude oil is normally classified using its' density or API gravity where API refers to the American Petroleum Institute, which is a trade association for the hydrocarbon industry established in the United States (Petroleum.co.uk). API gravity can be determined using the specific gravity of the crude oil at the standard temperature of 60oF and atmospheric pressure per Eq.1.

$$API_{60}^{60} = \frac{141.5}{Sp.Gr\ (\frac{60}{60})} - 131.5 \qquad \text{Equation 1}$$

Although classifications of the crude oil may differ from location to location, a rough idea of various types of crude oil is tabulated in **Table.1.1**

Table 1.1: Classification of crude oil per API gravity

Type of crude oil	**API Gravity of the crude oil**
Light	>31.1
Medium	22.3-31.1
Heavy	22.3-10
Extra Heavy	<10

In North America, often a second method of classifications might be used where oil viscosity is considered as an indication of the type of crude oil. Although might be used as reference with some cautious, researchers agreed to classify the heavy and extra heavy hydrocarbon resources per **Table 1.2** where oil viscosity is the demarcation factor (Butler et al., 1991).

Table 1.2: Classification of crude oil based on viscosity*

Type of crude oil	**Oil Viscosity (mPa.s.)**
Heavy	100-10,000
Tars and Bitumen	> 10,000

*Per 1982 United Nations Institute for Training and Research (UNITAR) agreement in Venezuela (Butler et al., 1991).

1.3. Production phases of oil reservoirs

Depending on the type of oil reservoir, production phases might fall into and follow primary, secondary, and tertiary stages. Primary stage of production is the result of natural energy existing in the reservoir that allows oil to flow into the wellbore naturally. Such sources of energy are normally from the solution gas existing in the oil, expansion of rock and fluids, gas cap expansion, gravity drainage, and aquifer support.

There is no doubt that primary production resulted from the natural energy of the reservoir is the most economical phase of production among the previously mentioned three phases as long as production rate is above the economic limit. Although recovery factor of primary stage of production is strongly depends on oil properties and reservoir conditions and characteristics, the overall recovery factor is merely exceeding 25% of the original oil inplace (OOIP).

During primary stage of oil production, energy of the reservoir continuously depletes with production and eventually reaches to a point that the differential pressure between the reservoir and well is not sufficient enough to mobilize the oil and move it to the surface at the desired rate. At this stage, installation of downhole pumps, gas recycling, and implementation of gas-lift is recommended to help lifting the oil to the surface and boosting the production rate.

It is noteworthy to mention that gas-lift operation is simply a process at which gas is introduced into the wellbore via a choke (released at a pre-designed depth into the oil) so that it reduces the oil density and ultimately the fluid's head and therefore improve the oil production. Re-injection of the associated gas produced with the oil (after removal of the water and sulfur contents) into the gas-cap of the oil reservoir, well known as pressure

maintenance, is also another strategy to maintain or improve the oil recovery immediately following the decline of the reservoir pressure and flow rate during the primary phase of production.

While pressure maintenance, gas-lift, and additional production engineering operations such as acid stimulation, re-perforation etc. may sustain the oil production for some time, depletion of the reservoir's energy will finally come to a point of low production rate that it is no longer feasible to continue, hence, forcing the production operation to be abandoned while significant amount of oil is still trapped in the reservoir as a means of residual oil saturation (Melzer, 2012; Mosavat & Torabi, 2013).

Producing oil from depleted oil reservoirs requires a displacement energy provided by injection of an external substance into the reservoir via injection wells. This is where the secondary recovery stage of an oil reservoir starts. According to the definition, secondary oil recovery stage is referring to that phase of production that the displacement of the oil to the wellbore is done by injecting water or immiscible gas. Injection of water and immiscible gas into the oil zone for the purpose of oil displacement are called waterflooding and gas flooding, respectively.

One important point is that gas flooding can be considered as secondary oil recovery process if additional oil recovery is purely the result of displacement of oil by gas and injected gas do not change the oil properties such as viscosity, etc.

In practice, secondary oil recovery is a synonym to the waterflooding and gas flooding operations are very rare. This is because the significant viscosity contrast between the gas and crude oil results in a very poor displacement efficiency of the gas flooding to an extent that there is no interest in implementing gas flooding as a means of secondary oil

recovery processes in many oil reservoirs. In contrast, research studies and field practices show that waterflooding is a very efficient and safe secondary oil recovery process particularly for light to medium oil reservoirs and have been practiced for number of oil reservoirs around the world (Mai & Kantzas, 2009).

Oil production resulting from secondary oil recovery processes may recover up to 25 to 35% of the residual oil of the primary phase. This means at the end of the secondary oil recovery still substantial amount of oil is remaining underground which justify the need for tertiary oil recovery stage. To understand the significance of the issue, if primary and secondary oil recovery stages recover 30% of OOIP and 25% of residual oil of the primary stage, respectively, the residual oil remaining in the reservoir after both primary and secondary stages of production will be 52.5% of the original oil inplace (OOIP). These values are substantially lower for the heavy and extra heavy oil reservoirs. **Figure 1.4** depicts the recovery potential of heavy oil reservoirs based on 20% and 10% recovery factors of primary and secondary oil recovery phases.

It must be noticed that primary and/or secondary oil recovery stages might be escaped during production life of heavy or extra heavy oil reservoirs. In the other words, if initial energy of the reservoir resulting from the solution gas drive and other mechanisms are ultra-low, it is not possible to produce oil through primary stage at a feasible rate. Also, if oil viscosity is substantially high compared to water viscosity (at reservoir conditions), injected water may quickly bypass the oil causing very poor displacement efficiency and uneconomical production scenario. Therefore, in any of these circumstances, primary, secondary or both stages could be staged and tertiary recovery stage and processes might be considered as the final solution.

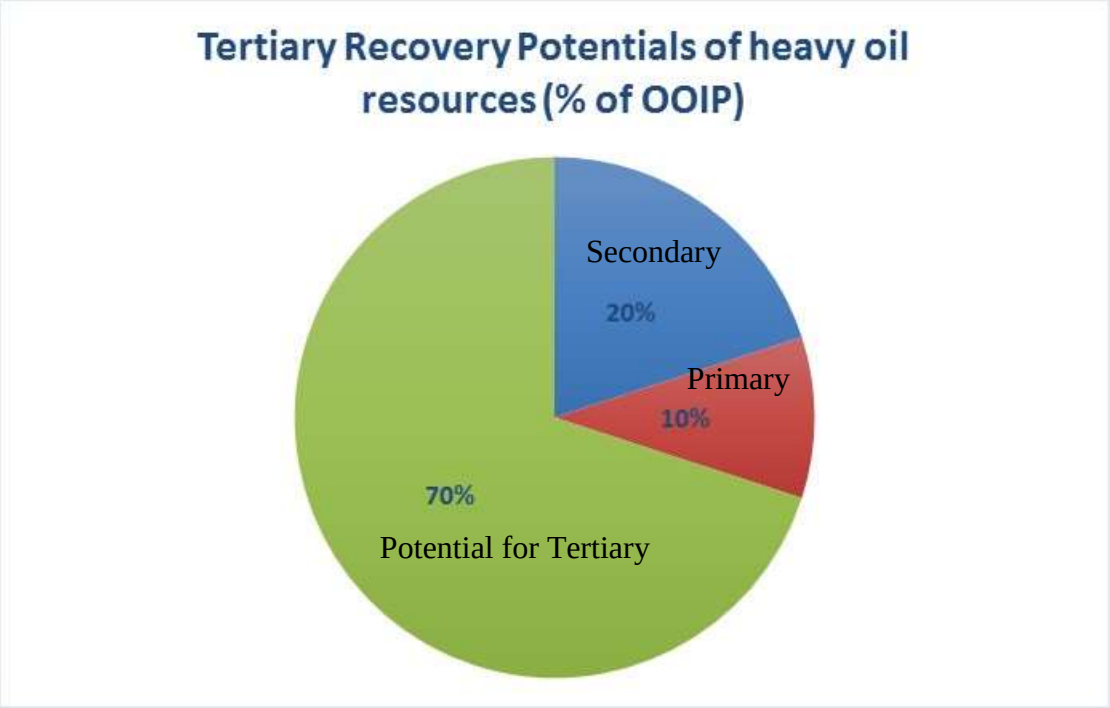

Figure 1.4: Oil recovery phases showing the approximate recovery factors for each phase and tertiary oil recovery potentials (original in color).

Tertiary recovery may involve one or more of the mobility control, oil viscosity reduction, and interfacial tension reduction processes. During this stage of production, one or more tertiary recovery processes will be used to mobilize the residual oil and produce it to the wellbore and ultimately to the surface.

Exploring and introducing an appropriate tertiary recovery process or sequence of processes is strongly depending on variety of parameters such as percentage of the residual oil saturation after primary and secondary phases, reservoir characteristics and conditions, oil properties at the latest reservoir conditions, depth of the reservoir, monetary factors, etc. For this fact, an extensive screening process is required to identify and perhaps rank the right tertiary recovery processes for a specific oil reservoir.

To date, performance of many tertiary oil recovery processes are investigated by means of experimental and/or simulation studies, pilot tests as well as field practices. In general, tertiary recovery processes might be classified as thermal and non-thermal groups.

Table 1.3 summarizes some of well-known tertiary recovery processes with their applications (Green & Willhite, 1998):

Table 1.3 Screening criteria for enhanced recovery methods (Green & Willhite, 1998)

EOR Method	**Gravity (ºAPI)**	**μ_o (mPa.s)**	**Oil Saturation**	**Average Permeability**	**Depth (ft)**	**Temperature (ºF)**
Nitrogen (&Flue Gas)	>35	<0.4	>40	N.C.	>6000	N.C.
Hydrocarbon Solvents	>23	<3	>30	N.C.	>4000	N.C.
Micellar/ Polymer *ASP	>20	<35	>35	>10	<9000	<200
Combustion	>10	<5000	>50	>50	<11500	>100
Steam	>8-13.5	<200k	>40	>200	<4000	N.C.
Carbonated Waterflooding	N.A					

In practice, each of the tertiary oil recovery processes presented in **Table 1.3** has some limitations and drawbacks. As an example, steam assisted gravity drainage (SAGD) and vapour assisted petroleum extraction (VAPEX) are limited to relatively thicker heavy oil formations while polymer and alkaline-surfactant-polymer (ASP) flooding recovery methods are limited to reservoirs with permeabilities higher than 200md and temperatures lower than 200^{o}F (Green & Willhite, 1998).

In addition to the technical and operational limitations, there are other factors that must be considered during the screening phase of tertiary recovery processes. Such factors include environmental impacts of the method, government policies and regulations related to the process, and costs associated with required infrastructures and implementation etc. As an example, thermal recovery methods are releasing large quantities of CO_2, while chemical flooding techniques are n United Nations Agreement for Training and Research ot environmentally friendly methods. VAPEX process involves injection of hydrocarbon solvents such as propane and butane which are expensive, hence, heavy oil operators are not keen to implement it.

Therefore, the implementation of a cost effective and environmentally friendly recovery technique with minimum upgrading of the surface facilities or changes in the downhole equipment are essential to continues production of crude oil during the downturn of the oil price. One such technique which take advantage of combining gas (e.g. CO_2) and water injection is carbonated water injection (CWF).

Carbonated waterflooding is simply referring to the injection of carbon dioxide (CO_2) saturated water in the oil zone where CO_2 is released from the water and diffused into the oil. During this process, water penetrates oil and get dispersed into the porous

media generating large contact area with oil. Carbon dioxide with higher diffusion rate in the oil is then released from water at the contact area and diffused into the oil. As diffusion of CO_2 into the oil continues, oil viscosity will reduce, hence, water displaces oil more efficiently. To enhance the processes of diffusion of CO_2 in the water and then releasing water and diffusing in the oil, use of solubility promoter and demoter are highly recommended (Mosavat, 2014).

Although CWF and its' application to enhanced oil recovery has been studied in great details, majority of those studies are focused on light oil systems (Mosavat, 2014; Riazi, 2011; Sohrabi et al., 2011) leaving a knowledge gap in the area of application of CWF to heavy oil reservoirs. The limited number of studies focused on the application of CWF in heavy oil reservoirs used relatively lower oil viscosities (e.g <100 mPa.s) with very few concentrating on oil viscosities above 100 mPa.s.

1.3. Why carbonated waterflooding?

As mentioned before, while waterflooding is a feasible secondary oil recovery technique for majority of light oil reservoirs which are not sensitive to water (e.g. reservoir containing shale strings), its performance in heavy oil reservoirs is much lower. **Figures 1.5** and **1.6** illustrates the vertical and areal sweep efficiency of both water and gas flooding when applied as a means of secondary oil recovery, particularly in a heavy oil reservoir. As it can be seen if **Figure 1.5 (a)** and **Figure 1.6 (a)**, low performance of water flooding, its poor vertical and areal displacement efficiency and early water breakthrough in heavy oil reservoirs is due to the viscous fingering and gravity underride (water bypasses the oil and moves beneath the oil as it is a heavier fluid compared to the oil).

Similar phenomenon but to a greater extent as depicted in **Figure 1.5 (b)** is happening during CO_2 flooding of a heavy oil reservoir. As it can be seen, extreme viscous fingering and gravity override (CO_2 moves on top of the oil and bypasses the oil as it is a much lighter fluid) results in the quick gas breakthrough and very poor vertical and areal sweep efficiency of the reservoir (see also Fig.1.6 (b) for areal sweep efficiency).

One solution that has been practiced to reduce the aforementioned problems and improve the performance of water and gas flooding in light oil reservoirs is to alternate the injection of gas and water, well known as water-alternating-gas injection (WAG). This particularly is very effective when gas is injected at miscible condition in light oil reservoirs. As illustrated in **Figure 1.5 (c)**, alternating gas and water injection could improve the displacement of oil by continuously displacing oil from the top and bottom of the reservoir and both small and large pores. As water is the wetting phase compared to the

gas, it tends to displace the oil from smaller and narrower pores while gas as non-wetting phase in presence of oil and water displaces oil from larger pores (Green & Willhite, 1998).

CO_2 injection in the form of miscible gas injection or miscible-WAG process in light oil reservoirs became of the interest of oil industry in the last three decades. In some cases where miscibility between light oil and CO_2 cannot be achieved, injection of CO_2 at near miscible condition is preferred compared to immiscible CO_2 injection. CO_2 has greater diffusion rate in light oils when compared to methane or nitrogen at the same pressure and temperature causing higher oil viscosity reduction and mobility. In addition, with the current policies and regulations to reduce the greenhouse gases, depleted oil reservoirs have great potentials to be used as CO_2 storage sites. In this regard, the higher the displacement efficiency, the larger the available space for CO_2 to be stored. Therefore, WAG provides an opportunity not only to improve the oil recovery but also to safely store large amount of CO_2 in the swept region of the oil reservoir at its abandonment time, hence, receiving carbon tax credit in many regions such as North America.

Although implementation of WAG in light oil reservoirs, and in particular miscible WAG, has shown significant improvement in ultimate oil recovery compared to injection of water or gas (individually), its application to heavy oil reservoir is limited. This is mainly because miscibility usually can't be achieved between heavy oil and injected gas at the reservoir condition, causing unfavorable mobility ratio between gas and oil during the displacement process.

For clarification, mobility ratio is a term used to describe the mobility of displacing phase over mobility of displaced phase while mobility of each phase is the ratio of its effective permeability to its viscosity. In petroleum engineering, favorable mobility ratio

is referred as the values of unity or lower, while mobility ratio values of more than unity is considered as unfavourable. Therefore, in the case of WAG in heavy oil reservoirs, mobility of both phases of water and gas are usually higher than the mobility of oil, causing unfavorable mobility ratio. The consequences of implementing an enhanced oil recovery process that results in unfavorable mobility ratio are fast breakthrough, poor displacement efficiency, and lower recovery factor.

Carbonated water injection (CWF) provides an opportunity to inject CO_2 as a dissolved phase in the water. When CO_2 arrived at the reservoir and while water is penetrating oil bank, it is released from the water and moves into the oil. This is due to the higher diffusion and solubility of CO_2 in the oil phase. This phenomenon causes the oil viscosity at the contact with the water to reduce, hence, improve the displacement efficiency of water. In addition, since CO_2 is not existing in the free form, gravity override is eliminated and displacement front is smoother than in the cases previously mentioned (**Figure 1.5 (d)**).

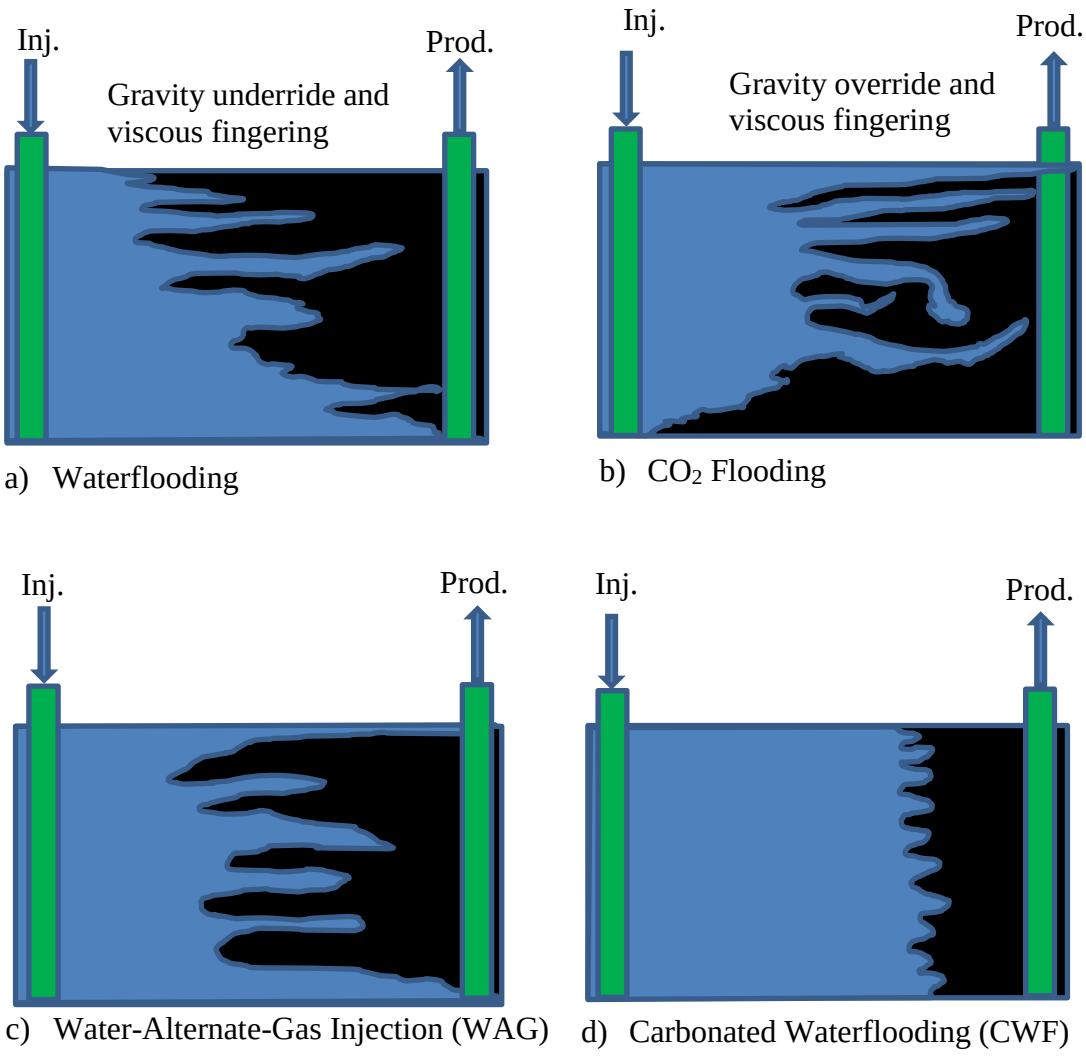

Figure 1.5: Vertical (side) view of oil displacement during (a) waterflooding, (b) CO_2 flooding, (c) WAG, and (d) CWF.

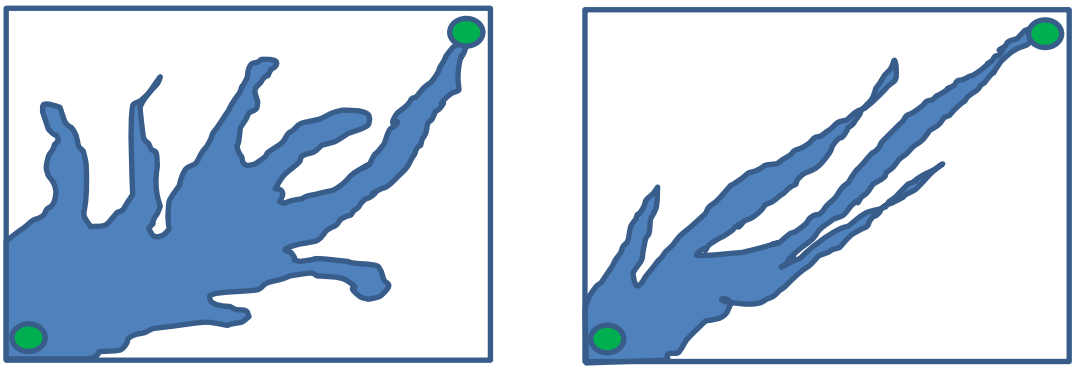

a) Water flooding

b) CO2 flooding

Figure 1.6: Areal view of oil displacement during (a) waterflooding, (b) CO_2 flooding.

In contrast to the light oil reservoirs that majority of them are either at the primary or secondary stages of production (Mosavat, 2014), most of heavy oil reservoirs are currently under waterflooding or already watered out and operators and researchers are looking for alternative enhanced oil recovery techniques for them. For the reasons mentioned earlier, neither carbon dioxide injection nor WAG are feasible options for some of those reservoirs. Also, switching from waterflooding to a completely different enhanced oil recovery technique is costly and perhaps might be beyond the monetary capacity of small to medium heavy oil operators.

Despite the lower contribution to the CO_2 storage, carbonated water injection (CWF) has been proved to be one of the successful alternatives to WAG, immiscible gas flooding, and even waterflooding in light oil reservoirs. This fact has been addressed by many researchers studying the performance of CWF in light oil systems both as a means of secondary and tertiary oil recovery techniques.

Due to the proven capability of CWF in improving microscopic and macroscopic sweep efficiencies, its implementation in heavy oil reservoirs might be viable. However, the viability of this enhanced oil recovery (EOR) is certainly depending on the oil viscosity and many other factors which needs to be investigated.

It must be noticed that one major difference between heavy oil reservoirs and those containing light oil is that primary and secondary stages of production in heavy oil reservoirs might be escaped due to the very low initial reservoir energy and poor displacement efficiency of waterflooding.

Therefore, because of all of the above reasons, this research study is mainly focused on investigating the performance of CWF, as an alternative to waterflooding and WAG, in

the heavy oil saturated porous media containing heavy oil samples of various viscosities. It is the intention of this study to address the knowledge gap existing in the area of CWF's application to heavy oil reservoirs.

1.4. Objectives of this study

The main objective of this study was to evaluate the performance of CWF in heavy oil reservoirs and its' range of applicability and extent of viability from oil viscosity point of view. For this fact, through a systematic approach, laboratory tests are conducted utilizing two different types of micromodels, with irregular grains, containing saturated with two different samples of heavy oil. Prior to the CWF experiments, additional tests were conducted to determine the physical properties of the fluids used, establish a base line of waterflooding for comparative evaluation purpose, and evaluate the phase behavior of the fluids under the test conditions. More specifically, the following steps were followed to the main objectives of this study:

- Two heavy oil samples and a synthetic brine were prepared and their physical properties were measured at the laboratory conditions.
- Variation in oil viscosity, oil swelling, etc. due to the dissolution of CO_2 for two heavy oil samples used in this study were determined. In addition, CO_2 capacity and variation in the properties of brine sample used in this study were investigated. All PVT studies were conducted at the laboratory conditions of this study. In some cases where predictions of the variations in the aforementioned properties were available through using correlations, available software, or previously conducted

experiments, those were either used directly or as the reference for comparison to the results obtained in this study.

- Two micro-models replicating unconsolidated porous media with and without dilated mediums (or fractures not connected to the injection and production wells) were prepared.
- A flexible experimental setup allowing injection of two types of heavy oil samples and brine in micromodels or sand packs was designed and assembled.
- Eighteen sets of CWF tests at secondary injection mode were conducted to evaluate the performance of CWF in heavy oil saturated porous media using two different heavy oil samples and utilizing two different micro-models.
- Image analysis was performed to analyze the results, evaluate the displacement efficiency of CWF in comparison to waterflooding, and identify the residual oil saturation at various injected pore volumes of carbonated water (CW).
- Furthermore, additional analyzes were performed to investigate the residual oil trapping phenomena, mechanisms involved in the oil production, contribution of the dilated regions of porous media to the displacement efficiency of CWF, effect of injection rate of carbonated water (residence time), effect of oil viscosity, and effect of temperature.
- Sandpack flooding tests were conducted to evaluate the displacement efficiency of both conventional and carbonated waterflooding for two heavy oil samples.
- Through sandpack flooding tests, effect of various parameters such as oil API gravity, injection rate, carbonation pressure, and temperature were studied for CWF.

1.5. Contributions and innovations of this study

The followings are the main contributions of this study:

- Performance evaluation of CWF in heavy oil reservoirs which has not been studied in detail and extensive in the past,
- Utilization of state-of-the-art micromodels to study the effect of fluid, and operation conditions on the performance of WF and CWF in heavy oil systems under various conditions,
- Inclusion of numerous high permeability channels in a micromodel to study the effect of dual permeability medium on the performance of WF and CWF in heavy oil reservoirs.

1.6. Organization of this dissertation

This dissertation is prepared in seven chapters. Chapter one is introduction. Chapter two is thorough literature review on the subjects of waterflooding, carbon dioxide flooding, water-alternating-gas injection, and carbonated water flooding. In chapter three, materials, safety percussions, fluid properties, experimental setups for pressure-volume-temperature (PVT) tests, and results of PVT tests are discussed. Preparation of micromodels, experimental setups for CWF tests, procedures, and results of the waterflooding (WF) tests are included in chapter four. Tests conducted using carbonated waterflooding (CWF) and discussion of the results are presented in chapter five. Results of sand-packed flooding (core flooding) tests conducted to investigate the effect of various fluid and operational conditions are included in chapter 6. Chapter seven is the conclusion and recommendations.

CHAPTER TWO: Literature review

In this chapter, available published studies related to the subjects of secondary oil recovery methods (gas and waterflooding), water-alternating-gas injection, and carbonated waterflooding are presented.

2.1. Review of measured and predicted fluid properties related to carbonated waterflooding

2.1.1. CO_2 physical properties

CO_2 is an interesting gas that has wide range of applications while it can be considered harmful to environment when it is released in the air. Fig.1.7 shows the pressure-temperature (P-T) diagram for CO_2 constructed from a data base generated by chemicalogic. As it can be seen, CO_2 is solid (dry ice) at all pressures above P=0.5 MPa when temperature T=-57^{o}C or lower. In the range of T=-56.4^{o}C to T=30^{o}C, and corresponding pressure range of P=0.5 MPa to 500 MPa CO_2 is liquid. Also, in the temperature range of T=-100 to 30^{o}C, and corresponding pressure range of P=0.01 MPa to 6.5 MPa, it will remain in the gas phase. Critical properties of CO_2 are T_c=31.1^{o}C and P_c=7.38 MPa. At pressures and temperatures above the critical values and below the melting line, CO_2 will turn into the supercritical condition (**Figure 1.7**).

CO_2 can be injected at miscible or immiscible conditions, in oil reservoirs, for the purpose of enhance oil recovery. CO_2 miscibility with oil could be achieved at relatively high pressure and low temperature and only when oil has relatively high API gravity

(higher than 36^{o}API). When injected at immiscible condition, CO_2 enhances oil recovery through viscosity reduction, oil swelling, and solution gas drive mechanisms. Interfacial tension (IFT) reduction is another enhancing mechanism that substantially contributes to the oil production at miscible condition.

An interesting point is that CO_2 could be converted into a dense fluid when subjected to high pressures (e.g., P=100 MPa at T=20^{o}C). While this behavior could help minimizing gravity override through proper design and optimization, it indicates that application of CO_2 to deep oil reservoirs might results in additional problems such as fracturing, gravity underride, etc.

To understand the role of CO_2 in the performance of carbonated waterflooding and its contribution to oil recovery, it is crucial to study the variation of physical properties of both oil and brine as a function of CO_2 concentration.

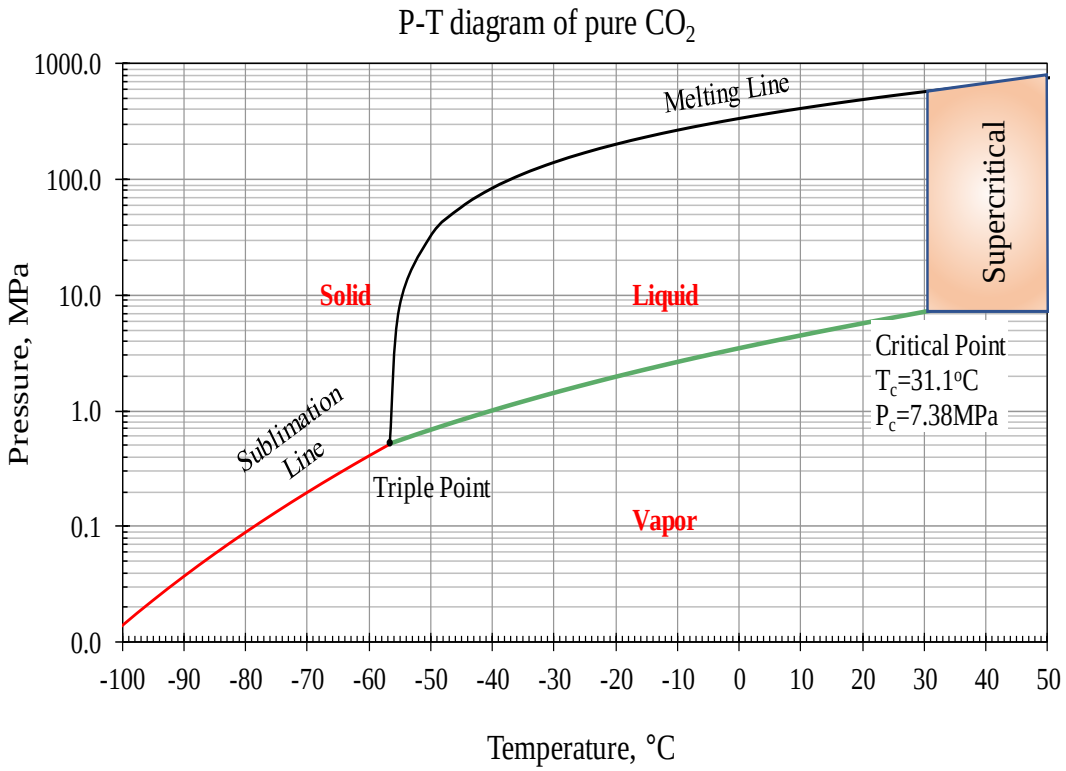

Figure 1.7: Phase diagram of pure CO_2 (constructed using data of chemicalogic)

2.1.2. CO_2 solubility in brine

Perhaps solubility of CO_2 in brine and oil could be considered as two key parameters in the success of all CO_2-based enhanced oil recovery processes. Water, when considered as an injectant in the oil reservoirs for enhanced oil recovery purpose, is not pure. Depending on the type of the oil reservoir and its sensitivity to the water, brine solutions of various concentrations of salts are the choices of enhanced oil recovery. For this fact, even though solubility of CO_2 in pure brine is widely available in the literatures and data bases (Bamberger et al., 2000; Chapoy, Mohammadi, et al., 2004; Chapoy, Mokraoui, et al., 2004; Diamond & Akinfiev, 2003; Duan & Sun, 2003; Han et al., 2009; Liu et al., 2011; Sabirzyanov & Shagiakhmetov, 2003), this study only focused on the review of CO_2 solubility data and related measurements and studies in brine solutions (Duan et al., 2006; ENICK & KLARA, 1990; Gu, 1998; Kiepe et al., 2002; Koschel et al., 2006; Mao et al., 2013; Mosavat & Torabi, 2013; Nighswander & Kalogerakis, 1989; Prutton & Savage, 1945; Rumpf et al., 1994). Unfortunately, such data sets are limited compared to those in pure water.

Review of some of the literatures showed that solubility of CO_2 in brine is depending on the concentration and types of dissolved salts in the water, pressure, and temperature. Data gathered from various sources (Nighswander & Kalogerakis, 1989; Prutton & Savage, 1945) and/or determined (from a correlation suggested by Enick et al., 1990) are plotted in **Figure 1.8** to show the effect of salt concentration on the solubility of CO_2 in water for three common salts at constant pressure of P = 9.0 MPa and T = 93.3 °C. As it can be seen, for all types of salts, CO_2 solubility in water decreases as salt concentration increase. Therefore, it is vital to optimize the concentration and types of salts in the injected brine to

maximize its CO_2 carrying capacity and ultimately oil recovery factor and CO_2 storage during carbonated waterflooding while compatible with reservoir condition.

Since CO_2 solubility in the brine is not available for all range and types of concentrations and operating pressures and temperatures, values of this key parameter have been measured experimentally for the specific brine and operating conditions of this study.

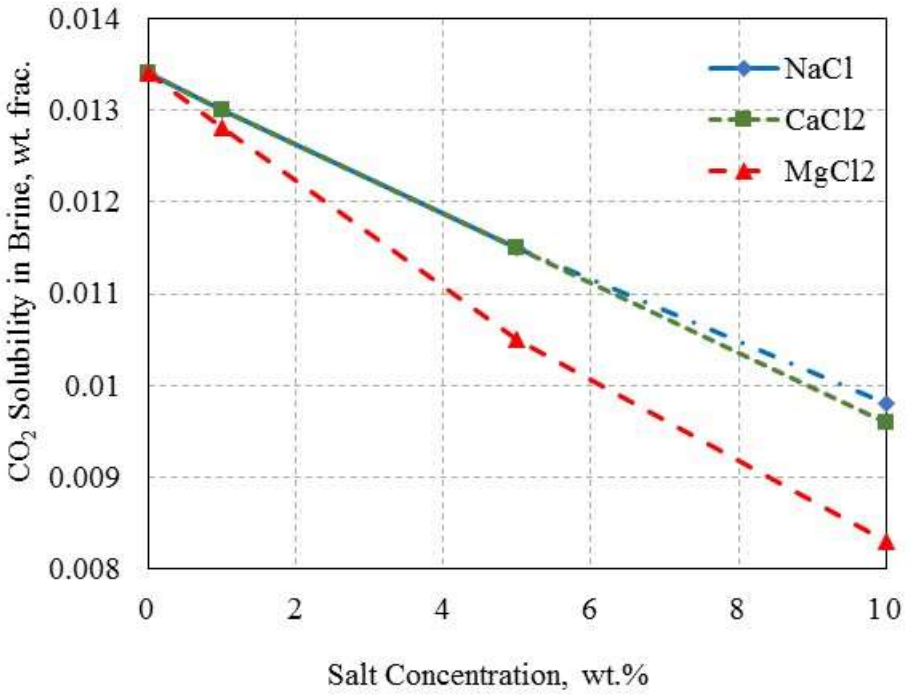

Figure 1.8: Solubility of CO_2 in three types of brines as a function of salt concentration at P = 9.0 MPa and T = 93.3 °C (constructed based on data gathered from (Enick et al., 1990; Nighswander et al., 1989; Prutton et al., 1945)

2.1.3. CO_2 solubility in oil

Although solubility of CO_2 in crude oil might be depending on many of the crude oil properties including saturates, aromatics, resins, and asphaltenes (SARA) contents, literatures usually referred to the oil viscosity, API gravity, pressure and temperature as the key parameters (Abedini et al., 2014; Emera & Sarma, 2007; Gu, 1998; Jamaluddin et al., 1991; Mosavat, 2014; Simon & Graue, 1965; Srivastava et al., 1995; Welker, 1963). As it is shown by Welker (1965), CO_2 solubility increases with increase in carbonation pressure (**Figure 1.9**) and decreases as the API gravity of oil decreases.

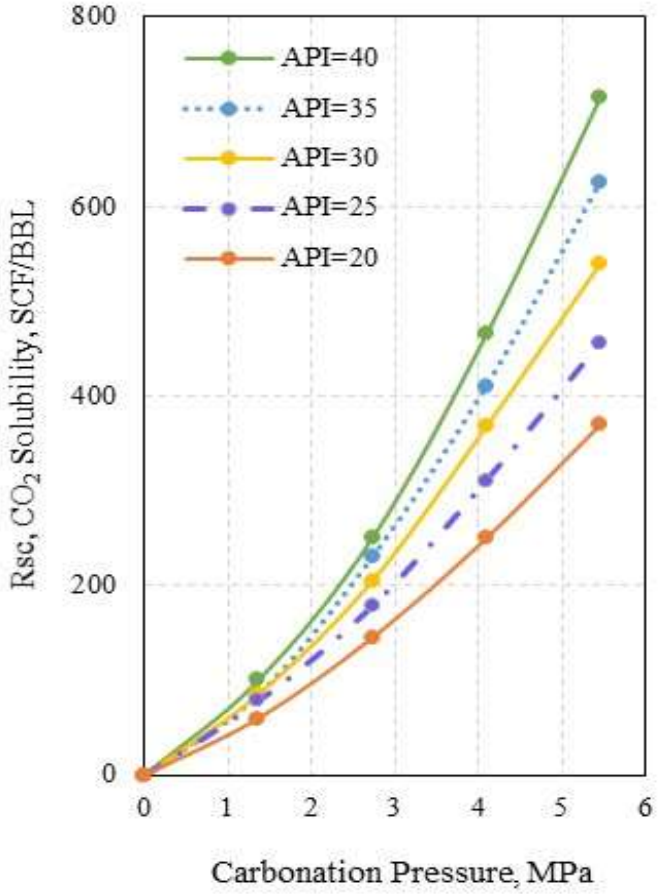

Figure 1.9: Solubility of CO_2 as a function of API gravity of oil at 26.7°C (reconstructed from Welker, 1963)

Solubility of CO_2 in crude oil could be also determined using suggested correlations by (Barclay & Mishra, 2016; Chung et al., 1988; Emera & Sarma, 2007; Mehrotra & Svrcek, 1982; Welker, 1963). Although these correlations can be used with reasonable accuracy, most of researchers prefer to experimentally measure the solubility values of CO_2 in crude oil at the desired pressures and temperatures of the EOR processes to ensure true values of those parameters are used in their analysis. In contrast to the effects of oil API

gravity and carbonation pressure on the CO_2 solubility, effect of temperature on the solubility is slightly complicated.

2.1.4. CO_2-oil viscosity

Diffusion of CO_2 in crude oil results in reduction of oil viscosity (**Figure 1.10**), a phenomenon that promotes further dissolution of CO_2 in the crude oil (Simon & Graue, 1965) and is considered as the main contributor to the improvement of oil recovery by CWF (Nevers, 1966).

Literature show variety of graphical approaches (Simon & Graue, 1965; Welker, 1963), and correlations (Barclay & Mishra, 2016; Beggs & Robinson, 1975; Emera & Sarma, 2007; Mehrotra & Svrcek, 1982) to estimate the CO_2-oil viscosity. **Table 2.1** shows some of available correlations for predicting viscosity of CO_2-oil, their developed conditions and range of applicability.

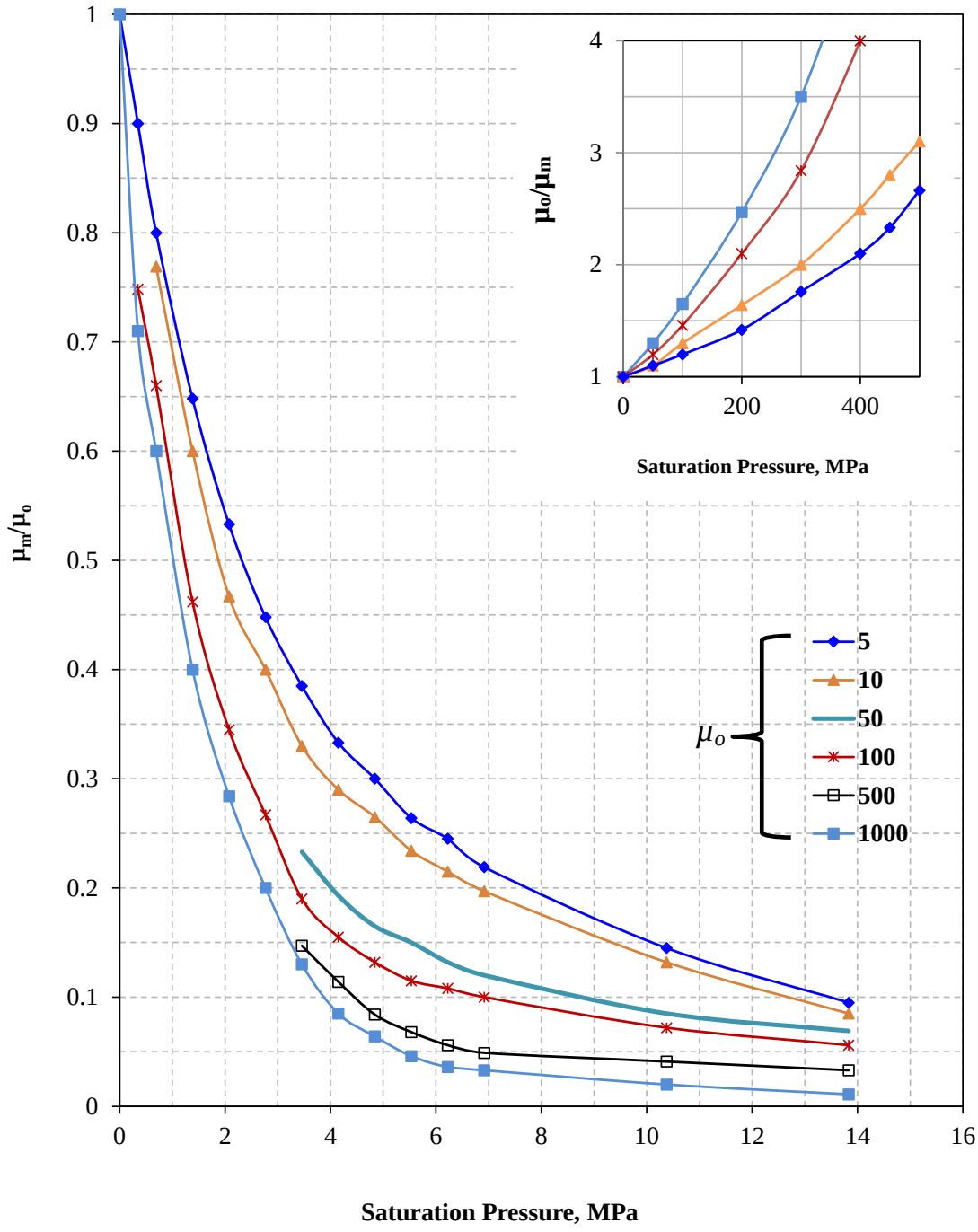

Figure 1.10: Viscosity of CO_2-crude oil mixture at 120°F (reconstructed from Simon & Graue, 1965 with pressure in terms of MPa)

Table 2.1: Available correlations for predicting density and viscosity of CO_2-Oil mixtures

Physical Properties	Author	Correlation
Density of CO_2-oil mixture	Quail et al. (1988)	$\rho = (C_1 - C_2 - C_3 P_s)\dfrac{exp(-C_4 sol\ (mole\ fraction))}{(1 + C_5(C_4, mole\ fraction))}$ Where (for Senlac region oil): $C_1 = 0.99,\ C_2 = 0.00036,\ C_3 = 5.51E-06, C_4 = 35.8E-04, C_5 = 50.86E-03$. Limited to: $P_s \leq 2{,}466\ psia$.
	Emera and Sarma (2007)	$\rho = \rho_i + 0.0008y - 0.0008y^{0.157}$ Where $y = \gamma\rho_i(P_s - P_b)/T\ and\ P_b = 14.7\ psia$.
Viscosity of CO_2-oil mixture	Welker and Dunlop (1963)	Graphical correlation. Function μ_i and P_s. Limited to: $T = 80°\text{F}\ and, P_s \leq 800\ psia, and\ 4\ cP\ \leq viscosity \leq 5{,}000\ cP$.
	Simon and Graue (1965)	Graphical correlation. CO_2-viscosity is a function of P_s, μ_i @ $120°\text{F}, T$, and CO_2 solubility. Limited to: $100°\text{F} \leq T \leq 250°\text{F}, P_s \leq 2{,}000\ psia, and\ viscosity \leq 1{,}300\ cP$.
	Beggs and Robinson (1975)	$\mu_d = 10^X - 1, where\ X = 10^{3.0324 - 0.02023\gamma_o}T^{-1.163}$ For dissolved gas (e.g., CO_2): $\mu = A\mu_d^B, where\ A = 10.715\ (Sol\ (scf/bbl) + 150)^{-0.338}$. Neglects oil viscosity dependence on composition and pressure.
	Mehrotra and Svrcek (1982)	$\log\log(\mu + 0.8) = a_1 + a_2 T + a_3 P_s + \dfrac{a_4}{(b_1 T + b_2)}P_s$, $where\ a_1 = -0.32029, a_2 = -0.002472, a_3 = 0.529E-03$ $a_4 = -0.23804, b_1 = 0.55556, b_2 = 255.3722$. Developed for saturated bitumen (for: $75°\text{F} \leq T \leq 207°\text{F}\ and\ P_s \leq 925\ psia$).
	Chung et al. (1986)	For $P \leq 3{,}000\ psia$: They modified Lederer (1933) equation as follows: $\ln(\mu_m) = x_o \ln(\mu_i) + x_s \ln(\mu_s)$, where $x_s = \frac{V_s}{\alpha V_o + V_s}\ x_o = 1 - x_s$ $\alpha = 0.255\gamma^{-4.16}T_r^{1.85}\left[\dfrac{e^{7.36} - e^{7.36(1-P_r)}}{e^{7.36-1}}\right]$, $T_r = (T + 460)/547.57,\ P_r = P_s/1{,}071$ Relationship among x_s, CO_2 solubility $\left(Sol\ (scf/bbl)\right)$, and SF is: $x_s = \dfrac{1}{\alpha\left(\frac{\theta}{B.Sol\ (scf/bbl)}\right)+1}$, $x_s = \dfrac{B.SF-1}{\alpha + B.SF - 1}$
	Emera and Sarma (2007)	$\mu = y\mu_i - 10.8\left(\dfrac{Sol\ (mole\ fraction)}{\mu_i}\right)$ Where $y = x^{-0.74}$ and $x = \left(\mu_i\left(\frac{P_s}{T}\right)^{0.2}\right)^{(y/Sol\ (mole\ fraction))}$

2.1.5. CO_2-oil density

Oil density also varies as a function of CO_2 amount dissolved in it, pressure, and temperature etc. Experimental data for density of CO_2-oil systems can be found in many data bases and published articles. Similar to other properties of CO_2-oil systems, Quail *et al.* (1988) presented a correlation to predict the density of CO_2-oil mixtures. Emera & Sarma, 2007 utilized genetic algorithms (GA) and developed more accurate correlations for the density of oil-CO_2 mixtures.

Available correlations for predicting density of CO_2-oil mixtures are also listed in **Table 2.2**.

2.1.6. Oil swelling resulted from CO_2 dissolution

Since oil swelling factor (SF) due to the solvent injection (e.g. CO_2) is one of the major factors contributing to the enhancement of the oil recovery processes, it has been experimentally measured for many types of oil-solvent systems at various operating conditions (Abedini et al., 2014; Mosavat & Torabi, 2014).

Literatures show very limited correlations which could predict the oil swelling factor resulted from the dissolution of hydrocarbon and/or non-hydrocarbon solvents (Welker, 1963). Available correlations to predict solubility of CO_2 in various types of crude oils and oil swelling factor resulting from CO_2 dissolution are also gathered from literature and tabulated in **Table 2.2**.

Table 2.2: Available correlations for predicting solubility of CO_2 in crude oil and oil swelling factor due to CO_2 dissolution

Physical Properties	Author	Correlation
CO_2-Solubility in oil	Welker and Dunlop (1963)	Graphical correlation. Function of: P_s and oil gravity ($°API$) at $T = 80$°F. Limited to: $20°API \leq oil\ gravity \leq 40°API$
	Simon and Graue (1965)	Graphical correlation. Function of CO_2 fugacity and $T\ or\ P_s\ and\ T$ at characterization factor $= 11.7$, with a correction factor function of the characterization factor and T (for characterization factors other than 11.7) Limited to: $110°\text{F} \leq T \leq 250°\text{F}, P_s \leq 2{,}300\ psia$, and $12°API \leq oil\ gravity \leq 33°API$.
	Mehrotra and Svrcek (1982)	$$Sol\ (scf/bbl) = C_1 + C_2 P_s + C_3 \left(\frac{P_s}{b_1 T + b_2}\right) + C_4 \left(\frac{P_s}{b_1 T + b_2}\right)^2,$$ Where $C_1 = -0.04127, C_2 = -0.57292, C_3 = 248.9543, C_4 = 1.327846, b_1 = 0.55556, b_2 = 255.3722.$ Solubility at $1\ atm\ (P_b) = 0$. Limited to: $P_s \leq 925\ psia, 75°\text{F} \leq T \leq 207°\text{F}$.
	Chung et al. (1986)	For $P \leq 3{,}000$ psia: Sol (scf/bbl) $= \frac{1}{C_1 \gamma^{C_2} T^{C_7 + C_3 T^{C_4} exp\left[-C_5 P_s - \frac{C_6}{P_s}\right]}}$ Where $C_1 = 0.4934 \times 10^{-2}, C_2 = 4.0928, C_3 = 0.571 \times 10^{-6}$, $C_4 = 1.6428, C_5 = 0.6763 \times 10^{-3}, C_6 = 781.334, C_7 = -0.2499.$
	Emera and Sarma (2007)	For $T > T_{c,CO_2} (for\ all\ pressure)\ and\ T < T_{c,CO_2}\ (for\ P > CO_2 liquefaction\ pressure)$: $Sol\ (mole\ fraction) = 2.238 - 0.33y + 3.235y^{0.6474} - 4.8y^{0.25656}$ Where $y = \gamma \left(\frac{T^{0.8}}{P_s}\right)^{exp\left(\frac{1}{MW}\right)}$, Assumption: $CO_2\ solubility\ at\ P_b = 1\ atm = 0$ For $T < T_{c,CO_2}\ and\ P > CO_2 liquefaction\ pressure$ $Sol\ (mole\ fraction) = 0.033 - 1.14y + 0.7716y^2 + 0.2176y^3 - 0.02183y^4$, Where $y = \gamma \left(\frac{P_s}{P_{liq}}\right)^{exp\left(\frac{T}{MW}\right)}$
Oil Swelling Factor due to CO_2 dissolution	Welker and Dunlop (1963)	$$SF = 1.0 + \frac{0.35\ (Sol(scf/bbl))}{1{,}000}.$$ Developed for oils at $T = 80$°F $and\ 20°API \leq oil\ gravity \leq 40°API$.
	Simon and Graue (1965)	Graphical correlation. Function of Co2 Solubility, oil MW, and oil density at 60°F. Presents lower accuracy at high pressures. Limited to $110°\text{F} \leq T \leq 250°\text{F}, P_s \leq$ 2,300 psia, and $12°API \leq oil\ gravity \leq 33°API$.
	Emera and Sarma (2007)	For oil $MW \geq 300$: $SF = 1 + 0.3302Y - 0.8417Y^2 + 1.5804Y^3 - 1.074Y^4 - 0.0318Y^5 + 0.21755Y^6$ Where $1{,}000.0 \times \left(\left(\left(\frac{\gamma}{MW}\right) \times Sol(mole\ fraction)^2\right)^{exp\left(\frac{\gamma}{MW}\right)}\right)$ For oil $MW < 300$: $SF = 1 + 0.48411Y - 0.9928Y^2 + 1.6019Y^3 - 1.2773Y^4 - 0.48267Y^5 + 0.06671Y^6$

2.1.7. CO_2 diffusion in crude oil

Diffusion of various pure solvents and solvent mixtures have been experimentally measured and reported by many researchers at various pressures and temperatures for different types of crude oils with some of them focused on the diffusion of CO_2 in both light and heavy oil systems (Renner, 1988; Yang & Gu, 2006; Zhang et al., 2000).

Table 2.3 shows the diffusion rates of multiple solvents and mixtures in various types of crude oils. As it can be observed, diffusion rate of CO_2 in the crude oil is reduced when temperature increased or API gravity of oil decreased. However, its value increased when oil viscosity decreased or pressure increased. Addition of methane to CO_2 stream resulted in lower diffusion rate while inclusion of propane or butane improved the rate of diffusion of CO_2-hydrocarbon solvent mixture in the crude oil.

Table 2.3: Measured values of diffusion rates of various gases in different types of crude oils

Solvent	Author	Crude oil	Pressure (MPa)	T(°C)	Viscosity (mPa.s)	Diffusivity (10^{-9} m^2/s)
CO_2	Yang and Gu (2006)	Lloydminster heavy oil	2.0-6.0	23.9	23,000 at 23.9°C	0.20-0.55
	Tharanivasan (2004)	Lloydminster heavy oil	3.5-4.2	23.9	20,267 at 23.9°C	0.46-0.53
	Schmidt (1989)	Athabasca bitumen	5.0	20	361,700 at 20°C	0.28
	Upreti and Mehrotra (2000)	Athabasca bitumen	3.1-4.1	25	767 at 80°C	0.16-0.22
	Upreti and Mehrotra (2002)	Athabasca bitumen	4.0	25	821,00 at 25°C	0.12-0.20
	Renner (1988)	Decane	1.54-5.83	37.8		1.97-5.05
	Grogan et al., (1988)	Pentane	1.54-2.83	25		3.72-5.84
		Decane	1.37-4.2	25		3.21-2.68
		Hexadecane	2.86-4.14	25		0.47-0.58
	Nguyen and Farouq-Ali (1995)	Aberfeldy heavy oil	3.45	21.15	1,842	3.25
	Zhang et al., (2000)		3.47	21	5000	4.8
CH_4	Yang and Gu (2006)	Lloydminster heavy oil	6.0-14.0	23.9	23,000 at 23.9°C	0.12-0.19
	Tharanivasan (2004)	Lloydminster heavy oil	4.9-5.0	23.9	20,267 at 23.9°C	0.21-0.22
	Upreti and Mehrotra (2002)	Athabasca bitumen	4.0	25	224,500 at 25°C	0.08-0.11
			4.0-8.0	25	821,000 at 25°C	0.06-0.08
	Zhang et al., (2000)		3.51	21	5000	8.6
	Schmidt (1989)	Athabasca bitumen	5.0	50	5000	0.4-0.75
C_2H_6	Yang and Gu (2006)	Lloydminster heavy oil	1.5-3.5	23.9	23,000 at 23.9°C	0.13-0.77
	Upreti and Mehrotra (2002)	Athabasca bitumen	4.0	25	821,000 at 25°C	0.21-0.38
	Ganapathy (2009)	Lloydminster heavy oil	2.0	24.9	13,443 at 16.9°C	0.38
	Renner (1988)	Decane	1.72-3.9	37.8		2.27-7.89
C_3H_8	Yang and Gu (2006)	Lloydminster heavy oil	0.4-0.9	23.9	23,000 at 23.9°C	0.09-0.68
	Tharanivasan (2004)	Lloydminster heavy oil	0.4-0.8	23.9	20,267 at 23.9°C	0.49-0.79
	Luo et al., (2007)	Lloydminster heavy oil	0.5	23.8	24,137 at 23.8°C	0.14
	Ganapathy (2009)	Lloydminster heavy oil	0.5	24.9	13,443 at 16.9°C	0.24

2.2. Waterflooding, CO_2 flooding and WAG

2.2.1 Waterflooding

The idea of injecting water into the oil reservoirs to enhance the oil recovery is probably started as early as 1920s. In 1930, Torrey indicated that "waterflooding has been widely practiced for many years". One of the earliest studies related to the waterflooding performance is conducted by Uren & Fahmy (1927). In their study, effect of oil viscosity, grain size, porosity, and temperature on the performance of waterflooding were experimentally studied indicating the importance of such parameters in the displacement efficiency of waterflooding. Later, Wyckoff et al. (1933), performed some theoretical analysis to explain the relationship between performance of waterflooding and distance between injectors and producers in various flooding patterns. Mechanism of displacement of oil by water was modelled by Buckley & Leverett (1942) where they showed that fractional flow of water in the absence of gravity and capillary terms can be determined by Equation 2.1:

$$f_w = \frac{1}{1+\frac{k_o \mu_D}{k_D \mu_o}} \qquad \text{Equation 2.1}$$

Holmgren & Morse (1951) and later Kyte et al. (1956) emphasized that performance of waterflooding in presence of an optimum saturation of free gas is substantially higher. Optimum saturation could be determined experimentally or with the help of correlations.

One of the major issues of waterflooding when applied to heavy oil reservoirs is viscous fingering and early water breakthrough. This is mainly because of the viscosity

contrast existing between the heavy oil and injected water that causes frontal instability (Peters & Flock, 1981).

Through a series of experiments, Mai & Kantzas (2009) investigated the effects of flow rate and oil viscosity on the performance of waterflooding in heavy oil saturated porous media. They have concluded that oil recovery can be continues if water is injected at low flow rate. Another finding of their study was that viscous forces are affecting the oil recovery at the earlier times while capillary forces are continually impact.

Overall, numerous factors are affecting the performance of waterflooding and to date literature shows lack of in depth understanding of the effects of some of them and correlations which could be widely used. Some of the most important parameters pointed out by researchers are: oil viscosity, mobility ratio, wettability, heterogeneity and lithology of the reservoir, injection rate, flood pattern, etc. (Aronofsky, 1952; Craig, 1971; Crawford, 1960; Dake, 2001; Kumar et al., 2008; Wardlaw, 1996; Willhite & G.P., 1986)

2.2.2 CO_2 flooding

CO_2 flooding is normally a better choice for light oil reservoirs as CO_2 can be injected at near miscible or miscible conditions. For many years, unfavorable economics didn't attract heavy oil operators to use CO_2 as an injectant (Khatib et al., 1981). In recent years, application of CO_2 in huff-and-puff (or cyclic CO_2 injection method) showed substantial recovery potential. This method involves injection of CO_2 in the reservoir for few days (e.g., 7-10 days) followed by a period of soaking (e.g., 5-7 days), and final period of production which could be continued for as many as few months. This injection-soaking-production process is considered one complete cycle. Cyclic injection is continued until it is no longer economy.

One of the comprehensive studies that referred to many facts about performance of CO_2 flooding in heavy oil reservoirs is by Spivak & Chima (1984). In their study, they concluded that during immiscible CO_2 flooding of heavy oil reservoirs, viscosity reduction is the main mechanism contributing to oil production. During CO_2 injection, methane is stripped out and form a methane bank ahead of the oil. Presence of nitrogen reduces the solubility of CO_2 in the heavy oil causing an early breakthrough due the fact that nitrogen is insoluble in the oil. Gravity override is also another serious issue of immiscible CO_2 injection.

Overall, CO_2 flooding contribution to oil recovery is through viscosity reduction (Saner & Patton, 1986), oil swelling (Klins & Ali, 1982), decrease of interfacial tension (Dryer & Ali, 1989), blow-down recovery (Gao et al., 2013; L. W. Holm & Josendal, 1974; Klins & Ali, 1981), solution gas drive mechanism, oil relative permeability improvement, skin factor reduction while suffering from early breakthrough, viscous fingering and gravity override (Gao et al., 2013).

It is a common believe among the researchers that injecting immiscible gas alternately with water improves sweep efficiency and recovery factor (Ahmadi et al., 2015; Dong et al., 2002; Jha, 1986; Kulkarni & Rao, 2005; Ma et al., 1995; Ma & Youngren, 1994; McGuire et al., 2005; Sanchez, 1999; Sohrabi et al., 2004, 2000, 2001; Spivak & Chima, 1984; Zhang et al., 2006).

2.2.3 WAG

Water-alternating-gas (WAG) is a name given to alternating injection of water and gas in the oil reservoirs for the purpose of enhanced oil recovery. When water and gas are injected simultaneously, it is called SWAG. Literature show that both immiscible and

miscible CO2 based WAG have been extensively studied and field practiced as early as 1950's. In heavy oil reservoirs, one of the earliest field implementations of the WAG North Pembina field project and until 1998, over 59 field trials of WAG were reported (Christensen, 1961).

WAG is receiving benefits from all of those mechanisms mentioned for CO_2 flooding combined with the displacement energy inserted by water. In addition, it is believed that in the water-wet formations, gas is normally intended to move in the larger pores while water moves into the smaller pores, hence, displacing oil from both types of pores.

Corrosion, formation of asphalthene and hydrates, and loss of water injectivity are some of the operational issues of WAG (Christensen *et al.*, 1998). Stephenson and Graham (1993) compared both WAG and SWAG performance from results obtained in Joffre Viking miscible CO_2 flood and concluded that SWAG's performance is substantially higher than WAG. Robie et al. (1995) analyzed the data of Rangeley Weber sand unit and found that injectivity of water during SWAG is not reducing as drastic as in the case of WAG.

Other types of WAGs are also suggested for heavy oil reservoirs. Viscosity-reduction WAG or VR-WAG is a process at which a viscosity reduction agent is injected prior to the implementation of WAG (McGuire et al., 2005). In this method, some heavy components are blended with lean gas to generate viscosity reduction injectant (VRI). This can be further promoted by mixing the blend with NGL to be applicable to more viscous oils.

Overall, it can be concluded that WAG, solvent-WAG (SWAG), variable-rate (VR-WAG) or any other types are more efficient compared to waterflooding and CO_2 flooding when applied to heavy oil reservoirs (Champion & Shelden, 1989; Christensen, 1961; Kulkarni & Rao, 2005; Sohrabi et al., 2000).

2.3. Carbonated water flooding

Carbonated water flooding or injection (CWF or CWI) is a process that involves injection of CO_2 saturated brine into the reservoir at the desired pressure and temperature. During this process, it is assumed that CO_2 will remain in the aqueous solution until it reaches the oil zone. At the contact, CO_2 is evolved from brine and diffuses into the oil because of higher solubility in the oil (solubility of CO_2 in oil is 3 to 7 times higher than that in the brine) (Y. Dong et al., 2011). Due to the diffusion of CO_2 into the oil phase, oil viscosity is substantially reduced and oil globules will be enlarged (swelled), hence, oil recovery is improved.

There are some interesting and important facts which distinguish the CWF from waterflooding and CO_2 flooding. During CWF process, CO_2 is carried to the reservoir as a dissolved phase in the brine and therefore, no free CO_2 should be existing causing early gas breakthrough or gravity override. In addition, evolution of CO_2 from water and its' dissolution into the oil is a mass transfer dominated process. Therefore, the higher the mas transfer, the higher the displacement efficiency (Y. Dong et al., 2011). Moreover, at abandonment time, CO_2 stored in the reservoir is expected to be remaining in the aqueous phase and overtime dissolves in the residual oil saturation. It must be emphasized that CWF

is an EOR technique and its CO_2 storage contribution is not substantially high though it is a bonus.

Application of CWF process in various types of oil reservoirs is reported as early as 1940's. Literature shows numerous studies and field practices of CWF, however, majority of them are focused on light oil reservoirs or heavy oils with viscosity (μ_o) of less than 100 mPa.s.(L. Holm, 1963a; Holmgren & Morse, 1951; Johnson et al., 1952; Latil, 1980; Martin, 1951; Mosavat & Torabi, 2013; Nevers, 1966; Riazi, 2011; Sohrabi et al., 2008, 2009; Steffens, 2010; Tran, 2009). Summary of the experimental studies as well as field practices of CWF applied to various types of oil reservoirs is presented in the next sections.

2.3.1. Experimental studies of CWF

As mentioned earlier, experimental studies related to CWF is reported as early as 1940's. Conclusion of the experimental studies performed by Martin (1951) was that to receive maximum benefit from CWF, fully saturated water with CO_2 must be injected. In his study, it was found that while CWF can increase the recovery factor by 12%, injection of 50% saturated water can drop the 12% to about 10.32% and 7.2% when applied to oil samples with API gravity of 43 and 50, respectively.

Experimental studies of CWF conducted at 5.28 MPa (carbonation pressure) and 23.9^{o}C showed 15% to 25% increase in recovery factor after conventional waterflooding (Johnson et al., 1952).

Tests conducted in a 30.48 cm long and 8.9 cm diameter Berea sandstone core using West Texas crude oil (5.1 mPa.s. at 21^{o}C) at operating temperature of 37.8^{o}C and pressure

of 8.4 MPa showed 20% improvement in recovery factor compared to WF (L. Holm, 1963a). L. Holm (1963b) conducted additional tests using oil samples of less than 5 mPa.s. and at temperature of 37.8^{o}C and pressure range of 4.25 MPa to 18.08 MPa while using CO_2 as chasing fluid. He observed 30% to 35% improvements in the recovery factor compared to when he used water as chasing fluid and concluded that some kind of miscibility might be achieved.

Analysis of the results obtained by Monteclaire research and later Earlougher Engineering (in 1940s) showed that oil recovery can be improved by 2 to 26% when CWF is implemented after waterflooding (Lake et al., 1984)

As mentioned earlier, majority of the CWF studies conducted in heavy oil systems used oil samples with viscosity of less than 100 mPa.s. During experimental studies of Holm (1963), when oil sample with viscosity of 90 mPa.s. was used in CWF tests, improvement of recovery factor was 69% compared to WF.

Another experimental study that focused on heavy oil was performed by Institut Francais du Petrole (IFP) using oil sample from Bati Raman oil field in Turkey (Khatib et al., 1981). In their study, core was saturated with oil sample from Bati Raman field (μ_o=290 mPa.s.) at 86%. Waterflooding was conducted at 2.9MPa and 65^{o}C until water cut reaches 100%. Core was then pressurized to 15.14 MPa using 88% purity CO_2 and closed for 24hrs. Thereafter, CWF was initiated and continued until water cut increased to 100%. About 13.9% improvement in recovery factor was observed, as the result of CWF.

Another set of experiments were conducted by (Mayer et al., 1988) where he used oil sample with viscosity of (μ_o=475 mPa.S. at T=51.7^{o}C) and saturated six core plugs each of approximate length of 12.2 cm. Core plugs were then waterflooded at 5.98 MPa with

large initial flow rate followed by stabilized flow rate of 0.0211 ml/min (equivalent to 1 ft/day). After water-oil-ratio (WOR) reached 100%, core was aged by injecting CO_2 at 5.98 MPa. Core plugs of various properties were then flooded using CW and overall improvements in the range of 13% PV to 21.5% PV were observed.

In similar set of experiments conducted by (Mayer et al., 1988) at P=7.02 MPa and T=51.7ºC using oil sample with viscosity of μ_o=406 mPa.s., some overall improvements of 15.9% to 24% were observed for CWF.

Micromodel studies are performed by various researchers to study the effectiveness of carbonated waterflooding (Mosavat & Torabi, 2013; Riazi et al., 2011; Sohrabi et al., 2008, 2009). In all of these studies, it was concluded that CWF has great potential to improve the recovery factor when used as means of secondary or tertiary recovery mechanisms.

Perhaps, experimental studies conducted by (Asghari et al., 2009) is the most related one to this study where they used oil samples with viscosity in the range of 1800 to 2000 mPa.s. CWF studies, conducted at T = 40 °C and P = 8.3 MPa, using those oil samples showed an improvement of 16.9 % OOIP for consolidated core and 13.9 % OOIP for sandpack models. Asghari et al. (2009) allowed soaking periods of 17 hrs to 34 hrs for their tests conducted in the consolidated and unconsolidated porous mediums, respectively.

Lastly, from the limited published data on the application of CWF in heavy oil systems, it can be observed that more fundamental, experimental, and practical studies are required to better correlate the performance of CWF to various reservoir and fluid parameters as well as operating conditions.

2.3.2. Field implementations of CWF

As mentioned earlier, it became appear that CWF has some advantages over waterflooding, CO_2 flooding and WAG. Two main advantages are i) higher recovery factor, ii) higher injectivity (Christensen, 1961). Because of such benefits, its application has been reported as late 1940s and early 1950s.

Martin (1951) reported that production rate from Allegany County near Richburg, New York, has increase from 92 to 1260 barrels/acre/year when CWF was implemented in 1947. Unfortunately, it was very difficult to find additional information about this early implemented CWF and aforementioned information has been gathered from other sources (Mosavat, 2014).

K&S project is considered as the first commercial CWF (Hickok & Jr, 1962; Martin, 1951). The producing formation in this 240-acre tract is Bartlesville, Oklahoma, at the depth of 396.24m with average pay zone of 10.06m. It contains oil with API gravity of 33, oil viscosity of 6.4 mPa.S.(at T=37.8^{o}C) and its porosity and permeability are 17.6% and 56 md, respectively. CWF was started in 1958 and increased oil production rate from 30 B/D to over 2300 B/D by late 1959.

Another tract located in the north of K&S, known as Wirt fields, was producing 15 B/D from Bartlesville sand using 4 wells in a 40-acre spacing. While oil properties of Wirt fields were similar to K&S, its sand permeability and porosity were 44md and 16%, respectively. Implementation of CWF by March 1959 increased the production rate from 15 B/D to 420 B/D and improved average injectivity from 700 B/D to about 1400 B/D, showing the significance of CWF (Christensen, 1961).

Domes unit is composed of 13 quarter-sections and is located in Osage county, Oklahoma, 15 miles west of Bartlesville (Scott and Forrester, 1965). This unit contains oil with API gravity of 32 degree and oil viscosity of μ_o=10 mPa.S. at T=36.7^{o}C. Average thickness, permeability, and porosity of the sand are 3.9m, 22md, and 14.5%, respectively. Production from Domes unit started in 1910 and until 1920s, 60 additional wells were drilled but all of them were plugged when waterflooding was started. Out of 90 wells drilled by 1953, 13 wells were converted into injectors. In 1961, carbonated water injection was started by injecting CO_2 and water into those 13 plus 3 newly drilled injectors. Analysis of the production data showed about 9% enhancement in the oil recovery (Riazi, 2011).

As it has been observed and reported in some of the field practices, CWF not only improved oil recovery but also improved the injectivity of the water when applied to various types of oil reservoirs. As an example, injectivity has been increased from an initial value of 700 B/D to over 1400 B/D in Wirt fields and substantially improved in Aleksandrovsk (Tuimazy) field after the implementation of CWF (Christensen, 1961; Kislyakov et al., 1967).

Such an increase in injectivity can be attributed to removal of the oil, reduction of water viscosity, reduction in oil viscosity, and improved permeability in the vicinity of the injection wells. In the other words, improvement in the rock permeability near the injectors is mainly due to the dissolution of the reservoir rock in the carbonic acid which is formed because of the reaction between CO_2 and water. Such improvement in rock permeability results in higher injection rate (Hickok & Jr, 1962; Jr & Small, 1964).

2.4. Chapter summary

An extensive literature review has been conducted on waterflooding, CO_2 flooding, and WAG processes. Experimental studies and field implementation cases of CWF were reviewed in detail. As stated by researchers and included in previous sections of the literature review, CWF improves oil recovery from light to heavy oil reservoirs through mechanisms such as: oil viscosity reduction, oil swelling, permeability and injectivity improvements, and interfacial tension reduction when compared to waterflooding, CO_2 flooding and WAG.

Parameters affecting the performance of CWF were identified per literature review to be: injection rate, temperature, oil viscosity, pressure, reservoir characteristics, brine salinity, and carbonation pressure.

In addition, implementation of CWF could result in additional benefits from carbon tax credit though its contribution to removal of greenhouse gases may not be as high as miscible CO_2 flooding, and both immiscible and miscible CO_2-WAG processes.

Although majority of the CWF field practices reported are from light oil reservoirs, and there are not many pilot tests and/or field applications available to public, experimental studies show that CWF can be also applied to heavy oils. The main knowledge gap identified during the literature review was the limited CWF studies conducted in heavy oil systems with oil viscosity of higher than 100 mPa.s.

Similar to the light oil cases, it is also crucial to investigate the effects of influencing parameters such as injection rate, temperature, oil viscosity, and etc. on the performance of CWF in heavy oil systems.

CHAPTER THREE: Phase behaviour study

3.1. Introduction

Phase behavior study is an essential part of performance prediction and analysis of most of EOR processes. In addition, changes in the physical properties of fluids when they interact with each other and, their implications on the mechanisms involved in the EOR processes must be studied prior to the commissioning of any EOR project.

As mentioned earlier, mechanisms involved in the improvement of recovery factor during CWF are oil viscosity reduction, oil swelling, IFT reduction, etc. All of these mechanisms are the result of dissolution of CO_2 in the oil (Abedini et al., 2014; Dryer & Ali, 1989; L. W. Holm & Josendal, 1974; Klins & Ali, 1982; Mosavat & Torabi, 2013; Saner & Patton, 1986).

The side benefit of implementing CWF for EOR is its contribution to greenhouse gas emission by trapping CO_2 in the aqueous phase (Ennis-King & Paterson, 2005; Lindeberg & Wessel-Berg, 1997; Nghiem et al., 2009). To evaluate the potential of CWF for CO_2 storage in the depleted oil reservoirs and aquifers, it is required to understand the dissolution of CO_2 in the brine and how salinity, pressure, temperature and total dissolved solids (TDS) may affect the solubility of CO_2 in the brine phase.

There are wide range of data and correlations available to predict the CO_2 solubility in brine solutions, and various types of crude oils (Beggs & Robinson, 1975; Standing, 1979). In this chapter, parameters such as CO_2 solubility in brine and oil, and changes in physical properties of both oil and brine phases due to the dissolution of CO_2 have been investigated.

3.2. The physical properties of the fluids

Fluids used in this study were: i) pure CO_2 (with purity of 99.99%) supplied by (Isfahan) , ii) synthetic brine with concentration of 20,000 PPM of NaCl dissolved in the deionized water (DI), and iii) two heavy crude oil samples of various viscosities by diluting an original extra heavy oil with kerosene.

Properties of CO_2 at various pressures and temperatures in the range of this study was determined (from www.peacesoftware.de/) and tabulated in **Table 3.1**. In addition, phase behavior (PT diagram) of pure CO_2 was prepared and presented in this report.

Brine solution was exactly similar to the one used by (Mosavat, 2014). Therefore, properties of brine solution were measured, determined and checked against his data. Viscosity was measured by a DV-II+Viscometer from Can-AM Instruments LTD. Values of brine viscosity (measured) and density (calculated) at various pressures and temperatures are presented in **Table 3.2**.

To investigate the applicability of CWF in heavy oil systems and evaluate the significance of oil viscosity on the displacement efficiency of CWF, two heavy crude oil samples were used. Viscosity of the two crude oil samples (named Type-I and Type-II in this study) were measured and reported to be 463 mPa.s and 1989 mPa.s at T=25^{o}C and P=101.325kPa. Carbon distribution and compositional analysis of various pseudo groups are presented in **Table 3.3-3.4** and **Figure 3.1**, respectively. Other physical properties of both types of crude oil samples such as density, viscosity and molecular weight measured at temperature of T = 25 °C and pressure of P= 101.325 kPa are tabulated in **Table 3.5**.

Table 3.1: Physical properties (density and viscosity) of CO_2 at various pressures and temperatures.

	Pressure *P* =101.325 kPa		Pressure *P* =345.8 kPa		Pressure *P* =691.6 kPa		Pressure *P* =1037.5 kPa		Pressure *P* =1383.3 kPa	
Temperature (°C)	Density (kg/cm^3)	Viscosity $(mPa.s)x10^{-3}$	Density (kg/cm^3)	Viscosity $(mPa.s)x10^{-3}$	Density (kg/cm^3)	Viscosity $(mPa.s)x10^{-3}$	Density (kg/cm^3)	Viscosity $(mPa.s)x10^{-3}$	Density (kg/cm^3)	Viscosity $(mPa.s)x10^{-3}$
21	1.83	14.74	6.38	14.76	12.99	14.79	19.83	14.83	27.28	14.89
25	1.8	14.93	6.27	14.95	12.75	14.98	19.45	15.03	26.71	15.08
30	1.77	15.17	6.15	15.19	12.51	15.22	19.05	15.27	26.12	15.32
35	1.74	15.41	6.05	15.43	12.28	15.46	18.69	15.5	25.58	15.55
40	1.71	15.65	5.94	15.67	12.06	15.71	18.34	15.74	25.05	15.79
45	1.69	15.89	5.85	15.91	11.85	15.94	18.01	15.97	24.56	16.02
50	1.66	16.13	5.75	16.15	11.64	16.18	17.68	16.21	24.07	16.26
55	1.64	16.37	5.66	16.39	11.45	16.42	17.37	16.45	23.63	16.5

Calculated from: www.peacesoftware.de/

Table 3.2: Density and viscosity of 20,000ppm brine sample at atmospheric pressure, *P*= 101.325 MPa and various temperatures.

Temperature (°C)	*Density (kg/cm^3)	Viscosity (mPa.s)	**Density (kg/cm^3)	**Density (mPa.s)
25	1012.08	0.94	1010	1010.2
30	1010.56	0.83		
35	1008.84	0.75	1008.2	1008.2
40	1006.94	0.67		
45	1004.88	0.62		
50	1002.66	0.06		
55	1000.31	0.53		

*Calculated from (www.csgnetwork.com/h2odenscalc.html)

** (Mosavat, 2014)

Table 3.3: Compositional analysis of the oil sample Type-I at T = 21°C and P=101.325 kPa

Carbon number	Mole %	Carbon number	Mole %	Carbon number(s)	Mole %
C_1	0.000	C_{14}'s	2.433	C_1–C_6's	0
C_2	0.000	C_{15}'s	2.498	C_{7+}'s	100
C_3	0.000	C_{16}'s	2.453		
i-C_4	0.000	C_{17}'s	2.469	C_1–C_{14}'s	50.527
n-C_4	0.000	C_{18}'s	2.410	C_{15+}'s	49.473
i-C_5	0.000	C_{19}'s	2.397		
n-C_5	0.000	C_{20}'s	2.234	C_1–C_{29}'s	78.841
C_5's	0.000	C_{21}'s	2.165	C_{30+}'s	21.159
i-C_6	0.000	C_{22}'s	1.794		
n-C_6	0.000	C_{23}'s	1.699		
C_6's	0.000	C_{24}'s	1.566		
C_7's	0.058	C_{25}'s	1.412		
C_8's	2.054	C_{26}'s	1.384		
C_9's	8.202	C_{27}'s	1.391		
C_{10}'s	17.061	C_{28}'s	1.258		
C_{11}'s	12.653	C_{29}'s	1.184		
C_{12}'s	4.945	C30's	1.154		
C_{13}'s	3.121	C_{31+}'s	20.005		

Table 3.4: Compositional analysis of the oil sample Type-II at T = 21°C and P=101.325 kPa

Carbon number	Mole %	Carbon number	Mole %	Carbon number(s)	Mole %
C_1	0.000	C_{14}'s	2.429	C_1–C_7's	0
C_2	0.000	C_{15}'s	2.446	C_{8+}'s	100
C_3	0.000	C_{16}'s	2.537		
i-C_4	0.000	C_{17}'s	2.467	C_1–C_{14}'s	40.585
n-C_4	0.000	C_{18}'s	2.399	C_{15+}'s	59.415
i-C_5	0.000	C_{19}'s	2.374		
n-C_5	0.000	C_{20}'s	2.209	C_1–C_{29}'s	68.742
C_5's	0.000	C_{21}'s	2.065	C_{30+}'s	31.258
i-C_6	0.000	C_{22}'s	1.879		
n-C_6	0.000	C_{23}'s	1.699		
C_6's	0.000	C_{24}'s	1.552		
C_7's	0.000	C_{25}'s	1.428		
C_8's	0.211	C_{26}'s	1.378		
C_9's	7.322	C_{27}'s	1.291		
C_{10}'s	13.234	C_{28}'s	1.248		
C_{11}'s	10.732	C_{29}'s	1.184		
C_{12}'s	4.536	C30's	1.090		
C_{13}'s	2.121	C_{31+}'s	30.169		

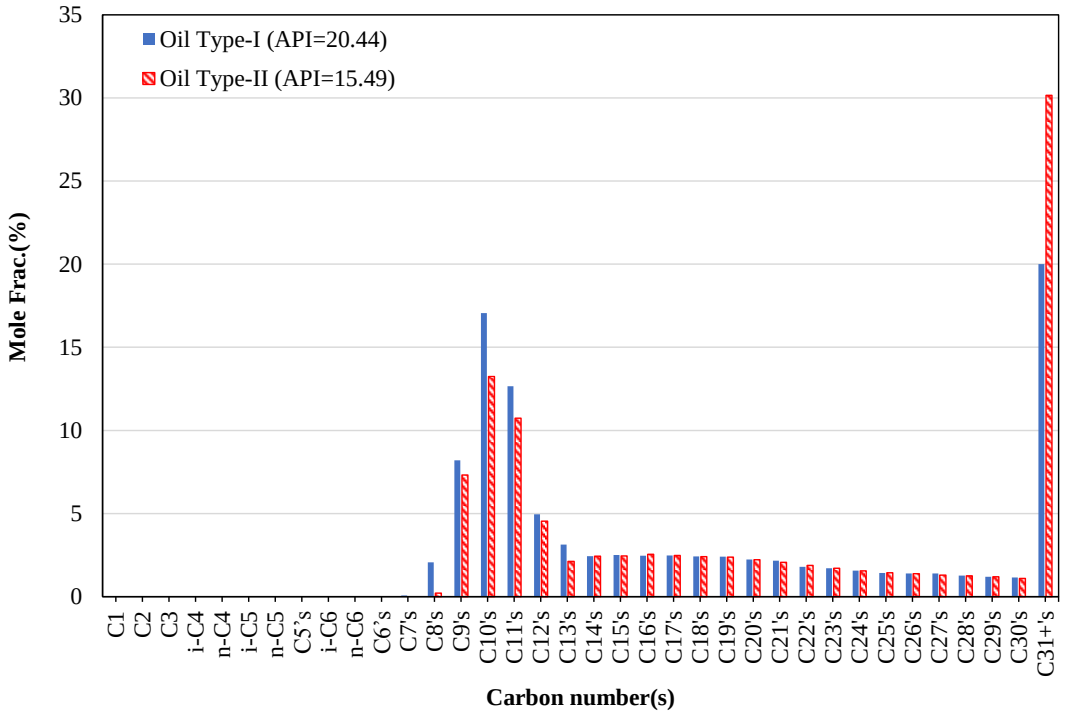

Figure 3.1: Carbon distribution (compositional analysis) of two heavy oil samples used in this study.

Table 3.5: Physical properties of two crude oil samples used in this study at P = 101.325 kPa and T = 21 °C.

Property and Conditions	Oil Type-I	Oil Type-II
Density (kg/m^3) at P =101.325 KPa and T =21^{o}C	930	962
Viscosity (mPa.S.) at P =101.325 KPa and T =21^{o}C	989	5265
Molecular Weight	354	427
API Gravity (15.6^{o}C/15.6^{o}C)	20.44	15.49

Changes in the oil viscosity of both samples as a function of temperature were measured using DV-II+Viscometer from Can-AM Instruments LTD and reported in **Figure 3.2**. Additionally, viscosities of both samples were predicted using correlation of Beggs & Robinson (1975) and plotted against experimental data. It became evident that calculated values are only within a reasonable range of accuracy compared to the measured values. Error calculations showed deviations of 1.5% to about 24% at various temperatures. As it can be seen in **Figure 3.2**, correlations of Beggs & Robinson (1975) slightly underestimated oil viscosity for Type-I (^{o}API=20.44) and largely overestimated viscosity values for Type-II (^{o}API=15.49) at the range of temperature of T=21 to 28^{o}C.

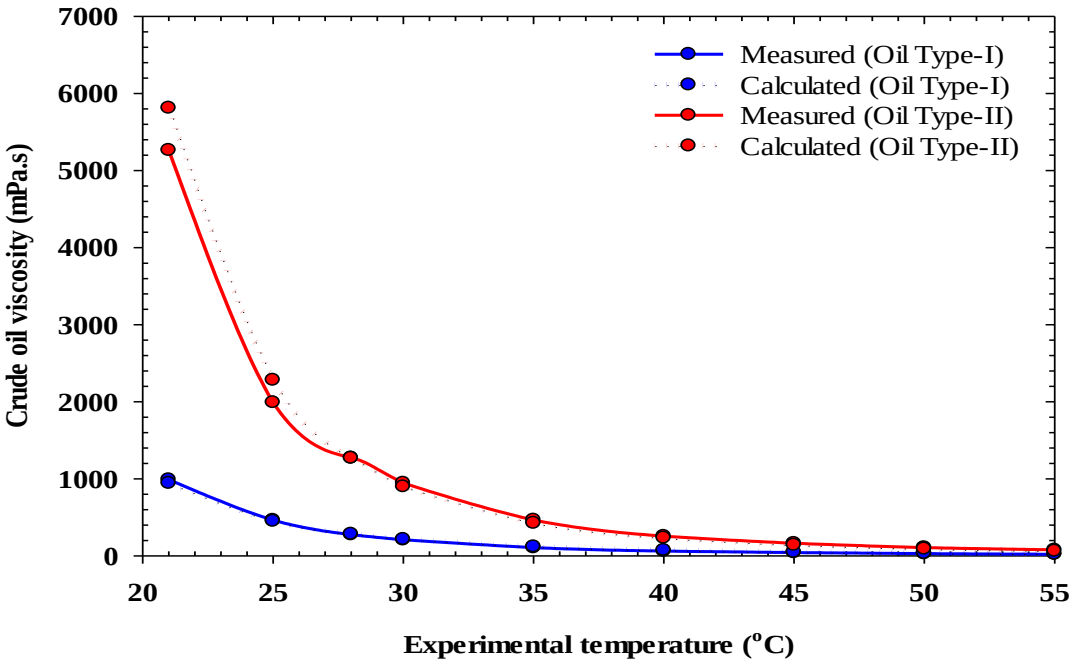

Figure 3.2: Measured crude oil viscosity for two types of crude oils used in this study at atmospheric pressure (P=101.325 kPa) and various temperatures versus calculated values (Beggs & Robinson, 1975)

CO_2–brine system

Perhaps one of the questions that has been always raised is why carbon dioxide is captured and used but no other gases such as nitrogen, methane, etc. are of interest to be captured? It is well known that presence of large quantity of carbon dioxide in the atmosphere significantly contributes to global warming. However, another reason for capturing CO_2 is that comparison of solubility of various gases shows that CO_2 solubility in water is much higher compared to other gases. Additionally, as mentioned earlier, CO_2 solubility is much higher in the crude oil compared to the brine or fresh water. Therefore, use of CO_2 for EOR and storage purposes is motivated by higher potential of CO_2 in reducing oil viscosity which in turn results in higher recovery factor while can be stored underground. **Figure 3.3** compares solubility of CO_2 and three other common gases, which are sometimes considered as alternatives for EOR processes, in fresh water. As it can be observed, solubility of CO_2 in fresh water is up to 25 times and nearly 100 times higher than solubility of ethane and nitrogen.

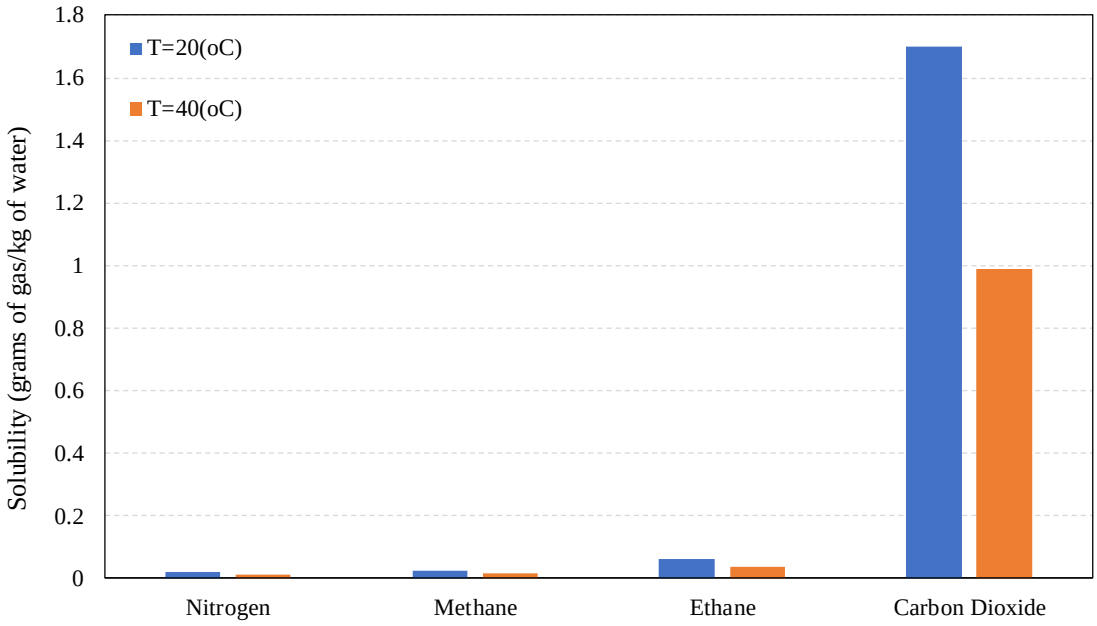

Figure 3.3: Solubility of four common types of EOR gases in pure water at pressure of P = 101.325 kPa and temperature of T = 20 °C and T = 40 °C (www.engineeringtoolbox.com).

While increase in pressure causes solubility of CO_2 in pure water to be increased, temperature has adverse effect. **Figure 3.4** depicts variation of solubility of CO_2 in pure water calculated in the range of T = 20 °C to 60 °C and atmospheric pressure of P = 101.325 kPa. The combination effect of pressure and temperature on the solubility of CO_2 in water is of more interest to the researchers, particularly those conducting research in the area of CO_2 storage in saline aquifers. Calculated values of solubility in the wide range of pressure and temperature are prepared by Dodds et al. (1956) and are reconstructed and presented in **Figure 3.5**.

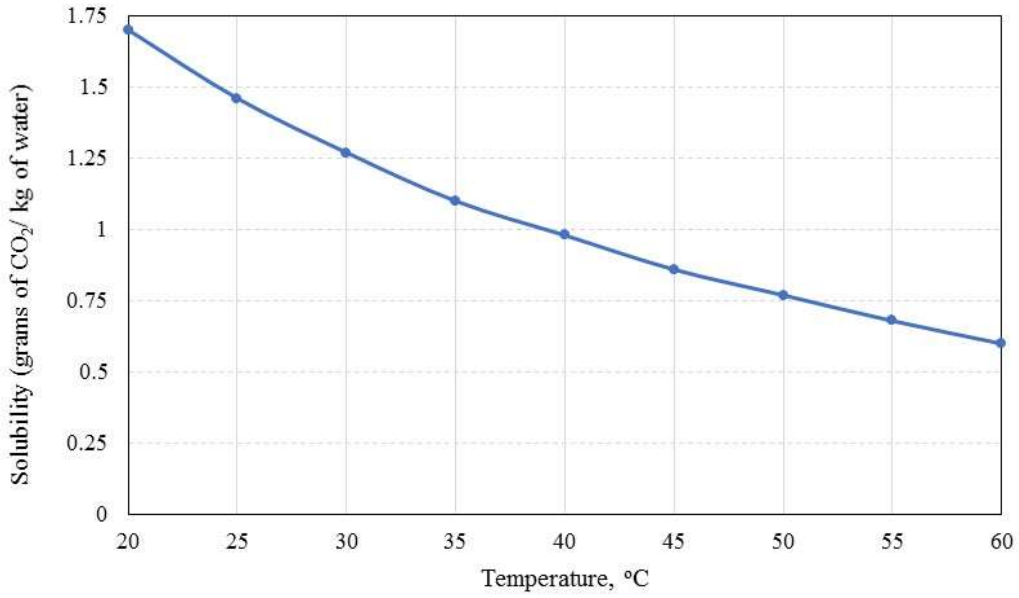

Figure 3.4: Solubility of CO_2 in fresh water as a function of temperature (http://www.rocketscientistsjournal.com)

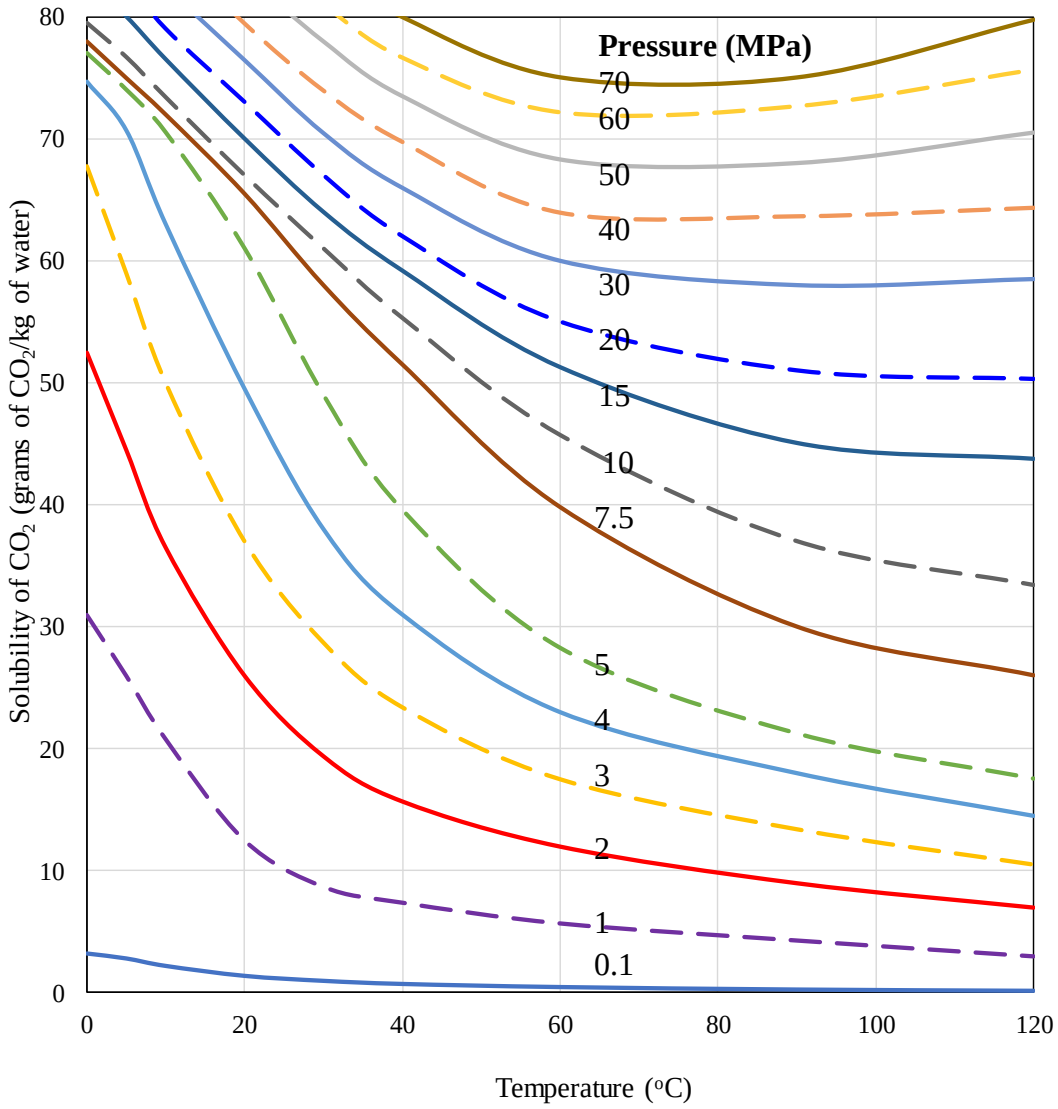

Figure 3.5: CO_2 solubility in fresh water at various pressures and temperatures (rebuilt and recalculated from (Dodds et al., 1956)).

3.2.1. Experimental setup, procedure and results of CO_2 solubility measurements in brine

As mentioned earlier, wide range of experimental data and correlations are available for CO_2 solubility in various types of brine solutions. However, due to the importance of the CO_2 solubility in evaluating the performance of CWF, accurate measurement of this parameter using the supplied CO_2 and synthetic brine solution used at the specific pressure and temperature is essential. Therefore, CO_2 solubility using the CO_2 supplied from Isfahan (with purity of 99.99%) and synthetic brine solution (20,000 ppm NaCl dissolved in DI water) has been measured for various temperatures and pressures and compared with those measured before (Mosavat, 2014) or determined (Duan & Sun, 2003).

Safety Percussions

Prior to each experiment, a safe operation procedure and personal protective equipment were prepared. Personal protective equipment such as safety goggles, proper shoes and gloves, as well as paper mask were always used during all stages of experiments in this study. Nitrogen, carbon dioxide, and transfer cylinders were all hooked-up and proper labels were attached with date, condition of the experiments (running or stopped), and safety percussions necessary in the case of emergency as well as the contact person information.

Experimental Setup

To measure solubility of CO_2 in DI water and brine solution used in this study," experimental setup showed in **Figure 3.6** was utilized. Experimental setup, measurement

procedure and analysis of the results were following a standard method used by (Abedini et al., 2014; Mosavat, 2014). Experimental setup consists of a computer-controlled pump (Agilent 1200 series), CO_2 cylinder (with purity of 99.99% from Isfahan), programmable oven (PetroAzma), digital pressure gauges (Heise Inc. and Ashcraft), a piston accumulator, a back-pressure regulator (BPR) with maximum operating pressure of P_{max} = 17.3 MPa (Equilibar, 2500 Psi series), and effluent fluid (CO_2 and water) collectors. The temperature of the air bath was maintained by its built-in temperature controller. Accuracy of temperature controller pressure gauges were $\pm$0.1 °C and 0.7 kPa, respectively. All systems were tested for leakage prior to the tests.

Experimental Procedure

Per safety regulations, during all experimental works conducted for this research, personal protective equipment (PPE) consists of nitrile gloves, safety goggles, lab coat, and proper shoes and dress were used and transfer of heavy parts were done following safe handling of heavy and dangerous equipment.

Prior to solubility tests, synthetic brine solution of 20,000 ppm was prepared using 2 grams of pure NaCl in 98 grams of DI water. Total amount of 2000mL of synthetic brine was prepared in a vertically mounted transfer cylinder (equipped with displacement piston) with a capacity of 1200mL. CO_2 was charged to the cylinder at desired pressure and temperature. While rocking at a constant temperature and pressure, solution was allowed to reach equilibrium for 48-72 hrs. During this process, CO_2 injection pressure was always kept constant using a pressure regulator and a digital pressure gauge. The mixture was homogenized for 48 hours inside the air bath at the experimental temperature while the outlet pressure of the CO_2 cylinder was kept constant. During the equilibration process, the

cylinder was kept connected to the CO_2 cylinder in order to provide the pressure support of the mixture. After solution reached equilibrium, CO_2 source was detached and pressure of the cylinder was observed for 3-4hrs to ensure absolute equilibrium has been reached. Brine solution was gently displaced through a BPR set at the same pressure of transfer cylinder to allow the free gas existing at the top of the cylinder be removed and to make sure that CO_2–brine solution is in liquid phase. In this process, a small differential pressure of less than 30kPa was utilized and effluent was carefully monitored until continues flow of carbonated water was observed from the BPR's outlet. All carbonated water solutions were prepared using aforementioned procedure at the desired pressures and temperatures of experiments.

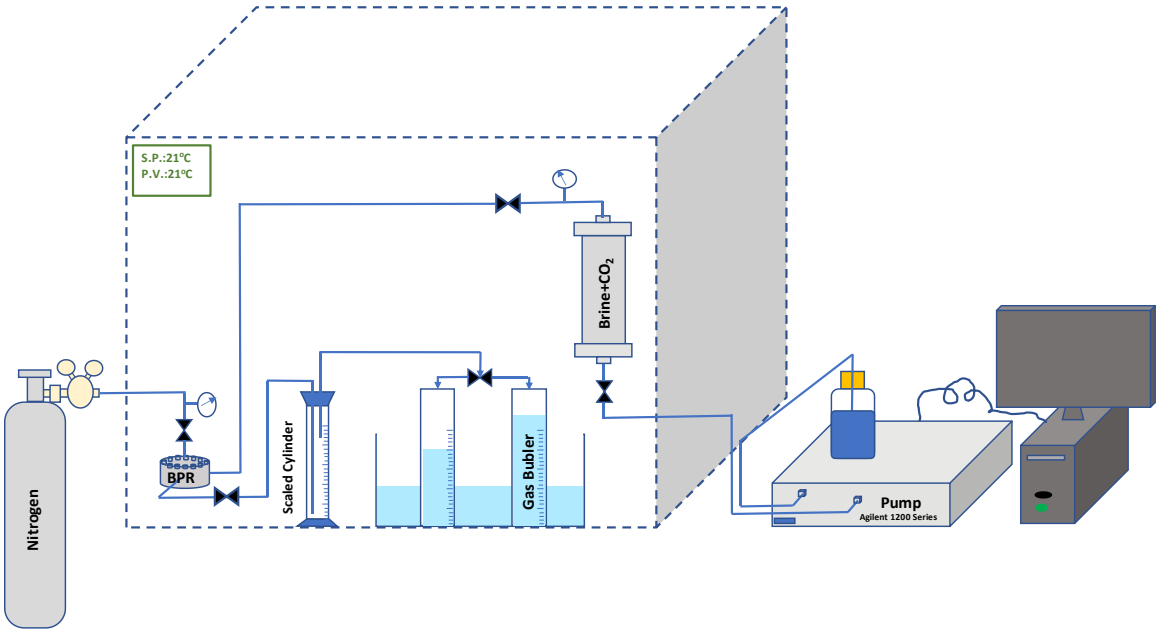

Figure 3.6: Schematic diagram of the experimental setup used to measure CO_2 solubility in brine at various pressures and constant temperatures.

CO_2 solubility measurement was then carried out for each pressure and temperature by taking samples from the BPR's outlet in a sealed scaled cylinder connected to an in-house made gas bubbler system. Volume of produced CO_2 was measured by adding the volume readings from two gas bubblers while volume of brine was directly read from the scaled cylinder. It must be noticed that the CO_2 gas cap presents on the top of the brine in the scaled cylinder was considered equal to the amount of air initially existing in the same space. Ratio of CO_2 gas to water (brine) solution (GWR) was calculated and CO_2 solubility in brine was determined using Equations 3.1 and 3.2.

$$GWR\left(\frac{cm^3 of\ CO_2}{cm^3 of\ water}\right) = \frac{Produced\ \ CO_2, cm^3}{Produced\ \ Water, cm^3} \quad \text{.....Equation (3.1)}$$

$$\chi_b = GWR \times \frac{\rho_{CO_2}\left(gr/cm^3\right)}{\rho_b\left(gr/cm^3\right)} \times 1000 \quad \text{.....Equation (3.2)}$$

In Equations 3.1 and 3.2, χ_b is the solubility of CO_2 in brine solution in gr of CO_2 per 1000 grams of water, GWR is the gas-water-ratio, and ρ_b is the brine density in gr/cm^3.

Results of CO_2 solubility measurements in brine solution

Solubility of CO_2 in brine was measured at a wide range of operating conditions covering the pressure and temperature range of the experiments conducted in this study (pressure and temperature). For each of these tests, CW was prepared at the desired pressure and temperature. Solubility of CO_2 in the brine solution was then measured following the previously mentioned procedure. As mentioned earlier, there are numerous experimental results of CO_2 solubility in various types of brines in the literature (Cramer & S.D., 1982; Mosavat, 2014; Rumpf et al., 1994). To validate the results and check the

repeatability of experiments, measured solubility values of this study were compared with those measured earlier (Mosavat, 2014) at various pressures and constant temperature of T=40^{o}C. At the same temperature, measured values were also compared with the calculated values from a correlation developed by Duan et al. (2006) .

The comparative evaluation of measured solubility values of this study with others is presented in **Figure 3.7** As it can be observed, measured values of this study are in a good agreement with both measured and calculated values from other researchers. It is noteworthy that quantitative error analysis has not been performed as measured values of (Mosavat, 2014) were at different pressures than those in this study and only trends are compared here. However, there were minimum of ±0.1 to ±2.0% deviation between the measured values of this study compared to the calculated values by (Duan et al., 2006).

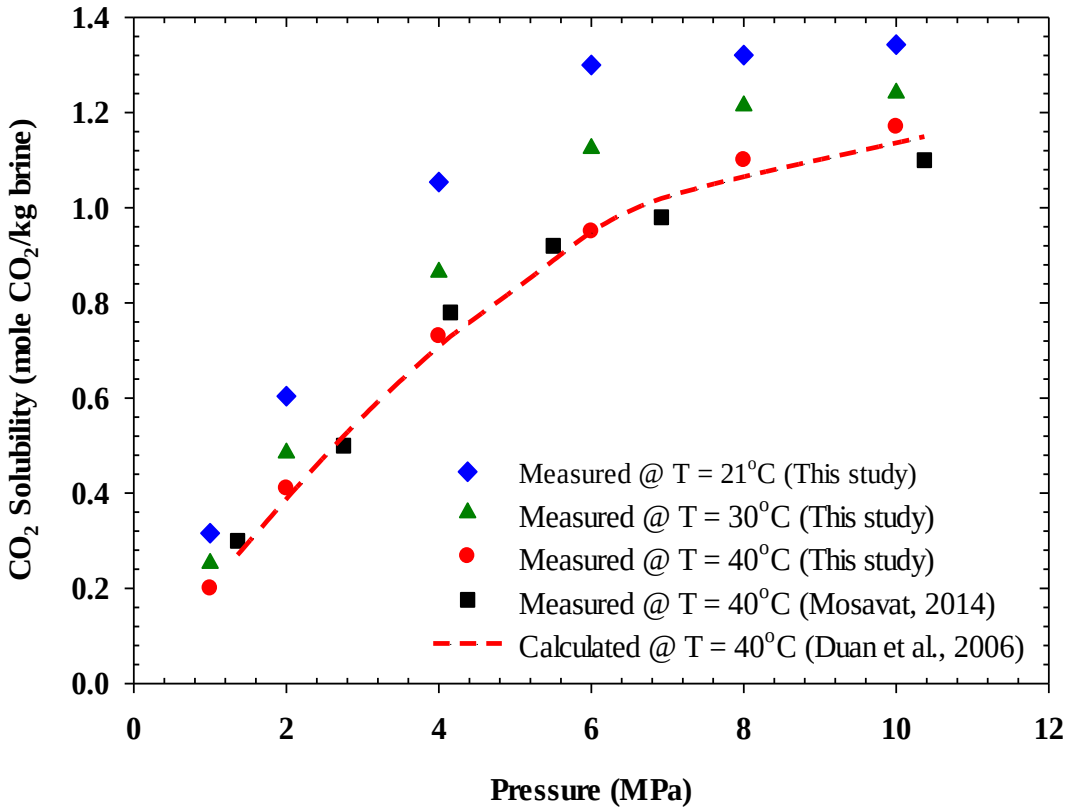

Figure 3.7: Comparison of measured and calculated CO_2 solubility in brine at various pressures and temperatures.

To further investigate the effect of NaCl salinity on the solubility of CO_2 in, three additional solubility tests were conducted at pressure of P=2 MPa and temperatures of T=21°C, 30°C, and 40°C in pure water with no salinity. Pressure of P=2 MPa was arbitrarily selected. **Figure 3.8** shows measured CO_2 solubility in 20,000ppm NaCl solution and fresh water. It became evident that addition of 2.0wt% NaCl to fresh water could decrease the CO_2 solubility in in the water by 8-12% at various temperatures.

Another important fact about CWF is its contribution to the improvement of permeability of the reservoir by dissolution of the formation rock. When CO_2 is dissolved in the water, it forms carbonic acid per the following chemical reaction.

$$CO_2 (aq) + H_2O \leftrightarrow H_2CO_3 (aq)$$

Although only a small portion of CO_2 reacts with water to form carbonic acid, the generated acid may have pH of 5.65 or lower. When CW is injected into the oil reservoir, formation rocks such as “limestone” and at much slower rate “dolomite” can be dissolved. Limestone and dolomite can be found in both carbonate and sandstone reservoirs. The dissolution of these types of rocks in carbonic acid during CWF improves the permeability of the reservoir particularly in the vicinity of the injection wells.

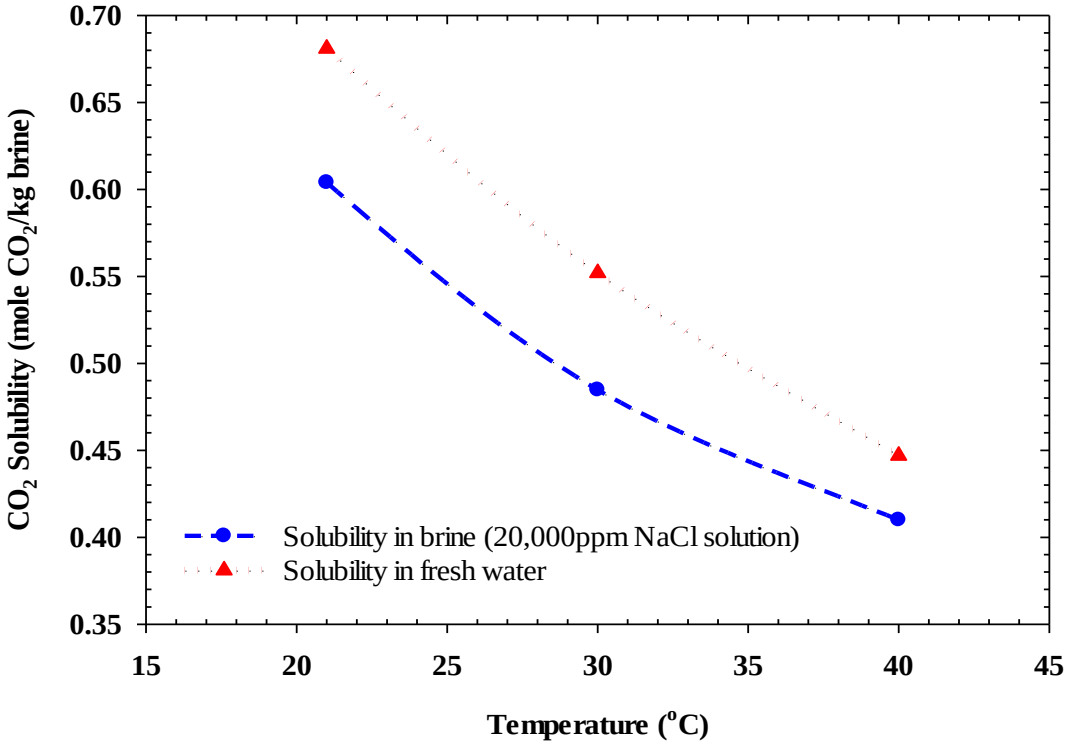

Figure 3.8: CO_2 Solubility in pure water and 20,000ppm NaCl solution at P = 2 MPa and experimental temperatures of this study.

3.3. CO_2–oil system

3.3.1. CO_2 solubility, oil swelling, and viscosity and density variation

CO_2 solubility in oil

Solubility is defined as the amount of solute dissolved in a solvent. It can be expressed in the units of volume of solute per volume of solvent (e.g. mL of solute/L of solvent), mass of solute per mass of solvent (e.g., gr of solute/ kg of solvent), mole fraction, etc.

As discussed before, solubility, oil swelling, and viscosity reduction are three main mechanisms contributing CWF's performance. All of these parameters are strongly dependent on the injected and inplace fluids' properties, and operating conditions. As an example, CO_2 solubility is decreasing when saturation pressure decreased at a constant temperature or when temperature increased at a constant pressure. Similarly, when oil API gravity decreased or viscosity increased, solubility of CO_2 in the crude oil also decreased.(Costa et al., 2012; Jamaluddin et al., 1991; Simon & Graue, 1965; Srivastava et al., 1995). Review of shows that other than in the case of miscible displacement process, CO_2 must be injected in the gas phase and below its dew point pressure. (Emera & Sarma, 2007; Yang & Gu, 2006).

Although there are number of suggested correlations for calculating CO_2 solubility in the crude oil, some of them are limited to a specific range of pressure, temperature, or API gravity of the crude oil (Chung et al., 1988; Emera & Sarma, 2007; Mehrotra & Svrcek, 1982; Simon & Graue, 1965; Welker, 1963). In this study, solubility of CO_2 was measured for both types of oil samples used and compared with the predicted values of one of the most recent correlations developed (Emera & Sarma, 2007). **Figure 3.9** and **3.10** are

showing calculated values of CO_2 solubility at various temperatures and pressures within this study's range for crude oil Type-I and II used in this study, respectively. Both of these figures confirm that CO_2 solubility increases with pressure and decreases with increase in temperature. As it can be observed, calculated values of CO_2 solubility in Type-I (API=20.44) and II (15.49) crude oils at maximum pressure of P=3.5 MPa and base temperature of T=21^{o}C, are 9.5 and 7.5 (gr/100grms) indicting the significant effect of the oil API gravity.

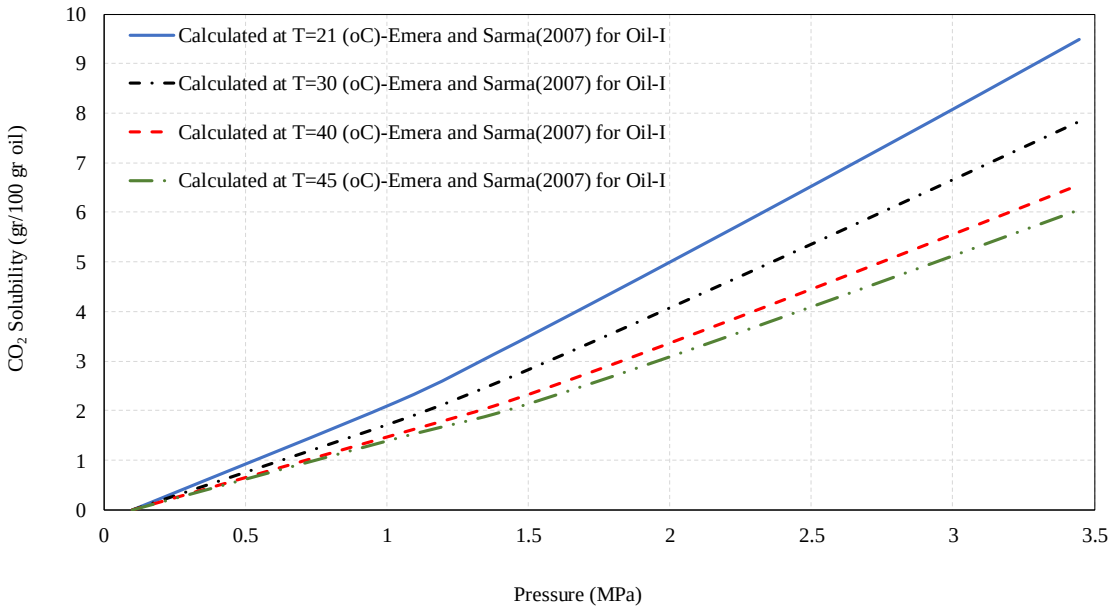

Figure 3.9: Calculated values of CO_2 solubility in Type-I (^oAPI=20.44) crude oil for the pressure range of P_{sat}=0.0 to 3.5 MPa (absolute) and various temperatures using correlation (Emera & Sarma, 2007).

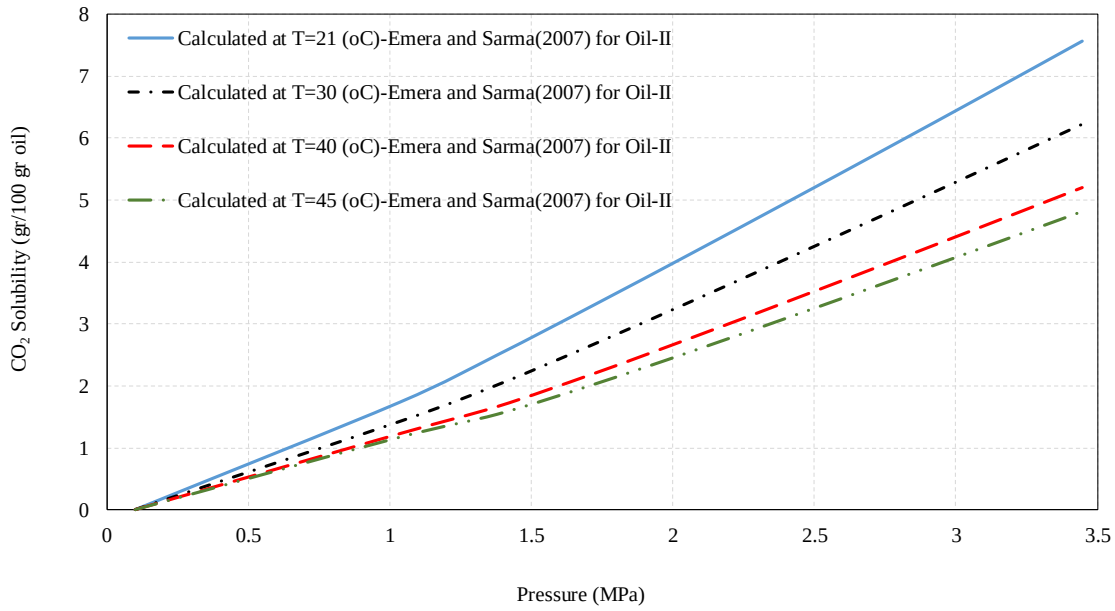

Figure 3.10: Calculated values of CO_2 solubility in Type-II (API=15.49) crude oil for the pressure range of P_{sat} =0.0 to 3.5 MPa (absolute) and various temperatures using correlation (Emera & Sarma, 2007).

Oil swelling factor

It is believed that when a gas molecule is dissolved in an oil globule, volume of oil is increased. This phenomenon is expressed as swelling factor (SF). Increase in volume of oil due to gas injection causes oil saturation to be increased, hence, displacement of oil by injected fluid will be more efficient. In order to determine the swelling factor of a crude oil sample, its saturated volume (with a specific gas) at desired pressure and temperature must be measured and divided by the original volume of the oil sample at atmospheric pressure and same temperature. This relationship can be mathematically expressed as Equation 3.3.

$$SF = \frac{Gas\ Saturated\ \ Oil\ Volume\left(P_R, T_R\right)}{Original\ \ Gas\ Free\ Oil\ Volume\left(P_{atm}, T_R\right)} \qquad \text{Equation (3.3)}$$

Same as solubility, swelling factor can be also determined using developed correlations (Emera & Sarma, 2007; Sankur et al., 1986; Simon & Graue, 1965; Welker, 1963). In this study, CO_2 solubility and oil swelling factor were measured during the same tests for both types of crude oil samples at various temperatures and pressures. Results were also compared with those calculated using correlations developed by Emera & Sarma (2007) at the temperature of T=30^{o}C and various pressures in the range of this study.

Oil viscosity changes

When CO_2 is dissolved in the crude oil, viscosity of the oil is substantially decreased. In this study, CO_2 saturated oil viscosity as a function of mole fraction of dissolved CO_2 is determined using correlations (Beggs & Robinson, 1975) and presented in **Figure 3.11**. As it can be seen from **Figure 3.11**, oil viscosity of both types of crude oil samples were reduced to one fifth of their original oil viscosity when subjected to the

dissolution of 10% by mole of CO_2.Recution of oil-CO_2 mixture viscosity is particularly more pronounced at lower temperatures.

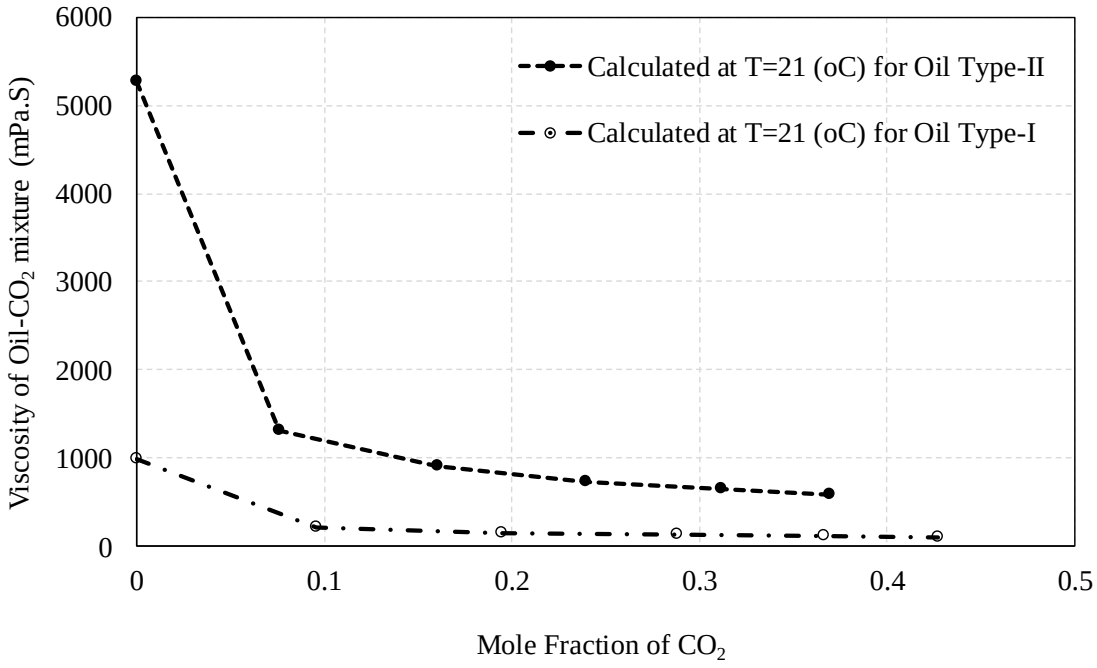

Figure 3.11: Calculated values of oil-CO_2 mixture viscosity as a function of CO_2 concentration (mole fraction) at temperature of T=21^{o}C using correlation (Beggs & Robinson, 1975).

Oil density variation

Figure 3.12 Shows density variations of oil-CO_2 mixture of both types of crude oils calculated by a correlation developed by Emera & Sarma (2007). Their developed correlation (Eq. 3.4) is the result of genetic algorithm's application.

$$\rho = \rho_i + 0.0008y + 0.0008y^{0.157} \qquad \text{Equation (3.4)}$$

Where y is:

$$y = \gamma \frac{(P_s - 14.7)}{T} \qquad \text{Equation (3.5)}$$

In the above equations, ρ and ρ_i are oil-CO_2 mixture, and initial oil densities in gr/mL, respectively. Also, P_{sat} and T are saturation pressure and temperature in Psia and ^oF, respectively.

As shown in **Figure 3.12**, oil-CO_2 mixture density for both types of oil are increasing as mole fraction of CO_2 increased. However, the maximum increase of oil-CO_2 mixture density is less than 0.5% for both oils which is happening at the pressure of P=3.5 MPa (CO_2 mole fractions of around 0.4%). It is speculated that increase in density of mixtures of oil and CO_2 are either within the error of the correlations or mainly because of the effect of pressure on the oil compressibility factor. Regardless, changes in the oil density for mixtures of oil and carbon dioxide are considered negligible in this study.

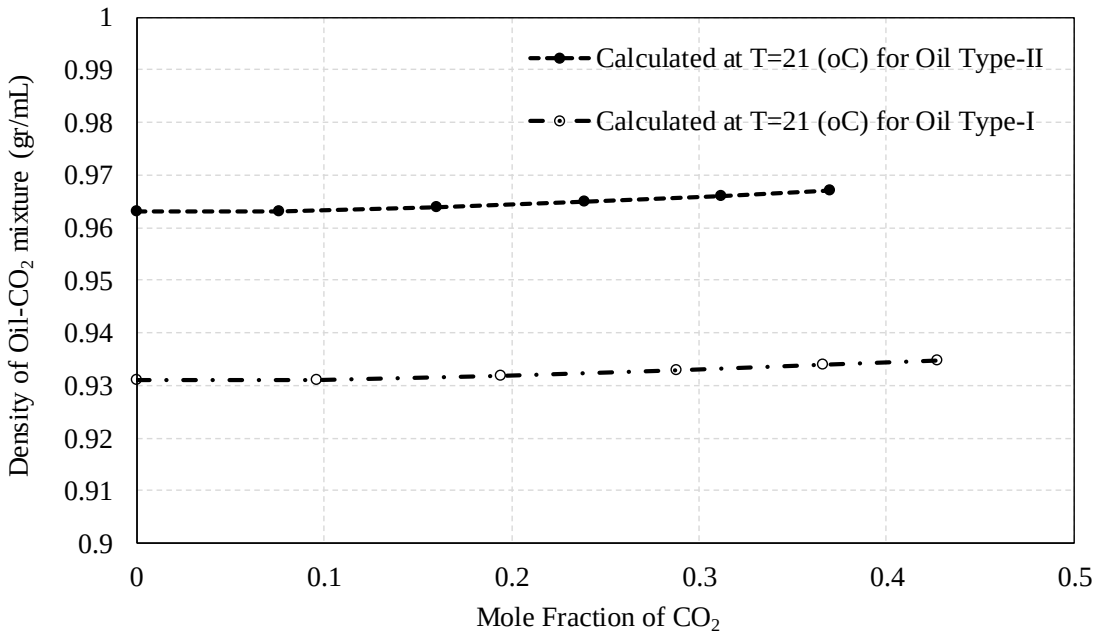

Figure 3.12: Calculated values of saturated oil-CO_2 mixture density as a function of CO_2 concentration (mole fraction) at temperature of T=21^{o}C using correlation of Emera & Sarma (2007).

3.3.2. CO_2 solubility measurements in two crude oil samples

Experimental setup and procedure for CO_2 solubility measurements in oils

Figure 3.13 depicts the schematic diagram of the experimental setup used for measuring the CO_2 solubility in the two crude oil samples of this study. Experimental setup consists of a high-pressure (HP) and high-temperature (HT) visual cell (AR Machinery), a separate rocking cell with heating jacket, computer-controlled Agilent pump (1200 series), a digital pressure gauge (Heise Inc), a high-pressure CO_2 cylinder (99.99% purity), and a high-pressure gas transfer cell, all placed in a temperature-controlled oven.

Visual cell was charged with an initial volume of 10 cm^3 of crude oil through its bottom injection port. CO_2 was then injected at the top at the desired pressure and allowed to diffuse and dissolve in the oil while maintained at the desired temperature and stirred using a mechanical rocking cell. To eliminate the vaporization of some fractions of the oil into the CO_2 phase existing in the transfer cell, CO_2 source was shut-in every time visual cell reached the desired pressure and opened to increase the pressure if needed. Mixture was allowed to reach equilibrium until no more pressure drop was observed. This processes sometimes was taking 5-7 days. At equilibrium state, initial pressure (P_i), final pressure (P_f), initial and final volumes of oil in the visual cell (V_{oi} and V_{of}), and initial and final volumes of CO_2 in both the visual cell ($V_{CO2,i}$ and $V_{CO2,f}$) and transfer cells were carefully recorded.

Using aforementioned data and Equations 3.6 To 3.8 (Abedini et al., 2014; Mosavat, 2014), CO_2 solubility in terms of grams of CO_2 in 100 grams of the crude oil was determined at various temperatures and saturation pressures.

$$m_{dis} = m_{CO_2,i} - m_{CO_2,f}$$
$$= \left(\frac{PV_{CO_2}M_{CO_2}}{ZRT}\right)_i - \left(\frac{PV_{CO_2}M_{CO_2}}{ZRT}\right)_f \quad \text{.....Equation (3.6)}$$
$$= \frac{M_{CO_2}}{RT}\left[\left(\frac{PV_{CO_2}}{Z}\right)_i - \left(\frac{PV_{CO_2}}{Z}\right)_f\right]$$

$$m_{oil} = \left(\rho_o V_{o,i}\right)_{@T_{exp}} \quad \text{..... Equation (3.7)}$$

$$\chi_{CO_2} = \frac{m_{dis}}{m_{oil}} \times 100$$
$$= \frac{M_{CO_2}}{RT\rho_{oil}V_{o,i}}\left[\left(\frac{PV_{CO_2}}{Z}\right)_i - \left(\frac{PV_{CO_2}}{Z}\right)_f\right] \quad \text{..... Equation (3.8)}$$

It is noteworthy that measurement tests conducted at higher temperatures or pressures were the continuation of the previous tests and there was no need to completely terminate the previous process and start from the beginning.

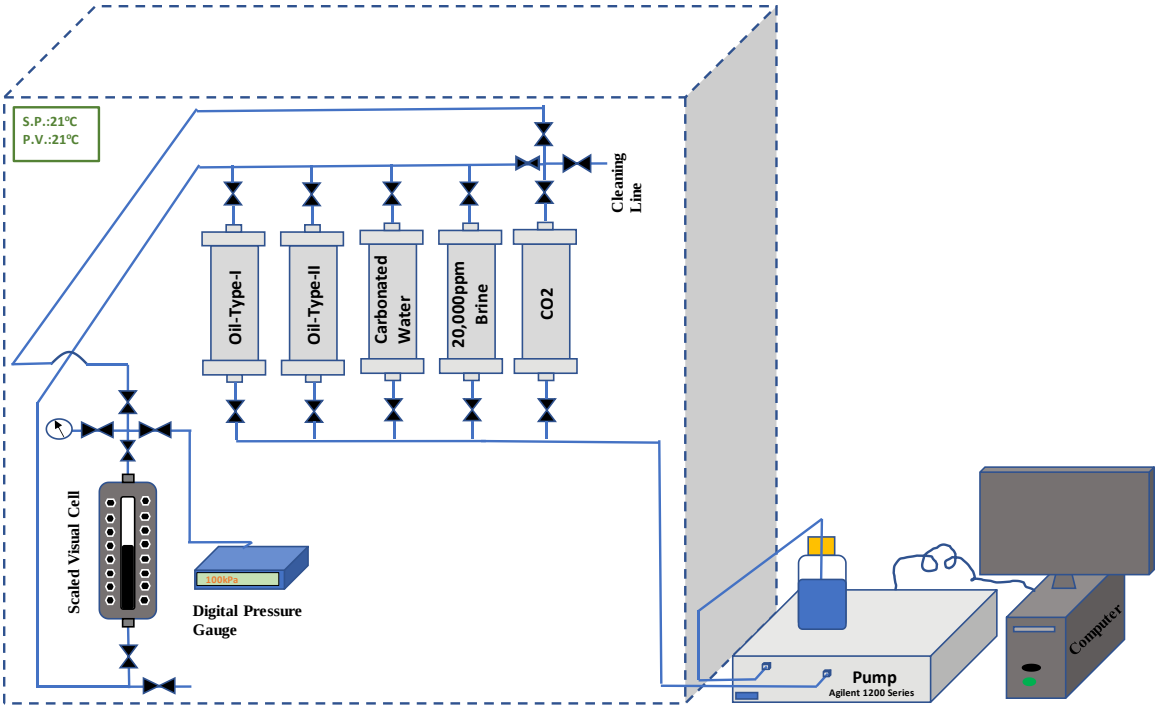

Figure 3.13: Schematic diagram of the experimental setup for measuring solubility of CO_2 in two crude oil samples (Type-I, °API=20.44 and Type-II, °API=15.49) at various pressures and constant temperatures of T = 21 °C,30 °C, 40 °C and 45 °C.

Results of CO_2 solubility tests in two crude oil samples

CO_2 solubility tests were conducted at five different pressures and four different temperatures for two types of crude oil samples used in this study. All test pressures and temperatures were selected to cover the range of core flooding and micromodel displacement tests of this research. **Figure 3.14, and 3.15** show values of measured solubility at different pressures and temperatures for crude oil Type-I and Type-II, respectively. As it can be seen from both figures, CO_2 solubility increased when saturation pressure increased. However, increasing temperature results in decreasing solubility of CO_2 in the crude oil. As an example, at a saturation pressure of about $P_{sat.}$ = 3.5 MPa, CO_2 solubility reduces from χ_b = 10.13 gr CO_2/100 gr of oil to χ_b = 5.72 gr CO_2/100 gr of oil for crude oil Type-I when temperature is increased from T = 21 °C to 45 °C. For Type-II oil this reduction is from χ_b = 7.84 gr CO_2/100 gr of oil to χ_b = 4.43 gr CO_2/100 gr of oil when experimental temperature increased from T = 21 °C to 45 °C.

Also, at the same temperature and pressure, CO_2 solubility in the heavier crude oil (Type-II with ^{o}API=15.49) is less than its value in the Type-I heavy oil (^{o}API=20.44). As an example, comparing values of solubility in two crude oil samples at T=21^{o}C and P_{sat}=3.5 MPa show that CO_2 solubility is χ_b = 10.13 gr CO_2/100 gr of oil and χ_b = 7.84 gr CO_2/100 gr, for Type-I and II crude oils, respectively. This corresponds to a reduction of over 22.6% which is due to the reduction in oil API gravity.

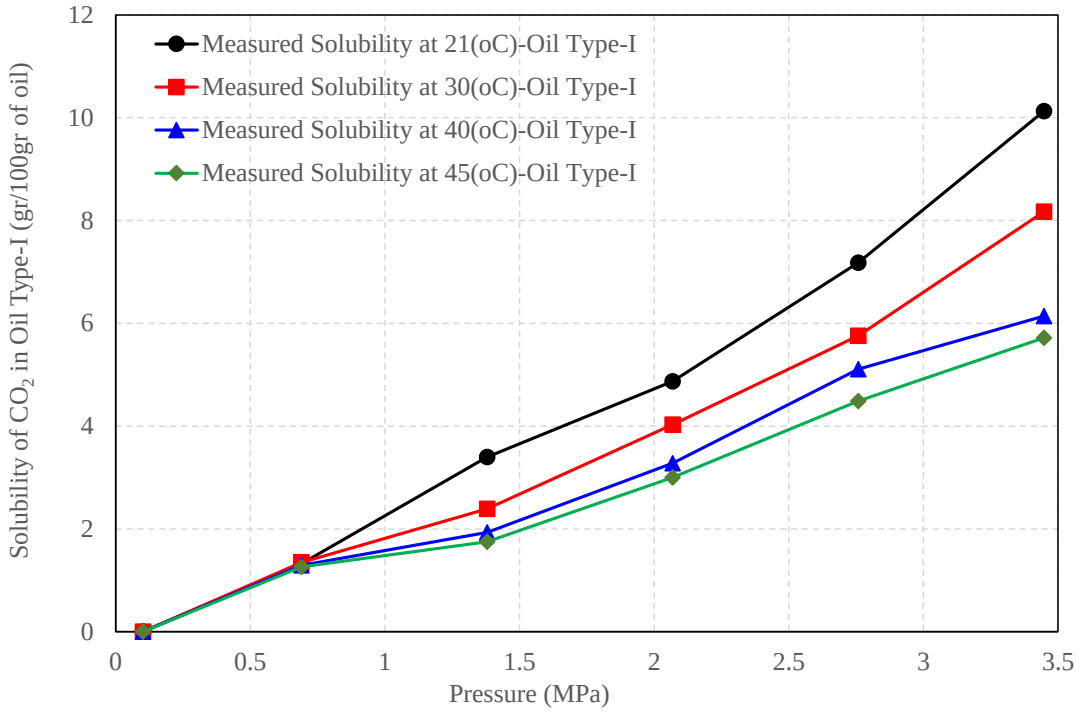

Figure 3.14: Measured solubility for CO_2–crude oil (Type-I, ^{o}API=20.44) mixture at various pressures and constant temperatures of T =21°C, 25 °C,30 °C and 45 °C.

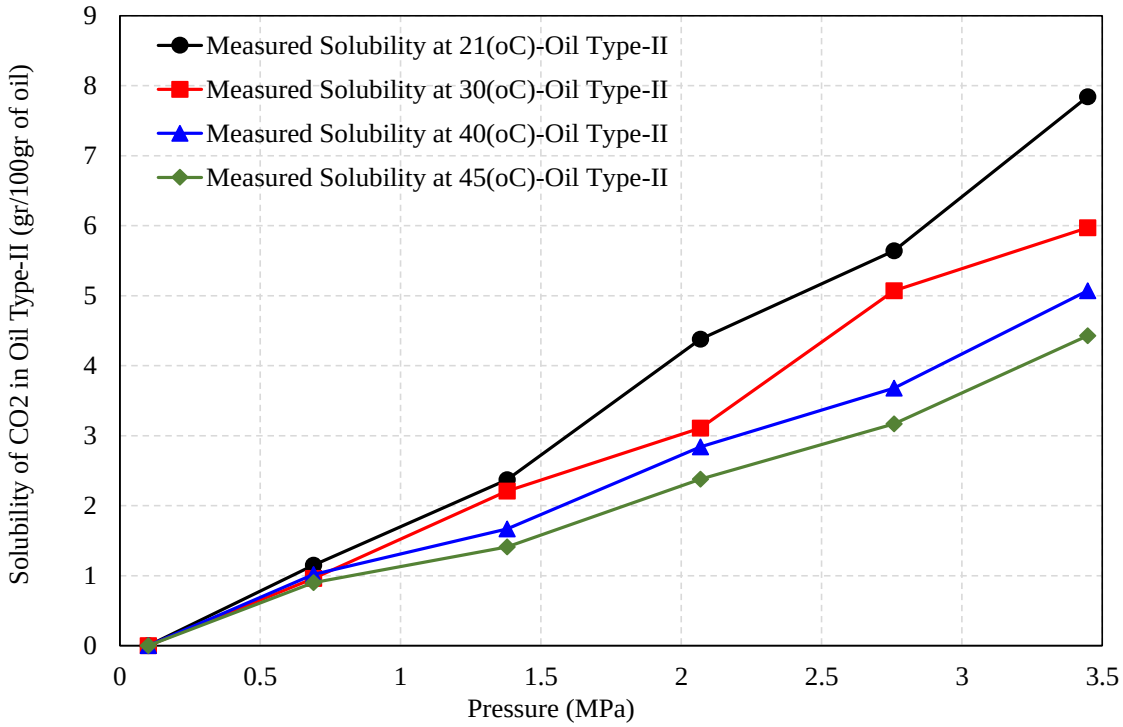

Figure 3.15: Measured solubility for CO_2–crude oil (Type-II, ^{o}API=15.49) mixture at various pressures and constant temperatures of T =21°C, 25 °C,30 °C and 45 °C.

The developed correlation of Emera and Sarma (2007) is also used to calculate CO_2 solubility values for the range of pressure and temperature of this study. **Figure 3.16** compares measured and calculated CO_2 solubility values in both types of crude oil samples as a function of saturation pressure and at the temperature of T=30^{o}C. Although measured and calculated CO_2 solubility trends are consistent and within a maximum deviation of 10%, it became evident that calculated values are lower for heavier oil (Type-II) while higher for the heavy oil (Type-I).

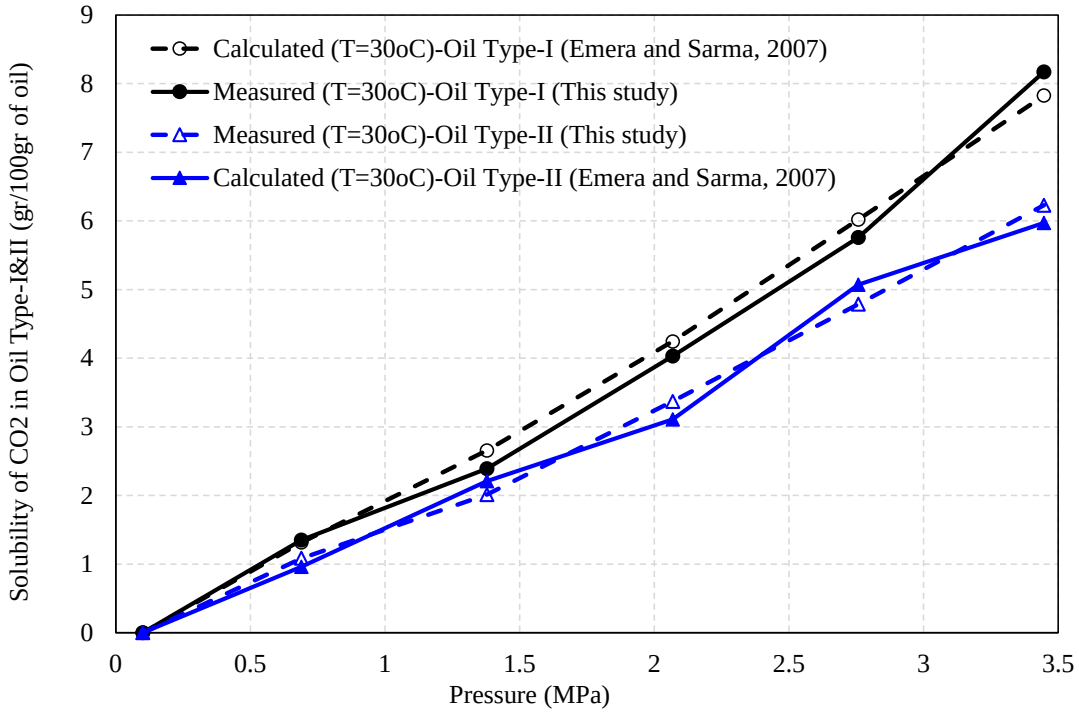

Figure 3.16: Measured solubility for CO_2–crude oil (Type-I, ^{o}API=20.44 and Type-II, ^{o}API=15.49) with calculated values from Emera and Sarma (2007) at various pressures and constant temperature of T = 30 °C.

3.3.3. Oil swelling tests

In order to determine the swelling factor (SF), initial (CO_2-free dead oil) and final (CO_2-saturated oil) height of crude oil before and after the visual cell charged with the CO_2 were carefully measured using a fine-scaled ruler at each experimental pressure and temperature. Heights were converted to volumes and SF values were determined using Equation 3.9.

$$SF = \frac{V_{o,f}\left(P_S, T_{Exp.}\right)}{V_{o,i}\left(P_{atm}, T_{Exp.}\right)} \quad \text{.....Equation (3.9)}$$

Figures 3.17 and **3.18** are showing SF values measured at various experimental pressures and temperatures for two types of crude oils used in this study. At atmospheric pressure, ratio of the initial volume to the final volume is equal to one, indicating no swelling effect as there is no dissolved gas in the oil.

As it can be seen from the figures, maximum values of 1.079 and 1.052 of oil swelling factor were achieved at pressure of P_{sat}=3.45 MPa and temperature of T=21^{o}C for Type-I (^{o}API=20.44) and Type- II (^{o}API=15.49) crude oils, respectively. This can be translated to about 34% reduction in oil swelling due to 5 degrees of reduction in crude oil API gravity.

Also, when values of swelling factor were compared at different experimental temperatures, it was calculated that swelling factor decreased from 1.079 to 1.037 for oil Type-I when temperature increased from T=21^{o}C to T=45^{o}C at constant pressure of P_{sat}=3.45 MPa. At the same temperature and pressure, the decrease was from 1.052 to 1.028, for Type-II crude oil. Therefore, reductions due to 24^{o}C increase in temperature at

a constant pressure of P_{sat}=3.45 MPa were 53% and 46% for crude oils Type-I and II, respectively.

As mentioned earlier, there are limited number of correlations available in the literature to estimate swelling factor (Emera & Sarma, 2007; Simon & Graue, 1965; Welker, 1963). (Welker, 1963) is limited to the temperature of T=80^{o}C and (Simon & Graue, 1965) is a graphical correlation. Emera & Sarma (2007) used a series of data and developed a simple correlation based on genetic algorithm as presented in Equations 3.10 to 3.12.

$$SF = 1 + 0.3302Y - 0.8417Y^2 + 1.5804Y^3 - 1.074Y^4 - 0.0318Y^5 + 0.21755Y^6 \quad \text{for } MW_o \geq 300 \qquad \text{Equation (3.10)}$$

and

$$SF = 1 + 0.48411Y - 0.9928Y^2 + 1.6019Y^3 - 1.2773Y^4 + 0.48267Y^5 - 0.06671Y^6 \quad \text{for } MW_o < 300 \qquad \text{Equation (3.11)}$$

Where:

$$Y = 1000\left(\frac{\gamma}{MW_o}{\chi_{CO2}}^2\right)^{exp(\gamma/MW_o)} \qquad \text{Equation (3.12)}$$

and χ_{CO2} $is\ in\ mole\ fraction$

For the comparison purpose only, values of SF were also calculated using Emera & Sarma (2007)at the temperature of T=30^{o}C and all experimental saturation pressures. For both types of crude oils and presented in **Figure 3.19**. Calculated and measured values were substantially deviating from each other particularly at higher pressures indicating poor estimation of the correlation for these two oil samples. As an example, the deviations were by about 36% and 30% at the maximum saturation pressure of P_{sat}=3.45 MPa for Type-I and Type-II crude oil samples, respectively.

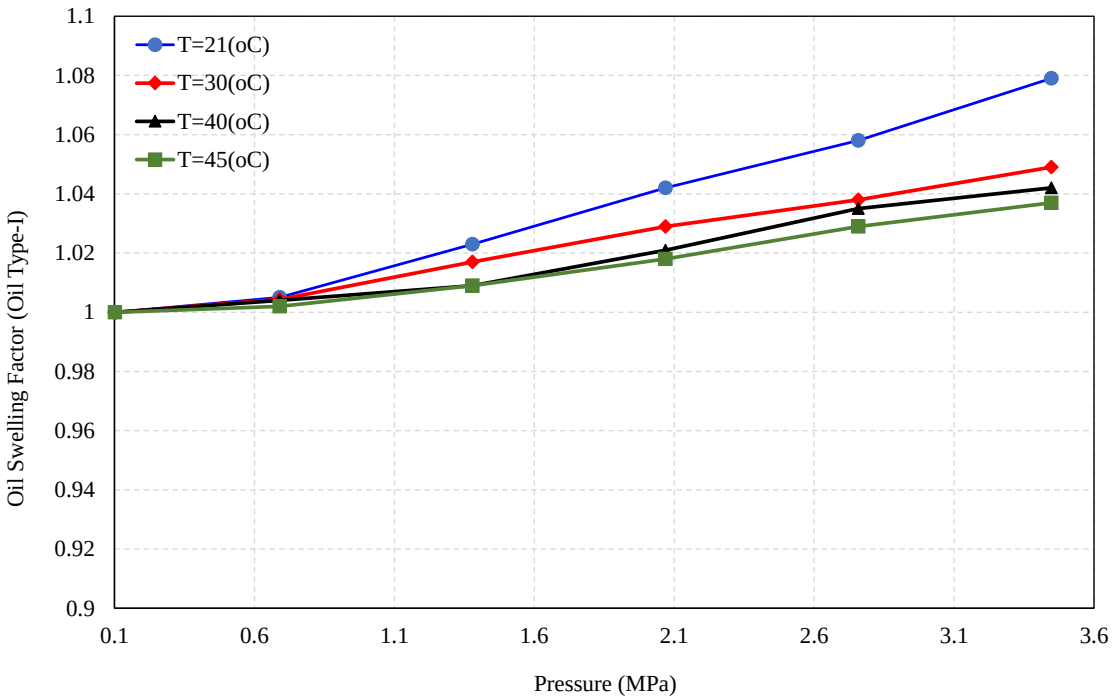

Figure 3.17: Measured oil swelling factor of the crude oil–CO_2 system (Type-I) versus equilibrium pressure at various experimental temperatures.

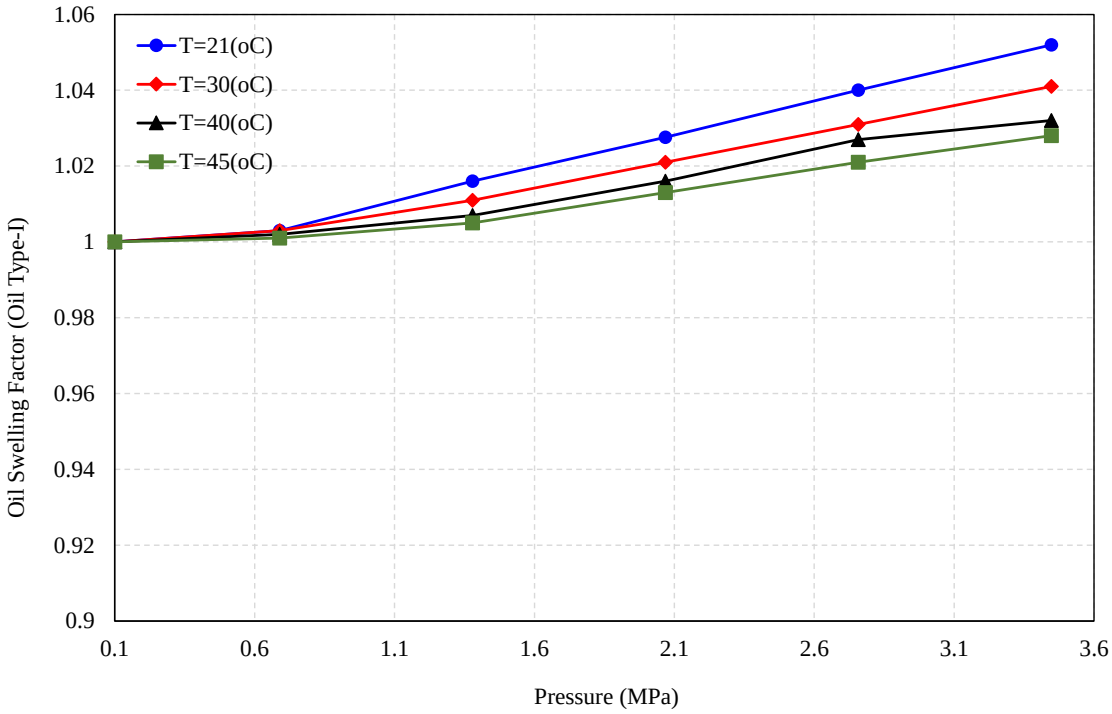

Figure 3.18: Measured oil swelling factor of the crude oil–CO_2 system (Type-II) versus equilibrium pressure at various experimental temperatures.

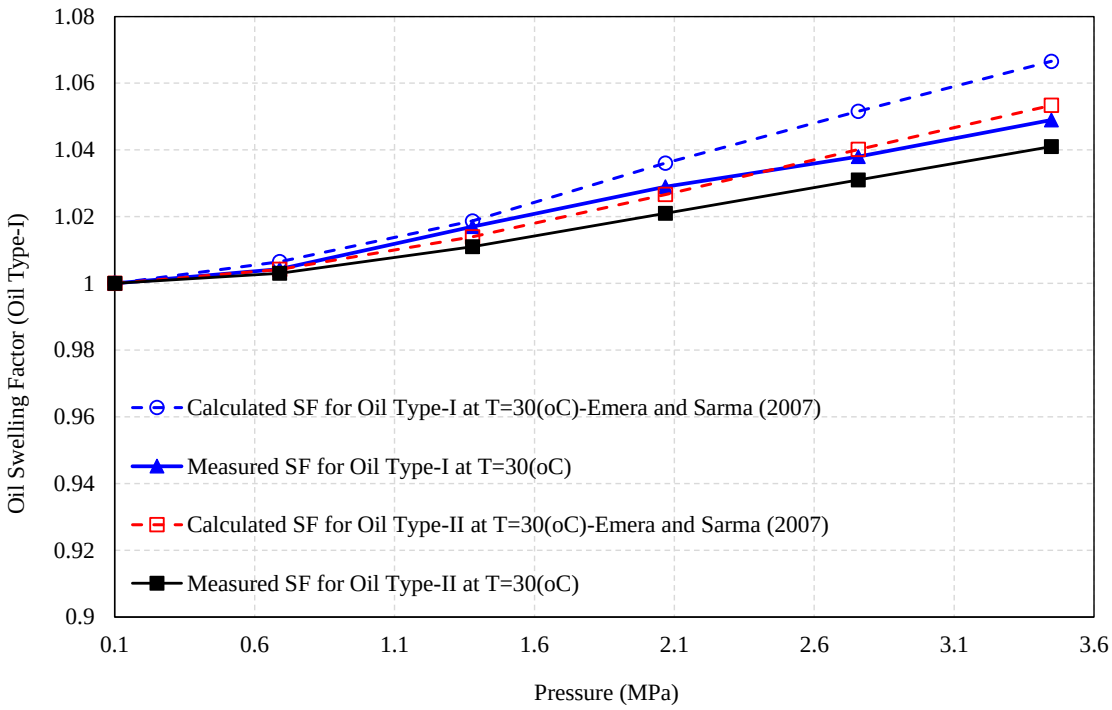

Figure 3.19: Measured oil swelling factor of the crude oil–CO_2 system versus equilibrium pressure at various experimental temperatures.

3.4. Chapter summary

Phase behavior study is an essential part of investigating the applicability and evaluating the performance of various enhanced oil recovery techniques. Parameters such as solubility of CO_2 in brine solutions and crude oil samples, swelling of crude oil due to the CO_2 dissolution, and variations in oil viscosity and density under various operating conditions are required to analyze the experimental results of coreflooding and to properly simulate and ultimately upscale the experimental findings.

Throughout this chapter, multiple experimental setups were designed and assembled to experimentally measure the values of CO_2 solubility in pure water, brine (20.000ppm) and two heavy oil samples with API gravities of 20.44 and 15.49. In addition, swelling factor resulted from dissolving CO_2 in both types of crude oil samples were determined from the obtained readings of experiments.

It was observed that solubility of CO_2 in water is not only a function of pressure and temperature but also it is depending on the salinity and types of the salts. Addition of 2% by weight of NaCl to deionized water resulted in reduction of CO_2 solubility in the solution. As perhaps expected, increase in temperature caused CO2 solubility reduction in both pure water and brine solutions while pressure increase boosted the CO_2 solubility substantially.

Solubility of CO_2 in the two crude oil samples were also highly depending on the pressure and temperature. Results of the experimental studies of this work showed that CO_2 solubility reduces as temperature increased. Interestingly, this decrease was more pronounced in the case of heavier oil.

Pressure showed opposite effect as CO_2 solubility in crude oil samples were increased when pressure increased. Increase in CO_2 solubility with pressure increase was more remarkable for the oil with higher API gravity.

Increase in crude oil API gravity caused reduction of CO_2 solubility when values were compared at the same temperature and pressure indicating lower diffusion and dissolution of CO_2 in the heavier oil due to the presence of higher amount of heavier components.

Values of oil viscosity and density for CO_2-oil mixtures were determined using available correlations of (Beggs & Robinson, 1975) and (Emera & Sarma, 2007), respectively. It was concluded that the trend of the reduction in the oil viscosity of CO_2-oil mixture as a function of CO_2 solubility are similar for both types of crude oil samples.

In this study, no extraction was observed within the range of temperatures and pressures of experiments. It was speculated that pressure was not sufficiently high and oil API gravities were possibly too low to observe extraction of lighter components into CO_2 phase. Previous studies (Abedini et al., 2014; Mosavat & Torabi, 2013) of the same nature showed an extraction pressure for light crude oil samples when CO_2 pressure was substantially high (e.g., in the range of P_{sat}=6-8 MPa at T=21^{o}C-40^{o}C for an oil with ^{o}API gravity of around 40).

CHAPTER FOUR: Micro-optical analysis of the effect of injection rate, temperature, crude oil viscosity, and dual permeability porous media on the performance of waterflooding

Utilization of micro-models to study the interactions of the fluids, displacement efficiency, and effect of parameters on the performance of various enhanced oil recovery techniques has been of the interest of researchers for many years. The unique capacity of the micro-model that provides the opportunity of visually investigating the processes and mechanisms involved in enhanced oil recovery is the cause of the growing interest and the improvements in manufacturing techniques of them. While the original models of micro-models were etched by acid, normally in a regular pattern, irregular, heterogeneous, and more complex micro-models could be manufactured using laser technology now a day.

In this study, two types of micro-models with different characteristics were utilized to better understand the effect of key parameters such as injection rate, oil viscosity, temperature, and structure of the pore networks on the performance of waterflooding in two heavy oil systems. These micro-models were designed and built to mimic the pore networks of the real porous media containing heavy oils. Furthermore, carbonated waterflooding tests at the temperature of T=21^{o}C and pressure of P=1MPa conducted in the heavy oil saturated micromodels and results were compared with those obtained during waterflooding.

As part of the analysis, breakthrough time (BT), recovery factor at BT and at higher pore volumes (PV) of injection and displacement efficiency in various parts of the porous media were investigated. In addition, effect of dual permeability zones, injection rate

(viscous forces), temperatures, and oil API gravity were evaluated. Overall, more than 26 micro-model tests were conducted and results of 20 tests were included in this report.

4.1. Introduction

Micro-models are considered 2-dimentional (2D) porous media etched on a piece of glass with pore depth of various sizes (e.g. 10^{-5}m) and different pore geometries. Earlier micro-models were etched using fluoric acid by drawing and engraving the desired pattern on a sticky and colored tape or on a polymer surface attached to the glass surface. Glass model was then placed in fluoric acid for certain time period to allow fluoric acid to dissolve the engraved channels. Major issues with micro-models manufactured by this method are uneven depth of the pores, failure of the method in manufacturing in many cases, difficulties in manufacturing micro-models with smaller grains, and health hazards related to the use of fluoric acid.

Chatzis & Dullien (1983) (1983) studied immiscible displacement process in micromodels. Paterson et al. (1984) and Hornof & Morrow (1988) utilized micro-models to study the performance of surfactant flooding. Multi-contact miscibility measurements and studies were conducted in micro-models by many researchers (Armitage & Dawe, 1989; Bahralolom et al., 1988; Campbell & Jr, 1985; Owete & Brigham, 1987). Other researchers investigated the performance of foam injection for EOR in micro-models (Romero et al., 2002).

The most relevant studies to this study conducted in micro-models are reviewed in this study (George et al., 2005; Grattoni & Dawe, 2003; Lago et al., 2002; Riazi, 2011; Sohrabi et al., 2008, 2012; Wang et al., 2006). Micro-models were also used for other types

of studies such as visualization of asphalthene precipitation (Danesh et al., 1988), interfacial tension (Mackay et al., 1998) and foamy oil flow (Bora et al., 2003) as well as investigation of capillary pressure (Smith et al., 2005). Other types of studies are conducted in the micro-models and reported in the literature which are not listed here.

4.2. Fluids

As mentioned in the previous chapter, two oil samples, namely oil Type-I and oil Type-II with API gravities of 20.44 and 15.49 (respectively) were prepared by diluting an original heavy oil with kerosene. Brine sample of 20,000 ppm concentration was made up of deionized water and NaCl salt (2.0 wt.%). Methylene blue with concentration 0.07gr in 1000 grams of water was added to the brine solution so that it become visible in blue color when flows in the micromodel. No significant changes were observed in the density and viscosity of water after dissolving methylene blue and therefore density and viscosity value of the brine were considered to be similar to the original solution.

4.3. Micromodel preparation using laser engraving technology

For this study, the first micromodel containing different flow patterns was manufactured using a high-precision laser machine (Boss Laser, LLC). For this fact, a heterogeneous flow pattern containing irregular-shape grains of various sizes was drawn to be used as the input file (for engraving) by the laser machine. Flow distributors and injection/production ports were added to the flow pattern. The laser machine (Boss Laser, LLC) used was a class-IV equipped with a computer controlled interface (Laser Cut 5.3). Two pieces of glasses with dimensions of 10 cm (W) and 23 cm (L) and thickness (H) of 1.25cm thickness were pre-ordered. One of the two glasses was ordered to have an

inlet/outlet holes with diameters (D) of 0.5 cm, each. Two stainless steel fittings were installed in those holes to be used as injection and production ports during the tests. After careful alignment of the second glass piece (with no holes) on the laser bench, flow pattern including inlet/outlet fluid distribution areas were engraved through a practiced set of laser settings. It is noteworthy that during alignment, it was checked that the inlet/outlet engraved points are exactly matching the two holes on the second glass piece. After engraving was completed, pore throats were carefully checked and cleaned to ensure flow can pass through them.

Two glass pieces were then placed in a programmable furnace where a 3-days procedure for glass fusion was followed. During the fusion process, furnace temperature was increased to a maximum of 690^{o}C.

Some of the specifications of the single permeability micromodel are listed in **Table 4.1**. In addition, histogram of the grain and pore size distributions are presented in **Figure 4.1** and **4.2**, respectively. Photos of single permeability micromodel containing brine solution (blue) and crude oil (black) are shown in **Figure 4.3(a)** and **(b)**.

Table 4.1: Properties of single-perm micromodel used in this study.

Property	**Single-Perm micromodel**
Number of grains	2635
Max throat size	5.049 mm
Min throat size	0.029 mm
Average grain size	0.775 mm^2
Max grain size	3.89 mm^2
Min grain size	0.001 mm^2
Pattern length, cm	123 mm
Pattern width, cm	38 mm
Engraving depth (pre-set), cm	0.0123 cm
Pore area	25.64 cm^2
Pore volume	0.317 cm^3
Porosity	56.0 %

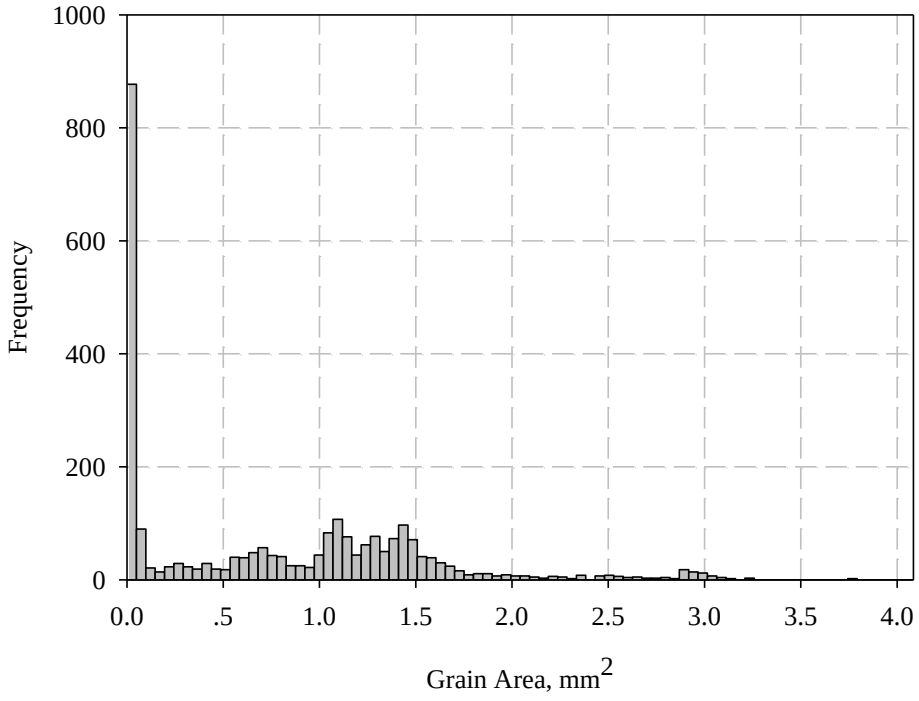

Figure 4.1: Grain size distribution of single permeability micromodel.

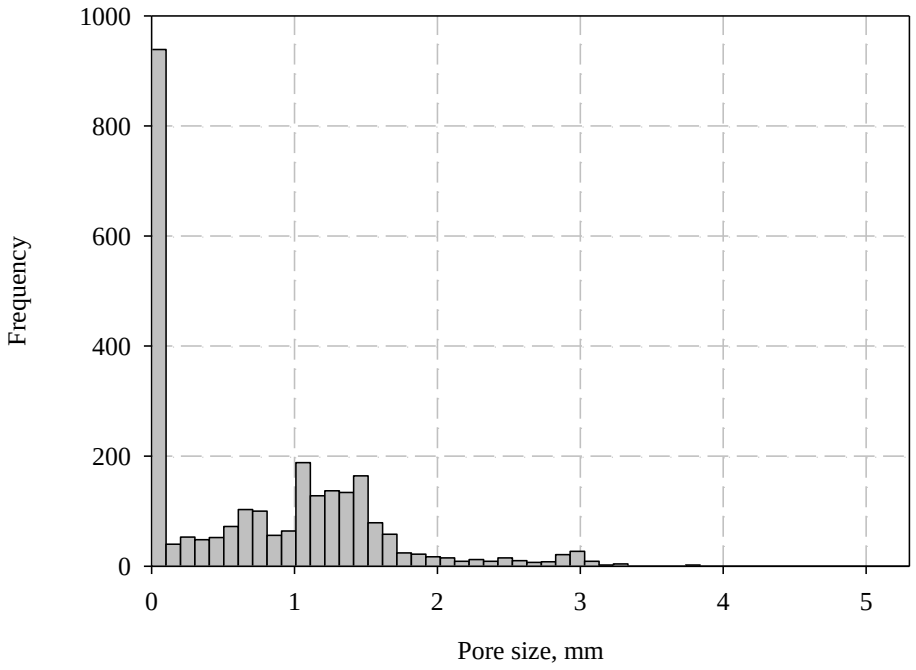

Figure 4.2: Pore size distribution of single permeability micromodel.

(a) Single perm micromodel saturated with brine

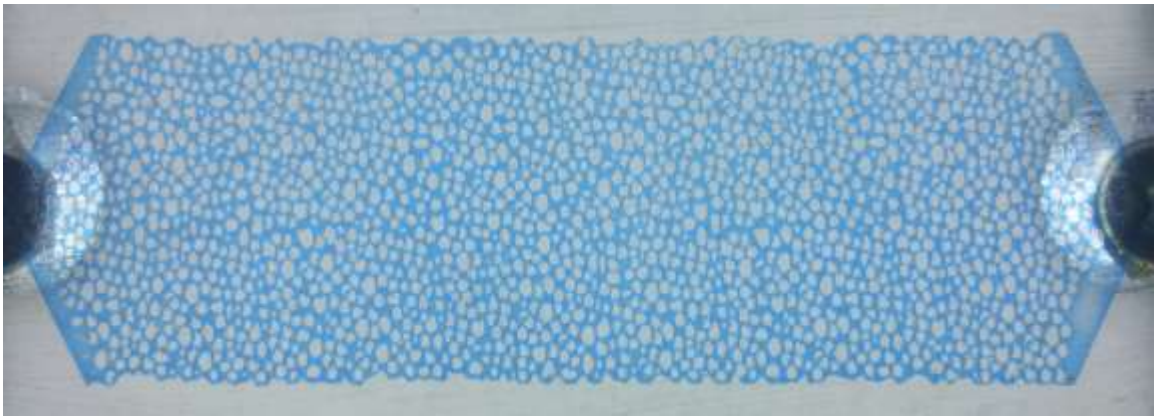

(b) Single-perm micromodel saturated with oil

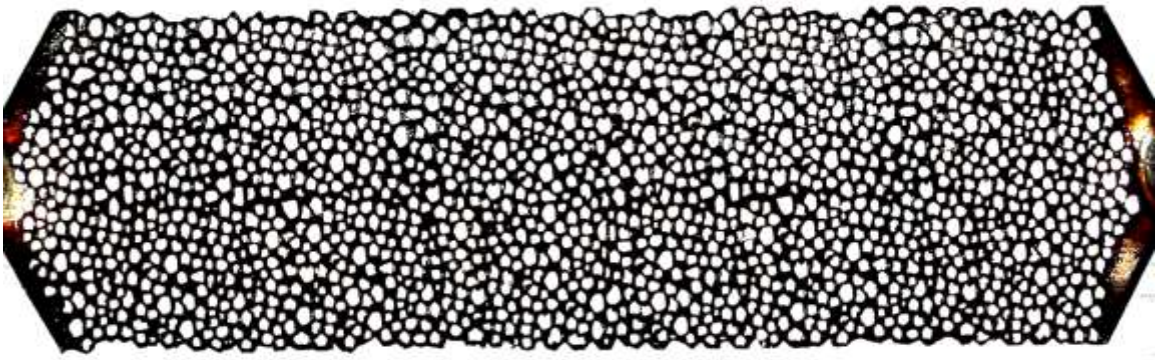

Figure 4.3: Photos of two types of micromodels used in this study, (a) single perm model containing brine, (b) single-perm model containing oil.

4.4. Micro-model flooding tests

4.4.1. Experimental setup

Experimental setup was designed to carry out both waterflooding and carbonated waterflooding tests while flexible for cleaning and preparation. The main components of the experimental setup for waterflooding were a temperature-controlled oven, a computer-controlled Agilent pump (1200 series from Agilent Comp.), three transfer cylinders (with displacement piston) for two types of crude oils and brine solution, a computer, high pressure gauges, a back-pressure-regulator (Equilibar, 2500 series), micromodel, LED light source with a light-filter (placed between the light and micromodel), a high-resolution camera (Canon, Rebel i4), a nitrogen cylinder with pressure regulator, a production cup and many high pressure stainless steel valves and fittings (Swagelok). A schematic diagram of the experimental setup for micro-model tests is depicted in **Figure 4.4**.

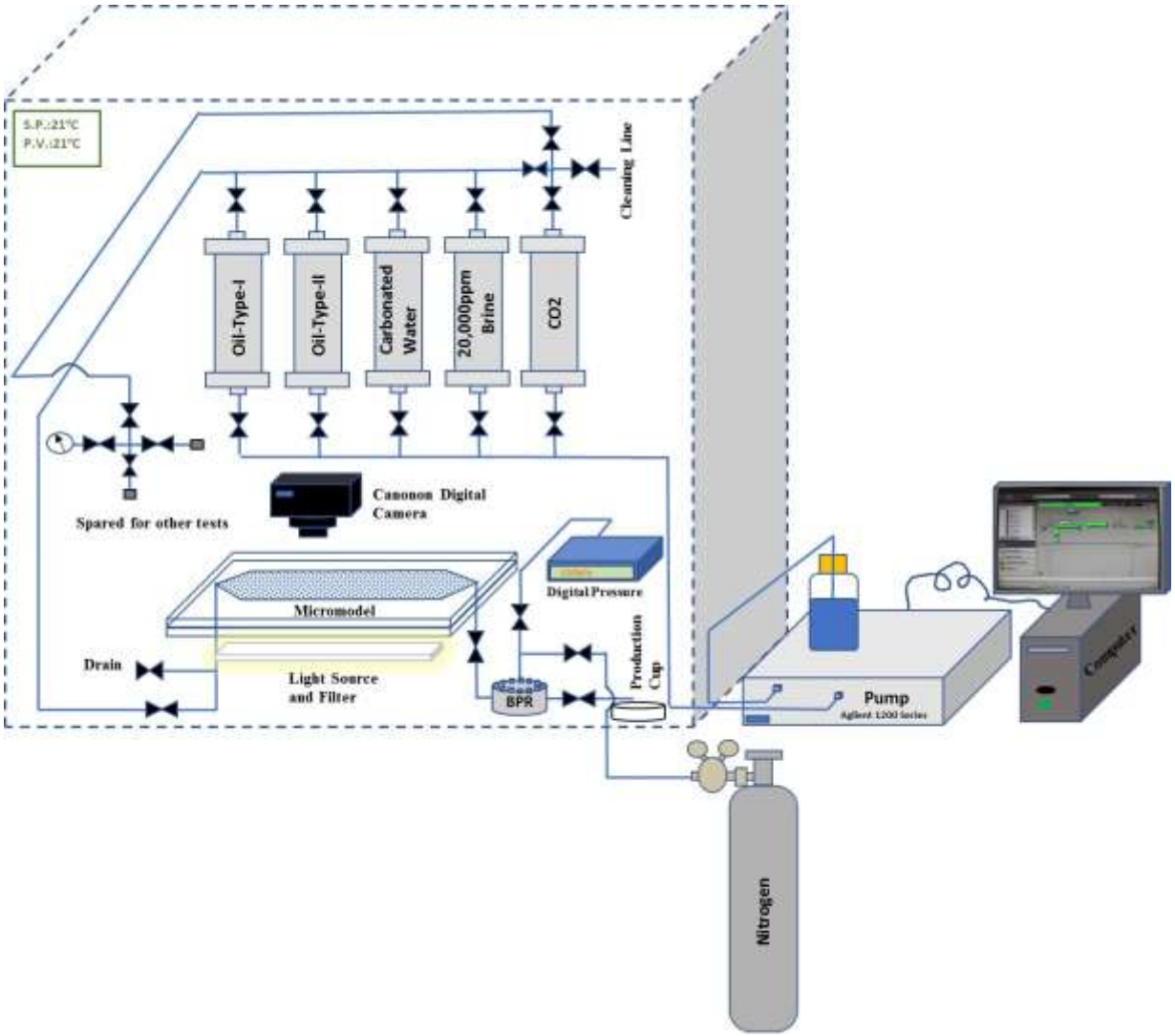

Figure 4.4: Schematic diagram of the micro-model experimental setup used in this study.

4.4.2. Experimental procedure

To perform waterflooding and later carbonated waterflooding tests, transfer cylinder and all connections and fittings were tested for leakage. Cylinders were charged with fluids (two heavy crude oils and brine solution) and tagged properly. Using a nitrogen cylinder, 1MPa pressure was applied to the top of the BPR. All flow lines were cleaned and brine solution was allowed to flow out of a drain near the micromodel under a pressure of P=1.01 MPa. Micromodel was then vacuumed for 2 hrs and saturated with brine. Amounts of injected and produced brine were carefully measured to evaluate the pore volume of the micromodel. Overall, about 10 PV of brine was injected to ensure maximum saturation is achieved.

Crude oil Type-I (^{o}API=20.44) was injected into the micromodel at the flow rate of 0.025 cm^3/min. During oil injection, significant increase in injection pressure was observed. As micromodels used in this study were only suitable for pressures up to P=4 MPa, injection rate was sometimes adjusted to avoid breaking them. About 5 PV of crude oil was injected while saturation process was visually observed and recorded.

After saturation was completed, all flow lines were cleaned using kerosene and alcohol followed by large volume of brine solution. This was done to reduce the time required for the displacement of the oil through the micromodel during waterflooding and to avoid leaving oil in the flow lines which might flow into the micromodel at some stages during the flooding process.

Waterflooding tests were then begin at the desired experimental temperature and pressure and at various injection rates. During flooding tests, the entire process was recorded on a high-resolution camera.

After a test was completed and no more oil is produced from the production port, test was terminated and setup was cleaned for the next test.

4.4.3. Method of analysis

Since micromodels have very small pore volumes (e.g. 0.3-0.4 cm^3), it is very difficult to perform quantitative measurements during the tests. Therefore, both qualitative analysis of the displacement of oil by injected fluid and quantitative analysis of the recovery performance were conducted using image analysis technique (MATLAB). Image analysis allow identifying and analyzing numerous mechanisms and phenomenon such as: multiphase flow, oil trapping, wettability nature of the medium, interactions of injected and inplace fluids (if existing), etc.

The major issue with image analysis is the time required for analysis of each test. This method requires taking photos at various time frames and whenever changes are happening and then convert the colors of the fluids into the numbers that software can read them. Because of various shades and saturations of colors, it takes a long time to processes each frame. Therefore, a short program code was prepared to convert the frames into the recognizable format by MATLAB so that displaced and remaining volumes of the oil could be determined. As an example, **Figure 4.5** shows the original and converted files of one of oil displacement process by water.

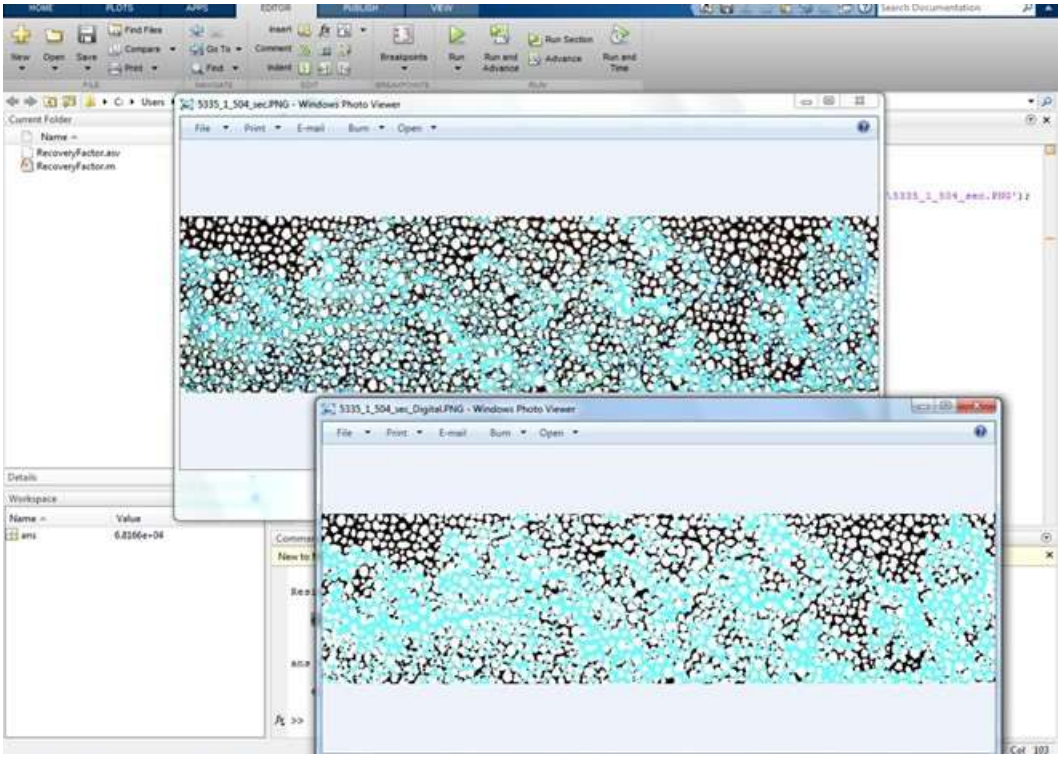

Figure 4.5: Original (top) and digitalized/converted (bottom) pictures of water displacing oil from micromodel by MATLAB software.

4.5. Experimental results and discussion

Although some studies were conducted by previous researchers to investigate the performance of waterflooding an carbonated waterflooding in micromodels (Mosavat & Torabi, 2014; Riazi, 2011; Sohrabi et al., 2008), most of those studies focused on the light oil systems. As mentioned earlier, the main objective of this study was to perform micro optical analysis of heavy oil displacement process by both water and carbonated water and investigate the effect of various parameters such as temperature, injection rate and heavy oil viscosity on the displacement efficiency of oil by water. In addition, inclusion of a secondary porous medium (dual permeability) which has not been investigated at the scale of this research is another contribution of this study.

4.5.1. Waterflooding of heavy oil (^{o}API=20.44) saturated micromodel-constructing a base case

To construct a base case for comparing other cases with it, micromodel was saturated with Type-I crude oil (^{o}API=20.44) and displaced with brine at an injection rate of q_{inj} = 0.05 cm^3/min. During the displacement processes, temperature was kept constant at T=21^{o}C and back pressure regulator was set at P_{BPR}=1 MPa. The displacement process of oil by injected water was recorded on camera for image analysis.

Figure 4.6(a) and **4.6(b)** illustrates the fully saturated micromodel and pore area considered for image analysis.

Displacement of oil by injected water at various time frames including the breakthrough time, t_{BT} is presented in **Figure 4.7**. As it can be observed in Figure 4.7 (c) breakthrough time of t_{BT}=112 *seconds* was observed for the base case.

(a) total pore area saturated with oil

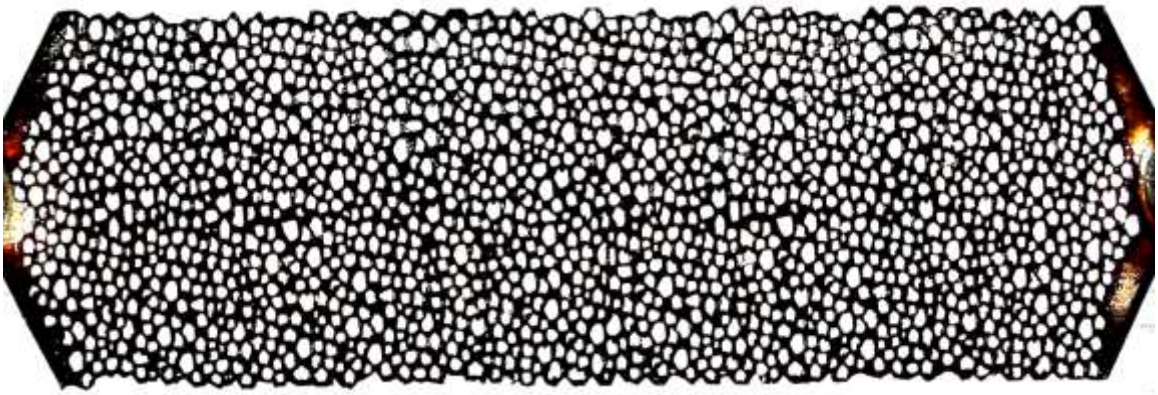

(b) pore area considered for image analysis

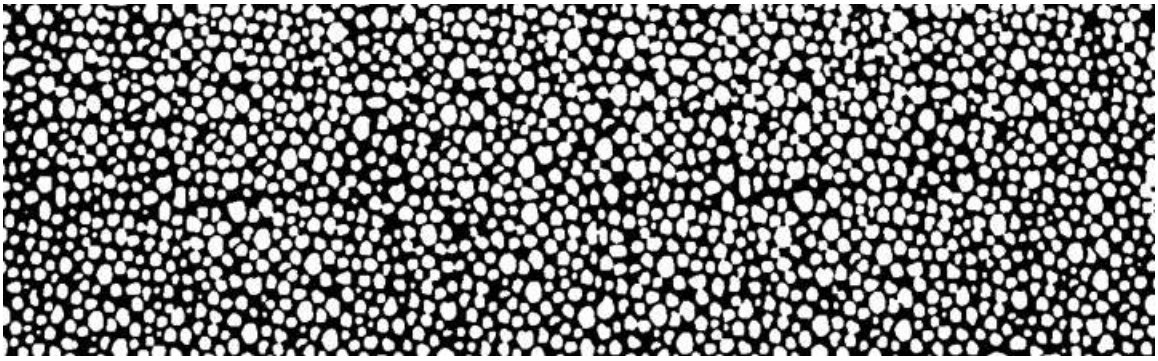

Figure 4.6: Actual photos of (a) oil saturated micro-model (total pore area) and (b) pore area considered for image analysis.

a: (t = 30 s)

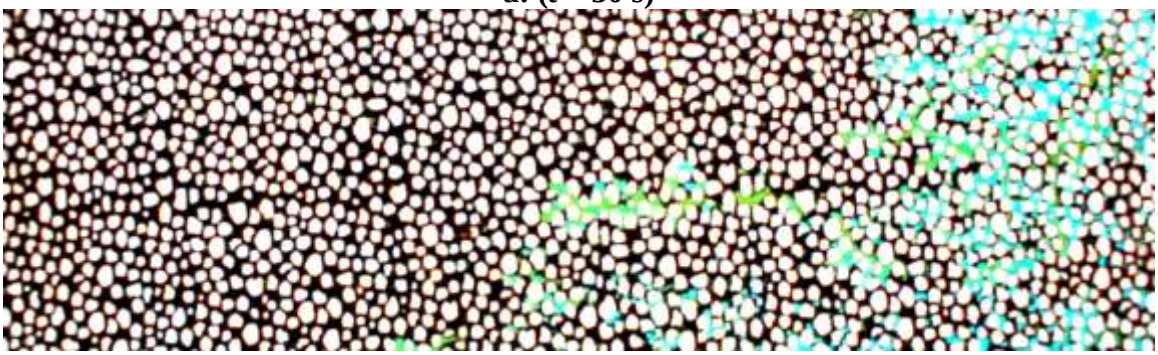

b: (t = 60 s)

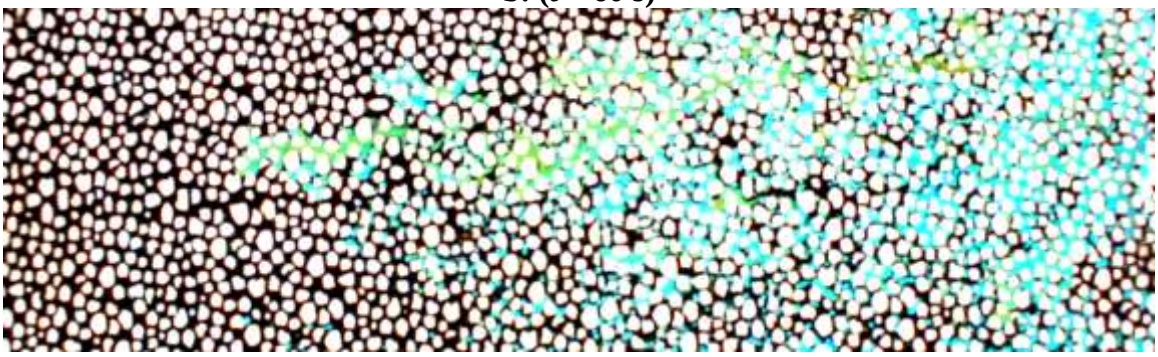

c: (t_{BT} = 112 s)

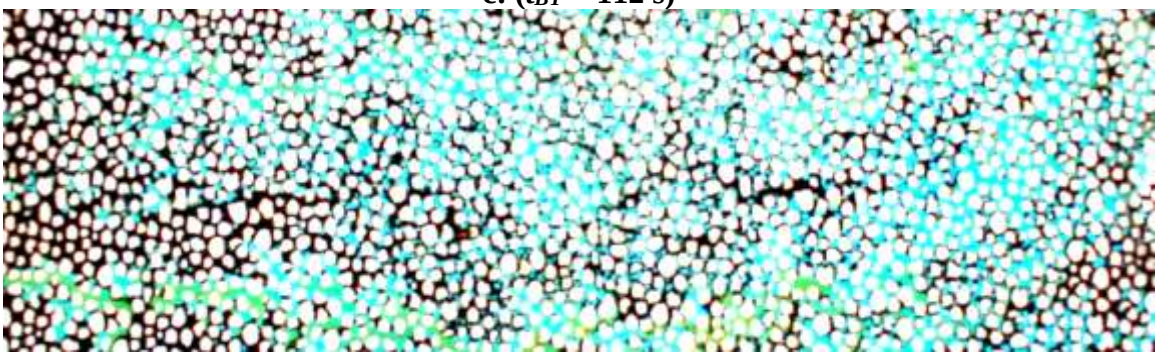

(Continue to next page …)

d: (t = 180 s)

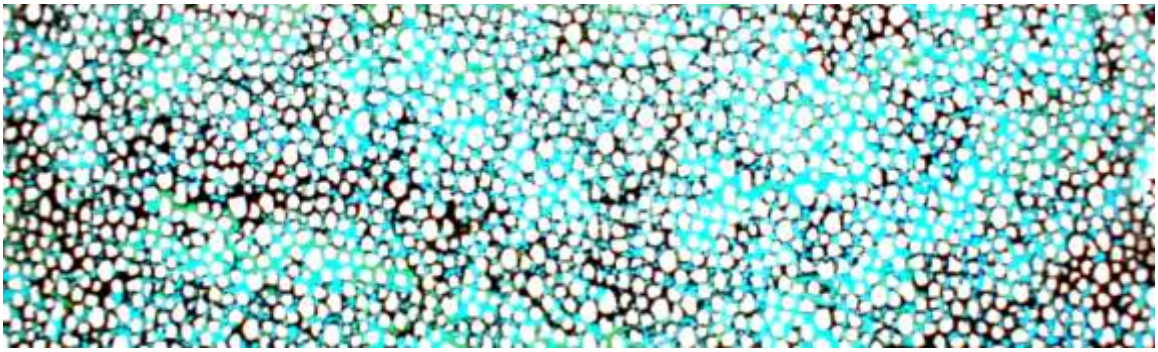

e: (t = 480 s)

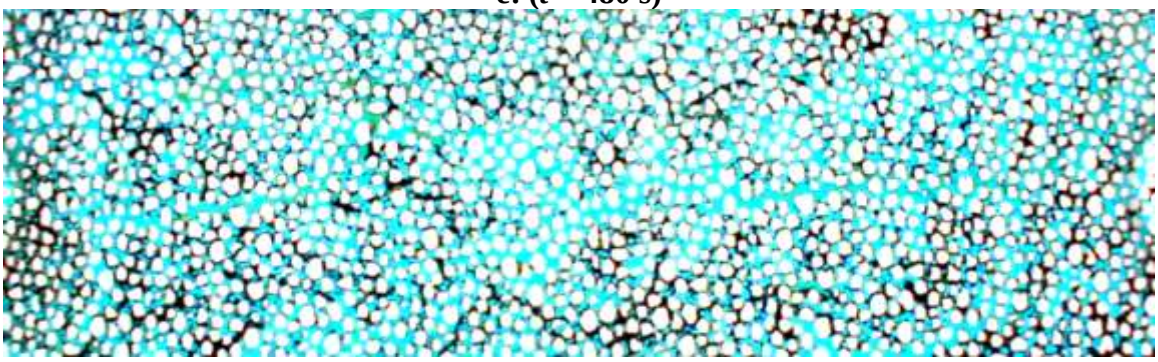

Figure 4.7: Advancement of waterfront during waterflooding of oil Type-I (°API=20.44): a) t = 30 s, b) t = 60 s, c) $t = t_{BT}$ = 112 s, d) t = 180 s, e) t = 480 s.

Figure 4.8 shows that while an ultimate oil recovery factor of 61% was achieved at about 1.6 PV of injection, 45.5% of it is before breakthrough happened. Analysis of the images (**Figure 4.9**) also show that most of the residual oil remaining in the micromodel after 1.6 PV of injected water are trapped in the larger pores mainly close to injection and production ports. This is mainly because water, as the wetting phase, tends to move into smaller pore throats and displace the oil from them.

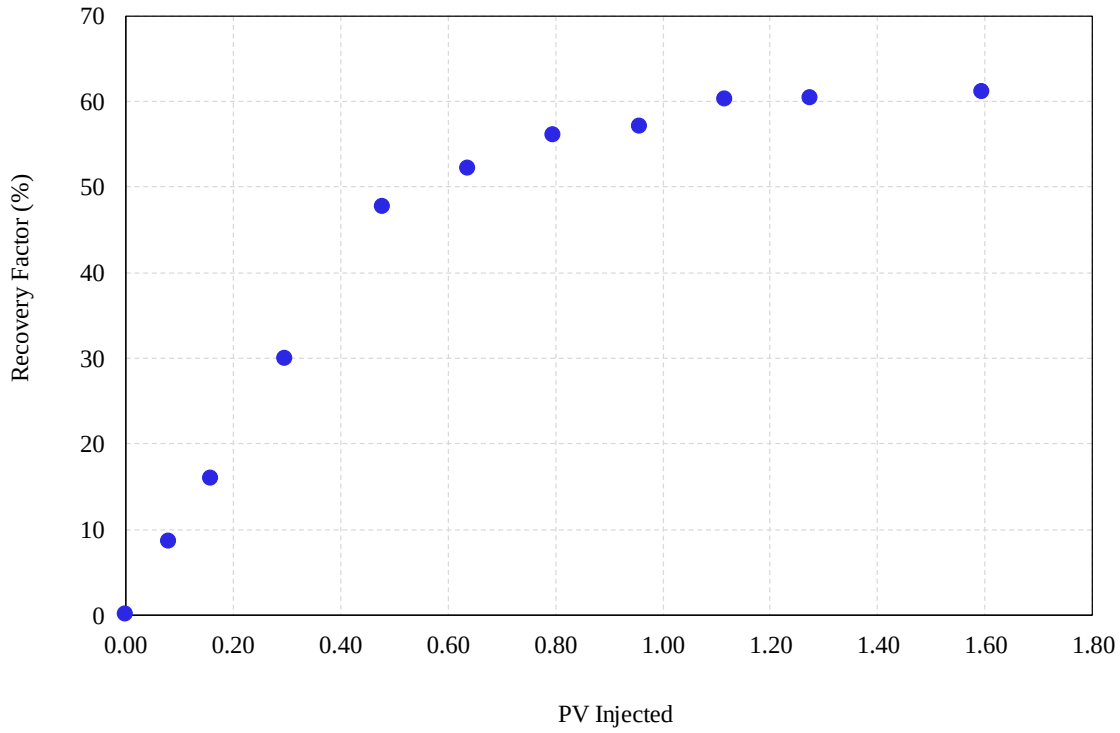

Figure 4.8: Recovery factor as a function of PV injected for the base case (waterflooding of oil Type-I, ^{o}API=20.44) at injection rate of q_{inj}=0.05 cm^3/min

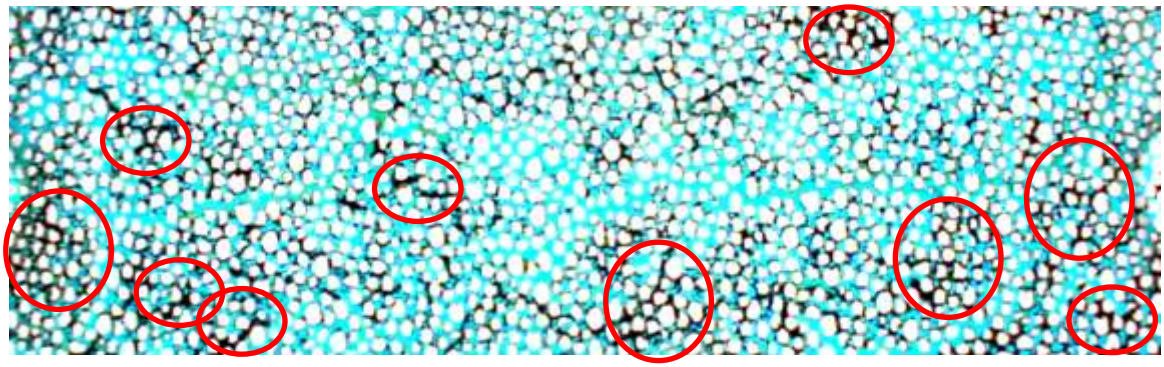

Figure 4.9: Residual oil saturation after injection of 1.6 PV of water (oil Type-I, ^{o}API=20.44) at injection rate of q_{inj}=0.05 cm^3/min

4.5.2. Effect of injection rate on waterflooding performance

To investigate the effect of injection rate on the performance of waterflooding in heavy oil reservoirs, two new tests were carried out. For each test, micromodel was saturated with Type-I (^{o}API=20.44) crude oil and waterflooding was performed in the same manner as the base case. Injection rates tested were q_{inj}=0.025 cm^3/min and q_{inj}=0.075 cm^3/min representing ±50% of changes in the injection rate.

Figure 4.10 shows recovery factor of waterflooding of Type-I oil at the injection rates compared to the base case (q_{inj}=0.05 cm^3/min). As it can be observed, in comparison to the base case, increasing or decreasing the injection rate by 50% caused higher recovery factors before breakthrough. However, both lower and higher injection rates resulted in lower ultimate recovery factor at the total injection of 1.6 PV with the lowest amount obtained from the lowest injection rate (q_{inj}=0.025 cm^3/min). Ultimate recovery factor of three cases in the order of increasing injection rates were 48%, 62 % and 50.7%, respectively.

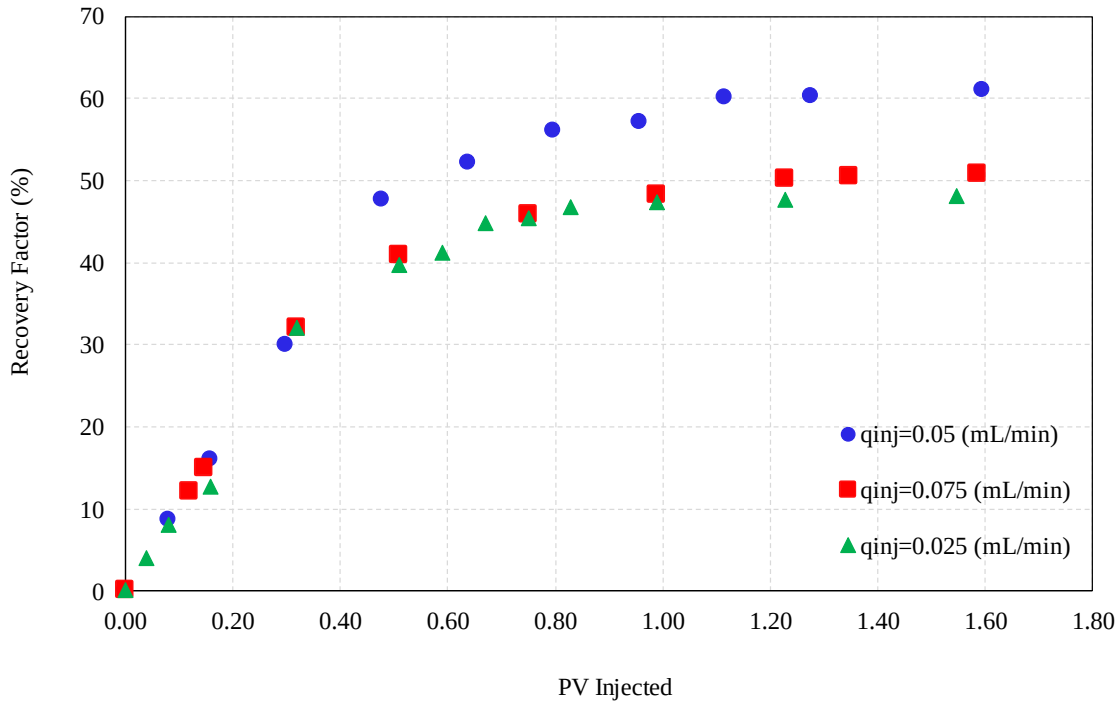

Figure 4.10: Waterflooding recovery factor of three injection rates as a function of injected PV of water for type-I heavy oil in the single permeability micromodel.

Figure 4.11(a) to 4.11(c) present images of the displacement efficiency at the breakthrough time for waterflooding of oil Type-I at three injection rates. As it can be seen, breakthrough time for the three cases of q_{inj}=0.025 cm^3/min, q_{inj}=0.05 cm^3/min and q_{inj}=0.075 cm^3/min are 120, 112 and 37 seconds, respectively. It was speculated that while viscous force is not sufficient enough during the lower injection rate of q_{inj}=0.025 cm^3/min to displace the oil, the higher velocity of water at the injection rate of q_{inj}=0.075 cm^3/min caused viscous fingering and early water breakthrough which consequently resulted in lower ultimate recovery factor. It must be noticed that the overall recovery factor of lower injection rate (q_{inj}=0.025 cm^3/min) was the minimum among the three cases.

(a) t_{BT}= 120 s

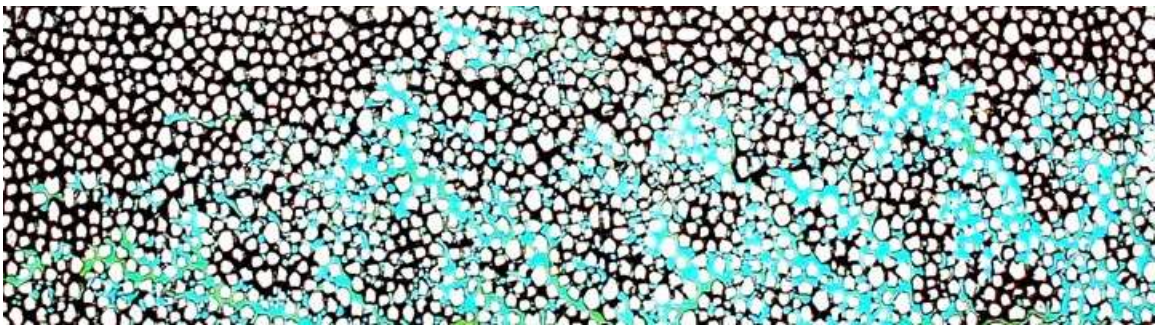

(b) t_{BT}= 112 s

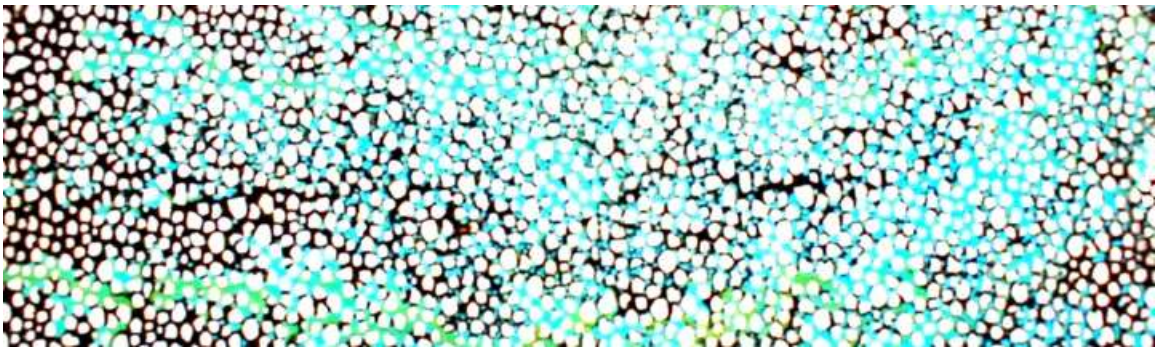

(c) t_{BT}= 37 s

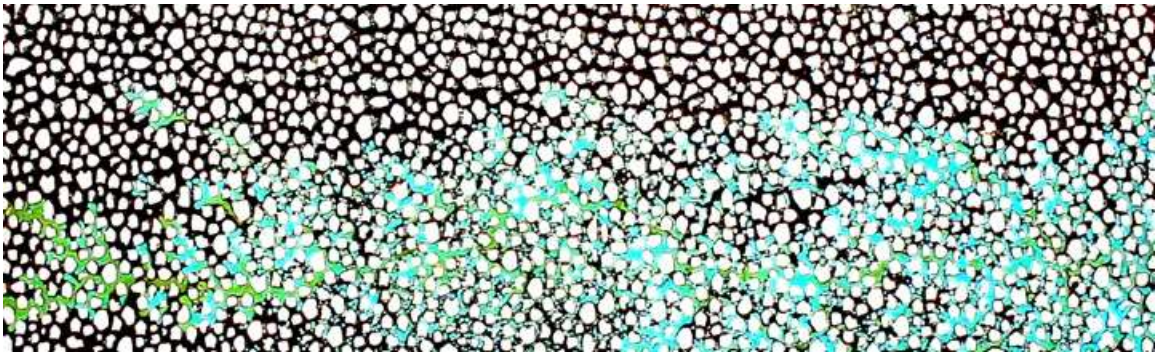

Figure 4.11: Displacement performance and residual oil saturation at breakthrough time for three injection rates of a) q_{inj}=0.025 cm^3/min, b) q_{inj}=0.05 cm^3/min, c) q_{inj}=0.075 cm^3/min

4.5.3. Effect of temperature on the performance of heavy oil waterflooding

To understand the effect of temperature on the recovery performance and displacement efficiency of waterflooding of Type-I crude oil (^{o}API=20.44), and also investigate if increasing water temperature could improve the oil production during waterflooding, two additional micromodel tests were conducted at T_{exp}=30^{o}C and T_{exp}=45^{o}C while injection rate was kept constant for both tests at q_{inj}=0.05 cm^3/min. Results obtained are also applicable to those heavy oil reservoirs with temperatures similar to the experiments.

Figure 4.12 illustrates the recovery factor of waterflooding of oil Type-I at injection rate of q_{inj}=0.05 cm^3/min and various temperatures. According to the results obtained in this study, oil recovery factor increased from an initial value of 61% to 69.3% when temperature increased from T_{exp}=21^{o}C to T_{exp}=30^{o}C and experienced a further increase to 73.7% when test was conducted at T_{exp}=45^{o}C.

While it was expected to see higher improvement in the recovery factor at the elevated temperature of T_{exp}=45^{o}C, it was speculated that water viscosity reduction might be the responsible mechanism for this inconsistency. It is noteworthy that water viscosity is reduced to μ_w=0.62 mPa.s when temperature increased to T_{exp}=45^{o}C.

Recovery trends at various temperatures could be also observed at 1.25 PV of injected water through **Figure 4.13(a)** to **(c)**.

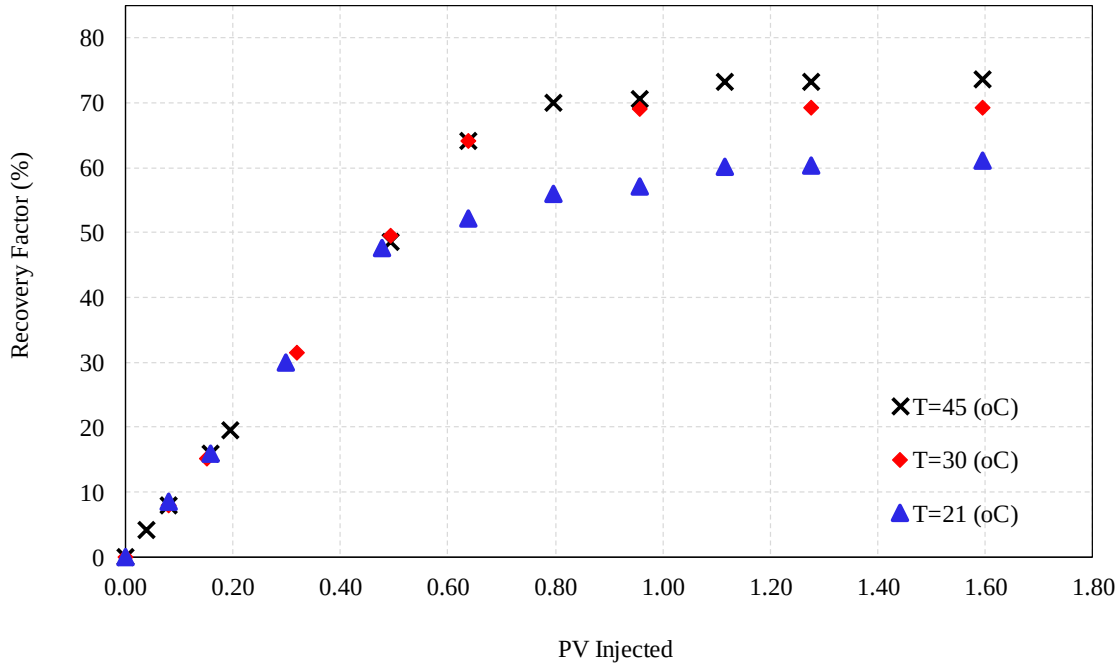

Figure 4.12: Recovery factor of waterflooding conducted at three different temperatures and constant injection rate of q_{inj}=0.05 cm^3/min for type-I heavy oil saturated micromodel

(a) T_{exp}=21 (°C)

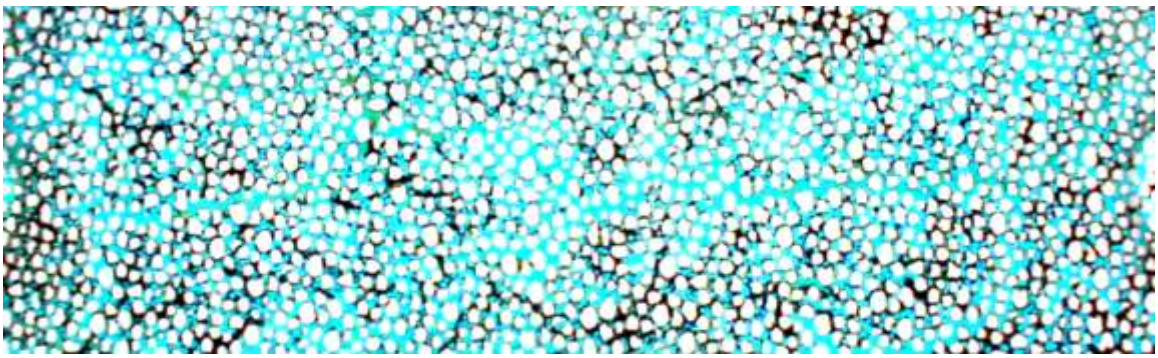

(b) T_{exp}=30 (°C)

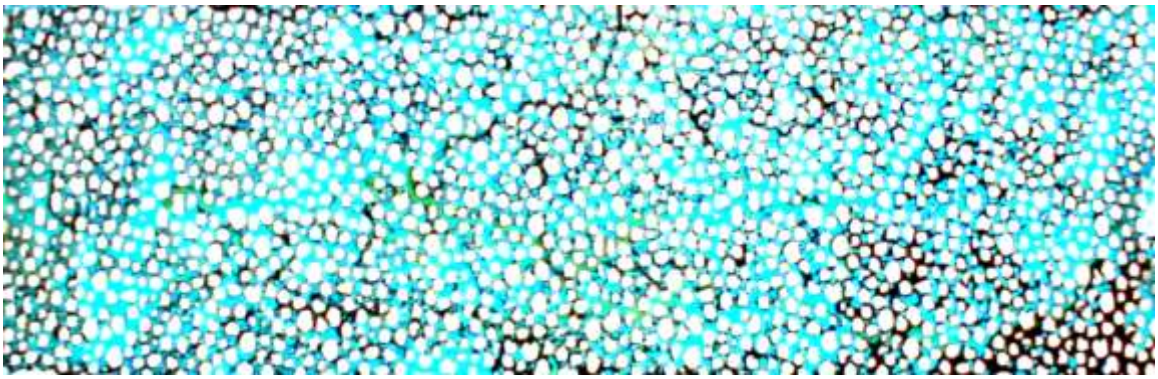

(c) T_{exp}=45 (°C)

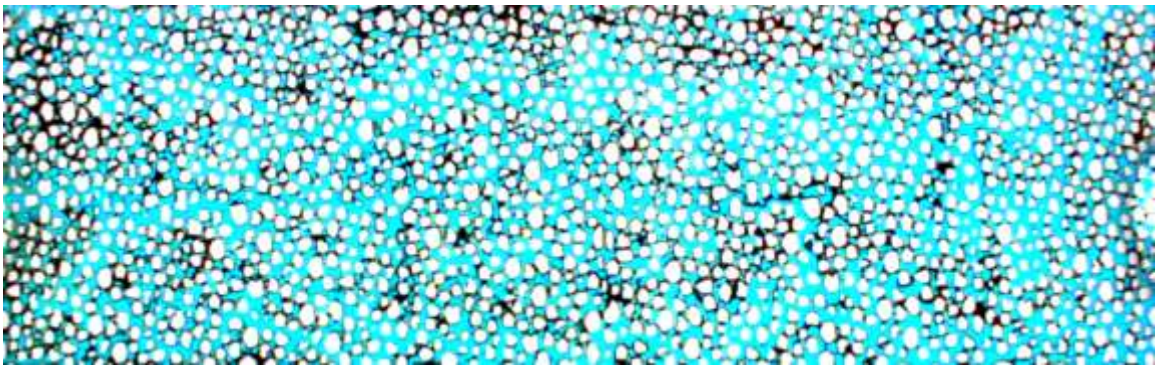

Figure 4.13: Displacement performance and residual oil saturation at about 1.25 PV of injection for three temperatures a) T_{exp}=21 (°C), b) T_{exp}=30 (°C), c) T_{exp}=45 (°C)

4.5.4. Effect of oil API gravity

To evaluate the performance of waterflooding in heavier oil system compared to oil Type-I, another sample of heavy oil with API gravity of 15.49 degrees was used. Similar micromodel flooding tests at various injection rates, and different temperatures were conducted using the heavier oil sample which is called oil Type-II in this study.

Figure 4.14 depicts the recovery factor of waterflooding of both types of heavy oil samples used at q_{inj}=0.05 cm^3/min and temperature of T_{exp}=21^{o}C.

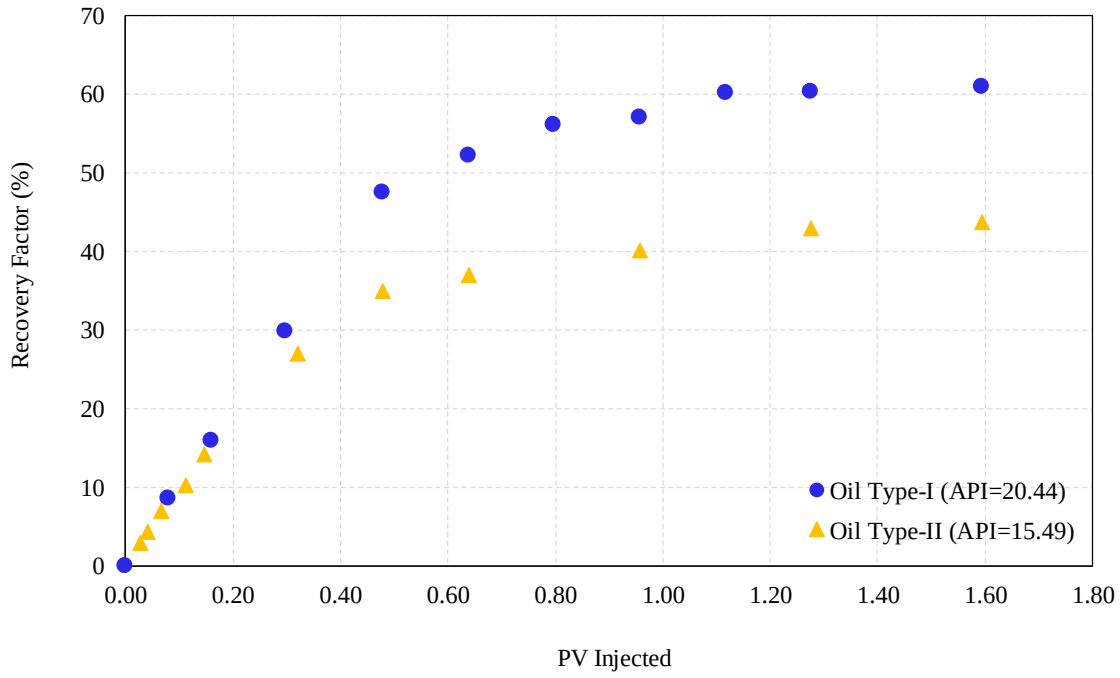

Figure 4.14: Waterflooding recovery factor for Type-I and Type-II heavy oil systems (API=20.44 and API=15.49) at q_{inj}=0.05 cm^3/min and temperature of T_{exp}=21^{o}C in the single permeability micromodel.

Comparison of the recovery factors of both cases after 1.6 PV of water injection shows that waterflooding was more successful in the heavy oil system with the oil API gravity of 20.44. As it can be seen, 5 degrees of reduction in the oil API gravity resulted in over 15% of reduction in recovery factor (from 61% to 43.8%). This is mainly due to the viscosity contrast existing between crude oil and injected water.

Figure 4.15 and **4.16** includes images of the residual oil saturation at the water breakthrough for Type-I and Type-II heavy oils during waterflooding at q_{inj}=0.05 cm3/min and temperature of T_{exp}=21^{o}C. As it can be observed, when water breakthrough happened, small amount of heavy oil with lower API gravity (^{o}API=15.49) has been displaced compared to oil Type-I (^{o}API=20.44). Consequently, images of displaced regions when ultimate recovery factor is achieved confirm lower performance of water injection in heavier oil.

The low performance of waterflooding in heavier oil system left large quantities of oil behind, making them suitable for tertiary oil recovery. One such tertiary recovery technique is carbonated waterflooding which requires minimum changes in surface facilities and infrastructures when considered for the field application. A comparative evaluation of the performance of carbonated waterflooding in both types of heavy systems of this study is included in the next chapter.

(a) t_{BT}=112 sec (oil API=20.44)

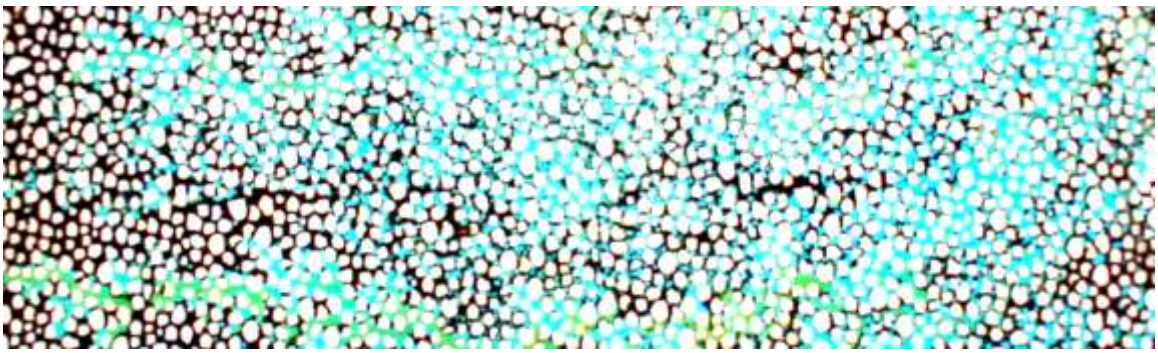

(b) t_{BT}=112 sec (oil API=15.49)

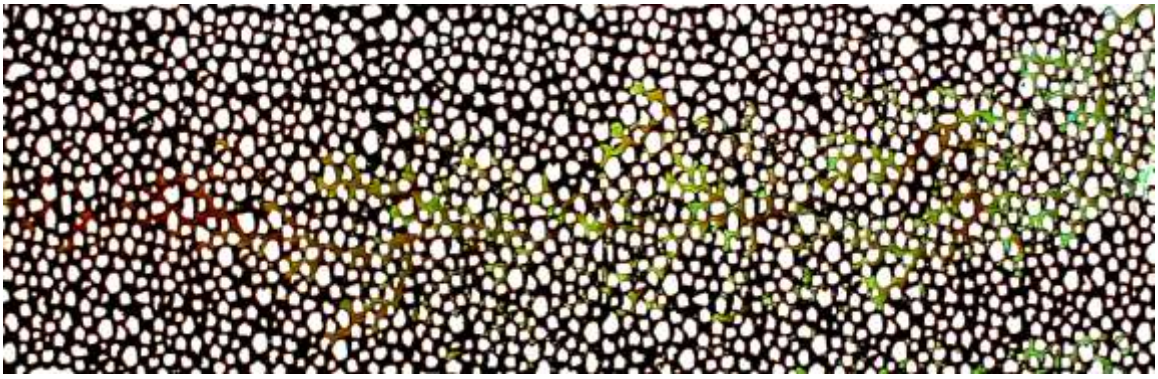

Figure 4.15: Displacement performance and residual oil saturation at the breakthrough time during waterflooding of oils with API gravity of (a) API=20.44 and (b) API=15.49 at q_{inj}=0.05 cm3/min and temperature of T_{exp}=21^{o}C.

(a) *at 1.28 PV or t=480 sec* (^{o}API=20.44)

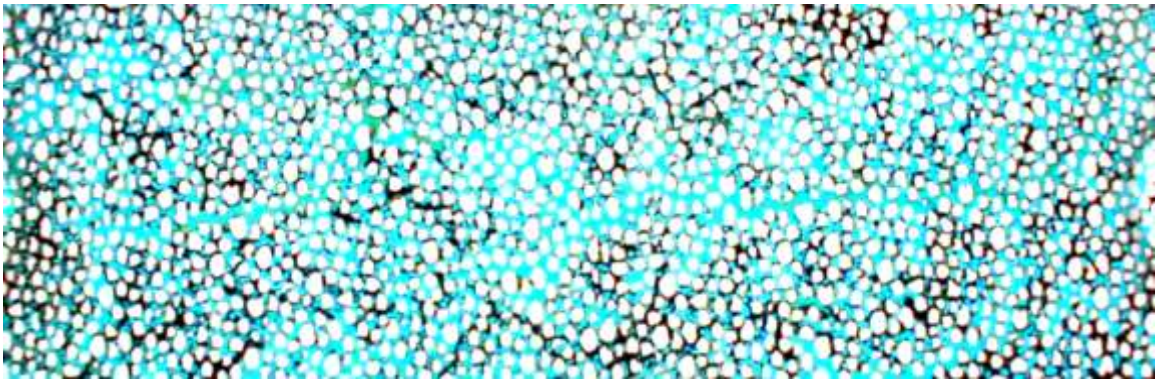

(b) *at 1.28 PV or t=480 sec* (^{o}API=15.49)

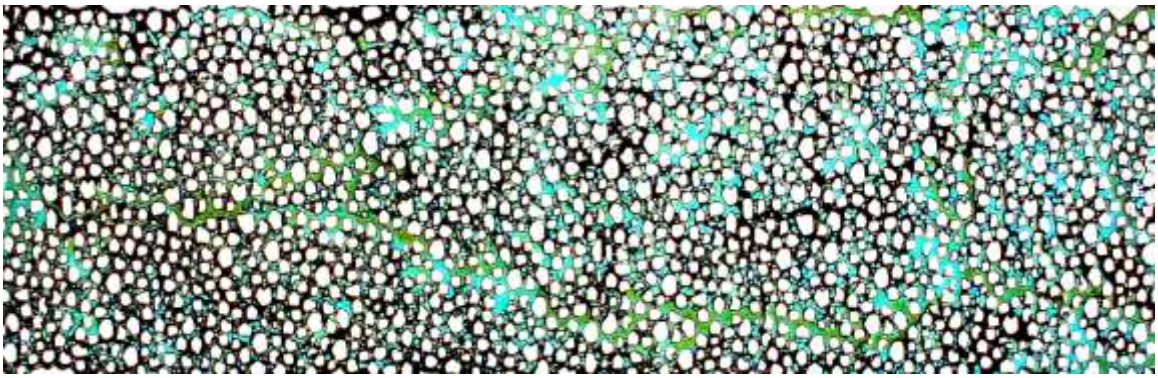

Figure 4.16: Displacement performance and residual oil saturation at 1.28 PV injection during waterflooding of oils with API gravity of (a) ^{o}API=20.44 and (b) ^{o}API=15.49 at q_{inj}=0.05 cm^3/min and temperature of T_{exp}=21^{o}C.

4.5.5. Effect of temperature on the performance of waterflooding in Type-II heavy oil

Effect of temperature on the performance of waterflooding in Type-II heavy oil sample was investigated through three micromodel tests conducted at the temperatures of T_{exp}=21^{o}C, 30^{o}C and 45^{o}C. Results of these tests are depicted in **Figure 4.17**. These results also confirmed that when temperature increased from T_{exp}=21^{o}C to T_{exp}= 30^{o}C recovery factor also increased from 43.79% to 48.18%. This can be translated to 0.488% of recovery increase per one degree of increase in temperature. However, when temperature was further increased to T_{exp}= 45^{o}C, recovery factor was only increased to 50.35% which is only about 0.145% recovery increase per one degree of increase in temperature. This is perhaps because of lower water viscosity at higher temperature (e.g 0.62 mPa.s).

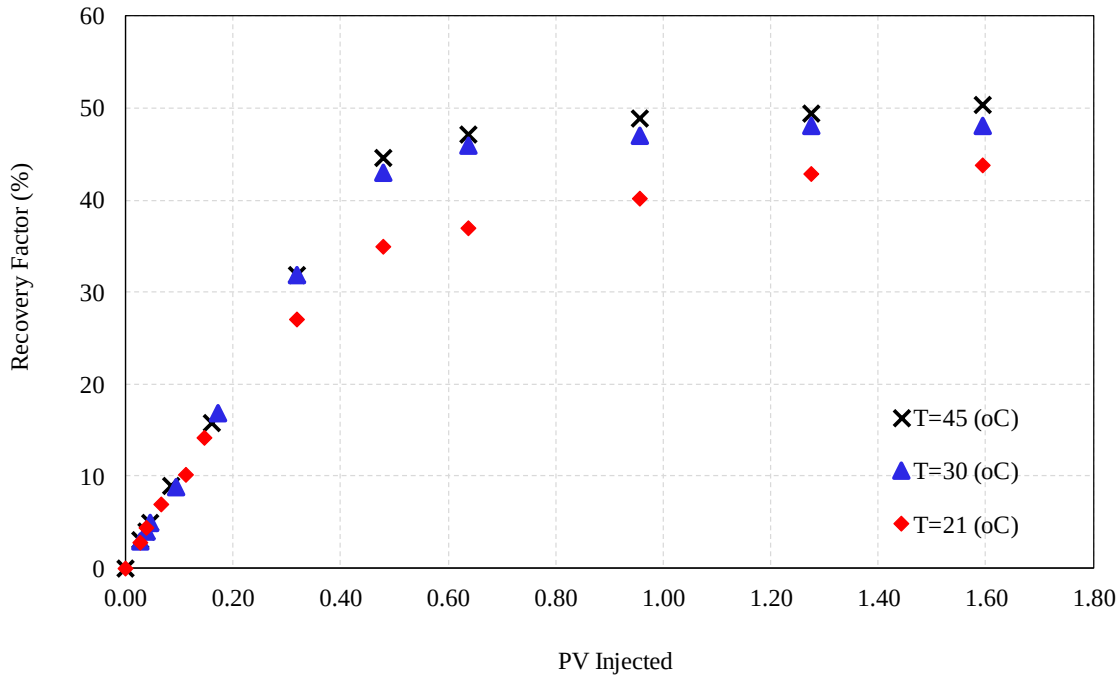

Figure 4.17: Waterflooding recovery factor at 1.6 PV water injection into a Type-II heavy oil saturated micromodel (single permeability) at q_{inj}=0.05 cm^3/min and temperatures of T_{exp}=21ºC, 30ºC and 45ºC.

4.5.6. Effect of flow rate on the displacement efficiency of waterflooding for Type-II heavy oil

Since some anomalies were observed during the investigation of the effect of injection rate on the displacement efficiency of waterflooding in Type-I heavy oil system, additional tests using Type-II heavy oil were conducted with the same objective. For this fact and to have more differentiable results, an injection rate of q_{inj}=0.01cm^3/min which is 5 times lower than the base case was considered for the waterflooding of Type-II heavy oil.

Recovery factors of both base-case and new lower injection rates are presented in **Figure 4.18** as a function of PV of water injected at the constant temperature of T_{exp}=21^{o}C. As it can be seen from the figure, lower injection resulted in higher recovery factor until water breakthrough. However, the ultimate recovery factor after injection of nearly 1.6 PV of water was much higher (43.8%) for the base-case injection rate of q_{inj}=0. 05 cm^3/min compared to 32.04% at the lower injection rate of q_{inj} =0.01cm^3/min.

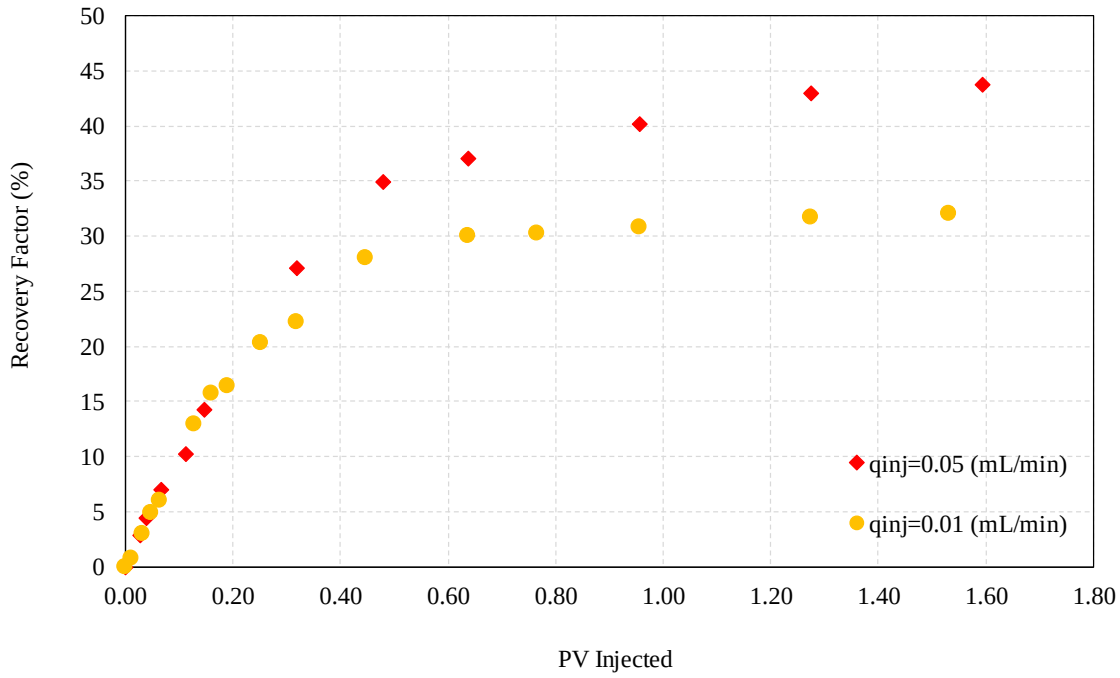

Figure 4.18: Waterflooding recovery factor at 1.6 PV water injection into a Type-II heavy oil saturated micromodel at two injection rates of q_{inj}=0.05 cm^3/min and 0.01 cm^3/min and constant temperature of T_{exp}=21°C.

4.5.7. Waterflooding of oil saturated dual permeability micromodel compared to single permeability (base case)

One of the main objectives of this study was to experimentally investigate if waterflooding and consequently carbonated waterflooding can be applied to the reservoirs containing fractures, wormholes and in general high permeability channels. To visually observe the displacement process of the oil by water in such mediums and quantify the displacement efficiency of waterflooding in the porous media containing high and low permeability channels compared to conventional porous media (single permeability), another micromodel was designed and manufactured. This new micromodel had similar pattern area, width, and engraving depth as the previously described one and most of the grains were remained the same. However, 17 connected and disconnected straight and oriented channels (with respect to flow direction) with various lengths and much higher permeability were included in various sections of the pattern. **Table 4.2** characteristics of the dual permeability micromodel. Grain and pore size distributions of the model are presented in **Figure 4.19** and **20**, respectively.

Actual photos of the oil saturated dual-permeability micromodel used in this study is shown in **Figure 4.21**.

Tests were conducted in the newly manufactured dual-permeability micromodel following the same procedure used for the tests performed in the single-permeability (previous cases) micromodel. Throughout number of tests, effect of temperature, injection rate, and API oil gravity on the displacement efficiency of waterflooding in a dual-permeability micromodel were evaluated.

Table 4.2: Properties of dual-perm micromodel used in this study.

Property	Dual- Perm micromodel
Number of grains	1775
Max throat size	5.208 mm
Min throat size	0.110 mm
Average grain size	1.113 mm^2
Max grain size	7.304 mm^2
Min grain size	0.012 mm^2
Pattern length, cm	123 mm
Pattern width, cm	38 mm
Engraving depth (pre-set), cm	0.0123 cm
Pore area	25.64 cm^2
Pore volume	0.334 cm^3
Porosity	59.0 %
Number of high-permeability channels	17
Length of high permeability channels	10-15 mm
Width of high permeability channels	3 mm

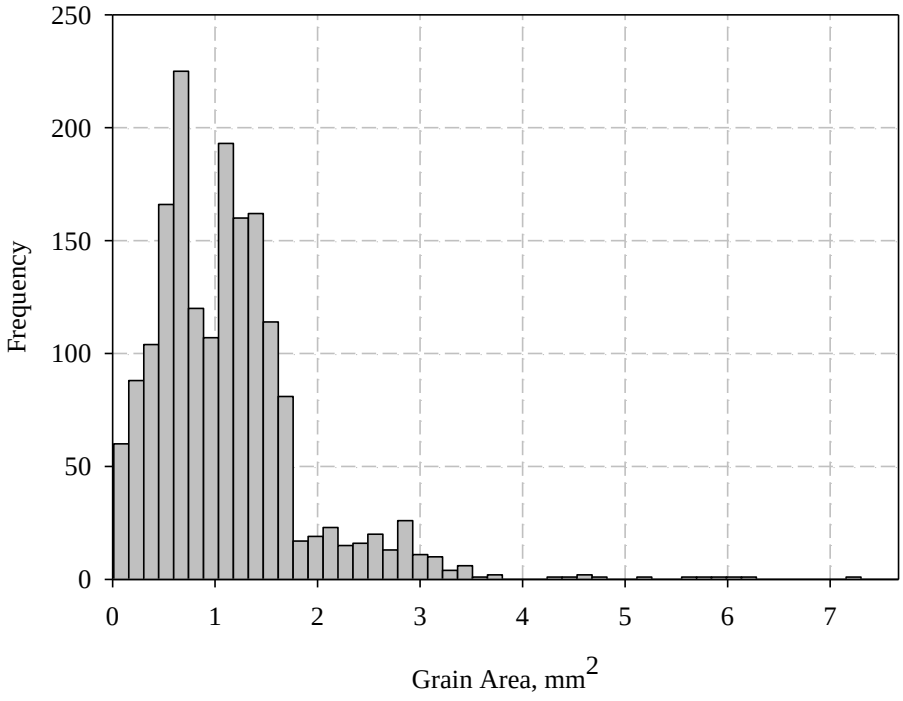

Figure 4.19: Grain size distribution for the dual permeability micromodel.

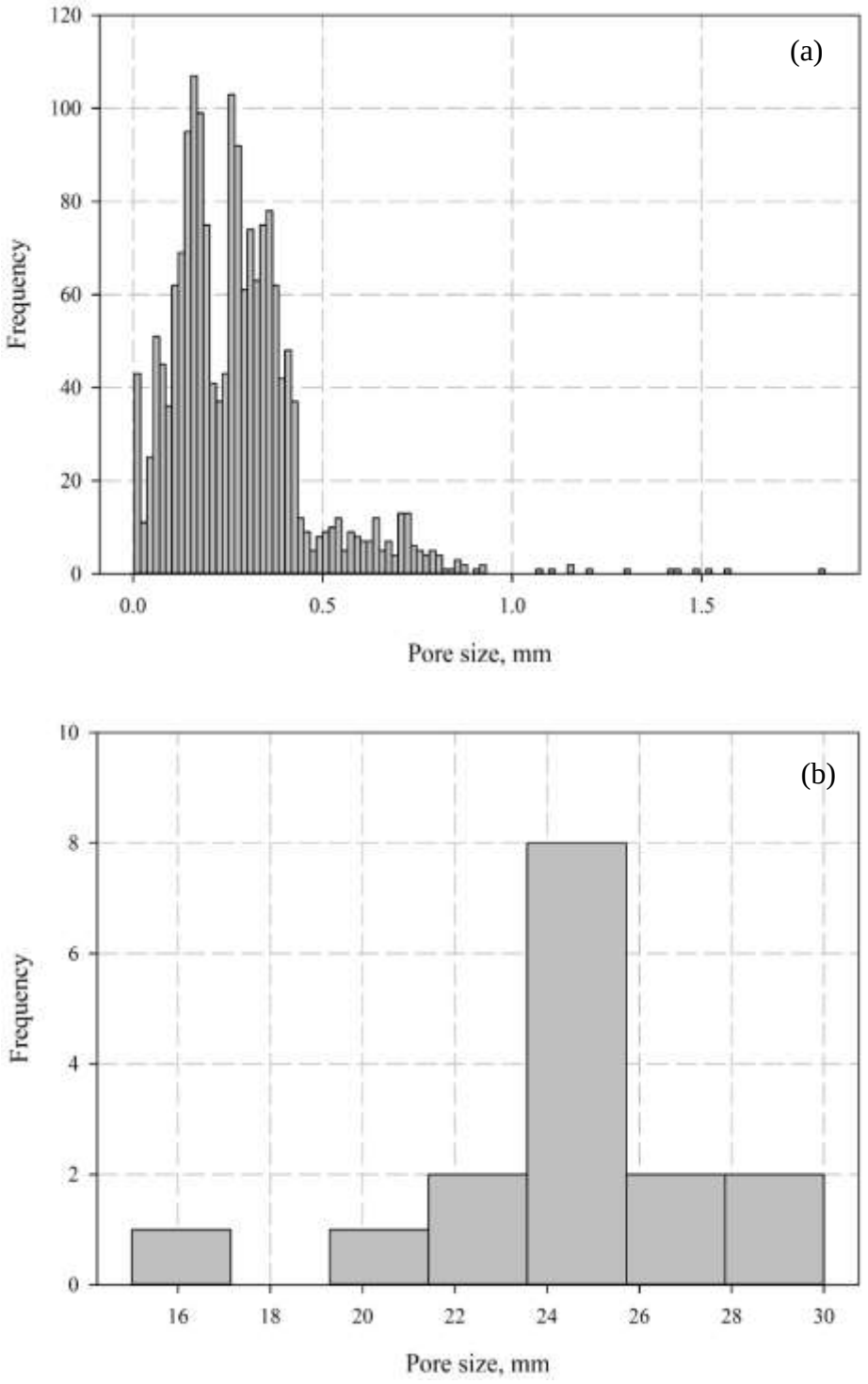

Figure 4.20: Pore size distribution for the dual permeability micromodel (a) low (matrix) permeability region, (b) high permeability region

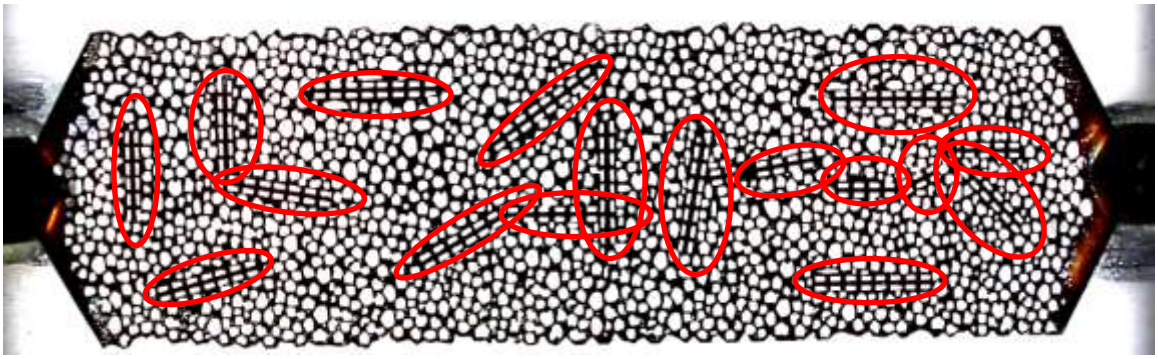

Figure 4.21: Photo of oil saturated dual-permeability model containing 17 high permeability channels manufactured and used in this study.

Effect of dual permeability porous media on the waterflooding of Type-I crude oil (API=20.44)

After saturating the dual permeability micromodel with Type-I crude oil, waterflooding was performed at the injection rate of q_{inj}=0.05 cm^3/min and constant temperature of T_{exp}=21°C to be consistent with experimental conditions of the base case. Analysis of the images taking from the displacement processes shows the early breakthrough happening through the high permeability channels causing the ultimate recovery factor to be lower compared to the base case. **Figure 4.22 (a)** to **(c)** shows the frontal advancement of water at various time frames from the beginning until the water breakthrough time, t_{BT}.

One of the interesting findings was the fast and perfect re-saturation of the high permeability channels as highlighted in **Figure 4.23 (a)** to **(c)** with tow ellipses on each figure. It is believed that this phenomenon helped producing additional oil, hence, the recovery factor not to be severely suffering from the early breakthrough of water. Both sets of Figures also confirm that the most inaccessible oil were contained in the pores with no high permeability channels though this was more noticeable prior to the water breakthrough. As it can be observed, after 1.6 PVs of water injected, most of high permeability channels are drained and highly saturated with water.

(a) t=10 seconds

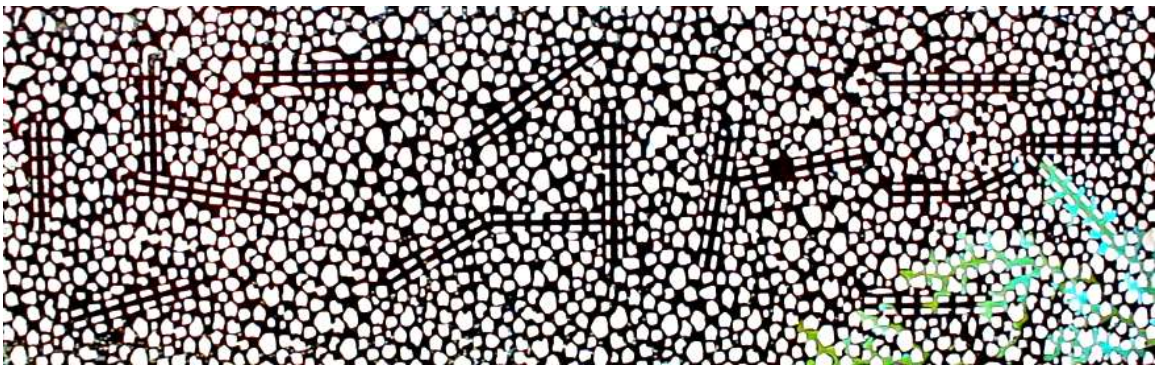

(b) t=30 seconds

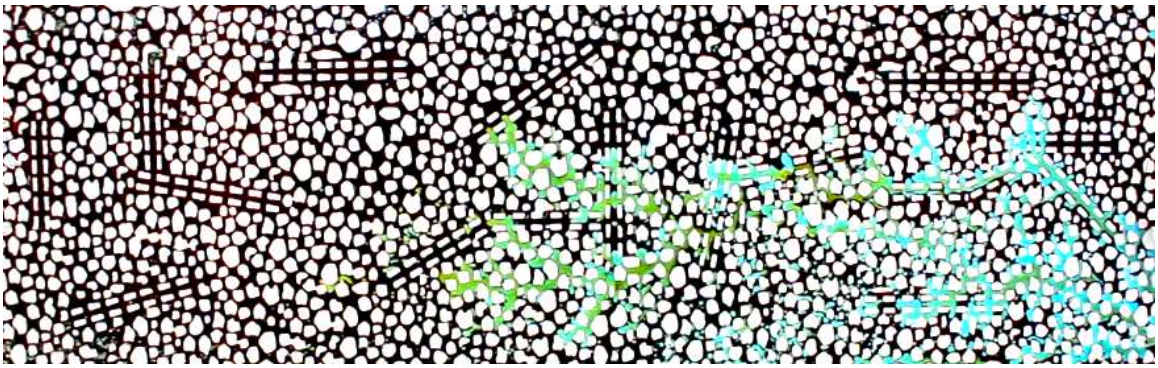

(c) t=40 seconds

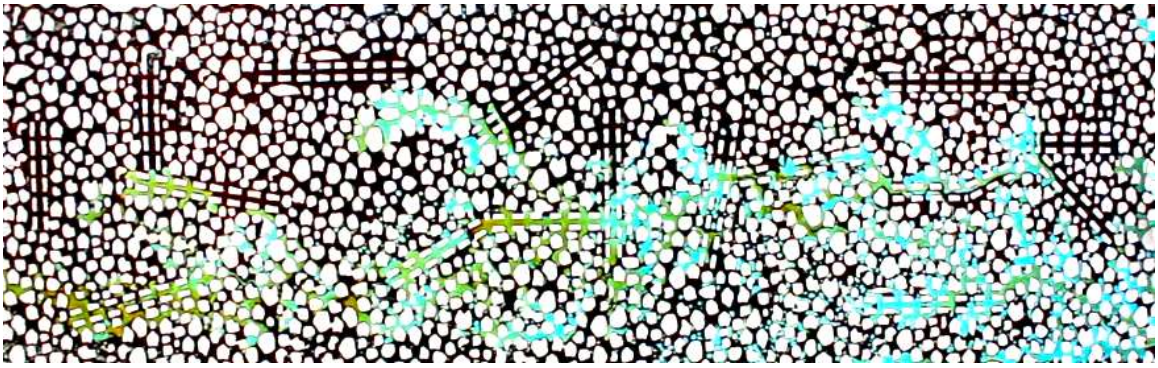

Figure 4.22: Frontal advancement of water during waterflooding of Type-I crude oil in the dual permeability micromodel before water breakthrough at q_{inj}=0.05 cm^3/min and constant temperature of T_{exp}=21°C.

(a) t=120 seconds

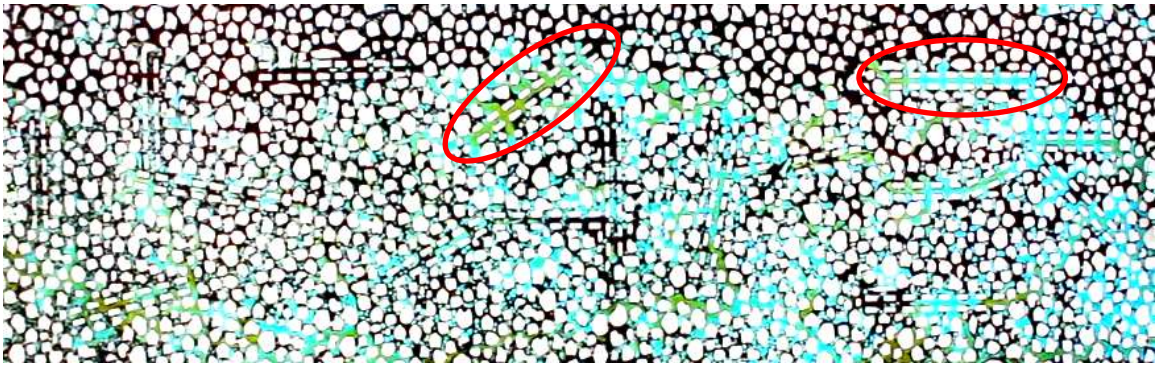

(b) t=240 seconds

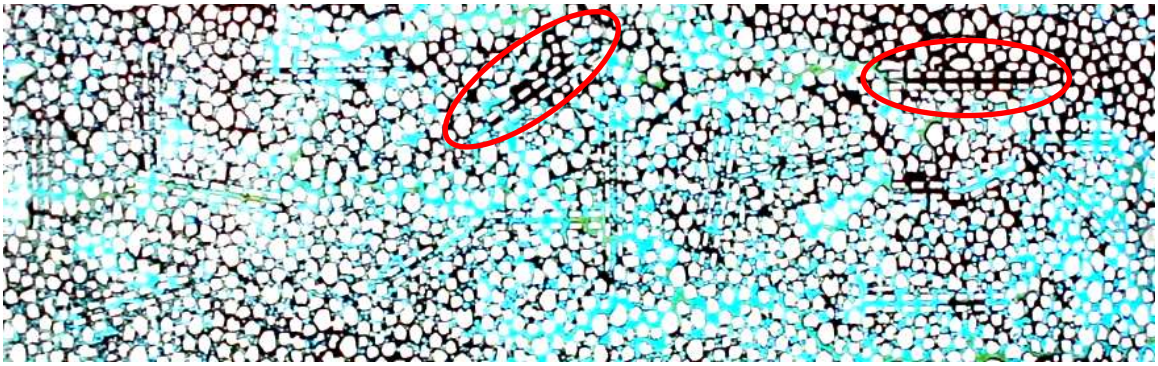

(c) t=480 seconds

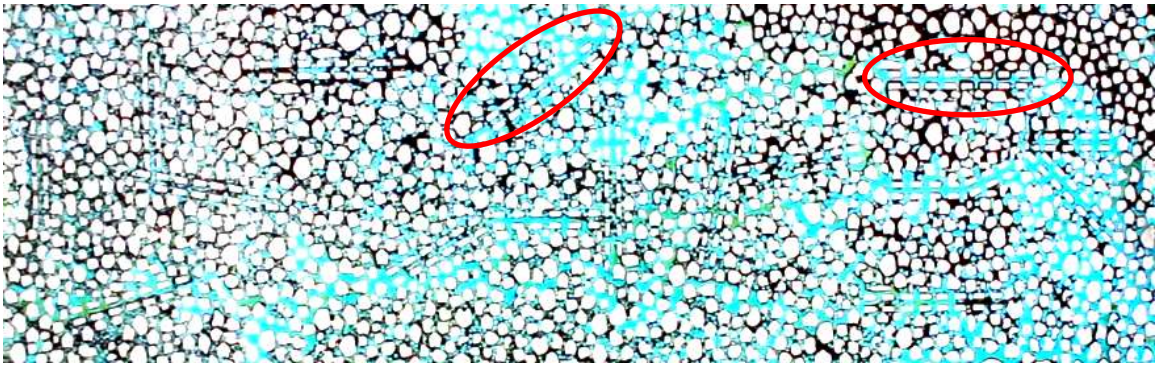

Figure 4.23: Frontal advancement of water during waterflooding of Type-I crude oil in the dual permeability micromodel after water breakthrough at q_{inj}=0.05 cm^3/min and constant temperature of T_{exp}=21^{o}C.

To perform a quantitative analysis, a comparative evaluation was performed by plotting the recovery factors obtained at various PVs of injected water for both single permeability and dual permeability cases. As shown in **Figure 4.24**, the ultimate oil recovery factor at about 1.6 PVs of injected water was 57.6% compared to the 61% recovery factor of the base case waterflooding which was conducted in a single permeability micromodel at the same injection rate and experimental conditions. As mentioned earlier, it was speculated that the 3.7% reduction in the recovery factor is because of the presence of high permeability channels causing earlier water breakthrough of $t_{BT\text{-}dual}$=40 seconds compared to $t_{BT\text{-}single}$=112 seconds.

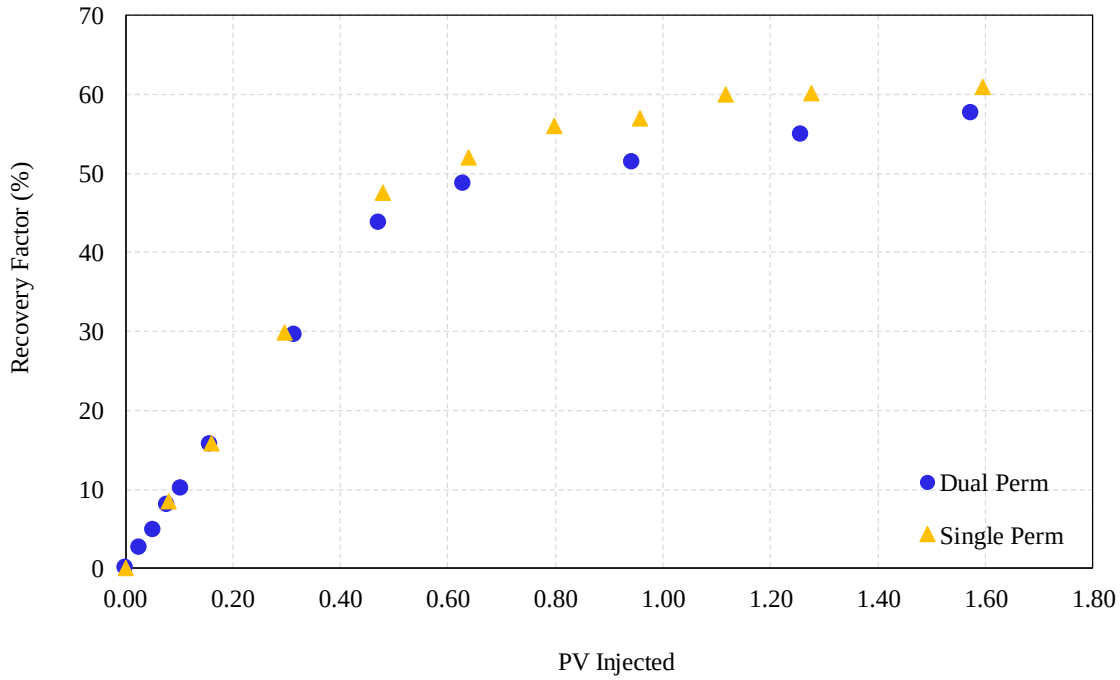

Figure 4.24: Recovery factor obtained during the waterflooding of dual-perm and single-perm micromodels saturated with Type-I heavy oil at injection rate of q_{inj}=0.05 cm^3/min and constant temperature of T_{exp}=21ºC.

Effect of dual permeability porous media on the waterflooding of Type-II crude oil (API=15.49)

Displacement efficiency of waterflooding in the dual permeability micromodel saturated with Type-II heavy oil was very poor compared to Type-I. As illustrated in **Figure 4.25 (a)** to **(c)**, significant amount of oil was left behind when nearly 1.6 PVs of water was injected. Areas highlighted with red ellipses in **Figure 4.25 (a)** to **(c)** shows that water was incapable of efficiently displacing oil from high permeability channels. This was also true for the regular pores. The pore displacement efficiency was attributed to the insufficient viscous force exerted by water during the displacement process causing severe viscous fingering. As it can be seen many of the high permeability channels are still partially or fully saturated with oil at 1.6 PVs of injected water. This was opposed to what was observed earlier for the case of waterflooding of oil Type-I.

(a) t=120 seconds

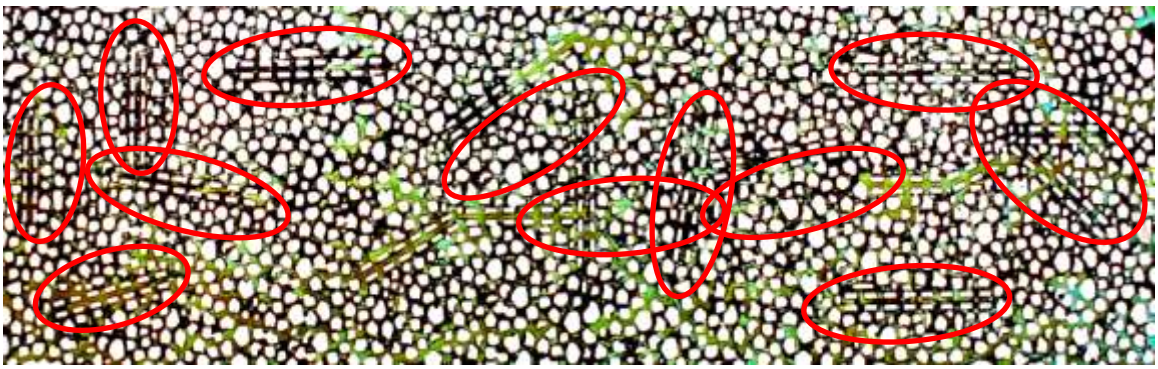

(b) t=240 seconds

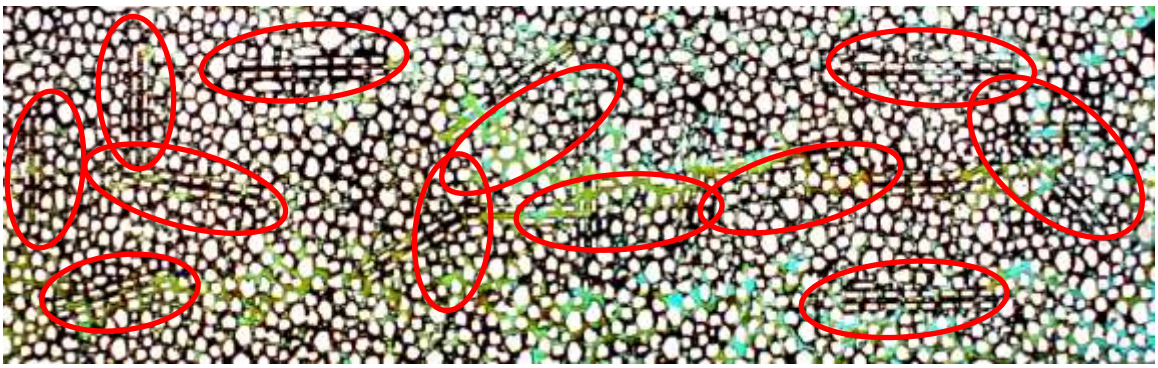

(c) t=480 seconds

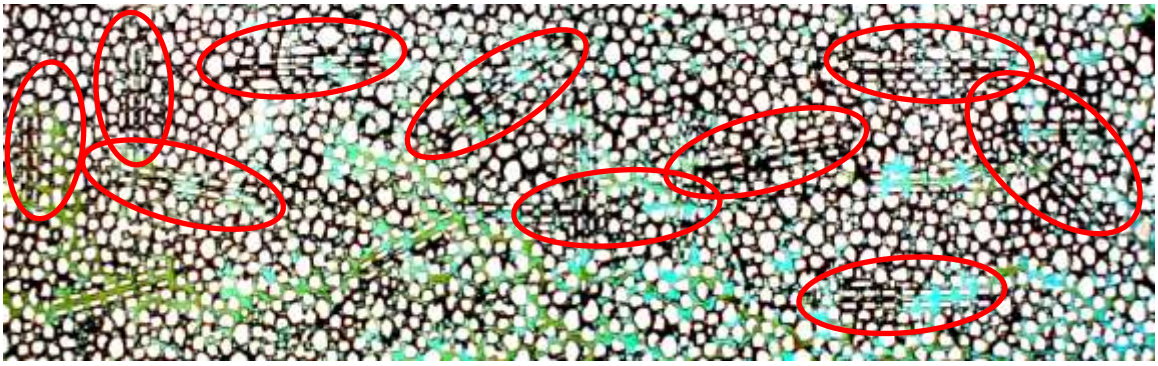

Figure 4.25: Frontal advancement of water during waterflooding of Type-II crude oil in the dual permeability micromodel after water breakthrough at q_{inj}=0.05 cm^3/min and constant temperature of T_{exp}=21^{o}C.

Recovery factor of waterflooding process conducted in Type-II crude oil (API=15.49) saturated micromodels representing single and dual permeability porous media are plotted as a function of PVs of water injected in **Figure 4.26**. The ultimate recovery factor of waterflooding in Type-II crude oil saturated micromodel with dual permeability porous media was 29.7% at 1.6 PVs of water injected which was 14.1% less than the recovery factor obtained for waterflooding of Type-I crude oil in the same dual permeability micromodel and at the same injection rate of q_{inj}=0.05 cm^3/min and temperature of T_{exp}=21°C. As mentioned earlier, this could be because of lower capillary number in the case of Type-II crude oil compared to Type-I. It is noteworthy that capillary number is defined as the ratio of viscous force to the capillary force. Since Type-II crude oil is heavier and has higher viscosity compared to Type-I, capillary force existing in the pore throats saturated with Type-II oil are considered to be higher causing the ratio of viscous force (exerted by water) to capillary force (due to the higher interfacial tension of the oil) to be lower. The lower the values of capillary number, the higher the residual saturation and the lower the recovery factor will be.

Comparison of the performance of waterflooding conducted in a dual permeability micromodel saturated with two types of crude oils (Type-I and II) is shown in **Figure 4.27** through plotting the recovery factor of both cases as a function of PVs of injected water. The maximum recovery factor achieved for both cases at 1.6 PVs of water injected were 57.6% and 29.7% for Type-I and Type-II oils, respectively. This can be translated to 48.5% reduction in recovery factor for 5 degrees of decrease in oil API gravity.

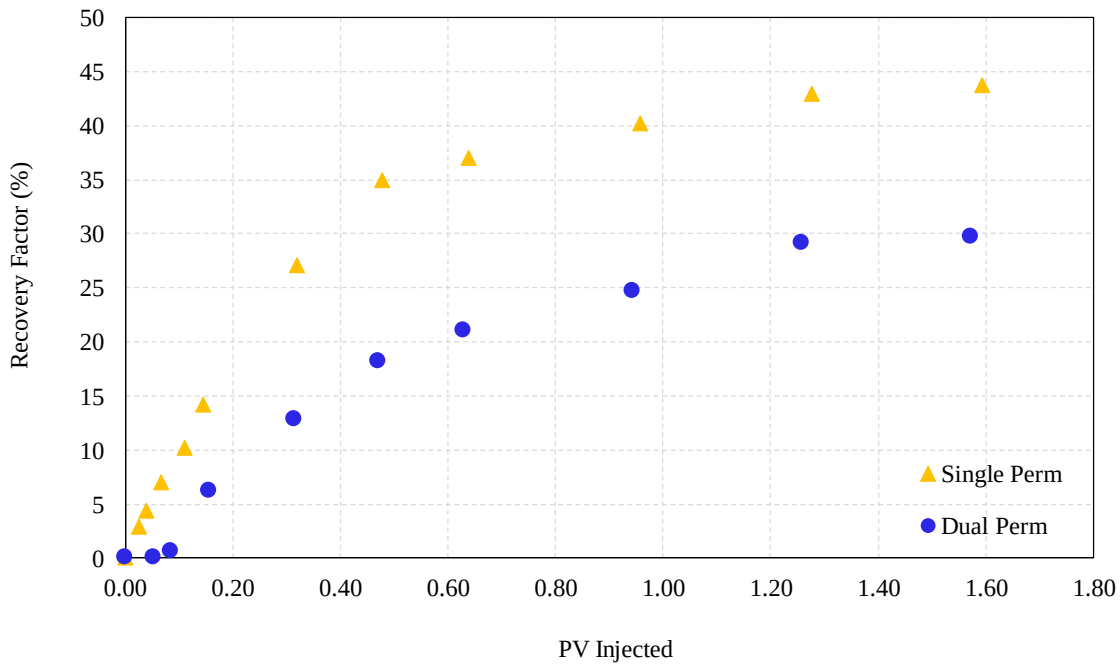

Figure 4.26: Recovery factor obtained during the waterflooding of dual-perm and single-perm micromodels saturated with Type-II heavy oil at injection rate of q_{inj}=0.05 cm^3/min and constant temperature of T_{exp}=21ºC.

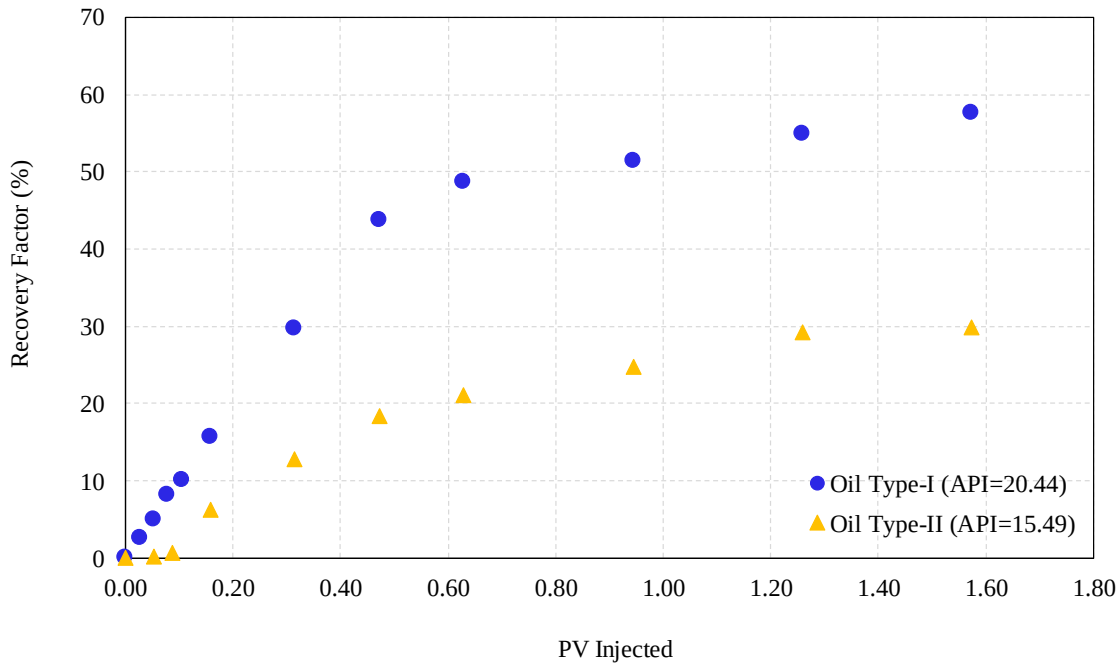

Figure 4.27: Recovery factor obtained during the waterflooding of dual-perm micromodel saturated with Type-I and Type-II heavy oils at injection rate of q_{inj}=0.05 cm^3/min and constant temperature of T_{exp}=21°C.

Effect of injection rate on the displacement efficiency of waterflooding in the dual permeability micromodel saturated with Type-II crude oil (API=15.49)

To observe and quantify the effect of water injection rate on the displacement performance of waterflooding in a Type-II oil saturated dual permeability micromodel, an additional test at the injection rate of q_{inj}=0.025 cm^3/min was conducted at the constant temperature of T_{exp}=21°C.

Images taken during the displacement processes at the same PVs of injected water for waterflooding of Type-II oil at two injection rates are presented in **Figures 4.28(a)** to **(b)** and **Figure 4.29(a)** to **(b)**. As it can be seen, prior to the breakthrough, water injection at lower rate of q_{inj}=0.025 cm^3/min resulted in better displacement of oil. However, the displacement efficiency of the base case waterflooding which was conducted at q_{inj}=0.05 cm^3/min was better compared to the lower injection rate.

(a) t=60 seconds (q_{inj}=0.025 cm^3/min)

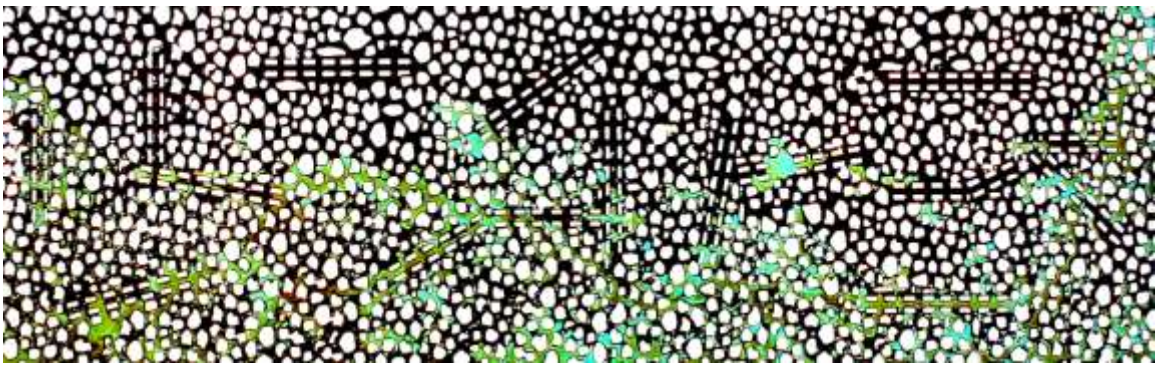

(b) t=60 seconds (q_{inj}=0.05 cm^3/min)

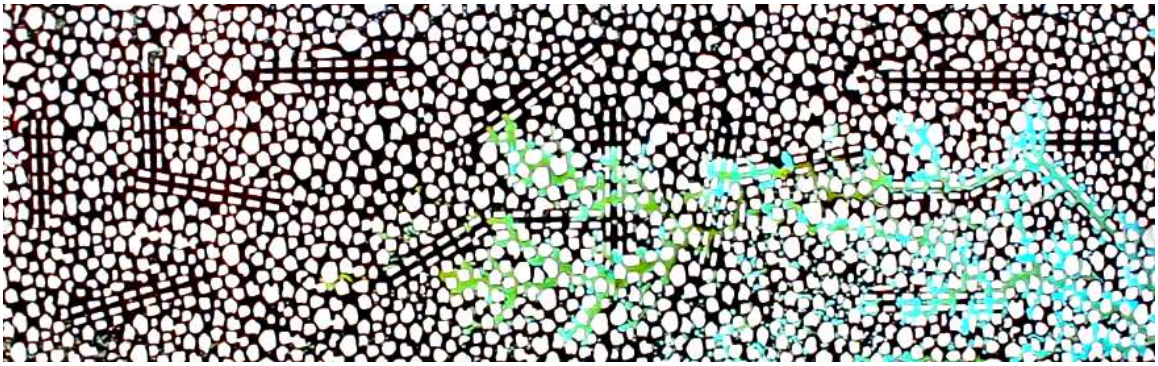

Figure 4.28: Frontal advancement of water during waterflooding of Type-II crude oil in the dual permeability micromodel before breakthrough at injection rates of (a) q_{inj}=0.025 cm^3/min, (b) q_{inj}=0.05 cm^3/min, constant temperature of T_{exp}=21^{o}C, and equal PVs of injected water.

(a) t=1320 seconds (q_{inj}=0.025 cm^3/min)

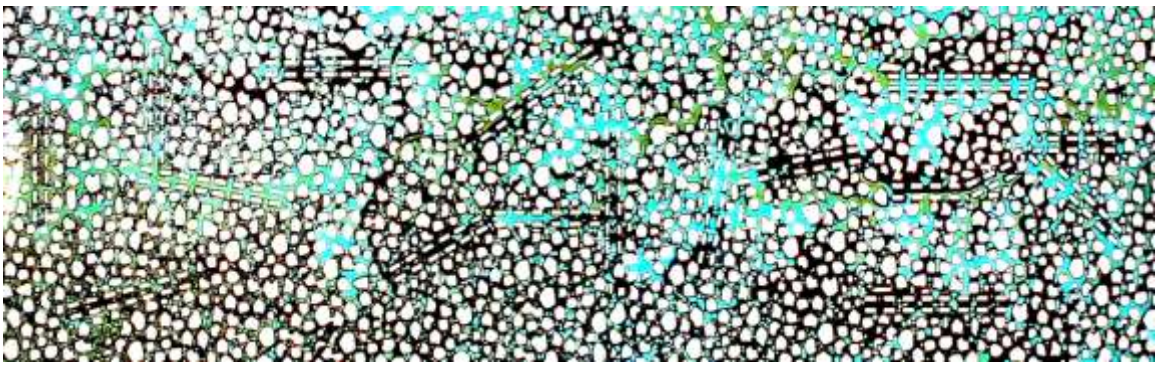

(b) t=660 seconds (q_{inj}=0.05 cm^3/min)

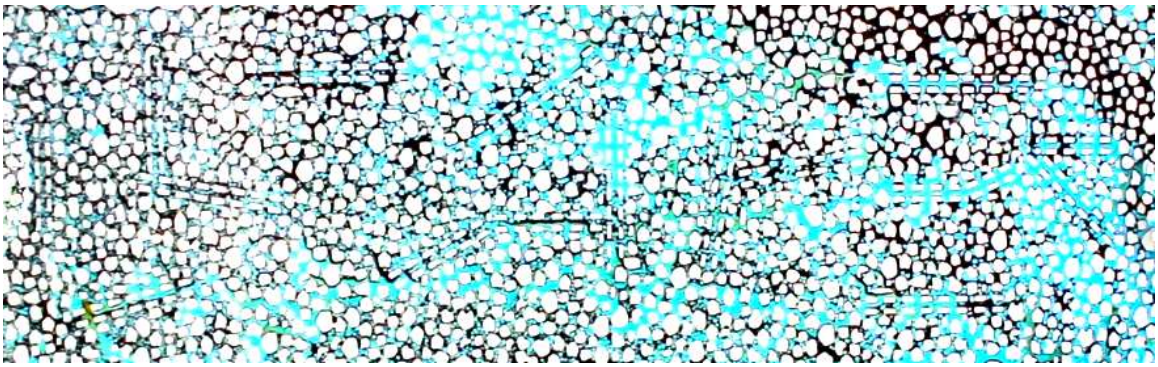

Figure 4.29: Frontal advancement of water during waterflooding of Type-II crude oil in the dual permeability micromodel after breakthrough at injection rates of (a) q_{inj}=0.025 cm^3/min, (b) q_{inj}=0.05 cm^3/min, constant temperature of T_{exp}=21^{o}C, and equal PVs of injected water.

Recovery factor of the displacement processes conducted at q_{inj}=0.025 cm^3/min is compared with the base case in **Figure 4.30**. As it can be seen, prior to the breakthrough, water injection at lower rate of q_{inj}=0.025 cm^3/min resulted in better displacement of oil. However, overall displacement efficiency of the base case waterflooding which was conducted at q_{inj}=0.05 cm^3/min (RF=29.7%) was better compared to the lower injection rate of q_{inj}=0.025 cm^3/min (RF=23.7%).

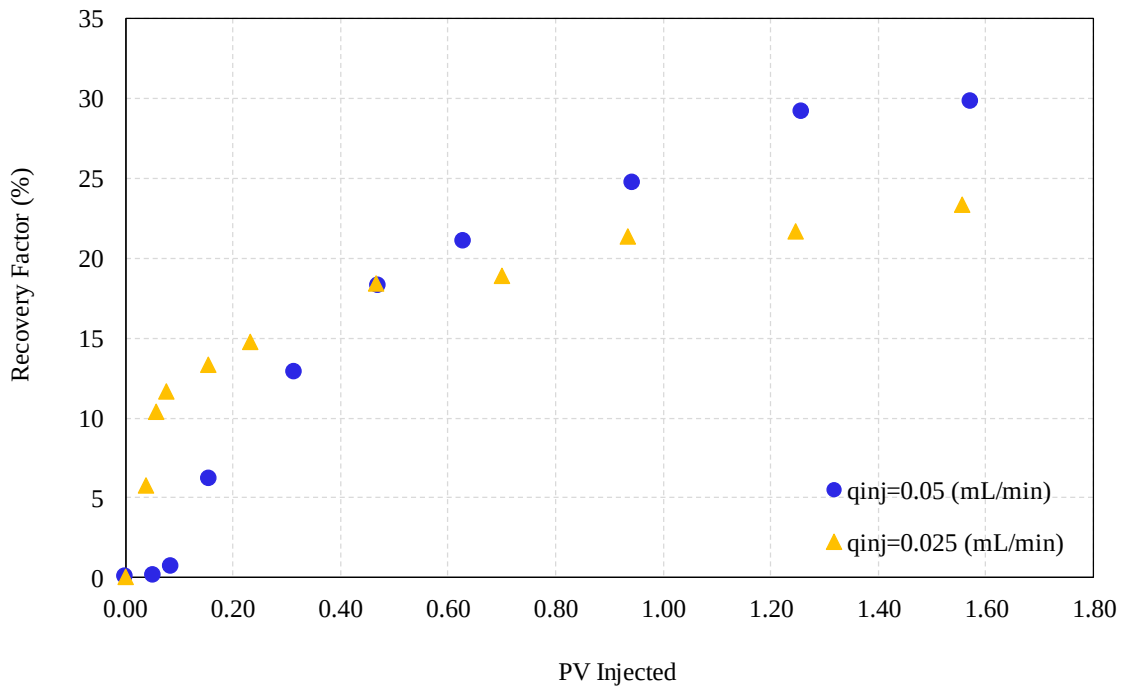

Figure 4.30: Recovery factor obtained during the waterflooding of dual-perm micromodel saturated with Type-II heavy oil at injection rates of q_{inj}=0.025 cm^3/min and q_{inj}=0.05 cm^3/min and constant temperature of T_{exp}=21ºC.

Effect of temperature on the displacement efficiency of waterflooding in the dual permeability micromodel saturated with Type-II crude oil (API=15.49)

The dual permeability micromodel saturated with Type-II crude oil was waterflooded at three temperatures of T_{exp}=21^{o}C, 30^{o}C, and 45^{o}C at the constant water injection rate of q_{inj}=0.05 cm^{3}/min, through three individual flooding tests.

Images of the water frontal advancement in the dual permeability micromodel for three cases of waterflooding conducted at various temperatures presented in Figure **4.31(a)** to **(c)** show that increasing temperature from T_{exp}=21^{o}C to 30^{o}C and 45^{o}C resulted in better displacement of oil particularly those contained in high permeability channels. This is simply because at higher temperatures, viscosity of the heavy oil is substantially decreased and consequently the capillary force is decreased. Reduction of the capillary force in the high permeability channels allow the viscous force exerted by the water to overcome and displace the oil.

A closer comparison of the three images presented in **Figure 4.31(a)** to **(c)** show that water was able to also move into more regular pores and pushing oil out of them when temperature increased.

Due to the lower oil and water viscosity at elevated temperatures, water spreads and breakdown into small droplets particularly in larger pores. This discontinuity of water which is somehow snap-off trapping of water in the oil regions are shown with red circles/ellipses on the **Figure 4.31(a)** to **(c)** and are more pronounced at higher temperatures.

(a) t=600 seconds (T_{exp}=21^{o}C)

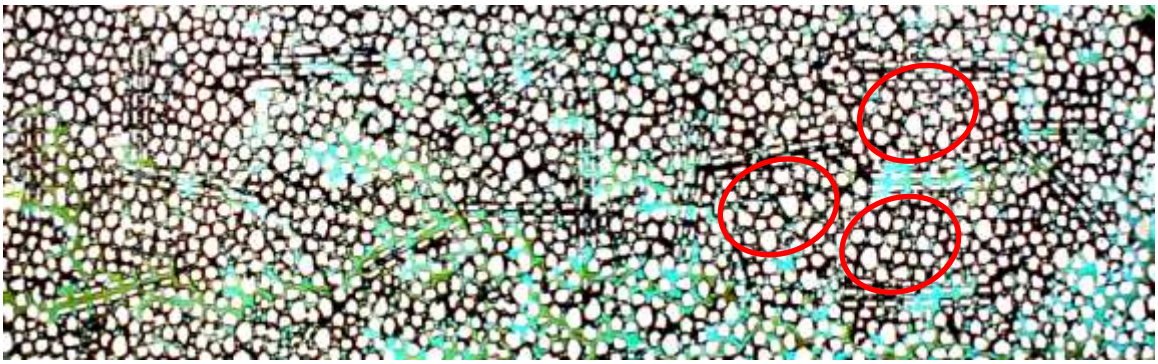

(b) t=600 seconds (T_{exp}=30°C)

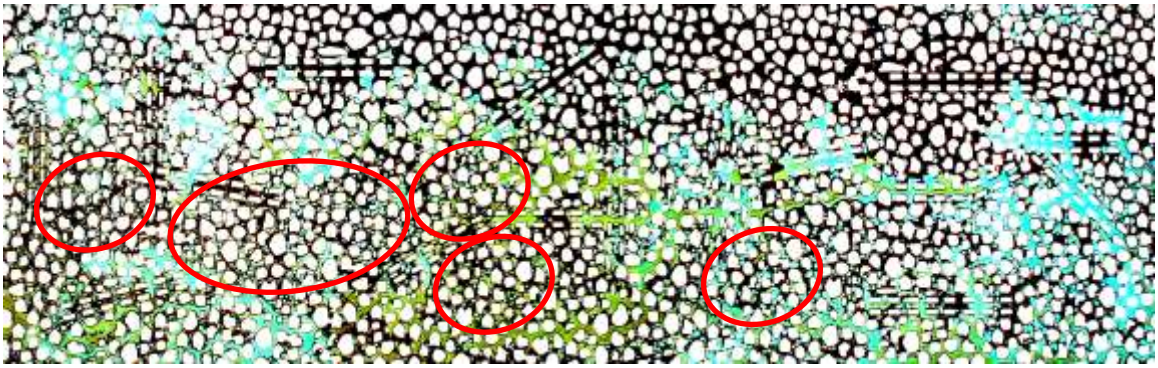

(c) t=600 seconds (T_{exp}=45°C)

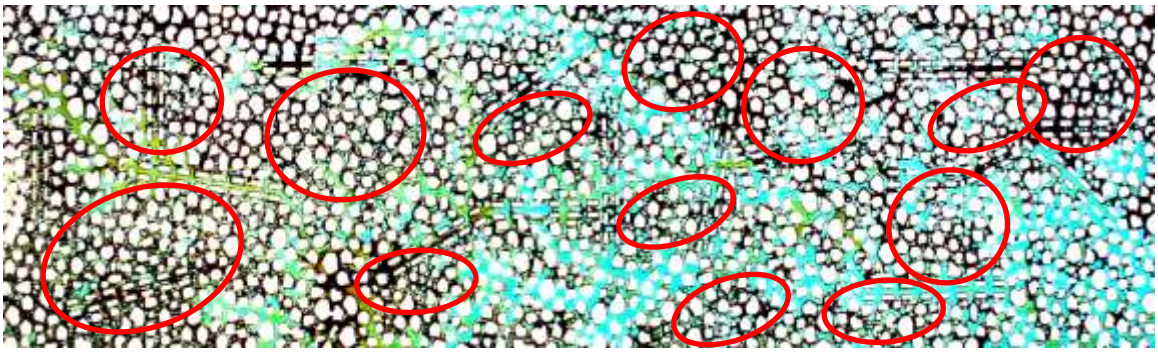

Figure 4.31: Frontal advancement of water during waterflooding of Type-II crude oil in the dual permeability micromodel after breakthrough at constant injection rate of q_{inj}=0.05 cm^3/min and temperatures of (a) T_{exp} =21°C, (b) T_{exp}=30°C, and (c) T_{exp} =45°C for the same 1.6 PVs of injected water.

Recovery factors of three cases of waterflooding conducted at aforementioned temperatures in the dual permeability micromodel at the constant water injection rate of q_{inj}=0.05 cm^3/min are plotted as a function of PVs of injected water and presented in **Figure 4.32**. The ultimate recovery factor of the three cases at 1.6 PVs of injected water were.29.7%, 36.3% and 63.8% for T_{exp}=21^{o}C, 30^{o}C and 45^{o}C, respectively. This can be translated into 1.42% of recovery increase per one degree of increase in the temperature.

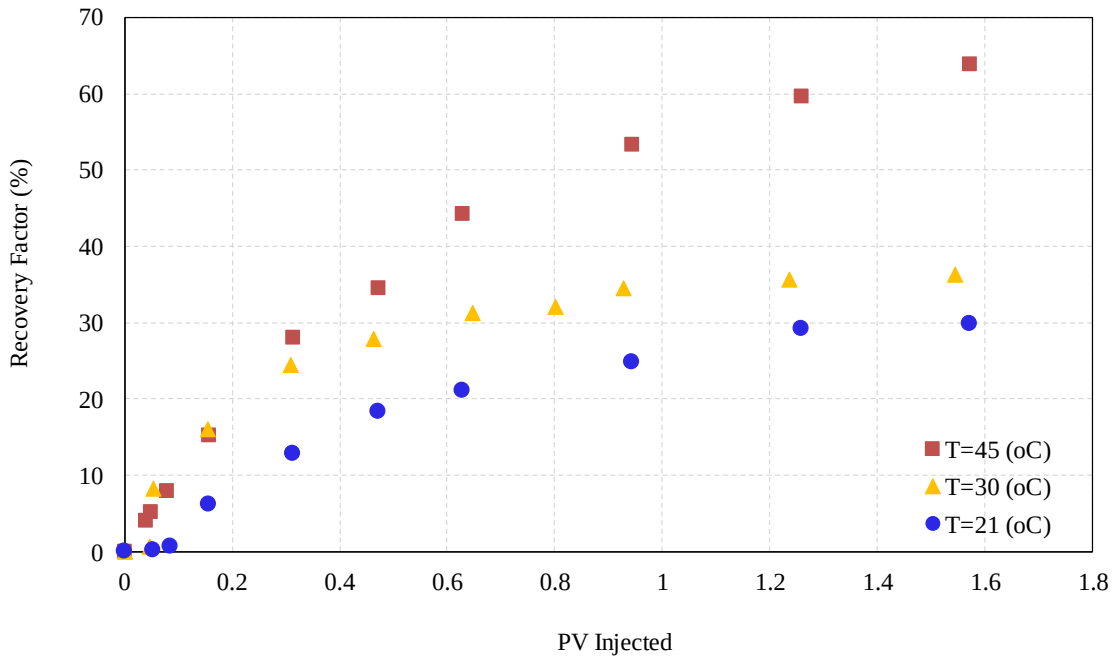

Figure 4.32: Recovery factor obtained during the waterflooding of dual-perm micromodel saturated with Type-II heavy oil at injection rate of q_{inj}=0.05 cm^3/min and temperatures of T_{exp}=21°C, 30°C, and 45°C.

4.6. Wettability analysis of the micromodels

As mentioned earlier, micromodels used in this study were showed oil wet tendency. To further validate this assumption, two cases were considered. **Figure 4.33(a)** shows the single-permeability micromodel that has been oil saturated after initially water saturated. As it can be observed from a zoomed-in portion of the model, no water has been remaining around the grains in the model during and after oil saturation or the amount is so negligible which was not captured by the camera. In addition, at it can be seen from **Figure 4.33(b)**, when oil saturated dual-permeability micromodel is displaced with carbonated water, oil has been remaining around the grains leaving the water to be dispersed in pore area. The zoomed-in fraction of the dual permeability micromodel also confirmed the snap-off mechanism where various sizes of water globules are formed and spread during the displacement process.

Similar behavior was found in almost all of the displacement scenarios described in this study. Therefore, it was concluded that micromodels used in this study are of the oil-wet nature though in some limited cases and only in small portions of the micromodels, mixed-wet scenarios were also observed.

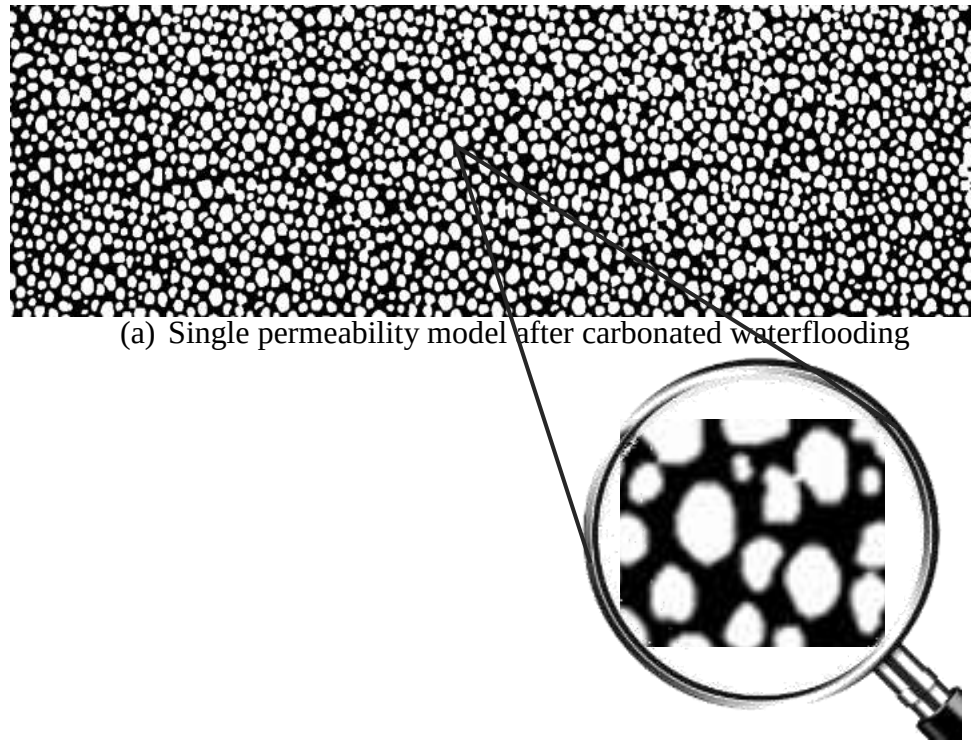

(a) Single permeability model after carbonated waterflooding

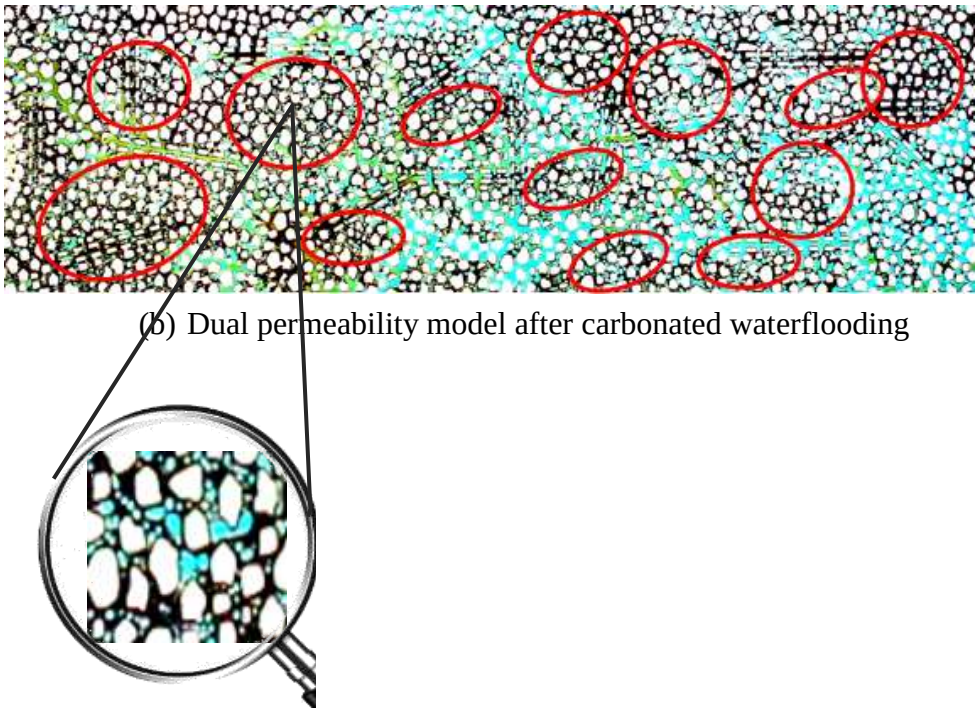

(b) Dual permeability model after carbonated waterflooding

Figure 4.33: Wettability analysis of the (a) single-permeability micromodel saturated with oil and, (b) dual-permeability micromodel saturated with heavy oil and displaced with carbonated water.

4.7. Chapter summary

In this chapter, glass micromodels were used to visually observe the effect of various parameters such as injection rate, temperature, dual permeability porous media, and oil API gravity on the performance of waterflooding. Results obtained with Type-II heavy oil with lower API gravity is highlighted here in the chapter summary.

Overall recovery factor of the various cases conducted using two different types of heavy oils show that water injection rate of q_{inj}=0.05 cm^3/min is the most efficient rate. As an example, the displacement efficiency of the base case waterflooding which was conducted at q_{inj}=0.05 cm^3/min resulted in 29.7% recovery factor whereas water injection at the rate of q_{inj}=0.025 cm^3/min produced only 23.7% of the oil in dual permeability porous media.

The ultimate recovery factor of the three cases of waterflooding in the dual permeability micromodel saturated with Type-II heavy oil at the temperatures of T_{exp}=21 ^oC, 30^oC and 40^oC and 1.6 PVs of injected water were.29.7%, 36.3% and 63.8%, respectively. These results show the significance of the effect of temperature on the waterflooding performance in dual permeability porous media.

Comparison of the waterflooding recovery factor in a dual permeability micromodel saturated with two types of crude oils (Type-I and II) showed that at 1.6 PVs of water injected, 57.6% of Type-I crude oil is recovered. When test was conducted using crude oil Type-II, only 29.7% of the oil could be recovered at the same experimental and operational conditions. This can be translated to 48.5% reduction in recovery factor for 5 degrees of decrease in oil API gravity.

CHAPTER FIVE: Carbonated waterflooding of heavy oils

In this chapter, results of performance evaluation of carbonated waterflooding (CWF) applied as the secondary oil recovery stage in two different types of micromodels saturated with two heavy crude oils are presented. Results obtained were compared with conventional waterflooding conducted in the same micromodels and under the same operational conditions. In addition, effects of parameters such as oil API gravity and dual permeability on the displacement efficiency of the carbonated waterflooding is visually and quantitively evaluated.

5.1. Introduction

As it was observed in previous chapter, increasing the temperature of the system resulted in higher recovery factor of waterflooding when tested in the heavy oil saturated micromodels. This was mainly because of the lower oil viscosity, lower interfacial tension of the oil and lower capillary force existing in the system at elevated temperatures. In practice, increasing the reservoir's temperature through injection of hot fluids is costly and may not be feasible for heavy oil reservoirs with small thickness. In the other side, presence of low API gravity and high viscosity oil cause the waterflooding performance to be poor. Therefore, carbonated waterflooding might be considered as an alternative in order to reduce the oil viscosity and improve the recovery factor of waterflooding processes in heavy oil systems. Based on this assumption, results obtained during carbonated waterflooding tests conducted in two different micromodels containing two different grades of heavy oils are discussed in this chapter.

5.2. Experimental setup and procedure

Experimental setup and procedure for carbonated waterflooding was very similar to the conventional waterflooding presented in chapter-4. One major difference is that an additional transfer cylinder containing carbonated water was added to the setup. Carbonated water was prepared at carbonation pressure of $P_{carbonation}$=1 MPa and T_{exp}=21^{o}C prior to the test by allowing CO_2 to be dissolved into the brine solution of 20,000 ppm and reaching equilibrium. Thereafter, injection of carbonated water into the heavy saturated micromodel at q_{inj}=0.05 cm^3/min and temperature of T_{exp}=21^{o}C was following the same procedure as described for conventional waterflooding.

5.2.1. Comparison of carbonated waterflooding with conventional waterflooding

Injection of carbonated water ($P_{carbonation}$=1 MPa) into the single permeability micromodel saturated with Type-I crude oil at the rate of q_{inj}=0.05 cm^3/min and temperature of T_{exp}=21^{o}C showed distribution of the water front throughout the pore networks compared to branched fingering phenomena happening during conventional waterflooding. As it can be observed in Figure 5.1, water front is spread and penetrated into the oil in most of the areas as time grows from 60 seconds to 420 seconds.

Figure 5.2(a) and (b) is comparing the two cases of conventional and carbonated waterflooding performed under the same conditions in the same heavy oil saturated, (crude oil Type-I) single permeability, micromodel. As it can be seen from the changes in the colors in the areas that water contacted, during carbonated waterflooding CO_2 moved out of the water and dissolved into the oil. This caused oil viscosity to be reduced hence, oil is displaced.

t=60 seconds

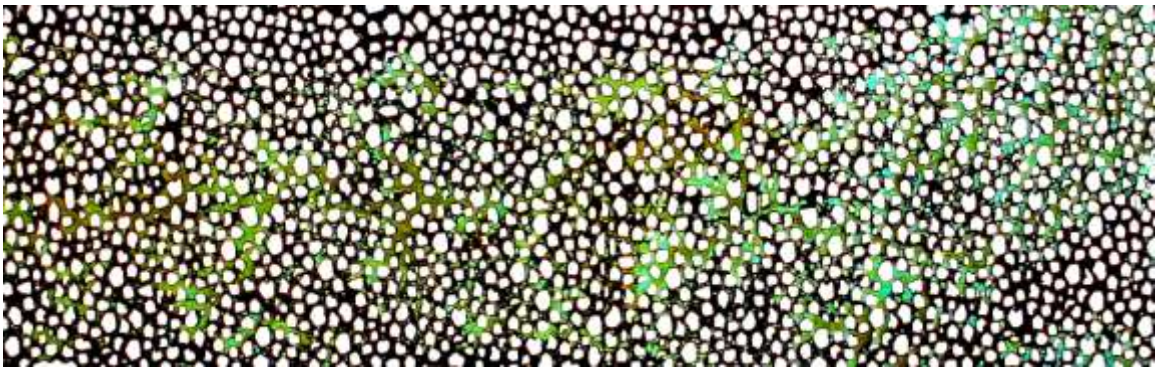

t=180 seconds

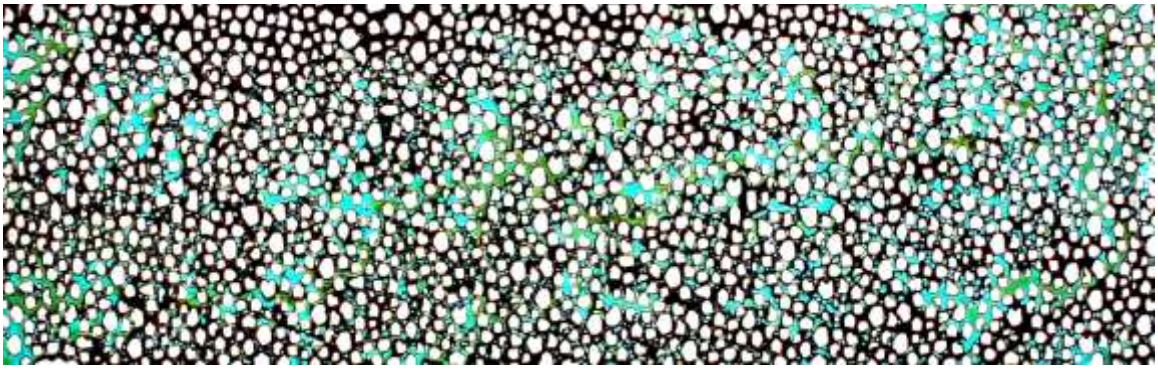

t=420 seconds

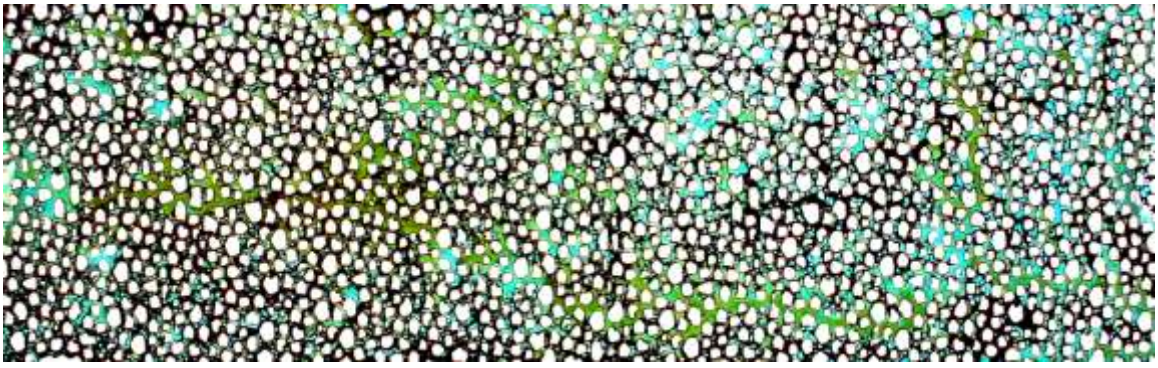

Figure 5.1: Frontal advancement of water during carbonated waterflooding of Type-I crude oil in the single permeability micromodel at constant injection rate of q_{inj}=0.05 cm^3/min and temperature of T_{exp} =21^{o}C at various time frames.

(a) conventional (t=60 seconds)

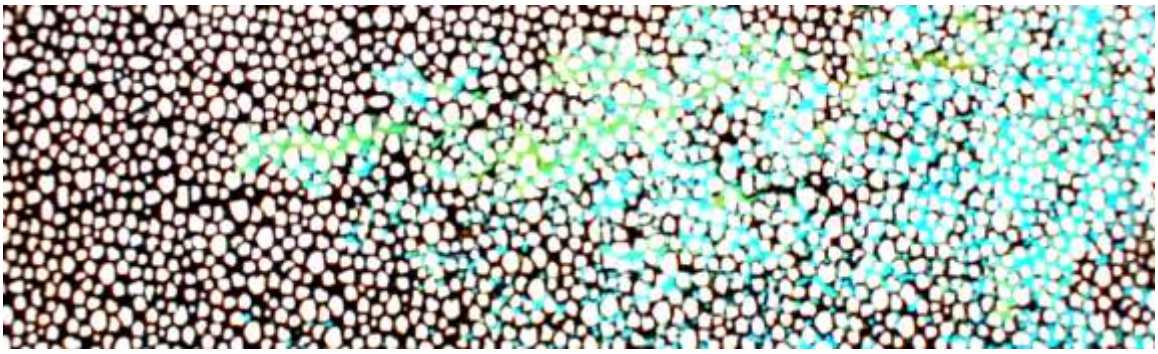

(b) carbonated waterflooding (t=60 seconds)

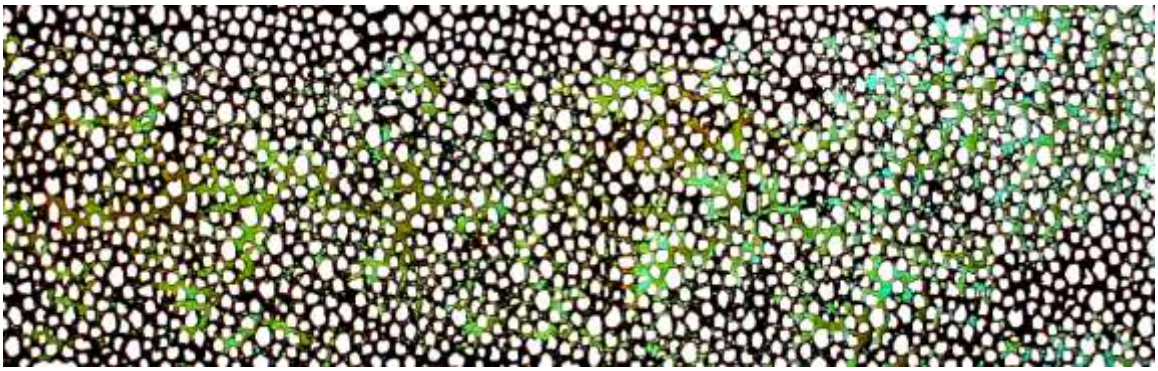

Figure 5.2: Frontal advancement of water during (a) conventional and (b) carbonated waterflooding of Type-I crude oil in the single permeability micromodel at constant injection rate of q_{inj}=0.05 cm^3/min and temperature of T_{exp} =21^{o}C at various time frames.

Figure 5.3 Shows recovery factor of both conventional and carbonated waterflood conducted in the single permeability micromodel saturated with Type-I crude oil. At about 1.6 PVs of injected water, recovery factor of carbonated waterflooding was estimated to be 70% while the conventional waterflooding recovered 61% of the same oil. This 9% improvement was mainly because of the contribution of the dissolved CO_2 in the water which left the water and dissolved in the oil at the contact interface of oil/water. Viscosity and IFT reduction and solution gas drive mechanisms were very clearly observed during the displacement process and recorded.

When carbonated waterflooding was implemented for the heavier oil system (Type-II crude oil with oil API gravity of 15.49) and results were compared with conventional waterflooding, the ultimate oil recovery was improved from 44.3% to 46.5% at about 1.6 PVs injected water (**Figure 5.4)**.

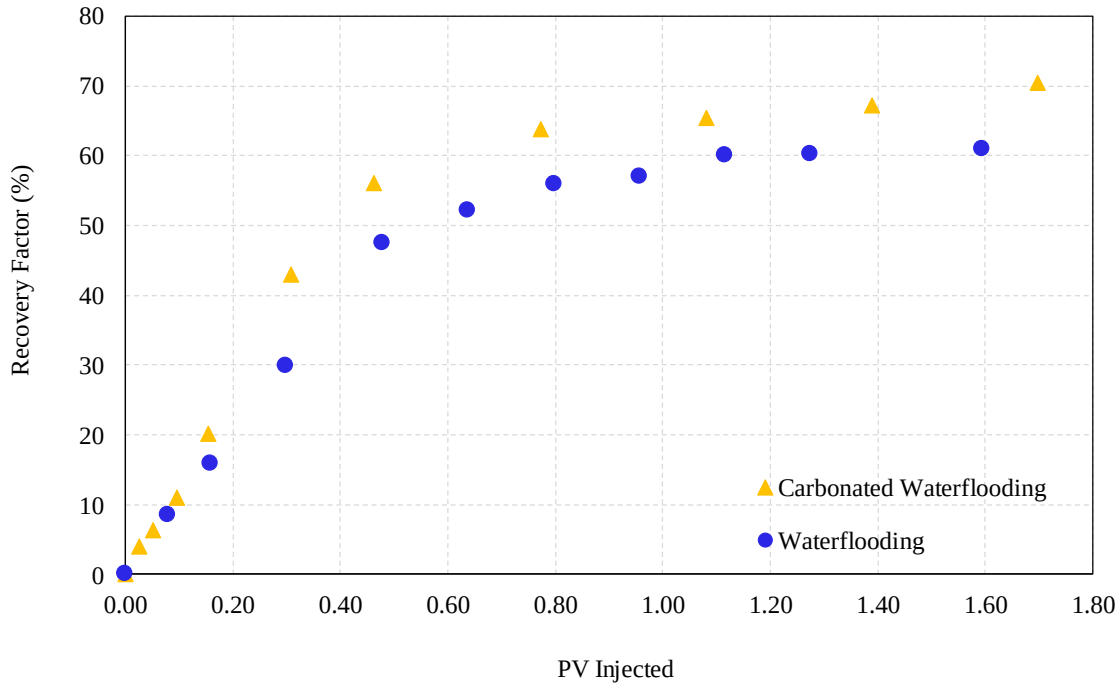

Figure 5.3: Recovery factor of conventional and carbonated waterflooding of single permeability micromodel saturated with Type-I heavy oil at injection rate of q_{inj}=0.05 cm^3/min and temperature of T_{exp}=21^{o}C.

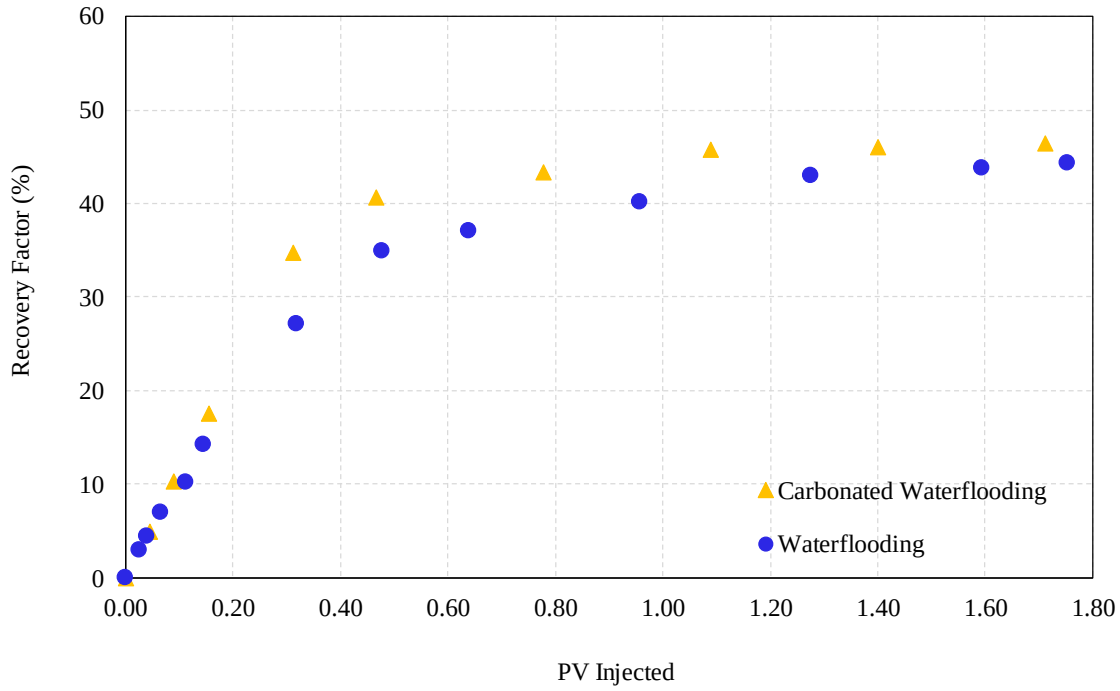

Figure 5.4: Recovery factor of conventional and carbonated waterflooding of single permeability micromodel saturated with Type-II heavy oil at injection rate of q_{inj}=0.05 cm^3/min and temperature of T_{exp}=21^{o}C.

Although 2.2% of improvements was observed when carbonated waterflooding was implemented, image analysis of the real photos of the displacement process clearly show the potential of carbonated waterflooding in reducing viscous fingering as presented in **Figure 5.5 (a) to (c)**. Compared to the oil Type-I, CO_2 diffusion in the heavier crude oil was less causing the carbonated waterflooding to also experience viscous fingering. **Figure 5.6 (a)** and **(b)** compares the frontal advancement and distribution of water after at about 1.74 PVs of water injected for both conventional and carbonated waterflooding, respectively. The amount of injected pore volume of 1.74 was selected as photos of both cases were available. Areas where improvements were very obvious during carbonated waterflooding are highlighted with red circles. Also, some areas where conventional waterflooding seems to displace the oil more efficiently compared to carbonated waterflooding are highlighted with dashed blue circles.

(a) t=60 seconds

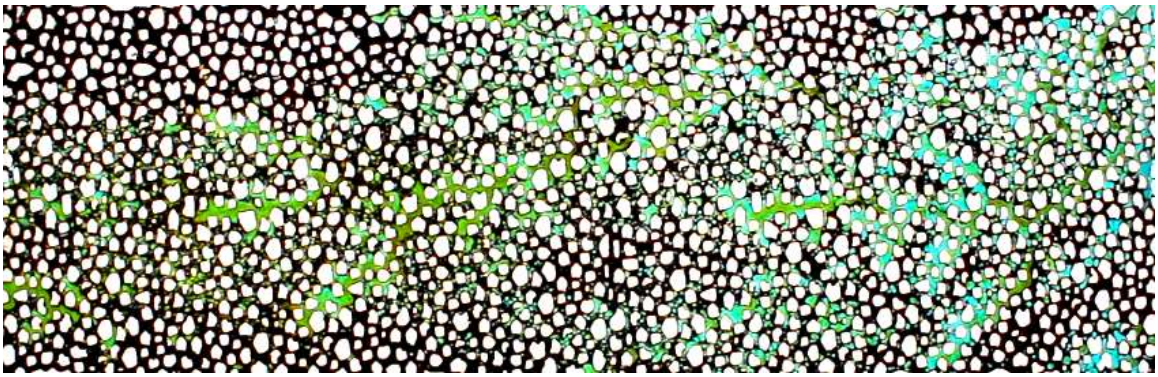

(b) t=330 seconds

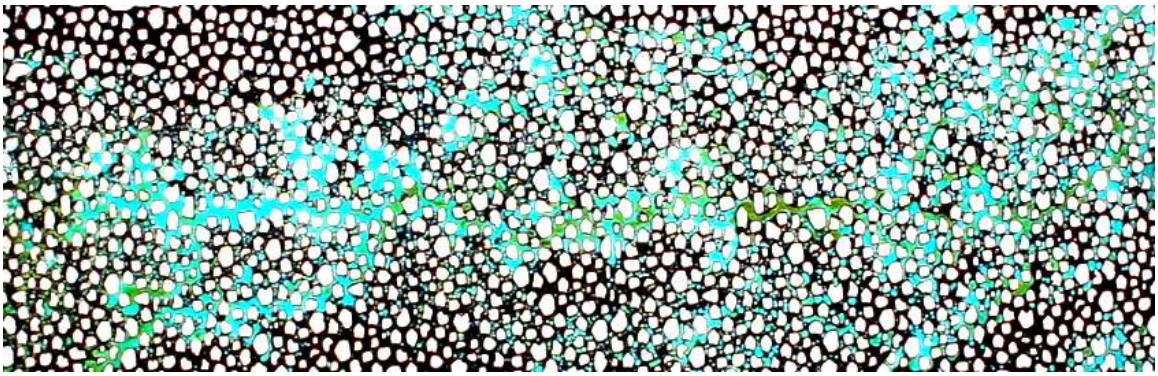

(c) t=540 seconds

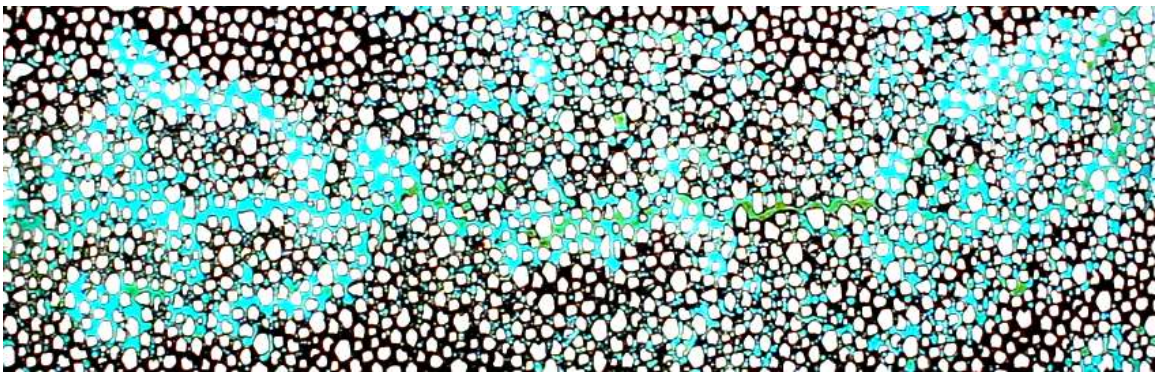

Figure 5.5: Frontal advancement of water during carbonated waterflooding of Type-II crude oil in the single permeability micromodel at various time frames and constant injection rate of q_{inj}=0.05 cm^3/min and temperature of T_{exp} =21^{o}C.

t=660 seconds, conventional waterflooding (oil Type-II, API=15.49)

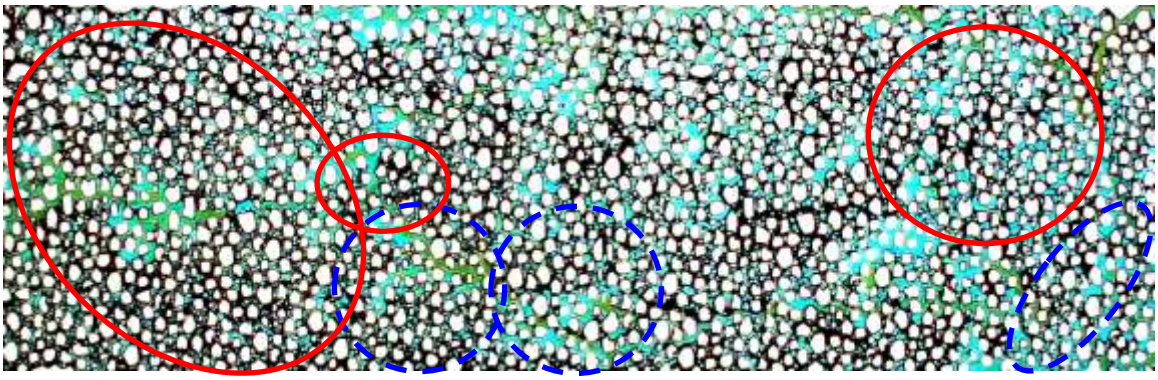

t=660 seconds, carbonated waterflooding (oil Type-II, API=15.49)

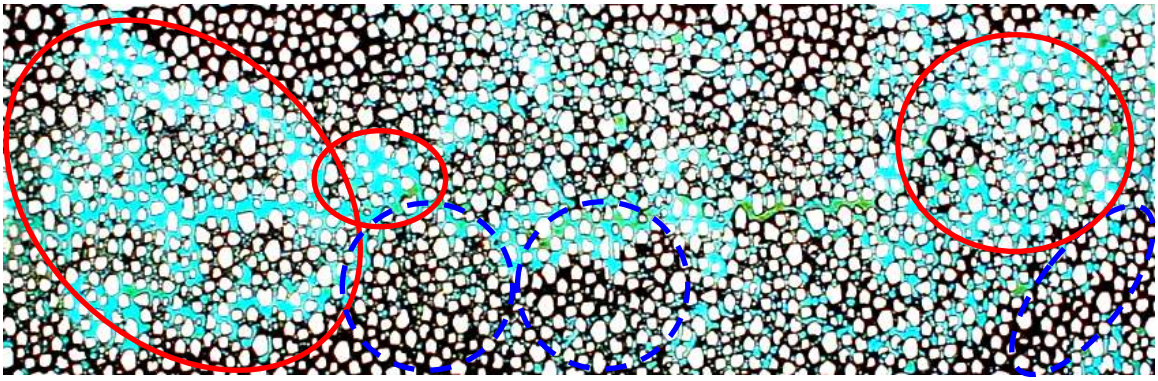

Figure 5.6: Frontal advancement of water during (a) conventional and (b) carbonated waterflooding of Type-II crude oil in the single permeability micromodel at constant injection rate of q_{inj}=0.05 cm^3/min and temperature of T_{exp} =21°C for various time frames.

5.2.2. Effect of oil API gravity on carbonated waterflooding

Figure 5.7 shows recovery factor of carbonated waterflooding applied to Type-I and Type-II heavy oil saturated micromodel with single permeability. The ultimate recovery factors achieved after injection of 1.7 PVs of injection were 70.5% and 46.5% for Type-I and Type-II heavy crude oils, respectively. This indeed confirms the significance of oil API gravity as one of the main screening criterion for carbonated waterflooding as a means of enhanced oil recovery.

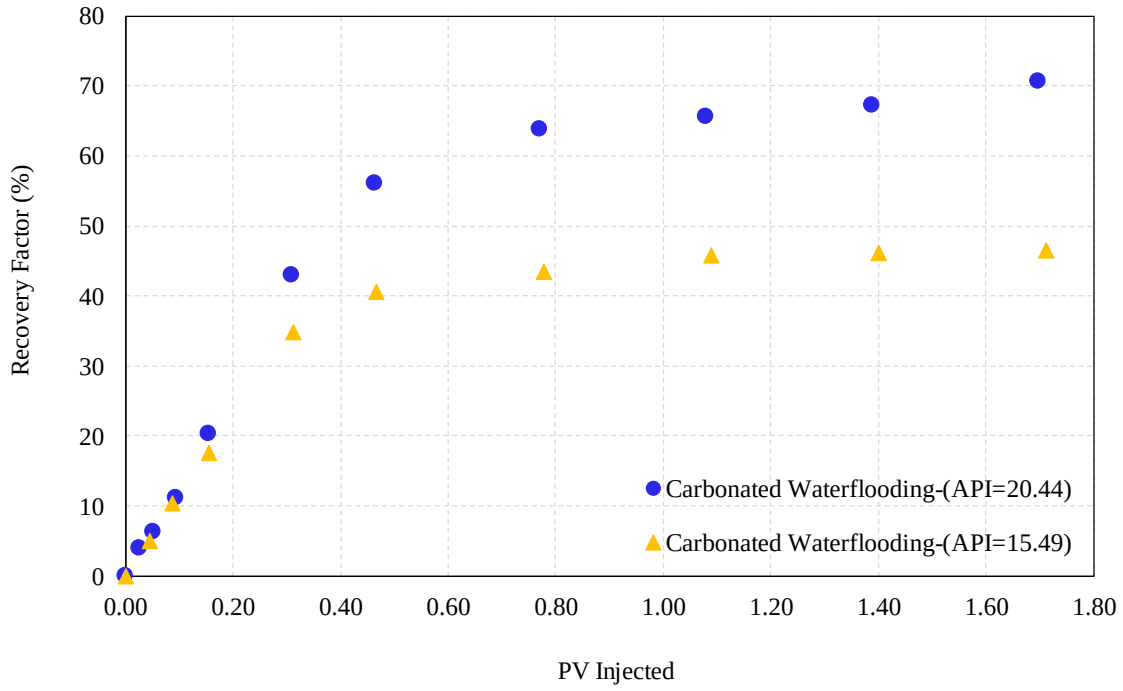

Figure 5.7: Recovery factor of carbonated waterflooding of single permeability micromodel saturated with Type-I and Type-II heavy oils at injection rate of q_{inj}=0.05 cm^3/min and temperature of T_{exp}=21^{o}C.

5.2.3. Carbonated waterflooding in dual-perm porous media

Carbonated waterflooding was also applied to dual permeability micromodel saturated with Type-II heavy oil (API=15.49). Results were compared with those obtained during the carbonated waterflooding of the same oil in single permeability model. As it can be observed from **Figure 5.8 (a)** to **(c)**, addition of carbon dioxide in the water resulted in better distribution of the oil in the reservoir where CO_2 was partially released into the oil, reduced the oil viscosity and helped producing oil via high permeability channels. Figure 5.9 illustrates that the frontal advancement of water in the case of carbonated waterflooding in dual permeability model is more spread compared to the sharper front observed in the case of singe permeability model.

Figure 5.10 compares the recovery factor of carbonated waterflooding conducted in two cases of single and dual permeability micromodels. As it can be seen, the ultimate oil recovery factor after 1.56 PVs of injected water were 67% and 46.3% for dual and single permeability cases, respectively. This concludes that presence of high permeability channels is beneficial to carbonated waterflooding as it continuously drained and filled because of the diluted oil with CO_2. In the other hand, water initially displaces oil from these channels but when CO_2 dissolves in the oil, the diluted oil will refill the channels, hence, recovery factor increased.

(a) t=60 seconds

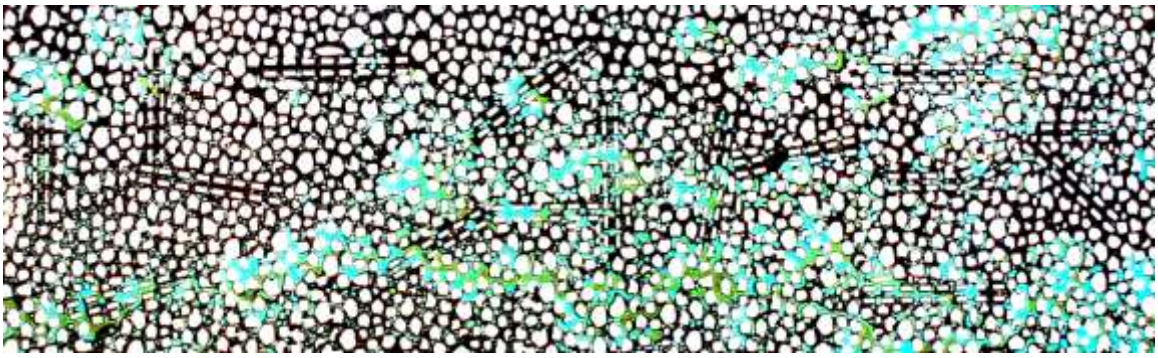

(b) t=240 seconds

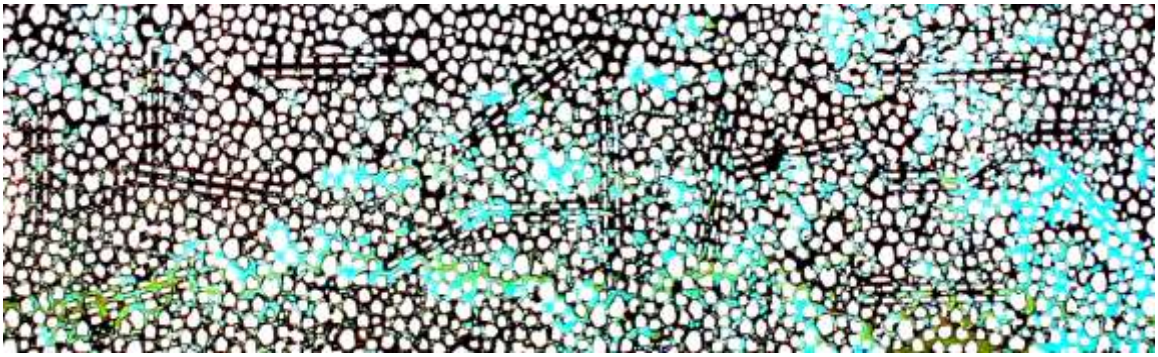

(a) t=540 seconds

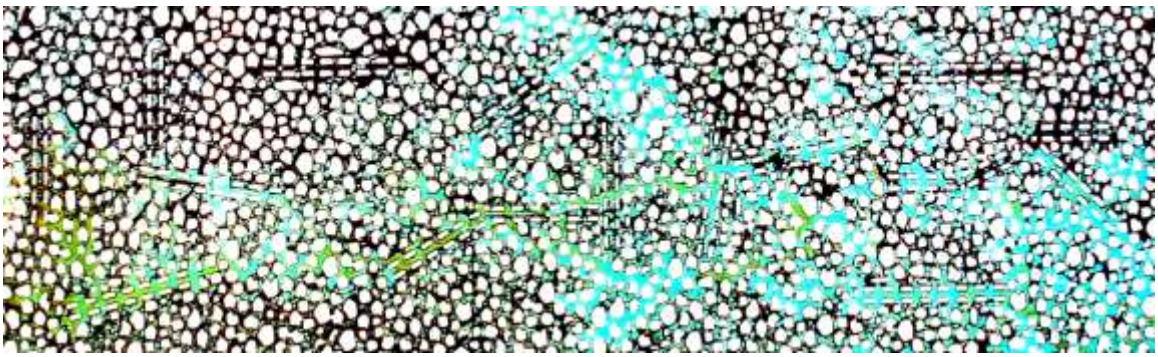

Figure 5.8: Frontal advancement of water during carbonated waterflooding of Type-II crude oil in the dual permeability micromodel at various time frames and constant injection rate of q_{inj}=0.05 cm^3/min and temperature of T_{exp} =21^{o}C.

t=600 seconds, carbonated waterflooding in single-perm micromodel (oil Type-II, ^{o}API=15.49)

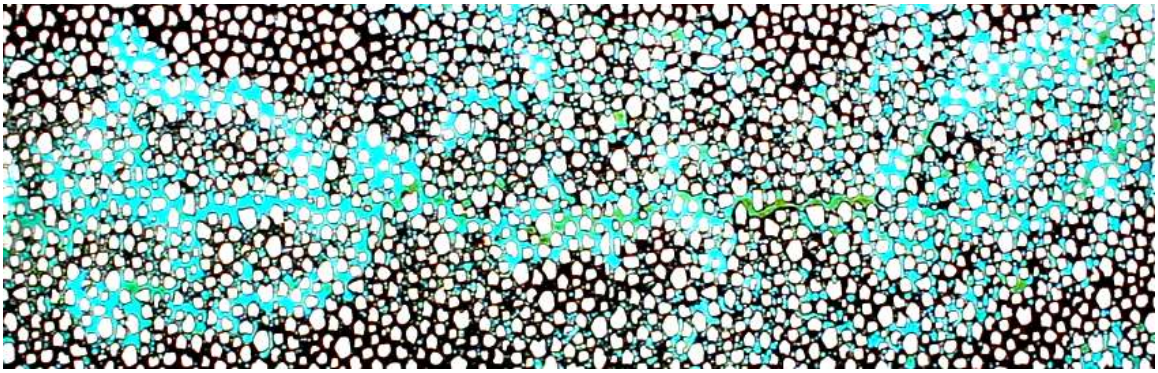

t=600 seconds, carbonated waterflooding in dual-perm micromodel (oil Type-II, ^{o}API=15.49)

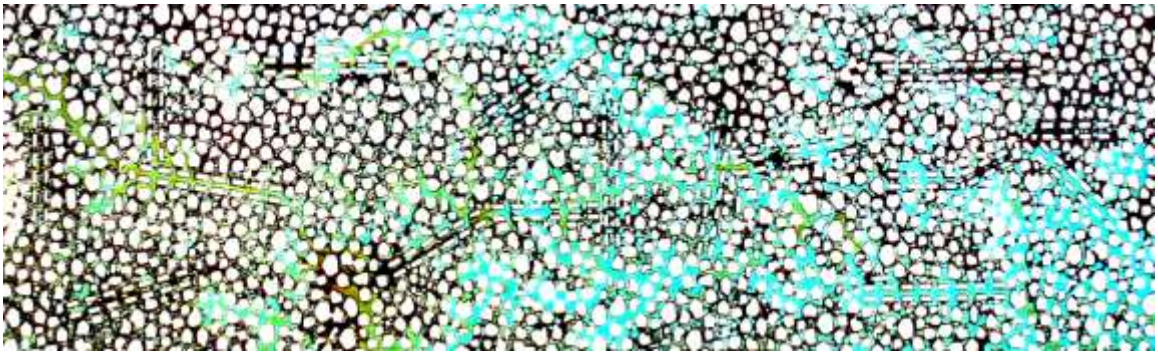

Figure 5.9: Frontal advancement of water during carbonated waterflooding in (a) single permeability (b) dual permeability micromodels saturated with Type-II crude oil, at constant injection rate of q_{inj}=0.05 cm^3/min and temperature of T_{exp} =21^{o}C for various time frames.

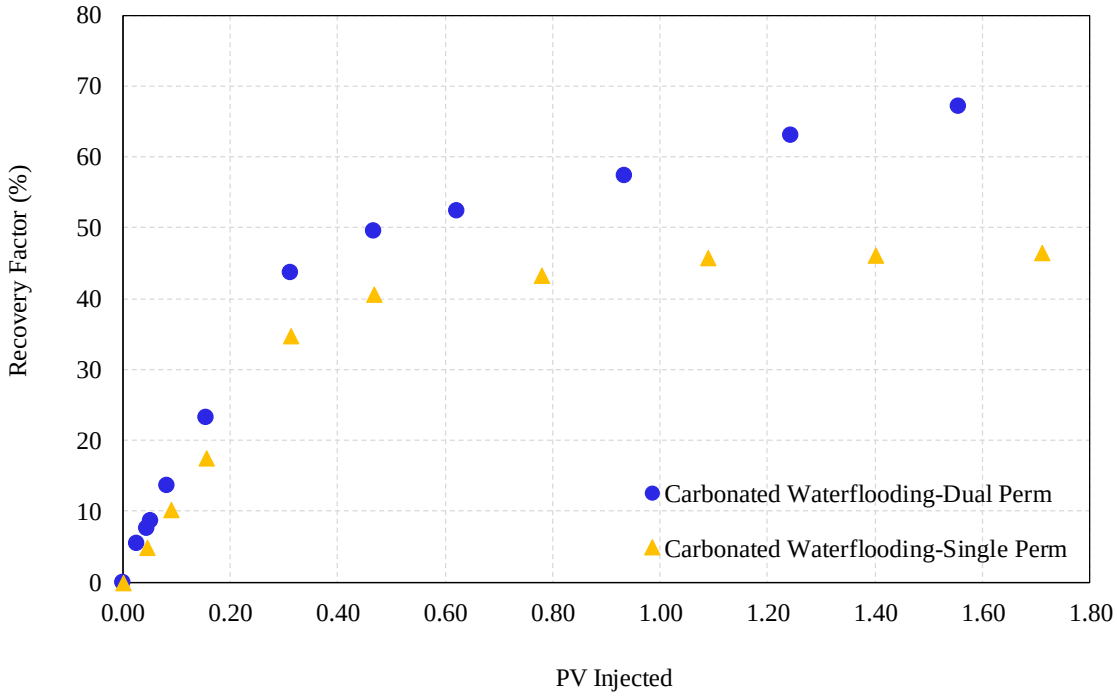

Figure 5.10: Recovery factor of carbonated waterflooding of single and dual permeability micromodels saturated with Type-II heavy oil at injection rate of q_{inj}=0.05 cm^3/min and temperature of T_{exp}=21°C.

5.3. Chapter summary

Carbonated waterflooding process was applied as a means of displacing phase to two types of heavy oils through utilization of two sate-of-the art micromodels designed and manufactured throughout this study. While irregular shape grains representing actual reservoirs were considered for both types of micromodels, high permeability channels representing connected and disconnected fractures or dilated mediums were included in one of them.

Comparative evaluation of the two cases of conventional and carbonated waterflooding showed about 9% improvements (from 61% to 70%, respectively) in the recovery factor of the Type-I oil (API=20.44) when carbonated water ($P_{carbonation}$=1 MPa, T_{exp}=21^{o}C) was injected at a constant rate of q_{inj}=0.05 cm^{3}/min for 1.6 PVs into the single permeability micromodel. This improvement was from 44.26% to 46.51% when applied to Type-II crude oil at the same experimental conditions and operations. The low performance of carbonated waterflooding of the second case (Type-II crude oil) was attributed to the significant viscosity contrast between carbonated water and oil and more importantly the low solubility of the carbon dioxide in the oil.

While Inclusion of high permeability channels in the micromodel had adverse effect on conventional waterflooding, it was beneficial to carbonated waterflooding. As an example, carbonated waterflooding implemented in the dual permeability micromodel saturated with heavy oil Type-II resulted in 23.5% improvements in the recovery factor over single permeability case at 1.6 PVs of injection at aforementioned experimental conditions and operations.

During this study, about 24% improvement was observed in recovery factor when carbonated waterflooding was applied to single permeability micromodel saturated with oil Type-I compared to Type-II.

Overall, it was concluded that carbonated waterflooding is a viable option for enhanced oil recovery of heavy oil reservoirs. Additional benefits will be through CO_2 storage, though less than immiscible and miscible CO_2 injection processes, and carbon tax credits. Some analysis and calculations will be included in the near future to address the potential of heavy oil carbonated waterflooding for CO_2 storage.

CHAPTER SIX: Sandpack Flooding

To investigate the performance of carbonated waterflooding at a larger scale and in a porous media, hence, series of experiments were conducted in s sandpack model. For this fact, three waterflooding tests were conducted using oil samples previously used in micromodel studies of this work. Furthermore, seven carbonated waterflooding experiments were performed at conditions similar to those in micromodel studies. Effect of parameters such as oil viscosity, saturation pressure, injection rate and temperature on the performance of carbonated waterflooding of the heavy oil sample were also studied.

6.1 Experimental Setup and Procedure

As mentioned earlier, experimental setup was designed to carry out both waterflooding and carbonated waterflooding tests while being flexible for other purposes such as coreflooding, cleaning and preparation. Therefore, a coreflooding physical model (sandpack) replaced the micromodel in the experimental setup and production collection system was accordingly changed to be appropriate for larger volume of effluents. Same as micromodel experimental setup, the main components for sandpack flooding were a temperature-controlled oven, a computer-controlled Agilent pump (1200 series from Agilent Comp.), three transfer cylinders (with displacement piston) for two types of crude oils and brine solution, a computer, high pressure gauges, a back-pressure-regulator (Equilibar, 2500 series), a sandpack model, a nitrogen cylinder with pressure regulator, scaled production collection cylinders (10 mL), high pressure stainless steel valves and other required fittings (Swagelok). An actual photo of the 1D sandpack model and

schematic diagram of the experimental setup for micro-model tests are presented in **Figure 6.1(a)** and **Figure 6.1(b)**, respectively.

Experimental procedure consists of number of steps which are listed below:

- Accurate measurement of the internal dimensions of the sandpack model
- Wet packing and drying the model with the sand
- Saturating sandpack model with brine and determination of porosity and absolute permeability of the sandpack model
- Saturating the sandpack model with the crude oil and determination of connate water saturation
- Waterflooding or carbonated waterflooding of the saturated sandpack model
- Determination of oil and water production rates and the recovery factor
- Cleaning the model for repacking and preparation for the next test

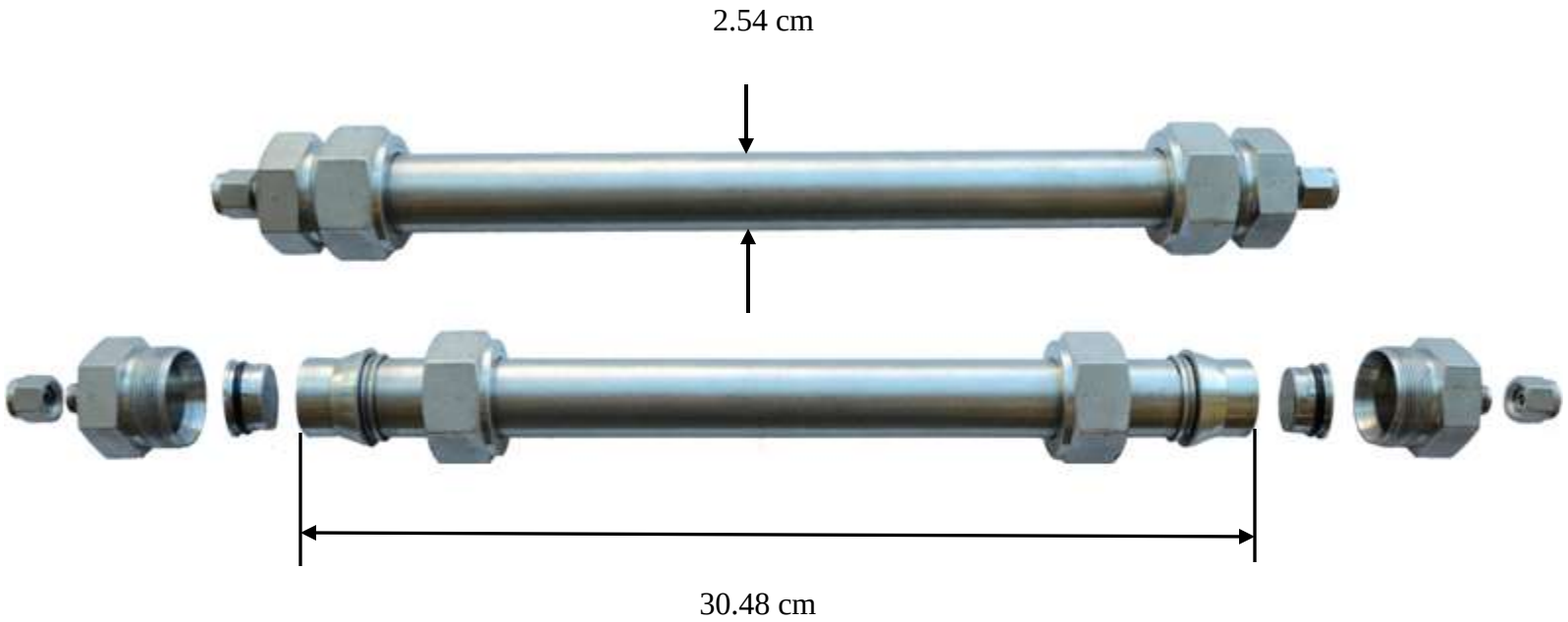

Figure 6.1(a): Photo of the assembled and disassembled sandpack model used in this study (reprinted from Pantus, 2012)

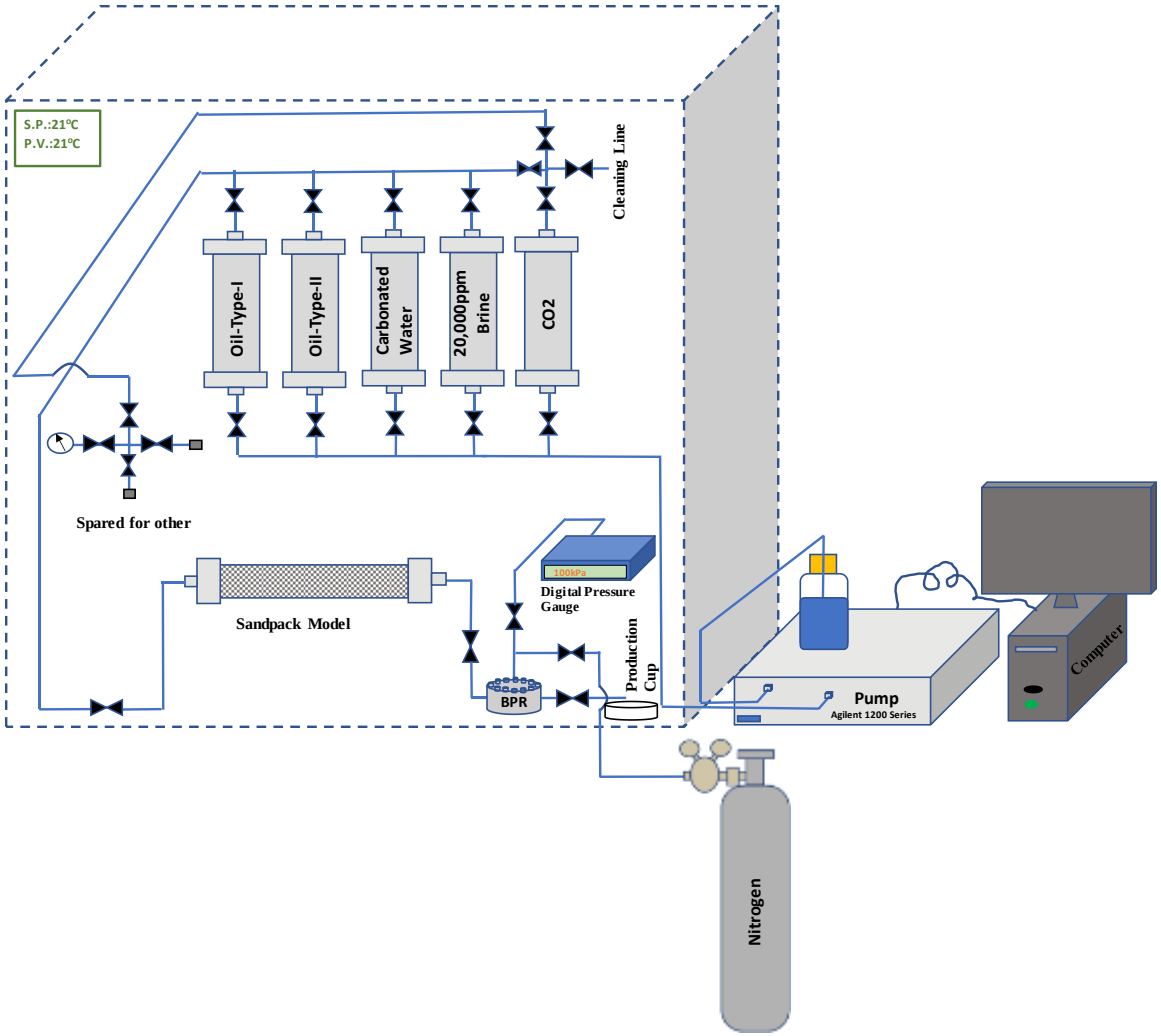

Figure 6.1(b): Schematic diagram of the coreflooding setup used in this study.

In this study, preparation of the sandpack was done following a simple yet thorough procedure. Since the sandpack model with dimensions of 30.48 (length) and 2.54 cm (diameter) had a smooth inner surface, it was coated with a thin layer of hydrocarbon and water proof liquid electrical tape (GB Gardner and Bender) capable of handling high temperatures. Sand-pack model was then wet-packed with sands from Bell and Mackenzie Company Ltd., with 99.88% of its composition as silicon dioxide (SiO_2). The particle mesh size ranged from ASTM 40 to 270 as previously reported by Mosavat (2014).

The wet packing procedure (with methanol) used by other researchers (Mosavat, 2014) was followed. Since methanol is a volatile fluid, the drying processes right after packing is relatively faster and easier than water as it can be achieved by injecting air for couple of hours. However, to ensure the wettability of the sand is not altered, model was vacuumed and then saturated with brine. Furthermore, about 20PVs of brine was injected, and an aging period of 48 hrs were allowed. It was then assumed that any alteration of the sand's wettability is reinstated.

Sandpack basic properties such as absolute permeability and porosity are very important when determining the performance of an enhanced oil recovery. All absolute permeability and porosity values measured for all sandpack models are listed in **Table. 6.1**. As it can be seen, values of permeability and porosity, and consequently, initial oil saturations and connate water saturations are different for various sandpack models. This is mainly because of the effect of sand packing and sorting of the sand grains which are most likely different for each test.

Table 6.1: Sand packs properties and experimental conditions.

Test No.	Type	^{o}API Gravity	Pressure (MPa)	Temperature (^{o}C)	Rate (cm^3/min)	Permeability (md)	Porosity (%)	S_{wc} (frac.)	S_{oi} (frac.)	S_{or} (frac.)
1	WF	20.44	1	21	0.1	6872	0.3	0.26	0.74	0.36
2	WF	15.49	1	21	0.1	7050	0.31	0.3	0.7	0.3
3	WF	15.49	3.1	21	0.1	6943	0.3	0.28	0.72	0.33
4	CWF	15.49	1	21	0.1	7137	0.31	0.32	0.68	0.3
5	CWF	15.49	3.1	21	0.1	7340	0.34	0.27	0.73	0.28
6	CWF	20.44	1	21	0.1	7083	0.32	0.31	0.69	0.31
7	CWF	20.44	3.1	21	0.1	7229	0.3	0.33	0.67	0.3
8	CWF	15.49	3.1	40	0.1	6905	0.29	0.26	0.74	0.33
9	CWF	15.49	3.1	21	1	7366	0.34	0.24	0.76	0.29
10	CWF	20.44	3.1	21	1	6748	0.28	0.25	0.75	0.35

6.2 Wateflooding of heavy oil saturated model

Waterflooding has been practiced as secondary oil recovery in both conventional and heavy oil reservoirs for several decades. Throughout years of practice in heavy oil reservoirs, it is suggested to inject water at a flux of 1 ft/day for an optimum recovery. Because of such practical recommendation by field engineers, an injection rate of 0.1 cm^3/min equivalent to 1 ft/day was considered for both waterflooding and carbonated waterflooding in sandpack models used in this study. The sand pack model had dimensions of 30.48 cm length and 2.54 cm diameter with two carefully designed distributors at both ends. As mentioned earlier, physical properties of sandpack such as absolute permeability, porosity, pore volume, initial and residual oil saturations and connate water saturation were measured for each test as tabulated in **Table 6.1**.

To establish two base lines for the two oil samples used in this study, three waterflooding tests were performed. Two base case scenarios of waterflooding were conducted at the temperature of T=21^{o}C, P=1 MPa, injection rate of q_{inj}=0.1 cm^3/min, using the two oil samples (^{o}API=15.49 and ^{o}API=20.44) previously used in the micromodel studies. A third base case of waterflooding was also conducted using the oil sample with ^{o}API=15.49 at conditions similar to the other two and operating pressure of P=3.1 MPa. This pressure is perhaps on the upper limit of the heavy oil reservoirs existing in unconsolidated shallow depths. However, compared to P=1 MPa, it allows higher amount of CO_2 to be carried out by brine, hence, performance evaluation at two substantially different operating pressures become easier.

Throughout this part of study significant effort was made to collect a minimum of 16 samples from effluent (each at 0.1 PV of injection) so that production trend can be

carefully determined. However, sometimes it was very difficult to have enough oil production and reading the produced oil volumes were challenging.

Figure 6.2 shows the cumulative recovery factor of the three aforementioned waterflooding tests. As it can be observed, conducting waterflooding in two sandpack models saturated with an oil sample with API gravity of 15.49 degree at operating pressure of P=3.1 MPa resulted in a small increase of 1.4% compared to waterflooding conducted at P=1MPa. This small increase could be attributed to the effect of pressure number of other factors such as variations in measurement from one test to another and some of the basic characteristics of sandpack models. Regardless, it clearly shows that for a gas-free oil, effect of operating pressure on the performance of waterflooding for the conditions of this study is minimum.

Comparison of the waterflooding results performed in two sandpack models saturated with two different oil samples shows significant increase of 6.5% in ultimate oil recovery factor. This is mainly because the oil sample with ^{o}API=20.44 has a lower viscosity compared with the heavier oil sample. In addition, as Table 6.1 depicts, when sandpack model was prepared and saturated with the oil sample of ^{o}API=20.44, higher initial oil saturation was achieved. Therefore, a small portion of the increase in the ultimate oil recovery of waterflooding could be attributed to the higher initial oil inplace and larger volume of oil contacted by water during waterflooding. This is indeed a known fact that the higher the initial oil saturation, the better the performance of secondary and tertiary oil recovery methods.

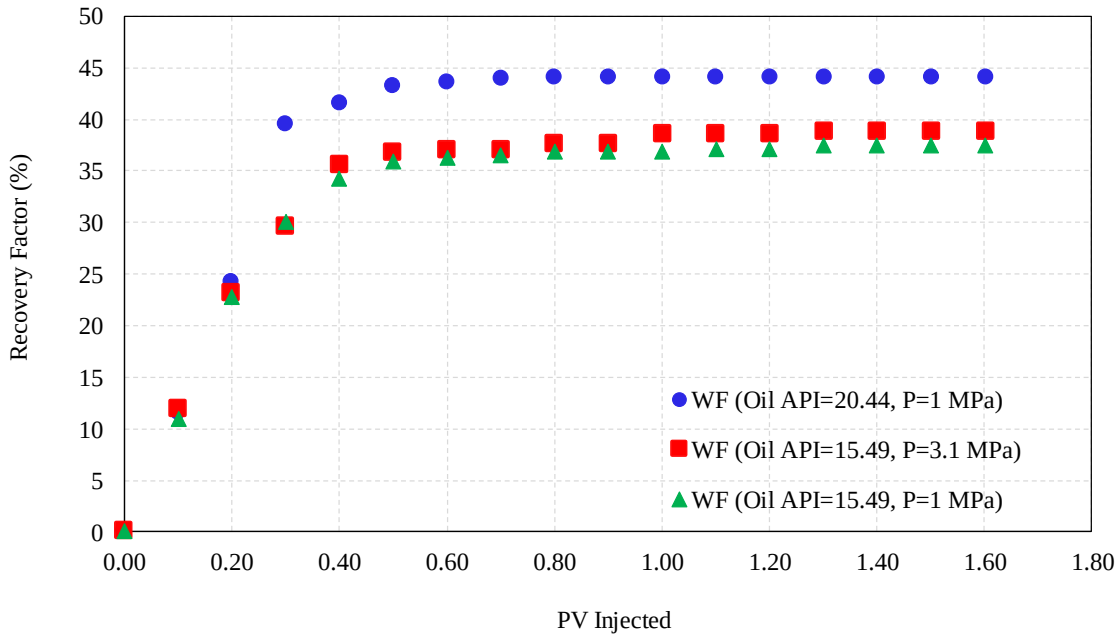

Figure 6.2: Waterflooding recovery factor of the sandpack models saturated with two different heavy oil samples at T=21°C, various pressures, and injection rate of 0.1 cm^3/min.

6.3 Carbonated Wateflooding of heavy oil saturated model

Carbonated waterflooding was performed at two different pressures of *P*=1 MPa and 3.1 MPa and constant temperature of *T*=21^{o}C for both oil samples. Carbonated water was prepared in similar manner as described in previous sections and injected at the same rate as waterflooding. **Figure 6.3** shows recovery factor of waterflooding and carbonated waterflooding tests performed at the two aforementioned tests in a sand-packed model saturated with the heavier oil sample (Type-II, ^{o}API=15.49). Waterflooding of this oil sample at two pressures of P=1 MPa and 3.1 MPa resulted in nearly similar recovery factors of 37.4 and 38.7%, respectively. In the other hand, carbonated waterflooding performed at those two pressures recovered 39.1 and 42% of the OOIP, respectively, after 1.6 PV of injection which means 1.7 and 3.3% higher than the waterflooding. Although the increased amount of recovery factor seems not substantial, they are very realistic for heavy oil reservoirs. As mentioned earlier, recovery factor of waterflooding in many of the heavy oil reservoirs are relatively low and sometimes a single digit. In addition, taking into account the large size of heavy oil reservoirs, an increase of 1 to 4%, results in recovery of large quantity of the heavy oil. More importantly, the amount of CO_2 injected via carbonated waterflooding is much lower compared to amount injected in the solvent injection scenarios. This, together with the benefit of using existing facilities waterflooding, turns carbonated waterflooding into a viable option for heavy oil reservoirs with the API within the range of those used in this study.

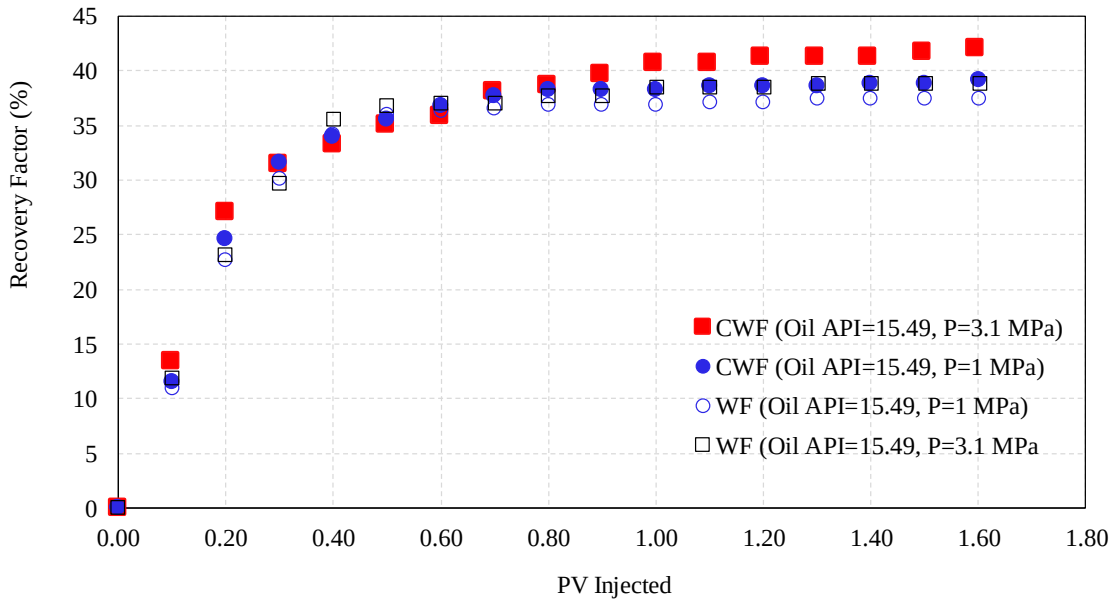

Figure 6.3: Recovery factor of waterflooding and carbonated waterflooding of the sandpack model saturated with type-II heavy oil samples at T=21^{o}C, various operating(carbonation) pressures, and injection rate of 0.1 cm^{3}/min.

6.3.1 Effect of oil API gravity on the performance of carbonated waterflooding

As mentioned in the literature review section, carbonated waterflooding has been well studied and recommended for conventional oil reservoirs. However, limited studies focused on the application of this technique to heavy oil reservoirs. Therefore, to better understand the range of applicability of carbonated waterflooding and role of oil API gravity on the performance of CWF results of four tests conducted using two oil samples are presented in **Figure 6.4**. As it can be observed from **Figure 6.4**, recovery factor of CWF conducted at *P*=1 MPa, in sandpack models saturated with two oil samples (Type-I, API Gravity=20.44; and Type-II, API Gravity=15.49) shows ultimate oil recovery factors of 50.7% and 39.1%, respectively. This shows that nearly 5 degrees of increase in API oil gravity could result in 11.6% increase in the recovery factor of CWF at P=1 MPa. Such significant increase is attributed to two main factors: higher amount of CO_2 mass transfer to the lighter oil (Type-I) and lower viscosity of Type-I oil compared with the heavier oil of Type-II. Similarly, at the higher carbonation pressure of *P*=3.1 MPa, recovery factor of 58.5% of OOIP was attained for CWF conducted in the sandpack model saturated with type-I (API Gravity 20.44). This was 16.5% higher compared to CWF conducted in a sandpack model saturated with oil type-II (API Gravity=15.49). Here also, the amount of CO_2 transferred from carbonated water to the type-II heavy oil is certainly larger and together with the effect of lower oil viscosity resulted in higher oil recovery factor for CWF conducted at *P*=3.1 MPa, *T*=21^{o}C, in the sandpack model saturated with type-I heavy oil (API Gravity=20.44). This comparative evaluation showed that the performance of CWF is more favourable when applied to a heavy oil reservoir with API gravity of 20 or higher and oil viscosity of 1000 mPa.s or lower.

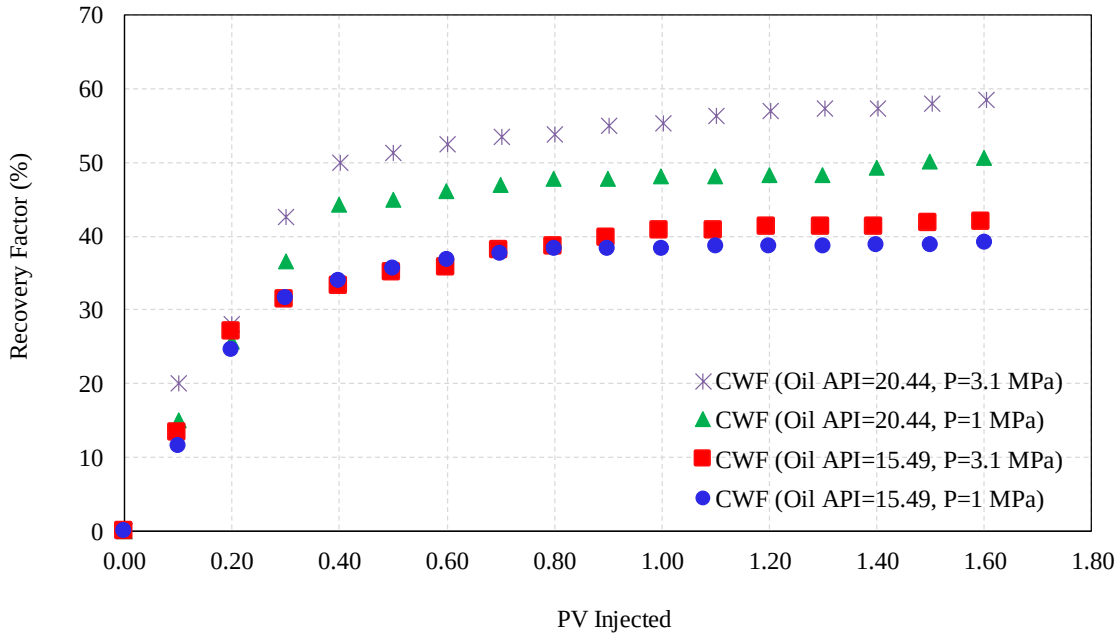

Figure 6.4: Recovery factor of carbonated waterflooding of the sandpack model saturated with two different heavy oil samples at T=21°C, at various carbonation pressures, and constant injection rate of 0.1 cm^3/min.

6.3.2 Effect of temperature on the performance of carbonated waterflooding

In addition to the carbonation pressure, another parameter which was of interest to study its effect on the performance of the CWF of heavy oil was temperature. Temperature was studied because of its dual effect. While temperature increase causes the oil viscosity to reduce, the diffusion rate and mass transfer of gases into the oil is inversely related to the temperature. Therefore, an additional carbonated waterflooding test was conducted at T=40^{o}C and its result was compared with that of base case CWF conducted at T=21^{o}C in **Figure 6.5**. As it is depicted in the figure, although within the first 0.6PV of CWF sometimes up to 3% of increase in the recovery factor was observed at the elevated temperature of 40^{o}C, the ultimate oil recovery factor was only increased by 1.1%. As almost no foamy oil behavior was observed during the CWF test conducted at T=40^{o}C, it was concluded that CO_2 minimally transferred to the oil and escaped during the displacement process. However, since oil viscosity reduced at T=40^{o}C, the ultimate oil recovery was slightly increased to 43.1% from an original amount of 42% at T=21^{o}C. Although higher increase was expected, it was speculated that lower water viscosity at the elevated temperature, lower quantity of the injected water as a small portion of the injection was dissolved CO_2 in the brine, and CO_2 evolution from brine while escaped without displacing oil could be mechanisms responsible for the lower increase in RF.

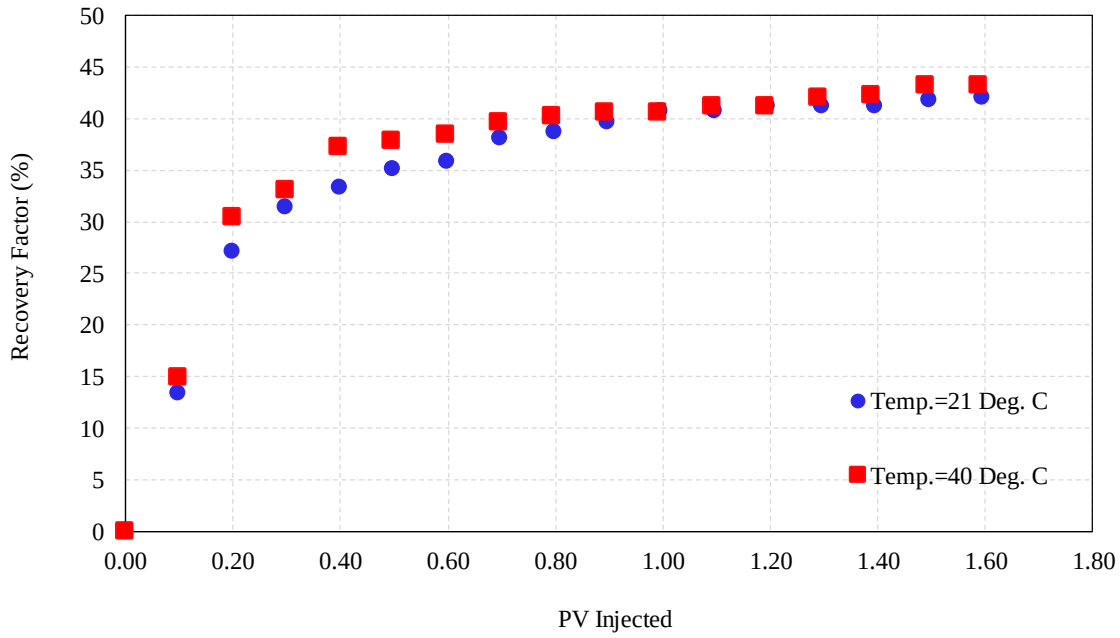

Figure 6.5: Recovery factor of carbonated waterflooding of the type-II heavy oil saturated sandpack model (^{o}API =15.49) at *P*=3.1 MPa, two different temperatures, and injection rate of 0.1 cm^3/min.

6.3.3 Effect of injection rate on the performance of carbonated waterflooding

By practice, one of the key factors in performing successful conventional waterflooding in heavy oil reservoirs is maintaining the injection flux of 1ft/day, equivalent to 0.02 cm/min. At the scale of the laboratory tests of this study where a 2.54 cm diameter sandpack model was used as the porous media, the injection rate was set to 0.1 mL/min to satisfy the flux condition of 1 ft/day (or 0.02 cm/min). However, to further study the effect of injection rate on the performance of CWF, an additional test was conducted at 1 mL/min corresponding to 10 folds of the practical injection rate in Type-II (^{o}API=15.49) oil saturated sand-pack. As it can be observed from **Figure 6.6**, results of the two flooding tests were nearly similar up until 1 PV of injection. However, injection at the higher flow rate of 1 mL/min for 1.6 PV, resulted in the ultimate recovery factor of 44.6%, which is about 2.6% higher than the achieved recovery factor at the base case injection rate of 0.1 mL/min.

As shown in **Table 6.1**, the base case CWF was conducted in a sandpack model with the initial oil inplace of 73%, porosity of 34% and absolute permeability of 7340 md. However, the sandpack model that was used for the CWF at 1 mL/min had characteristics of 76% oil inplace, 34% porosity and permeability of 7366 md. Although reservoir properties were very close in both sandpack models, 2% difference in the original oil inplace makes the comparison very difficult when the difference in recovery factor is also around 2-3%. Because of this difficulty, it can be concluded that micromodels are more reliable tools as properties of the porous media will remain the same during all tests.

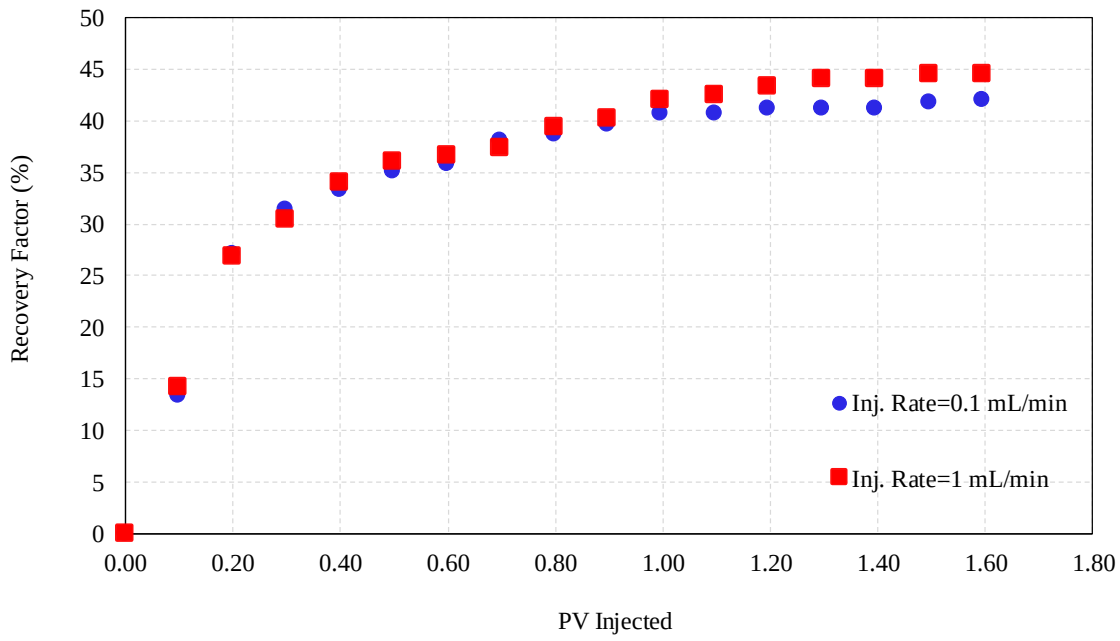

Figure 6.6: Recovery factor of carbonated waterflooding of the sandpack model saturated with a type-II heavy oil sample (API gravity of 15.49), at *T*=21°C, P=3.1 MPa, and various injection rates.

Carbonated waterflooding was also conducted in a sandpack model saturated with the type-I heavy oil (^{o}API=20.44) at 1 mL/min injection rate and at the constant pressure of P=3.1 MPa and temperature of T=21^{o}C. Results are presented in **Figure 6.7**. The ultimate oil recovery factor obtained at 1.6 PV of injection was 65.2% when CWF was conducted at 1 mL/min injection rate. This means increasing the injection rate by 10 folds resulted in 11.5% increase in the recovery factor of CWF conducted in the sandpack model saturated with type-I heavy oil (RF of base case=58.5%). Here again, the initial oil inplace for the test conducted at 1 mL/min was 75% compared to the lower value of 69% for the test conducted at 0.1 mL/min injection rate using heavy oil type-I. As it has been proved that performance of almost all enhanced oil recovery processes and in particular both WF and CWF are directly related to the oil inplace, it is difficult to draw a solid conclusion using the results obtained. At the same time, it is nearly impossible to prepare identical sandpack models and achieve exactly the same initial fluid saturations in all models. Therefore, it is just speculated that higher injection rate which results in higher capillary number may increase the recovery factor, however, more tests are required to formulate the relationship of CWF injection rate and its extent to which it increase the recovery factor in heavy oil reservoirs. As mentioned earlier, CWF tests performed at various injection rate in micromodels provide better comparative evaluations than those conducted in various cores or sandpack models.

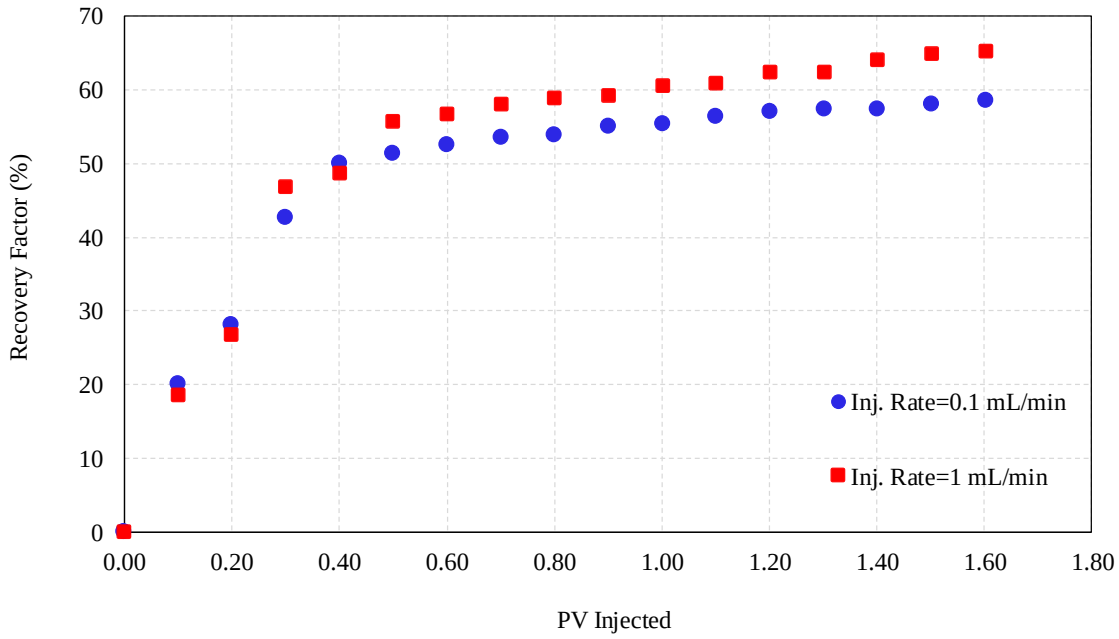

Figure 6.7: Recovery factor of carbonated waterflooding of the sandpack model saturated with type-I heavy oil sample (°API= 20.44), at *T*=21°C, P=3.1 MPa, and various injection rates.

6.4 Chapter Summary

Waterflooding and carbonated waterflooding tests were conducted in a sandpack model at various conditions. Effect of carbonation pressure, oil API gravity, injection rate and temperature were studied on two types of heavy oil samples. All experiments were conducted at constant temperature of T=21^{o}C and pressure of P=1 MPa and injection rate of q_{inj}=0.1 mL/min except those conducted to investigate the effect of the three aforementioned parameters. Comparison of carbonated waterflooding tests conducted at P=1 MPa and T=21^{o}C using both oil samples (Type-I, ^{o}API=20.44; Type-II, ^{o}API=15.49) showed 11.6% increase in ultimate recovery factor for the type-I oil in comparison to type-II. Similarly, at the higher carbonation pressure of P=3.1 MPa, recovery factor of 58.5% of OOIP was attained for CWF conducted in the sandpack model saturated with type-I heavy oil (API Gravity 20.44). This was 16.5% higher compared to CWF conducted in a sandpack model saturated with oil type-II (API Gravity=15.49). This demonstrates that CO_2 mass transfer from carbonated water to the heavy oil type-I is higher than that for type-II.

Carbonated waterflooding conducted in a sandpack model saturated with type-II heavy oil (^{o}API=15.49), at carbonation pressure of P=3.1 MPa, and two temperatures of 21^{o}C and 40^{o}C showed a small increase of 1.1% increase in oil recovery at higher temperature. Such a small increase was attributed to the balance of lower amount of CO_2 mass transfer to the oil and lower viscosity of the oil at the elevated temperature. At the elevated temperature of T=40^{o}C, although oil viscosity is lower which is expected to cause a higher displacement efficiency, the amount of CO2 transferred from the carbonated water as well as the water viscosity are much lower compared to the scenario of lower

temperature. The overall balance of these effects resulted in an insignificant improvement in recovery factor.

To study the effect of injection rate, two scenarios of 0.1 and 1.0 mL/min injection rate were compared for CWF in both heavy oil systems. Carbonated water injection at the higher flow rate of 1 mL/min for 1.6 PV, resulted in 2.6% higher recovery factor compared to the RF achieved at 0.1 mL/min for type-I heavy oil (P=3.1 MPa, and T=21^{o}C). For type-I heavy oil (^{o}API=20.44) carbonated water injection at the flow rate of 1 mL/min and similar conditions, resulted in the ultimate recovery factor of 65.2% which was 11.5% higher than that of CWF conducted at 0.1 mL/min injection rate in the same heavy oil system and at the same experimental conditions (RF of base case=58.5%).

Overall, throughout the sandpack flooding tests conducted in this study, it was proved that carbonation pressure, oil API gravity, temperature, and injection rate are all key parameters in the success of carbonated waterflooding. However, the extent of the effect of such parameters are very difficult to be determined as maintaining similar reservoir characteristics during the packing processes of various sand-packed models is nearly impossible. The deviation of the sandpack properties is mainly because of the packing, sand grains distribution. Such challenges justify the importance of displacement tests conducted in the micromodels where properties such as porosity, permeability, grains distribution, and to some extend the initial fluid saturations will remain constant. Also, cleaning process of the micromodels to ensure no residual oil or asphaltene contents are remaining in the model can be visually observed.

CHAPTER SEVEN: Conclusions and Recommendations

7.1 Conclusions

Two state-of-the-art micromodels with irregular shape and variable size grains were designed and manufactured to perform extensive experimental studies on waterflooding and carbonated waterflooding in heavy oil systems. Through an innovative idea, dual permeability porous media was generated in one of the micromodels and effect of influential parameters such as injections rate, temperature and oil API gravity on the performance of waterflooding carbonated waterflooding was studied. For this fact two heavy oil samples with API gravity of 20.44 and 15.49 and viscosities of 989 mPa.s and 5265 mPa.s at atmospheric pressure and temperature of T=21^{o}C were used. Waterflooding was conducted using synthetic brine with NaCl concentration of 20,000 ppm. Carbonated waterflooding was also implemented using carbon dioxide saturated brine at $P_{carbonation}$=1 and 3.1 MPa and T_{exp}=21^{o}C, 30^{o}C and 45^{o}C.

Thorough optical analysis, and quantitative evaluations were performed on the experimental results obtained. Conclusions of various sections of this study are presented below.

7.1.1 Fluid properties and interactions of fluids in binary systems

Prior to the micromodel flooding tests, detailed experimental studies were conducted to determine the key parameters such CO_2 solubility in brine solution and crude oil samples and swelling factor of the crude oil due to the dissolution of CO_2. Changes in the oil viscosity as a function of temperature were measured for both crude oil samples. In

addition, changes in oil and brine physical properties such as density and viscosity were estimated using available and popular correlations.

As the result, viscosity of both oils was significantly reduced when temperature increased. Type-I and II oil viscosities were reduced to 21 mPa.s and 78 mPa.s at T=55^{o}C from the initial values of 989 mPa.s and 5265 mPa.s at T=21^{o}C. These values were averaged over 5 measurements with deviations of up to 3%. Calculated results of viscosity variations as a function of dissolved CO_2 reveals that oil viscosity reduced to 590 mPa.s and 113 mPa.s after dissolution of about 0.37 moles of CO_2 in Type-I and Type-II crude oils, respectively.

Analysis of the measured CO_2 solubility values at various pressures and temperatures showed that solubility of CO_2 in Type-I and II crude oil reduced substantially when temperature increased. As an example, CO_2 solubility at pressure of P_{sat}=3.45 MPa was reduced by a consistent value of 43.4%-43.5% when temperature increased from 21^{o}C to 45^{o}C for both oil samples.

Maximum and minimum values of measured swelling factors for Type-I oil were 1.079 and 1.002 at two conditions of P_{sat}=3.45 MPa,, T_{exp}=21^{o}C and P_{sat}=689 kPa, T_{exp}=45^{o}C, respectively. These values were 1.052 and 1.001 for oil Type-II at the same conditions.

7.1.2 Waterflooding of heavy oils in micromodels

In this study effect of key parameters such as injection rate, temperature, oil API gravity, and reservoir extreme heterogeneity (dual permeability) on the performance of waterflooding, one of the most widely used secondary oil recovery processes, have been studied though series of experiments conducted in micromodels saturated with different

types of heavy oil samples. For this fact, the base case waterflooding was set at q_{inj}=0.05 cm^3/min at T=21°C. IN this section of the report, ultimate recovery factors of various cases were compared mainly at 1.6 PVs of injected water.

Effect of Injection Rate

To investigate the effect of injection rate on the performance of waterflooding in heavy oil systems, two additional tests were conducted using q_{inj}=0.025 cm^3/min and q_{inj}=0.075 cm^3/min representing ±50% of changes in the injection rate.

It was observed that, in comparison to the base case, increasing or decreasing the injection rate by 50% caused higher recovery factors before breakthrough. However, both lower and higher injection rates resulted in lower ultimate oil recovery factor at the total injection of 1.6 PV with the lowest amount obtained from the lowest injection rate (q_{inj}=0.025 cm^3/min). Ultimate recovery factors of three cases in the order of increasing injection rates were 48%, 62 % and 50.7%, respectively.

Effect of temperature

Temperature plays significant rule in the success of various types of EOR techniques when applied to heavy oil reservoirs due to the significant changes in oil viscosity and IFT. To visualize and quantify the effect of temperature on the recovery performance and displacement efficiency of waterflooding of oils (°API=20.44) two micromodel tests were conducted at T_{exp}=30°C and T_{exp}=45°C in addition to the base case of T_{exp}=21°C while injection rate was kept constant for both tests at q_{inj}=0.05 cm^3/min. Results obtained are also applicable to those heavy oil reservoirs with temperatures similar to the experiments.

Results obtained for Type-I crude oil showed that recovery factor increased from an initial value of 61% to 69.3% when temperature increased from T_{exp}=21°C to T_{exp}=30°C and experienced a further increase to 73.7% when test was conducted at T_{exp}=45°C.

For Type-II crude oil, ultimate recovery factors were 43.8, 48.2 and 50.4% in the increasing order of three temperatures.

While it was expected to see higher improvement in the recovery factor at the elevated temperature of T_{exp}=45°C, it was speculated that water viscosity reduction might be the responsible mechanism for this inconsistency. It is noteworthy that water viscosity is reduced to μ_w=0.62 mPa.s when temperature increased to T_{exp}=45°C.

Effect of oil API gravity

Comparison of the recovery factors in two heavy oil systems at 1.6 PVs of water injection shows that waterflooding was more successful in the heavy oil system with the oil API gravity of 20.44. Results showed that, 5 degrees of increase in the oil API gravity resulted in over 15% of increase in recovery factor (from 43.8% to 61%). This is mainly due to the viscosity contrast existing between crude oil and injected water.

Image analysis revealed that, when water breakthrough happened, only small amount of heavy oil with lower API gravity (API=15.49) was displaced compared to oil Type-I (API=20.44). Overall, images taken after water breakthrough confirmed lower performance of water injection in heavier oil (Type-II).

Dual-Permeability Effect

As mentioned earlier, one of the most innovative ideas of this research was to incorporate high permeability channels of different lengths and directions in the

micromodel to mimic the reservoirs with dilated porous media (e.g. dual permeability porous media, wormholes, fractures, etc.).

Comparative evaluation of the performance of waterflooding in two micromodels (with and without dual permeability regions showed that inclusion of the dual permeability reduced the ultimate oil recovery factor (at about 1.6 PVs of injected water) to 57.6% from the initial value of 61% obtained in single permeability model. As mentioned earlier, it was speculated that the 3.7% reduction in the recovery factor is because of the presence of high permeability channels causing earlier water breakthrough of $t_{BT\text{-}dual}$=40 seconds compared to $t_{BT\text{-}single}$=112 seconds obtained in the absence of high permeability channels.

7.1.3 Carbonated waterflooding of heavy oil in micromodels

The idea of applying carbonated waterflooding as a means of enhanced oil recovery is to dissolve CO_2 in the injected water and inject it into the oil reservoir. At the reservoir condition, when water contacted the oil, CO_2 leaves water and dissolves in the oil mainly because of its' higher solubility in the crude oil. As mentioned in the literature review section of this report (Chapter-2), carbonated waterflooding has been used as a means of enhanced oil recovery in many light oil systems. However, there is a large knowledge gap in the applicability of this technique to heavy oil reservoirs particularly those with API gravities of lower than 25 degree and viscosity of over 500 mPa.s. In this study, two heavy oil samples with characteristics mentioned earlier were used to experimentally investigate the performance of carbonated waterflooding in heavy oil saturated micromodels with and without high permeability channels. It is noteworthy that high permeability channels are typical dilated channels in unconsolidated sandstone reservoirs where sand is allowed to be produced with oil.

Carbonated waterflooding test conducted in the single permeability micromodel saturated with Type-I crude oil at about 1.6 PVs of injected water and under the base case conditions of q_{inj}=0.05 cm^3/min and T_{exp}=21°C showed an estimated recovery factor of 70%. This means, compared to the 61% recovery factor obtained during conventional waterflooding in the same oil system and under similar operating conditions, recovery factor was improved by 9%. This 9% improvement is attributed to the oil viscosity and IFT reduction, and solution gas drive mechanisms due to the dissolution of carbon dioxide in the oil at the contact interface of oil/water.

Effect of oil API gravity

Carbonated waterflooding was implemented to displace the heavier oil (Type-II crude oil with oil API gravity of 15.49) from single permeability micromodel at the rate of q_{inj}=0.05 cm^3/min and T_{exp}=21°C, a condition similar to the base case. Results of carbonated waterflooding applied to Type-II heavy oil showed 2.2% improvements in recovery factor at about 1.6 PVs compared to conventional waterflooding.

Comparison of recovery factor of carbonated waterflooding applied to Type-I and Type-II heavy oil saturated micromodel with single permeability at 1.7 PVs of water injection were 70.5% and 46.5% for Type-I and Type-II heavy crude oils, respectively. This shows that oil API gravity is one of the main screening criterion for carbonated waterflooding recovery technique.

Dual permeability effect

Carbonated waterflooding was also applied to dual permeability micromodel containing 17 high permeability channels in various directions and with different lengths. Micromodel was saturated with Type-II heavy oil (API=15.49), to mimic a real field scenario. Results were compared with those obtained during the carbonated waterflooding of the same oil in single permeability model and under the same conditions.

Analysis of the images taken during the displacement process showed wider distribution of frontal advancement compared to conventional waterflooding conducted in the same micromodel. This was attributed to the partial dissolution of CO_2 into the oil through multiple contacts of water, reduced oil viscosity and improved displacement efficiency via high permeability channels.

Overall, carbonated waterflooding conducted in two cases of single and dual permeability micromodels resulted in the ultimate oil recovery factor of 67% and 46.3%, at 1.57 PVs of injection, for dual and single permeability cases, respectively. This concludes that presence of high permeability channels is beneficial to carbonated waterflooding as channels are continuously drained from and refilled with the oil due to the dilation of the oil resulted from CO_2 dissolution. In the other hand, water initially displaces oil from these channels but when CO_2 dissolves in the oil, the diluted oil will refill the channels, hence, recovery factor increased.

7.1.4 Waterflooding and carbonated water flooding of heavy oils in sandpack model

Effect of carbonation pressure, oil API gravity, injection rate and temperature were studied on two types of heavy oil samples through utilization of sand-packed flooding process. Comparison of carbonated waterflooding tests conducted at *P*=1 MPa and P=3.1 MPa and *T*=21^{o}C using both oil samples (Type-I, ^{o}API=20.44; Type-II, ^{o}API=15.49) showed superiority of the performance of CWF in type-I heavy oil saturated model by additional recovery of 11.6%, and 16.5%, respectively. This demonstrates that CO_2 mass transfer from carbonated water to the heavy oil type-II is higher than that for type-I due to its higher API gravity and lower viscosity.

Carbonated waterflooding conducted in a sand-packed model saturated with type-II heavy oil (^{o}API=15.49), at carbonation pressure of P=3.1 MPa, and *T*=40^{o}C showed a small increase of 1.1% in oil recovery when compared with similar tests conducted at *T*=21^{o}C. Such a small increase was attributed to the balance of lower amount of CO_2 mass transfer to the oil and lower viscosity of the oil at the elevated temperature.

Flooding tests conducted at two carbonated water injection rates of 0.1 and 1.0 mL/min revealed that at the higher flow rate of 1 mL/min, an additional recovery factor of 2.6% is achieved for type-I heavy oil (*P*=3.1 MPa, and *T*=21^{o}C). For type-I heavy oil (^{o}API=20.44) carbonated water injection at the flow rate of 1 mL/min and similar conditions, resulted in an additional recovery factor of 11.5% when compared with the base case injection rate of 0.1 mL/min (RF of base case=58.5%).

Overall, throughout the sandpack flooding tests conducted in this study, it was proved that carbonation pressure, oil API gravity, temperature, and injection rate are all

key parameters in the success of carbonated waterflooding. However, the extent of the effect of such parameters are very difficult to be determined as maintaining or achieving similar reservoir characteristics during the packing process of various sand-packed models is nearly impossible. This will further make the comparative evaluation very difficult particularly for those cases where the effect of a specific parameter is very small. The deviation of the sandpack properties is mainly because of the packing and grain size distribution. Such challenges show the importance of displacement tests conducted in the micromodels where properties such as porosity, permeability, grain size distribution, and to some extend the initial fluid saturations will remain constant. Also, cleaning processes in micromodels can be visually monitored to ensure no asphaltene precipitation or residual oil are remaining in the model.

7.2 Recommendations

To validate the results obtained in this study and be able to implement carbonated waterflooding in the filed with confidence, the following future works are recommended:

- Utilization of the dual-permeability micromodels with connected fractures to wellbores are highly recommended. Extension of fractures to both injector and/or producer could mimic some actual scenarios.
- Since the main focus of this study was to investigate the applicability of carbonated waterflooding as a secondary oil recovery method, it is viable to study the performance of CWI in tertiary mode and be compared with the current results.
- Experimental studies of waterflooding and carbonated waterflooding in the large 3D sandpack models to compare the results with the micromodel and coreflooding results obtained in this study.
- Mathematical modeling of the pore networks and upscaling from micromodel to large field scale case.
- Utilization of hydrocarbon soluble nanoparticles which are able to encapsulate solvents and carry them to the reservoir while injected in the water may promote the solvent/waterflooding processes.
- Combination of carbonated waterflooding and polymer and/or surfactant flooding needs to be investigated and compared with both waterflooding and carbonated waterflooding in heavy oil systems.

- Utilization of the available commercial simulators to simulate the sandpack flooding process and history match the results and ultimately upscaling to a larger scale scenario is recommended.
- Investigating the contribution of carbonated waterflooding to CO_2 storage in heavy oil reservoirs using a field scale model is suggested.
- Asphaltene precipitation is one of the major concerns of the solvent injection processes. Conducting tests at elevated pressures and measurement of asphaltene precipitation for various scenarios and its relationship to other fluid and rock properties are recommended.

REFRENCES

Abedini, A., Mosavat, N., & Torabi, F. (2014). Determination of minimum miscibility pressure of crude oil–CO2 system by oil swelling/extraction test. *Energy Technology*.

Ahmadi, Y., Eshraghi, S., & Bahrami, P. (2015). Comprehensive Water–Alternating-Gas (WAG) injection study to evaluate the most effective method based on heavy oil recovery and asphaltene precipitation tests. *Journal of Petroleum*.

Alboudwarej, H., Felix, J., Taylor, S., & Badry, R. (2006). Highlighting heavy oil. *Oilfield*.

Armitage, P., & Dawe, R. (1989). What Is the Rheology of Foam in Porous Media? A Micromodel Study. *SPE International Symposium on Oil field*.

Aronofsky, J. S. (1952). Mobility Ratio - Its Influence on Flood Patterns During Water Encroachment. *Journal of Petroleum Technology*, *4*(01), 15–24.

Asghari, K., Araghi, M., & Ahmadloo, F. (2009). Utilization of CO for Improving the Performance of Waterflooding in Heavy Oil Recovery. *Canadian International*.

Bahralolom, I., Bretz, R., & Jr, F. O. (1988). Experimental investigation of the interaction of phase behavior with microscopic heterogeneity in a CO2 flood. *SPE Reservoir Engineering*.

Bamberger, A., Sieder, G., & Maurer, G. (2000). High-pressure (vapor+liquid) equilibrium in binary mixtures of (carbon dioxide+water or acetic acid) at temperatures from 313 to 353 K. *The Journal of Supercritical Fluids*, *17*(2), 97–110.

Barclay, T. H., & Mishra, S. (2016). New correlations for CO2-Oil solubility and viscosity reduction for light oils. *Journal of Petroleum Exploration and Production Technology*, *6*(4), 815–823.

Beggs, H. D. H., & Robinson, J. J. R. (1975). Estimating the Viscosity of Crude Oil Systems, *27*(09), 1140–1141.

Bora, R., Chakma, A., & Maini, B. (2003). Experimental investigation of foamy oil flow using a high pressure etched glass micromodel. *SPE Annual Technical Conference*.

Buckley, S., & Leverett, M. (1942). Mechanism of fluid displacement in sands. *Transactions of the AIME*.

Butler, Engineering, R. M. (Dept. of C. and P., Calgary, U. of, Calgary, & (CA)), A. (1991,

January 1). Thermal recovery of oil and bitumen. Old Tappan, NJ (United States); Prentice Hall Inc.

Campbell, B., & Jr, F. O. (1985). Flow visualization for CO2/crude-oil displacements. *Society of Petroleum Engineers Journal*.

Champion, J. H., & Shelden, J. B. (1989). An Immiscible WAG Injection Project in the Kuparuk River Unit. *Journal of Petroleum Technology*, *41*(05), 533–540.

Chapoy, A., Mohammadi, A., & Chareton, A. (2004). Measurement and modeling of gas solubility and literature review of the properties for the carbon dioxide− water system. *Industrial &*.

Chapoy, A., Mokraoui, S., Valtz, A., & Richon, D. (2004). Solubility measurement and modeling for the system propane–water from 277.62 to 368.16 K. *Fluid Phase*.

Chatzis, I., & Dullien, F. (1983). Dynamic immiscible displacement mechanisms in pore doublets: theory versus experiment. *Journal of Colloid and Interface Science*.

Chisholm, H. (1911). The Encyclopædia britannica: a dictionary of arts, sciences, literature and general information.

Christensen, R. J. (1961). Carbonated Waterflood Results--Texas And Oklahoma. In *Annual Meeting of Rocky Mountain Petroleum Engineers of AIME*. Society of Petroleum Engineers.

Chung, F., Jones, R., & Nguyen, H. (1988). Measurements and correlations of the physical properties of CO2-heavy crude oil mixtures. *SPE Reservoir Engineering*.

Costa, G., Rocha, P., & Ribeiro, A. (2012). An improved method for calculating CO 2 minimum miscibility pressure based on solubility parameter. *Journal of Petroleum*.

Craig, F. F. (1971). *The reservoir engineering aspects of waterflooding*. H. L. Doherty Memorial Fund of AIME.

Cramer, & S.D. (1982, August 1). The solubility of methane, carbon dioxide, and oxygen in brines from 0 deg to 300 deg c. Report of investigations/1982.

Crawford, P. B. (1960). Factors Affecting Waterflood Pattern Performance and Selection. *Journal of Petroleum Technology*, *12*(12), 11–15.

Dake, L. (2001). *The practice of reservoir engineering (revised edition)*.

Danesh, A., Krinis, D., & Henderson, G. (1988). Asphaltene deposition in miscible gas flooding of oil reservoirs. *Engineering Research*.

Diamond, L., & Akinfiev, N. (2003). Solubility of CO 2 in water from− 1.5 to 100 C and from 0.1 to 100 MPa: evaluation of literature data and thermodynamic modelling. *Fluid Phase Equilibria*.

Dodds, W., Stutzman, L., & Sollami, B. (1956). Carbon dioxide solubility in water. *Industrial&Engineering*.

Dong, M., Foraie, J., Huang, S., & Chatzis, I. (2002). Analysis of immiscible water-alternating-gas (WAG) injection using micromodel. *Canadian International*.

Dong, Y., Dindoruk, B., Ishizawa, C., Lewis, E. E., & Kubicek, T. (2011). No Title. *SPE Annual Technical*.

Dryer, S., & Ali, S. (1989). The potential of the immiscible carbon dioxide flooding process for the recovery of heavy oil. *Technical Meeting/Petroleum Conference of The*.

Duan, Z., & Sun, R. (2003). An improved model calculating CO 2 solubility in pure water and aqueous NaCl solutions from 273 to 533 K and from 0 to 2000 bar. *Chemical Geology*.

Duan, Z., Sun, R., Zhu, C., & Chou, I. (2006). An improved model for the calculation of CO_2 solubility in aqueous solutions containing Na^+, K^+, Ca^{2+}, Mg^{2+}, Cl^-, and SO_4, *Marine Chemistry*.

Emera, M., & Sarma, H. (2007). Prediction of CO_2 solubility in oil and the effects on the oil physical properties. *Energy Sources, Part A*.

ENICK, R., & KLARA, S. (1990). CO2 solubility in water and brine under reservoir conditions. *Chemical Engineering Communications*.

Ennis-King, J., & Paterson, L. (2005). Role of convective mixing in the long-term storage of carbon dioxide in deep saline formations. *Spe Journal*.

Gao, C., Li, X., Guo, L., & Zhao, F. (2013). Heavy oil production by carbon dioxide injection, *3*(3), 185–195.

George, D., Hayat, O., & Kovscek, A. (2005). A microvisual study of solution-gas-drive mechanisms in viscous oils. *Journal of Petroleum Science And*.

Grattoni, C., & Dawe, R. (2003). Gas and oil production from waterflood residual oil: effects of wettability and oil spreading characteristics. *Journal of Petroleum Science and Engineering*.

Green, D., & Willhite, G. (1998). Enhanced oil recovery.

Gu, F. (1998). Solubility of carbon dioxide in aqueous sodium chloride solution under high pressure. *J. Chem. Eng. Chin. Univ*.

Han, J., Shin, H., Min, B., Han, K., & Cho, A. (2009). Measurement and correlation of high pressure phase behavior of carbon dioxide+ water system. *Journal of Industrial And*.

Hickok, C., & Jr, H. R. (1962). Case histories of carbonated waterfloods in Dewey-Bartlesville field. *SPE Secondary Recovery Symposium*.

Holm, L. (1963a). CO2 Requirements in CO2 Slug and Carbonated Water Recovery Processes. *Producer Monthly. September*.

Holm, L. (1963b). CO2 Slug and carbonated water oil recovery processes. *Producers Monthly*.

Holm, L. W., & Josendal, V. A. (1974). Mechanisms of Oil Displacement By Carbon Dioxide. *Journal of Petroleum Technology*, *26*(12), 1427–1438.

Holmgren, C., & Morse, R. (1951). Effect of free gas saturation on oil recovery by water flooding. *Journal of Petroleum Technology*.

Hornof, V., & Morrow, N. (1988). Flow visualization of the effects of interfacial tension on displacement. *SPE Reservoir Engineering*.

Jamaluddin, A., Kalogerakis, N., & Chakma, A. (1991). Predictions of CO2 solubility and CO2 saturated liquid density of heavy oils and bitumens using a cubic equation of state. *Fluid Phase Equilibria*.

Jha, K. (1986). A laboratory study of heavy oil recovery with carbon dioxide. *Journal of Canadian Petroleum Technology*.

Johnson, W., Macfarlane, R., Breston, J., & Neil, D. (1952). Laboratory experiments with carbonated water and liquid carbon dioxide as oil recovery agents. *Prod. Monthly*.

Jr, H. R., & Small, F. (1964). Use of carbon dioxide for water injectivity improvement. *Journal of Petroleum Technology*. Retrieved from https://www.onepetro.org/journal-paper/SPE-595-PA

Khatib, A. A. K., Earlougher, R. C. R., & Kantar, K. No Title (1981). Society of Petroleum Engineers. https://doi.org/10.2118/9928-MS

Kiepe, J., Horstmann, S., & Fischer, K. (2002). Experimental determination and prediction of gas solubility data for CO2+ H2O mixtures containing NaCl or KCl at temperatures between 313 and 393 K and. *Industrial & Engineering*.

Kislyakov, Y., Kovalenko, K., & Babalyna, G. (1967). Treatment of well-Bore Area of Injection Wells with Carbonated Water. *Neft Khoz*.

Klins, M. A., & Ali, S. M. F. (1981). Oil Production in Shallow Reservoirs By Carbon Dioxide Injection. In *SPE Eastern Regional Meeting*. Society of Petroleum Engineers.

Klins, M. A., & Ali, S. M. F. (1982). Heavy Oil Production By Carbon Dioxide Injection. *Journal of Canadian Petroleum Technology*, *21*(05).

Koschel, D., Coxam, J., Rodier, L., & Majer, V. (2006). Enthalpy and solubility data of CO 2 in water and NaCl (aq) at conditions of interest for geological sequestration. *Fluid Phase Equilibria*.

Kulkarni, M., & Rao, D. (2005). Experimental investigation of miscible and immiscible Water-Alternating-Gas (WAG) process performance. *Journal of Petroleum Science and Engineering*.

Kumar, M., Hoang, V. T., Satik, C., & Rojas, D. H. (2008). High-Mobility-Ratio Waterflood Performance Prediction: Challenges and New Insights. *SPE Reservoir Evaluation & Engineering*, *11*(01), 186–196.

Kyte, J., Jr, R. S., Jr, S. S., & Rapoport, L. (1956). Mechanism of water flooding in the presence of free gas.

Lago, M., Huerta, M., & Gomes, R. (2002). Visualization study during depletion experiments of Venezuelan heavy oils using glass micromodels. *Journal of Canadian Petroleum*.

Lake, L. W., Carey, G. F., Pope, G. A., & Sepehrnoori, K. (1984). Isothermal, multiphase, multicomponent fluid flow in permeable media. *In Situ; (United States)*, *8:1*.

Latil, M. (1980). *Enhanced oil recovery*.

Lindeberg, E., & Wessel-Berg, D. (1997). Vertical convection in an aquifer column under a gas cap of CO 2. *Energy Conversion and Management*.

Liu, Y., Hou, M., Yang, G., & Han, B. (2011). Solubility of CO 2 in aqueous solutions of NaCl, KCl, CaCl 2 and their mixed salts at different temperatures and pressures. *The Journal of Supercritical Fluids*.

Ma, T., Rugen, J., & Stoisits, R. (1995). Simultaneous water and gas injection pilot at the Kuparuk River Field, reservoir impact. *SPE Annual Technical*.

Ma, T., & Youngren, G. (1994). Performance of immiscible water-alternating-gas (IWAG) injection at Kuparuk River Unit, North Slope, Alaska. *SPE Annual Technical Conference And*.

Mackay, E., Henderson, G., & Tehrani, D. (1998). The importance of interfacial tension on fluid distribution during depressurization. *Reservoir Evaluation & …*.

Mai, A., & Kantzas, A. (2009). Heavy Oil Waterflooding: Effects of Flow Rate and Oil Viscosity. *Journal of Canadian Petroleum Technology*, *48*(03), 42–51.

Mao, S., Zhang, D., Li, Y., & Liu, N. (2013). An improved model for calculating CO 2 solubility in aqueous NaCl solutions and the application to CO 2–H 2 O–NaCl fluid inclusions. *Chemical Geology*.

Martin, J. (1951). Additional oil production through flooding with carbonated water. *Producers Monthly*.

Mayer, E., Sr, R. E., & Spivak, A. (1988). Analysis of heavy-oil immiscible CO2 tertiary coreflood data. *SPE Reservoir*.

McGuire, P. P. L., Redman, R. R. S., Jhaveri, B. S. B., Yancey, K. E., & Ning, S. X. No Title (2005). Society of Petroleum Engineers.

Mehrotra, A., & Svrcek, W. (1982). Correlations for properties of bitumen saturated with CO2, CH4 and N2, and experiments with combustion gas mixtures. *Journal of Canadian Petroleum*.

Melzer, L. (2012). Carbon dioxide enhanced oil recovery (CO2 EOR): Factors involved in adding carbon capture, utilization and storage (CCUS) to enhanced oil recovery. *Center for Climate and Energy Solutions*.

Mosavat, N. (2014). Utilization of Carbonated Water Injection (CWI) as a Means of Improved Oil Recovery in Light Oil Systems: Pore-Scale Mechanisms and Recovery Evaluation.

Mosavat, N., & Torabi, F. (2013). Performance of secondary carbonated water injection in light oil systems. *Industrial & Engineering Chemistry Research*.

Mosavat, N., & Torabi, F. (2014). Experimental evaluation of the performance of carbonated water injection (CWI) under various operating conditions in light oil systems. *Fuel*.

Nevers, N. De. (1966). Carbonated waterflooding. *World Oil;(United States)*.

Nghiem, L., Shrivastava, V., Kohse, B., Hassam, M., & Yang, C. (2009). Simulation of Trapping Processes for CO2 Storage in Saline Aquifers. In *Canadian International Petroleum Conference*. Petroleum Society of Canada.

Nighswander, J., & Kalogerakis, N. (1989). Solubilities of carbon dioxide in water and 1 wt.% sodium chloride solution at pressures up to 10 MPa and temperatures from 80 to 200. degree. C. *Journal of Chemical And*.

OPEC Annual Statistical Bulletin, 2017. (n.d.). OPEC : World Proven Crude Oil Reserves: Cumulative production versus net additions. Retrieved September 12, 2017, from http://www.opec.org/opec_web/en/data_graphs/331.htm

Owete, O., & Brigham, W. (1987). Flow behavior of foam: a porous micromodel study. *SPE Reservoir Engineering*.

Pantus, P. (2012). *Experimental Investigation of Viscosity Ratio Effect on Displacemenet Performance of Polymer Systems During Heavy Oil Recovery*. University of Regina.

Paterson, L., Hornof, V., & Neale, G. (1984). Visualization of a surfactant flood of an oil-saturated porous medium. *Society of Petroleum Engineers*.

Peters, E., & Flock, D. (1981). The onset of instability during two-phase immiscible displacement in porous media. *Society of Petroleum Engineers Journal*.

Prutton, C., & Savage, R. (1945). The solubility of carbon dioxide in calcium chloride-water solutions at 75, 100, 120 and high pressures1. *Journal of the American Chemical*.

Renner, T. A. (1988). Measurement and Correlation of Diffusion Coefficients for CO 2 and Rich·Gas Applications.

Riazi, M. (2011). Pore scale mechanisms of carbonated water injection in oil reservoirs.

Riazi, M., Sohrabi, M., & Jamiolahmady, M. (2011). Experimental study of pore-scale mechanisms of carbonated water injection. *Transport in Porous Media*.

Robie, D. R., Roedell, J. W., & Wackowski, R. K. (1995). Field Trial of Simultaneous Injection of CO2 and Water, Rangely Weber Sand Unit, Colorado. In *SPE Production Operations Symposium*. Society of Petroleum Engineers.

Romero, C., Alvarez, J., & Müller, A. (2002). Micromodel studies of polymer-enhanced foam flow through porous media. *SPE/DOE Improved Oil Recovery*.

Rumpf, B., Nicolaisen, H., **?**cal, C., & Maurer, G. (1994). Solubility of carbon dioxide in aqueous solutions of sodium chloride: Experimental results and correlation. *Journal of Solution Chemistry*, *23*(3), 431–448.

Sabirzyanov, A., & Shagiakhmetov, R. (2003). Water solubility of carbon dioxide under supercritical and subcritical conditions. *Of Chemical Engineering*.

Sanchez, N. (1999). Management of water alternating gas (WAG) injection projects. *Latin American and Caribbean Petroleum Engineering*.

Sandrea, I., & Sandrea, R. (2007). Global Oil Reserves-1: Recovery factors leave vast target for EOR technologies. *Oil and Gas Journal*.

Saner, W. B., & Patton, J. T. (1986). CO2 Recovery of Heavy Oil: Wilmington Field Test. *Journal of Petroleum Technology*, *38*(07), 769–776.

of Wilmington Tar Zone CO2 injection project. *SPE Reservoir*.

Simon, R., & Graue, D. (1965). Generalized correlations for predicting solubility, swelling and viscosity behavior of CO2-crude oil systems. *Journal of Petroleum Technology*.

Smith, J. D., Chatzis, I., & Ioannidis, M. A. (2005). A New Technique to Measure the Breakthrough Capillary Pressure. *Journal of Canadian Petroleum Technology*, *44*(11).

Sohrabi, M., Henderson, G., & Tehrani, D. (2000). Visualisation of oil recovery by water alternating gas (WAG) injection using high pressure micromodels-water-wet system. *SPE Annual Technical*.

Sohrabi, M., Kechut, N., Riazi, M., & Jamiolahmady, M. (2012). Coreflooding studies to investigate the potential of carbonated water injection as an injection strategy for improved oil recovery and CO2 storage. *Transport in Porous*.

Sohrabi, M., Riazi, M., & Jamiolahmady, M. (2008). Carbonated water injection for oil recovery and CO2 storage*: Meeting the Science.*

Sohrabi, M., Riazi, M., Jamiolahmady, M., & Ireland, S. (2009). Mechanisms of oil recovery by carbonated water injection. *SCA Annual*.

Sohrabi, M., Riazi, M., Jamiolahmady, M., & Kechut, N. (2011). Carbonated water injection (CWI)–A productive way of using CO2 for oil recovery and CO2 storage. *Energy Procedia*.

Sohrabi, M., Tehrani, D., & Danesh, A. (2001). Visualisation of oil recovery by water alternating gas (WAG) injection using high pressure micromodels-oil-wet & mixed-wet systems. *SPE Annual Technical*.

Sohrabi, M., Tehrani, D., Danesh, A., & Henderson, G. (2004). Visualization of oil recovery by water-alternating-gas injection using high-pressure micromodels. *SPE Journal*.

Spivak, A., & Chima, C. M. (n.d.). Mechanisms of Immiscible C0 2 Injection in Heavy Oil Reservoirs, Wilmington Field, CA.

Srivastava, R., Huang, S., & Dyer, S. (1995). Measurement and prediction of PVT properties of heavy and medium oils with carbon dioxide.

Standing, M. (1979). A set of equations for computing equilibrium ratios of a crude oil/natural gas system at pressures below 1,000 psia. *Journal of Petroleum Technology*.

Steffens, A. (2010). Modeling and laboratory study of carbonated water flooding.

Tran, T. S. (2009). Electromagnetic assisted carbonated water flooding in heavy oil recovery.

Uren, L., & Fahmy, E. (1927). Factors influencing the recovery of petroleum from unconsolidated sands by waterflooding. *Transactions of the AIME*.

Vogel, H. (1993). The great well of China. *Scientific American*.

Wang, J., Dong, M., & Asghari, K. (2006). Effect of Oil Viscosity on Heavy Oil-Water Relative Permeability Curves. *SPE/DOE Symposium on Improved Oil*.

Wardlaw, N. C. (1996). Chapter 10 Factors affecting oil recovery from carbonate reservoirs and prediction of recovery (pp. 867–903).

Welker, J. (1963). Physical properties of carbonated oils. *Journal of Petroleum Technology*.

Willhite, & G.P. (1986, January 1). Waterflooding. Society of Petroleum Engineers,Richardson, TX.

Wyckoff, R., Botset, H., & Muskat, M. (1933). The mechanics of porous flow applied to water-flooding problems. *Transactions of the AIME*.

Yang, C., & Gu, Y. (2006). Diffusion coefficients and oil swelling factors of carbon dioxide, methane, ethane, propane, and their mixtures in heavy oil. *Fluid Phase Equilibria*.

Zhang, Y., Hyndman, C., & Maini, B. (2000). Measurement of gas diffusivity in heavy oils. *Journal of Petroleum Science And*. Retrieved from http://www.sciencedirect.com/science/article/pii/S0920410599000315

Zhang, Y., Sayegh, S., & Huang, S. (2006). Enhanced heavy oil recovery by immiscible WAG injection. *Canadian International Petroleum*. Retrieved from https://www.onepetro.org/conference-paper/PETSOC-2006-014